

**Lean-On Bracing Refined Design Methods and Field Assessment**

by

Claire Elizabeth Gasser

A dissertation submitted to the Graduate Faculty of  
Auburn University  
in partial fulfillment of the  
requirements for the Degree of  
Doctor of Philosophy

Auburn, Alabama  
May 4, 2024

Keywords: lean-on bracing, brace stiffness,  
stability bracing, cross-frame, steel bridge

Copyright 2024 by Claire Elizabeth Gasser

Approved by

Matthew Yarnold (Chair), Associate Professor of Civil & Environmental Engineering  
James Davidson, Professor of Civil & Environmental Engineering  
Robert Barnes, Professor of Civil & Environmental Engineering  
Kadir Sener, Assistant Professor of Civil & Environmental Engineering  
Todd Helwig, Professor of Civil, Architectural & Environmental Engineering

## Abstract

Cross-frames are critical for the stability of steel bridges during construction and play a significant role in completed bridges. Historically, brace locations have been regions of fatigue concerns, and each brace requires significant handling and processing during fabrication. The braces represent one of the most expensive bridge components per unit weight. Therefore, there are significant benefits to minimizing the number of cross-frames in a bridge in terms of economics and structural performance.

Lean-on bracing concepts replace select cross-frames in certain bracing lines with top and bottom struts, which allow a single cross-frame to brace several girders as a method of minimizing the number of cross-frames in a bridge. Lean-on concepts were developed for the Texas Department of Transportation (TxDOT) in the early 2000s. Previous studies developed design guidelines, but recent applications of lean-on bracing in TxDOT bridge designs demonstrated the need for improved efficiency and clarity.

The stiffness and strength of a given line of bracing are functions of the number and location of cross-frames in the line, as well as the specific cross-frame geometry (X, K, or Z-frames). While previous lean-on bracing equations were applicable to systems with one X- or Z-shaped cross-frame positioned in an exterior bay, derivations and model validation have been completed to extend the application of the design guidance. Derived equations with simplified design expressions for lean-on brace stiffness and strength will be discussed in terms of stability implications, with consideration for future application.

## **Dedication**

This work is dedicated in memory of Leo Santschi.

Thank you for the encouragement to pursue impossible goals.

## Acknowledgments

I express my deepest gratitude to my advisor, whose support, guidance, and expertise have been instrumental throughout my graduate studies. His mentorship has exemplified a commitment to excellence coupled with genuine care for his students. I am profoundly grateful for the opportunities and confidence he has given me to extend my capabilities. Thank you, Dr. Matthew Yarnold, for your impact on my academic development and personal growth.

This dissertation is part of a larger study of lean-on bracing, which was a collaboration between the University of Texas at Austin, Texas A&M University, and Auburn University. I am grateful to have been part of this effort and extend my gratitude to the professors involved in the project: Dr. Todd Helwig, Dr. Stefan Hurlebaus, Dr. Michael Engelhardt, Dr. Matthew Hebdon, and Dr. Eric Williamson. Thank you for your thoughtful insight and feedback.

The exchange of ideas and collaborative efforts have been vital in the progression of this research, and in this regard, I am extremely appreciative of my colleagues on the research team. Thank you, Aidan Bjelland, for complementarily sharing the workload with me, and David Fish, for your commitment to unravelling the research question from the outset.

This project would not have been possible without the financial support provided by the Texas Department of Transportation. Particular thanks to the panel who helped guide the study: Martin Dassi, Jamie Farris, Michelle Romage-Chambers, and Greg Turco.

Transferring universities midway through a PhD program is not the simplest undertaking. I am immensely grateful to the Auburn faculty members who were willing to invest in me. Thank you, Dr. James Davidson, Dr. Robert Barnes, and Dr. Kadir Sener for serving on my committee.

My graduate school experience would not have been as enjoyable without the camaraderie of my peers at Texas A&M and Auburn. I express my gratitude to all those who have indirectly contributed to the completion of this dissertation. Your support has been indispensable, and I am truly thankful for the community you have provided for me.

As this is a terminal degree, I feel it would be remiss not to mention the people who ignited and encouraged my interest in engineering from the beginning. Thank you to my high school math and science teachers, Mark Hoffman and Peter Scheetz, for going above and beyond to fuel my appetite for learning. And thank you to the faculty and students at the University of Notre Dame for introducing me to research and providing opportunities for me to ask questions, especially Dr. Robert Devine, Dr. Yahya Kurama, Dr. Ashley Thrall, and Dr. Kevin Walsh.

My heartfelt appreciation extends to my family for their constant support and encouragement. Mom and Dad, thank you for your love, guidance, and sacrifices to provide a springboard for my pursuits. To my Nana, Grandad, and Grandma, your affection and unwavering faith in me have been a constant source of motivation. Thank you to my siblings, Anna, Rudy, and Robbie, for bringing levity and mirth to my trips back home.

I am immensely grateful for my soon-to-be husband, who has been my rock through every trial and triumph of this endeavor. Nick, your patience and profound confidence in me mean the world. Thank you.

Finally, I am thankful to God for putting this opportunity and all of these incredible people in my life. He used this research project to reveal Himself through the intrinsic order of His creation and has remained steadfast with me throughout my studies.

## Table of Contents

Abstract .....	i
Dedication .....	ii
Acknowledgments .....	iii
Table of Contents .....	v
List of Tables .....	xii
List of Figures .....	xiv
List of Symbols .....	xxv
Chapter 1. Introduction .....	1
Chapter 2. Background .....	6
2.1. Bridge Girder Stability .....	6
2.1.1. Lateral-Torsional Buckling .....	6
2.1.2. System (Global) Lateral-Torsional Buckling .....	9
2.2. Stability Bracing .....	13
2.2.1. Torsional Bracing .....	13
2.2.2. Lateral Bracing .....	14
2.2.3. Lean-On Bracing .....	14
2.3. Torsional Bracing Stiffness Requirement .....	17
2.3.1. Brace Stiffness Requirement .....	17
2.3.2. Ideal Stiffness .....	19
2.3.3. Initial Imperfection .....	20

2.4. Lateral Bracing Stiffness Requirement.....	24
2.5. Conventional Torsional Bracing System Stiffness .....	25
2.5.1. In-Plane Girder Stiffness, $\beta g$ .....	26
2.5.2. Torsional Brace Stiffness, $\beta br$ .....	28
2.5.3. Cross-Section Stiffness, $\beta sec$ .....	32
2.6. Lean-On Torsional Bracing System Stiffness .....	34
2.6.1. In-Plane Girder Stiffness, $\beta g$ .....	34
2.6.2. Cross-Section Stiffness, $\beta sec$ .....	34
2.6.3. Torsional Brace Stiffness, $\beta br$ .....	35
2.7. R-Factors.....	36
2.8. Torsional Bracing Strength Requirements.....	37
2.8.1. Conventional Bracing .....	37
2.8.2. Lean-On Bracing.....	39
Chapter 3. Lean-On Brace Stiffness Derivations for One Exterior X- or K-Frame .....	40
3.1. Current Brace Stiffness Derivations .....	40
3.1.1. Twin Girder System Derivation.....	40
3.1.2. Original Lean-On Bracing Derivation .....	43
3.2. Derivations for Other Cross-Frame Shapes .....	45
3.2.1. Two-Dimensional Model Validation .....	45
3.2.2. Lean-On with K-Frames .....	46
3.2.3. Lean-On with Full X-Frames.....	52
Chapter 4. Lean-On Brace Stiffness Equation Modifications for Multiple Cross-Frames.....	57
4.1. Approaches for Multiple Cross-Frames.....	58

4.1.1. Cross-Section Slice Approach .....	58
4.1.2. Displacement Combination Approach .....	59
4.1.3. Stiffness Superposition Approach.....	60
4.1.4. Cross-Frame Coefficient Approach .....	60
4.2. Comparison of Approaches .....	61
4.3. Generalized Equation for Cross-Section Slice Approach.....	62
4.4. Detailed Validation of CSS Approach for Z-Frames.....	62
4.5. Validation of CSS Approach for Other Cross-Frame Shapes.....	68
4.5.1. Lean-On K-Frames .....	68
4.5.2. Lean-On X-Frames .....	71
4.6. Summary of CSS Equation .....	73
 Chapter 5. Lean-On Brace Stiffness Equation Modifications for Interior Bay Cross- Frames.....	 74
5.1. Performance of Cross-Section Slice with Interior Cross-Frame Placement.....	74
5.1.1. Revised Idealizations and Equation .....	76
5.1.2. Modified Equation Performance .....	77
5.2. Adjustments for Nonadjacent Cross-Frames .....	78
5.2.1. Checkerboard Layouts .....	78
5.2.2. Other Nonadjacent Cross-Frame Patterns.....	81
5.3. Summary of Brace Stiffness Equation.....	82
 Chapter 6. Field Instrumentation .....	 84
6.1. Identification of Existing Lean-On Bridges.....	84
6.2. Lubbock Bridge .....	87



6.2.1. Background .....	87
6.2.2. Data Archive .....	89
6.3. SH 105 Bridge at Brazos River.....	90
6.3.1. Overview .....	90
6.3.2. Sensor Layout .....	92
6.3.3. Data Acquisition .....	97
6.3.4. Live Loading.....	99
6.4. Chisholm Trail Bridge at FM1902.....	101
6.4.1. Overview.....	101
6.4.2. Sensor Layout .....	104
6.4.3. Data Acquisition .....	107
6.4.4. Live Loading.....	108
6.5. Data Processing.....	111
6.5.1. Strain Gauge Readings to Axial Forces .....	111
6.5.2. Deflection Measurements .....	113
Chapter 7. Bridge Model Validation.....	114
7.1. Objective Functions .....	115
7.2. SH 105 Bridge Model Validation .....	116
7.3. Chisholm Trail Bridge Model Validation.....	119
7.4. Lubbock Bridge Model Validation .....	122
7.4.1. Overview of Lubbock Bridge .....	122
7.4.2. Field Instrumentation and Testing .....	123
7.4.3. Validated Model Results.....	127

Chapter 8. Study of Bridge Models .....	129
8.1. Live Load Stress Response of Lean-on Systems .....	129
8.1.1. SH 105 Bridge.....	130
8.1.2. Chisholm Trail Bridge .....	133
8.2. Cross-Frame Layout Study .....	136
8.2.1. Findings From Phase 1: Initial Layout Study .....	136
8.2.2. Findings From Phase 2: Layout Effect with Isolated Brace Stiffness .....	137
8.2.3. Findings from Phase 3: Layout Effect with Isolated In-Plane Girder Stiffness.....	138
8.2.4. Summary of Recommended Layouts.....	141
Chapter 9. System Stiffness Equation Performance Comparison with 3D Models.....	142
9.1. Differences Between Brace Stiffness Derivation and 3D Bridge System Models .....	142
9.2. Equation Validation for Constant Cross-Frame Placements .....	144
9.3. Performance Improvement for Staggered Layouts .....	145
9.4. Performance of Recommended Layouts.....	148
9.5. Relationship of $\beta g$ and $\beta br$ for Design.....	150
Chapter 10. Revised Expressions for Brace Strength Design.....	152
10.1. Previous Strength Requirement Equations .....	153
10.2. Z-Frame Revised Strength Equations .....	154
10.3. X-Frame Revised Strength Equations.....	155
10.4. K-Frame Revised Strength Equations.....	156
10.5. Summary of Brace Force Equations .....	157
Chapter 11. Refined Design Methodology for Lean-On Bracing.....	159
11.1. Determine Girder Layout and Geometry .....	159

11.2. Determine Cross-Frame Locations Based on Recommended Layouts .....	160
11.3. Determine Moment Demands at Each Brace Line .....	160
11.3.1. Calculate the Moment Loading at Each Cross-Frame Line.....	161
11.3.2. Check System Global Buckling Moment .....	161
11.3.3. Check the Conventional Lateral-Torsional Buckling Moment.....	162
11.4. Determine Minimum Brace Area for Each Bracing Line.....	163
11.4.1. Determine Required System Stiffness .....	163
11.4.2. Calculate In-Plane Girder Stiffness.....	163
11.4.3. Calculate Cross-Sectional Stiffness .....	164
11.4.4. Use Brace Stiffness Equation to Determine Minimum Brace Area .....	165
11.4.5. Select Brace Member Size .....	166
11.5. Check Strength Requirements .....	166
11.5.1. Determine the Total Brace Force Demand in Diagonals and Struts.....	166
11.5.2. Check Strength Capacity.....	167
11.5.3. Other Design Requirements .....	168
Chapter 12. Design Examples.....	169
12.1. Design Example 1 .....	169
12.1.1. Determine Girder Layout and Geometry .....	169
12.1.2. Determine Cross-Frame Locations Based on Recommended Layouts.....	171
12.1.3. Check Moment Demands.....	173
12.1.4. Determine Minimum Brace Area for Each Bracing Line .....	175
12.1.5. Check Strength Requirements for Each Bracing Line .....	177
12.2. Design Example 2 .....	182

12.2.1. Determine Girder Layout and Geometry .....	182
12.2.2. Determine Cross-Frame Locations Based on Recommended Layouts.....	184
12.2.3. Check Moment Demands.....	185
12.2.4. Determine Minimum Brace Area for Each Bracing Line .....	188
12.2.5. Check Strength Requirements for Each Bracing Line .....	190
Chapter 13. Conclusions .....	196
13.1. Research Contributions.....	196
13.2. Future Work.....	197
References.....	199
Appendix A. Lubbock Bridge Live Load Testing Layouts .....	202
Appendix B. SH 105 Bridge Sensor List Conventions.....	204
Appendix C. SH 105 Bridge Sensor List.....	205
Appendix D. SH 105 Bridge Live Load Testing Layout .....	208
Appendix E. Chisholm Trail Bridge Sensor List Conventions.....	211
Appendix F. Chisholm Trail Bridge Sensor List .....	212
Appendix G. Chisholm Trail Bridge Live Load Testing Layouts .....	216
Appendix H. Axial Force Sample Calculations.....	218
Appendix I. Lubbock Bridge Axial Forces.....	222
Appendix J. SH 105 Bridge Axial Forces and Deflections .....	228
Appendix K. Chisholm Trail Bridge Axial Forces and Deflections.....	237
Vita.....	245

## List of Tables

Table 2-1. System Warping Stiffness Factor Values .....	12
Table 2-2. Brace Coefficient used in Equation 2.16.....	25
Table 3-1. Virtual Work Calculations for Two Girders and One K-Frame.....	48
Table 3-2. Virtual Work Calculations for Three Girders and One K-Frame.....	50
Table 3-3. Virtual Work Calculations for Four Girders and One K-Frame.....	51
Table 3-4. Virtual Work Calculations for Three Girders and One X-Frame.....	54
Table 3-5. Virtual Work Calculations for Four Girders and One X-Frame.....	55
Table 4-1. Preliminary Comparison of Approaches: $\beta_{br}$ , <i>approach</i> / $\beta_{br}$ , <i>SAP model</i> .....	62
Table 5-1. Revised CSS Idealization .....	77
Table 5-2. Effective Values for Checkerboard Patterns .....	80
Table 5-3. Example Idealizations for Non-Checkerboard Nonadjacent Cross-Frame Patterns.....	82
Table 5-4. Correct Values for Brace Stiffness Equation.....	83
Table 6-1 SH 105 Bridge Measured Truck Weights .....	100
Table 6-2 Truck Weights for Live Load Testing of the Chisholm Trail Bridge.....	109
Table 8-1. Lean-on $\beta g$ and $Mg$ Recommendations adapted from Bjelland (2024).....	140
Table 8-2. Recommended Lean-On Layout Summary adapted from Bjelland (2024) and Helwig (2024).....	141
Table 9-1. Results for 1 CFL with 10 Foot Girder Spacing.....	145
Table 9-2. Results for 3 CFL with 80 Foot Girder Spacing.....	146

Table 9-3. Results from 3 staggered CFL parametric study on leaning girders .....	147
Table 9-4. Results from recommended layout study .....	148
Table 11-1. Recommended Lean-On Layout Summary .....	160
Table 11-2. System Warping Stiffness Factor ( $\alpha x$ ) Values .....	162
Table B-1. SH 105 Bridge Sensor List Conventions .....	204
Table C-1. SH 105 Bridge Sensor List .....	205
Table E-1. Chisholm Trail Bridge Sensor List Conventions .....	211
Table F-1. Chisholm Trail Bridge Sensor List.....	212

## List of Figures

Figure 1-1. Lateral-Torsional Buckling (Helwig and Wang, 2003) .....	1
Figure 1-2. (A) Conventional Cross-Frame System and (B) Lean-On System .....	3
Figure 2-1. Various Forms of Cross-Frames .....	13
Figure 2-2. Lean-on Bracing in Lubbock, Texas Implementation Study (TxDOT Project 5-1772).....	15
Figure 2-3. Typical Lean-On Bracing Layout .....	16
Figure 2-4. Lean-On Bracing Detailed Layout .....	16
Figure 2-5. (A) Brace Stiffness Less than Ideal Stiffness and (B) Brace Stiffness Greater than Ideal Stiffness.....	19
Figure 2-6. Braced Winter Column with Initial Out-of-Straightness (Yura, 2001).....	21
Figure 2-7. In-Plane Girder Stiffness.....	27
Figure 2-8. Girder Deformation with Zero Brace Stiffness.....	29
Figure 2-9. Twin Girder Tension Model Brace Stiffness Idealization .....	29
Figure 2-10. Twin Girder Compression Model Brace Stiffness Idealization .....	31
Figure 2-11. Twin Girder K-Frame Brace Stiffness Idealization .....	32
Figure 2-12. Force Distribution along Lean-On Bracing Line .....	36
Figure 2-13. Idealized Cross-Frame Forces.....	37
Figure 3-1. Twin Girder Brace Stiffness Idealization.....	41
Figure 3-2. Lean-On Bracing Stiffness Idealization.....	44

Figure 3-3. Twin Girder Tension Model Idealization and Deformed Shape .....	45
Figure 3-4. Twin Girder K-Frame Idealization.....	47
Figure 3-5. Twin Girder K-Frame Real Force Distribution.....	47
Figure 3-6. Twin Girder K-Frame Virtual T2 Force Distribution .....	47
Figure 3-7. Twin Girder K-Frame Virtual B2 Force Distribution .....	47
Figure 3-8. Force Distribution for One K-Frame and Three Girders .....	49
Figure 3-9. Force Distribution for One K-Frame and Four Girders .....	49
Figure 3-10. Generalized Lean-On K-Frame Force Distribution .....	49
Figure 3-11. Force Distribution for One X-Frame and Three Girders .....	53
Figure 3-12. Force Distribution for One X-Frame and Four Girders .....	53
Figure 3-13. Generalized Lean-On X-Frame Distribution .....	53
Figure 4-1. Four Girder, One Z-Frame Lean-On Bracing Stiffness Idealization .....	57
Figure 4-2. Four Girder, Two Z-Frame Lean-On Bracing Stiffness Idealization.....	57
Figure 4-3. Cross-Section Slice Approach.....	59
Figure 4-4. Displacement Combination Approach .....	59
Figure 4-5. Stiffness Superposition Approach.....	60
Figure 4-6. Cross-Frame Coefficient Approach .....	61
Figure 4-7. $\beta_{br}$ , $leanZ$ , $CSS/\beta_{br}$ , $SAP$ model for Exterior Z-Frames.....	64
Figure 4-8. $\beta_{br}$ , $leanZ$ , $CSS/\beta_{br}$ , $SAP$ model for Checkerboard Z-Frames .....	65
Figure 4-9. $\beta_{br}$ , $leanZ$ , $CSS/\beta_{br}$ , $SAP$ model for Interior and Exterior Z-Frames.....	65
Figure 4-10. $\beta_{br}$ , $leanZ$ , $CSS/\beta_{br}$ , $SAP$ model for One Z-Frame Varied Location.....	66



Figure 4-11 $\beta_{br}$ , $leanZ$ , $CSS/\beta_{br}$ , $SAP$ model for Two Z-Frames Varied Location .....	67
Figure 4-12. $\beta_{br}$ , $leanZ$ , $CSS/\beta_{br}$ , $SAP$ model for Z-Frames Three Cross-Frames Varied Location .....	67
Figure 4-13. $\beta_{br}$ , $leanK$ , $CSS/\beta_{br}$ , $SAP$ model for K-Frames Cross-Frames Aligned Exterior .....	69
Figure 4-14. $\beta_{br}$ , $leanK$ , $CSS$ , $reduced/\beta_{br}$ , $SAP$ model for Simplified K-Frame Equation Cross-Frames Aligned Exterior .....	70
Figure 4-15. $\beta_{br}$ , $leanX$ , $CSS/\beta_{br}$ , $SAP$ model for X-Frames Cross-Frames Aligned Exterior .....	72
Figure 4-16. $\beta_{br}$ , $leanX$ , $CSS$ , $reduced/\beta_{br}$ , $SAP$ model for Simplified X-Frame Equation Cross-Frames Aligned Exterior .....	73
Figure 5-1. Brace Stiffness Increase due to Interior Cross-Frame Placement .....	75
Figure 5-2. Overlay of Brace Stiffness Increase due to Interior Cross-Frame Placement.....	76
Figure 5-3. Modified Brace Stiffness Equation with Interior Cross-Frames.....	78
Figure 5-4. Model Stiffness of Checkerboard Bracing Lines .....	79
Figure 5-5. Checkerboard Model Stiffness/Idealized Stiffness .....	80
Figure 6-1. Lubbock Bridge Instrumentation Plan (Romage, 2008) .....	88
Figure 6-2. Lubbock Bridge (a) Brace Angle and (b) Girder Gage Locations (Romage, 2008) .....	88
Figure 6-3. Lubbock Bridge Strut and Cross-Frame Strain Gage Locations (Romage, 2008) .....	89
Figure 6-4. Lubbock Bridge Truck Positions (Romage, 2008) .....	90

Figure 6-5. SH 105 Bridge Framing Plan .....	91
Figure 6-6. Typical Transverse Section on SH 105 Bridge.....	91
Figure 6-7. SH 105 Bridge Span 7-8 .....	92
Figure 6-8. SH 105 Bridge Span 6.....	92
Figure 6-9. SH 105 Bridge Span 6 Strain Gauge Layout .....	94
Figure 6-10. SH 105 Bridge Span 6 Girder Displacement Layout.....	94
Figure 6-11. Strain Gage Placement on Angles.....	95
Figure 6-12. Revised Strain Gauge Placement on Top Struts .....	95
Figure 6-13. Strain Gage Placement on Cross-Frames and Struts.....	96
Figure 6-14. Strain Gage Placement on Center Girder .....	97
Figure 6-15. SH 105 Bridge Wiring Diagram .....	98
Figure 6-16. Sensor Monitoring During Loading.....	98
Figure 6-17. SH 105 Bridge Truck Dimensions for Live Load Testing.....	99
Figure 6-18. Truck Setup for SH 105 Bridge Load Case #1 .....	100
Figure 6-19. Measuring the Distance Between Trucks.....	101
Figure 6-20. Chisholm Trail Bridge Framing Plan.....	102
Figure 6-21. Chisholm Trail Bridge Typical Transverse Section.....	103
Figure 6-22. Chisholm Trail Bridge Spans.....	104
Figure 6-23. Chisholm Trail Bridge Span 1 Strain Gauge Layout .....	105
Figure 6-24. Chisholm Trail Span 1 Girder Displacement Layout.....	105

Figure 6-25. Chisholm Trail Double Angle Top and Bottom Strut Strain Gauge Placement.....	106
Figure 6-26. Chisholm Trail Single Angle Top and Bottom Strut Strain Gauge Placement.....	106
Figure 6-27. Chisholm Trail Strain Gauge Placement on Cross-Frames and Struts .....	107
Figure 6-28. Chisholm Trail Strain Gauge Placement on Cross-Frames and Struts .....	108
Figure 6-29. Chisholm Trail Bridge Truck Dimensions for Live Load Testing.....	109
Figure 6-30. Chisholm Trail Bridge Load Case 4.....	110
Figure 7-1. SH 105 Spring and Deck Stiffness Objective Function .....	117
Figure 7-2. SH 105 Bridge Girder Displacements Load Case 1 .....	118
Figure 7-3. SH 105 Bridge Girder Displacements Load Case 2.....	118
Figure 7-4. SH 105 Bridge Girder Displacements Load Case 3 .....	119
Figure 7-5. SH 105 Bridge Girder Displacements Load Case 4.....	119
Figure 7-6. Chisholm Trail Deck and Barrier Stiffness Objective Function .....	120
Figure 7-7. Chisholm Trail Girder Displacements Load Case 1 .....	121
Figure 7-8. Chisholm Trail Girder Displacements Load Case 2 .....	121
Figure 7-9. Chisholm Trail Girder Displacements Load Case 3 .....	122
Figure 7-10. Chisholm Trail Girder Displacements Load Case 4 .....	122
Figure 7-11. Lubbock Bridge During Deck Pour (Romage, 2008) .....	123
Figure 7-12. Lubbock Bridge Deck Pour Sequence Timeline (Helwig <i>et al.</i> , 2024) .....	124
Figure 7-13. Lubbock Overhang Loading During Construction (Helwig <i>et al.</i> , 2024).....	125

Figure 7-14. Lubbock Overhang Load Positions of Screed and Deck Pour (Helwig <i>et al.</i> , 2024) .....	126
Figure 7-15. Lubbock Model used for Validation (Bjelland, 2024) .....	127
Figure 7-16. Results from 6:00 AM Model .....	128
Figure 8-1. SH 105 Load Case One Conventional vs. Lean-On Bracing Line Forces .....	131
Figure 8-2. SH 105 Load Case Two Conventional vs. Lean-On Bracing Line Forces .....	132
Figure 8-3. SH 105 Load Case Four Conventional vs. Lean-On Bracing Line Forces .....	133
Figure 8-4. Chisholm Trail Load Case Three Conventional vs. Lean-On Bracing Line Forces .....	134
Figure 8-5. Chisholm Trail Load Case Two Conventional vs. Lean-On Bracing Line Forces .....	134
Figure 8-6. Chisholm Trail Load Case Five Conventional vs. Lean-On Bracing Line Forces .....	135
Figure 8-7. Phase 1 Lean-On Layouts (Bjelland, 2024) .....	136
Figure 9-1. Bridge Cross-Frame Line Displacement with Supports Under Each Girder .....	142
Figure 9-2. Bridge Cross-Frame Line Displacement with Supports at Ends of Span .....	143
Figure 9-3. Schematic of Non-Staggered vs. Staggered Lean-On Layouts .....	147
Figure 9-4. Buckled Shape of Optimized X Bridge System (Bjelland, 2024) .....	149
Figure 9-5. Relationship Between Stiffness Components Relative to the Ideal Stiffness (Bjelland, 2024) .....	151
Figure 10-1. Brace Forces (Helwig and Wang, 2003) .....	153
Figure 10-2. Z-Frame Single Brace Forces Exterior Bay .....	154

Figure 10-3. Z-Frame Brace Forces Multiple Cross-Frames.....	155
Figure 10-4. Z-Frame Brace Forces Interior Bay .....	155
Figure 10-5. X-Frame Single Brace Forces .....	156
Figure 10-6. X-Frame Generalized Brace Forces .....	156
Figure 10-7. K-Frame Single Brace Forces .....	157
Figure 10-8. K-Frame Generalized Brace Forces .....	157
Figure 12-1. Example 1 Girder Elevation View .....	169
Figure 12-2. Example 1 Cross-Frame Layout.....	172
Figure 12-3. Example 1 CFL 1 Section View.....	172
Figure 12-4. Example 2 Girder Elevation View .....	182
Figure 12-5. Example 2 Cross-Frame Layout.....	184
Figure 12-6. Example 2 CFL 4 Section View.....	185
Figure 12-7. Example 2 Maximum Moment Locations.....	186
Figure A-1. Lubbock Bridge Load Case 1: Staggered Ahead Station.....	202
Figure A-2. Lubbock Bridge Load Case 2: Staggered Behind Station.....	202
Figure A-3. Lubbock Bridge Load Case 3: Side-by-Side South .....	202
Figure A-4. Lubbock Bridge Load Case 4: Side-by-Side North .....	203
Figure A-5. Lubbock Bridge Load Case 5: End-to-End South.....	203
Figure A-6. Lubbock Bridge Load Case 6: End-to-End Central .....	203
Figure D-1. SH 105 Bridge Load Case 1 .....	208
Figure D-2. SH 105 Bridge Load Case 2.....	208

Figure D-3. SH 105 Bridge Load Case 3 .....	208
Figure D-4. SH 105 Bridge Load Case 4 .....	209
Figure D-5. SH 105 Bridge Load Case 5 .....	209
Figure D-6. SH 105 Bridge Load Case 6 .....	209
Figure D-7. SH 105 Bridge Load Case 7 .....	210
Figure D-8. SH 105 Bridge Load Case 8 .....	210
Figure D-9. SH 105 Bridge Load Case 9 .....	210
Figure G-1. Chisholm Trail Bridge Load Case 1 .....	216
Figure G-2. Chisholm Trail Bridge Load Case 2 .....	216
Figure G-3. Chisholm Trail Bridge Load Case 3 .....	216
Figure G-4. Chisholm Trail Bridge Load Case 4 .....	217
Figure G-5. Chisholm Trail Bridge Load Case 5 .....	217
Figure G-6. Chisholm Trail Bridge Load Case 6 .....	217
Figure I-1. Lubbock Bridge Load Case 1 CFL 7 Axial Force [kip] .....	222
Figure I-2. Lubbock Bridge Load Case 1 CFL 3 Axial Force [kip] .....	222
Figure I-3. Lubbock Bridge Load Case 2 CFL 7 Axial Force [kip] .....	223
Figure I-4. Lubbock Bridge Load Case 2 CFL 3 Axial Force [kip] .....	223
Figure I-5. Lubbock Bridge Load Case 3 CFL 7 Axial Force [kip] .....	224
Figure I-6. Lubbock Bridge Load Case 3 CFL 3 Axial Force [kip] .....	224
Figure I-7. Lubbock Bridge Load Case 4 CFL 7 Axial Force [kip] .....	225
Figure I-8. Lubbock Bridge Load Case 4 CFL 3 Axial Force [kip] .....	225

Figure I-9. Lubbock Bridge Load Case 5 CFL 7 Axial Force [kip] .....	226
Figure I-10. Lubbock Bridge Load Case 5 CFL 3 Axial Force [kip] .....	226
Figure I-11. Lubbock Bridge Load Case 6 CFL 7 Axial Force [kip] .....	227
Figure I-12. Lubbock Bridge Load Case 6 CFL 3 Axial Force [kip] .....	227
Figure J-1. SH 105 Bridge Load Case 1 CFL 3 Axial Force [kip] .....	228
Figure J-2. SH 105 Bridge Load Case 1 CFL 5 Axial Force [kip] .....	228
Figure J-3. SH 105 Bridge Load Case 1 CFL 5 Deflections [in].....	228
Figure J-4. SH 105 Bridge Load Case 2 CFL 3 Axial Force [kip] .....	229
Figure J-5. SH 105 Bridge Load Case 2 CFL 5 Axial Force [kip] .....	229
Figure J-6. SH 105 Bridge Load Case 2 CFL 5 Deflections [in].....	229
Figure J-7. SH 105 Bridge Load Case 3 CFL 3 Axial Force [kip] .....	230
Figure J-8. SH 105 Bridge Load Case 3 CFL 5 Axial Force [kip] .....	230
Figure J-9. SH 105 Bridge Load Case 3 CFL 5 Deflections [in].....	230
Figure J-10. SH 105 Bridge Load Case 4 CFL 3 Axial Force [kip] .....	231
Figure J-11. SH 105 Bridge Load Case 4 CFL 5 Axial Force [kip] .....	231
Figure J-12. SH 105 Bridge Load Case 4 CFL 5 Deflections [in].....	231
Figure J-13. SH 105 Bridge Load Case 5 CFL 3 Axial Force [kip] .....	232
Figure J-14. SH 105 Bridge Load Case 5 CFL 5 Axial Force [kip] .....	232
Figure J-15. SH 105 Bridge Load Case 5 CFL 5 Deflections [in].....	232
Figure J-16. SH 105 Bridge Load Case 6 CFL 3 Axial Force [kip] .....	233
Figure J-17. SH 105 Bridge Load Case 6 CFL 5 Axial Force [kip] .....	233

Figure J-18. SH 105 Bridge Load Case 6 CFL 5 Deflections [in].....	233
Figure J-19. SH 105 Bridge Load Case 7 CFL 3 Axial Force [kip] .....	234
Figure J-20. SH 105 Bridge Load Case 7 CFL 5 Axial Force [kip] .....	234
Figure J-21. SH 105 Bridge Load Case 7 CFL 5 Deflections [in].....	234
Figure J-22. SH 105 Bridge Load Case 8 CFL 3 Axial Force [kip] .....	235
Figure J-23. SH 105 Bridge Load Case 8 CFL 5 Axial Force [kip] .....	235
Figure J-24. SH 105 Bridge Load Case 8 CFL 5 Deflections [in].....	235
Figure J-25. SH 105 Bridge Load Case 9 CFL 3 Axial Force [kip] .....	236
Figure J-26. SH 105 Bridge Load Case 9 CFL 5 Axial Force [kip] .....	236
Figure J-27. SH 105 Bridge Load Case 9 CFL 5 Deflections [in].....	236
Figure K-1. Chisholm Trail Bridge Load Case 1 CFL 9 Axial Forces [kip] .....	237
Figure K-2. Chisholm Trail Bridge Load Case 1 CFL 13 Axial Forces [kip] .....	237
Figure K-3. Chisholm Trail Bridge Load Case 1 CFL 15 Axial Forces [kip] .....	237
Figure K-4. Chisholm Trail Bridge Load Case 1 CFL 8 Deflections [in] .....	238
Figure K-5. Chisholm Trail Bridge Load Case 1 CFL 10 Deflections [in] .....	238
Figure K-6. Chisholm Trail Bridge Load Case 2 CFL 9 Axial Forces [kip] .....	239
Figure K-7. Chisholm Trail Bridge Load Case 2 CFL 13 Axial Forces [kip] .....	239
Figure K-8. Chisholm Trail Bridge Load Case 2 CFL 15 Axial Forces [kip] .....	239
Figure K-9. Chisholm Trail Bridge Load Case 2 CFL 8 Deflections [in] .....	240
Figure K-10. Chisholm Trail Bridge Load Case 2 CFL 10 Deflections [in] .....	240
Figure K-11. Chisholm Trail Bridge Load Case 3 CFL 9 Axial Forces [kip] .....	241



Figure K-12. Chisholm Trail Bridge Load Case 3 CFL 13 Axial Forces [kip] .....	241
Figure K-13. Chisholm Trail Bridge Load Case 3 CFL 15 Axial Forces [kip] .....	241
Figure K-14. Chisholm Trail Bridge Load Case 3 CFL 8 Deflections [in] .....	242
Figure K-15. Chisholm Trail Bridge Load Case 3 CFL 10 Deflections [in] .....	242
Figure K-16. Chisholm Trail Bridge Load Case 5 CFL 9 Axial Forces [kip] .....	243
Figure K-17. Chisholm Trail Bridge Load Case 5 CFL 13 Axial Forces [kip] .....	243
Figure K-18. Chisholm Trail Bridge Load Case 5 CFL 15 Axial Forces [kip] .....	243
Figure K-19. Chisholm Trail Bridge Load Case 5 CFL 8 Deflections [in] .....	244
Figure K-20. Chisholm Trail Bridge Load Case 5 CFL 10 Deflections [in] .....	244

## List of Symbols

$A_d$  = cross-sectional area of the cross-frame diagonals

$A_h, A_s$  = cross-sectional area of the cross-frame struts

$b_s$  = width of stiffener

$c$  = distance from the centroid of the compression flange to the neutral bending axis

$C_b$  = moment gradient factor

$C_{bb}$  =  $C_b$  factor corresponding to a beam fully braced at intermediate brace locations

$C_{bu}$  =  $C_b$  factor corresponding to a beam with no intermediate braces

$C_{bs}$  = system mode moment gradient factor

$C_{CF}$  = cross-frame shape coefficient

$C_L$  = lateral top flange loading factor

$C_{LO}$  = lean-on layout factor

$C_T$  = top flange loading modification factor

$C_w$  = torsional warping constant

$E$  = modulus of elasticity

$F$  = unit load applied at the top and bottom of each girder

$F_{br}$  = force applied to bracing line

$F_{d,leanZK}$  = maximum diagonal member force in lean-on cross-frame line with Z- or K-frames

$F_{d,leanX}$  = maximum diagonal member force in lean-on cross-frame line with X-frames

$F_{s,leanZK}$  = maximum top/bottom strut force in lean-on cross-frame line with Z- or K-frames

$F_{d,leanX}$  = maximum top/bottom strut force in lean-on cross-frame line with X-frames

$G$  = shear modulus of elasticity

$h, h_b$  = depth of the cross-frame

$h_0$  = distance between flange centroids

$h_w$  = height of web

$I_{eff}$  = effective moment of inertia of a single girder

$I_x$  = strong-axis moment of inertia of a single girder

$I_y$  = weak-axis moment of inertia of a single girder

$I_{yc}$  = out-of-plane moment of inertia of the compression flange

$I_{yt}$  = out-of-plane moment of inertia of the tension flange

$J$  = torsional constant

$K$  = effective length factor used to account for warping restraint

$L$  = span length

$L_b$  = unbraced length

$L_d$  = length of the cross-frame diagonal members

$M$  = moment applied to the system

$M_{br}$  = moment applied to bracing line

$M_{bp}$  = buckling capacity of the girder when buckling occurs between the brace points

$M_{cr}$  = buckling moment

$M_g$  = elastic global buckling resistance

$M_{g,conventional}$  = global lateral torsional buckling capacity of the conventional system

$M_{g,lean}$  = global lateral torsional buckling capacity of the lean-on system

$M_{gs}$  = modified elastic global buckling resistance

$M_0$  = buckling capacity of a girder with no intermediate bracing

$M_u$  = factored design moment

$M_y$  = yield moment

$N$  = contact length of torsional brace

$n$  = number of discrete intermediate braces

$n_c$  = number of cross-frames in the bracing line

$n_{c,eff}$  = effective number of cross-frames in the bracing line

$n_{CFL}$  = number of cross-frame lines

$n_g$  = number of girders

$n_{g,eff}$  = effective number of girders

$n_{gc}$  = number of girders per cross-frame (Helwig and Wang, 2003)

$n_{lean}$  = maximum number of adjacent lean-on bays

$n_{lean,eff}$  = effective number of adjacent bays without cross-frames

$P_f$  = equivalent elastic buckling capacity of the compression flange

$N$  = contact length of torsional brace

$N_i$  = lateral brace coefficient

$R$  = reduction factor to account for connection eccentricity

$S$  = girder spacing

$t$  = distance from the centroid of the tension flange to the neutral bending axis

$t_s$  = thickness of stiffener

$t_w$  = thickness of web

$\alpha_x$  = system warping stiffness factor

$\bar{\beta}_b$  = continuous torsional brace stiffness

$\beta_{br}$  = brace stiffness

$\beta_{br,lean}$  = lean-on brace stiffness

$\beta_g$  = in-plane girder stiffness

$\beta_{sec}$  = stiffness of the cross section related to cross sectional distortion

$\beta_T$  = total brace stiffness of the torsional system

$\beta_{Ti}$  = ideal stiffness for discrete torsional bracing

$\bar{\beta}_T$  = equivalent effective continuous torsional brace stiffness

$\bar{\beta}_{Ti}$  = ideal stiffness for continuous torsional bracing

$\Delta_{crit}$  = total displacement of the critical girder

$\theta$  = rotation of the girder

$\theta_0$  = initial rotation of the girder

# Chapter 1. Introduction

I-shaped girders are often utilized in steel bridge systems as an efficient and economical solution in a wide range of bridge applications. Steel girders provide significant flexibility for applications in highway bridges because the bridge girders can be fabricated in shorter lengths, shipped to the site, spliced together, and quickly erected. However, the high strength-to-weight ratio of steel often results in relatively slender components that are susceptible to stability-related limit states that must be considered in design. The primary stages for which stability is critical is generally during erection and other construction phases when the steel girders support the entire load, and the bracing conditions can be highly variable. The controlling stability limit state is generally lateral-torsional buckling (LTB) of the bridge girders, which is a failure mode that involves lateral movement of the compression flange and twist of the section, as depicted in Figure 1-1. Once the composite concrete deck has cured, the deck and shear studs provide continuous lateral and torsional restraint to the girder. As a result, conventional LTB is not typically a concern in the completed bridge.

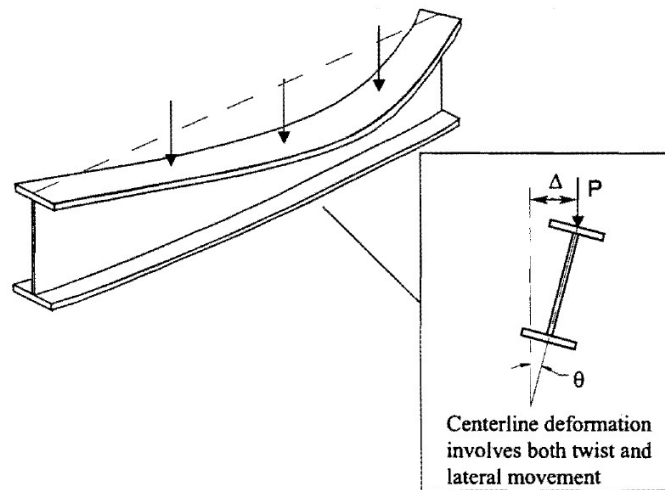


Figure 1-1. Lateral-Torsional Buckling (Helwig and Wang, 2003)

An increase in the LTB capacity is achieved by providing bracing that reduces the unsupported length of the girders. Effective beam bracing can be achieved by either restraining lateral displacement of the compression flange (lateral bracing), or by controlling the twist of the section (torsional bracing). The most common form of bracing used in steel bridges consists of cross-frames or diaphragms that control girder twist and therefore are categorized as torsional point braces. Though the braces are necessary for girder stability, they introduce some complexities into the design and require strategic placement along the length and width of the framing system. These complexities range from difficulties during fabrication and erection to concerns regarding the fatigue performance during the service life of the bridge. Due to the significant handling and fabrication requirements, the braces are often the most expensive component of steel bridges per unit weight. Therefore, it is advantageous to refine the design and detailing of cross-frame systems.

The AASHTO LRFD Bridge Design Specification (BDS) provides design, detailing, and analysis guidance for cross-frames and diaphragms, but this guidance is primarily limited to the fatigue limit state. The 9<sup>th</sup> edition of the AASHTO LRFD BDS (2020) provided no formal guidance on stability bracing requirements of cross-frames and diaphragms. A recent study (Reichenbach *et al.*, 2021) that investigated the stability bracing characteristics of conventional cross-frames in steel I-girder systems resulted in recommendations that will be included in the 10<sup>th</sup> edition of the AASHTO LRFD BDS due out in 2024. However, due to the absence of formal design requirements in all current and previous editions of the AASHTO BDS, the typical practice has been to utilize standard brace details and layouts that are specified by state departments of transportation. Historically, the braces in straight bridges have not generally been sized for stability forces or demands. For example, a common member size in cross-frames specified by many bridge owners is an L4x4x3/8 angle.

For cross-frames in steel bridges, conventional detailing practice is to provide braces between adjacent girders across the full width of the bridge, as shown in Figure 1-2 (A). However, in some applications, such a layout can lead to large live-load induced forces, as well as difficulty installing bracing, particularly in bridges with significant support skew. Instead of providing cross-frames across the full width of the bridge, selectively positioning cross-frames within the bridge cross-section and using top and bottom struts to “lean” other girders on the braced locations, as depicted in Figure 1-2 (B), can provide improved behavior and efficiency. This concept is referred to as lean-on bracing.

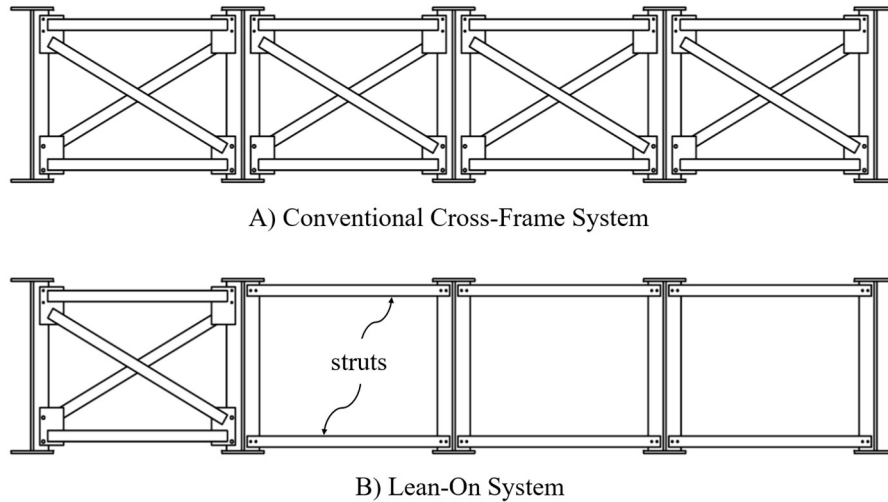


Figure 1-2. (A) Conventional Cross-Frame System and (B) Lean-On System

Lean-on concepts are often employed in steel building frames where column bracing may be located in a bay and provide stability to columns in adjacent bays connected through the beams in the frame. In the early 2000s, lean-on concepts were adapted for implementation into steel I-girder bridges (Helwig and Wang, 2003). Lean-on braces offer a cost-effective solution by combining the versatility of a torsional bracing system with the simplicity of a lateral brace. In these systems, torsional braces (typically in the form of cross-frames) are strategically placed throughout the bridge and provide the primary source of stability to the girders.



As noted previously, the current AASHTO LRFD provides no guidance on the design of cross-frames for stability bracing requirements. The provisions approved for inclusion in the 10<sup>th</sup> edition of AASHTO focus on the stability bracing requirements for conventional bracing. Provisions for lean-on bracing are not included in the 10<sup>th</sup> edition of the AASHTO LRFD BDS; however, there is interest in inclusion of guidance on lean-on concepts for future editions. Based upon the recommendations from TxDOT project 0-1772 (Helwig and Wang, 2003; Romage, 2008) there have been successful applications of lean-on bracing in bridges with both skewed and normal supports, primarily in the state of Texas. Some of the more recent applications have identified aspects of lean-on bracing that would benefit from additional research. Furthermore, there has been an abundance of research conducted over the past few decades with respect to LTB and the bracing characteristics of cross-frames, but the application towards lean-on systems was not considered. Therefore, the present research investigation was conducted to refine the design process and develop improved guidance on design procedures for wider applications of lean-on bracing.

The objective of TxDOT Project 0-7093-1 was to study the behavior of lean-on bracing systems for the development of improved guidance allowing engineers to better implement lean-on bracing into steel bridge designs. If cross-frames are properly detailed and distributed along the bridge length and width, lean-on bracing systems can reduce the number of full cross-frames required while potentially improving the long-term bridge behavior. A well-designed and detailed lean-on bracing system potentially offers significant savings in fabrication costs, simplifies the erection process, and alleviates in-service cross-frame force demands in heavily skewed bridges. In short, the strategic use of lean-on braces can serve as an efficient alternative to traditional cross-frame systems.

The work contained in this dissertation includes research conducted as part of TxDOT Project 0-7093-1 (Helwig *et al.*, 2024) related to the refinement of lean-on brace stiffness and strength equations, field monitoring, and equation-based design methodologies. Additional information particularly related to the refinement of other stiffness components and parametric finite element analysis studies for lean-on layouts can be found in Bjelland (2024) and Fish (2021; 2024).

This dissertation consists of 13 chapters. Following this introductory chapter, a review of the literature and pertinent background information is provided in Chapter 2. While there are multiple components of the total stiffness of a lean-on bracing system, derivations and refinements for the lean-on brace stiffness equation are provided in Chapters 3-5. To accompany the theoretical study, results from the field instrumentation and testing of three bridges with lean-on bracing are provided in Chapter 6. The results from the field monitoring and tests provided valuable data for the validation of FEA models of lean-on bracing systems, which is summarized in Chapter 7. A summary of the parametric study of lean-on bracing layouts is provided in Chapter 8. The focus of Chapter 9 is the implementation of the revised stiffness equations in the calculation of the total system stiffness. The brace strength requirements are then covered in Chapter 10. Finally, Chapter 11 outlines the proposed design methodology for lean-on bracing systems, and detailed equation-based design examples are provided in Chapter 12. An overview of the research contributions is provided in Chapter 13.

## **Chapter 2. Background**

The lateral-torsional buckling (LTB) limit state is a critical consideration in steel I-girder bridges. Although the LTB resistance can be improved by increasing the section properties (by way of adjusting the girder geometries), a more economical approach is often to apply some kind of bracing, typically in the form of cross-frames, or a combination of cross-frames and lateral struts called lean-on bracing to reduce the unbraced length.

This chapter outlines the past research that is most pertinent to the present study. The following sections provide background information on the critical conditions for bridge girder stability, as well as an overview of methods of stability bracing concepts. Solutions for determining the required system stiffness requirement are presented, as well as expressions for the stiffness and strength of bracing systems. Current bracing design provisions are discussed, including lean-on bracing adaptations to these provisions developed by Helwig and Wang (2003).

### **2.1. Bridge Girder Stability**

---

#### **2.1.1. Lateral-Torsional Buckling**

I-shaped girders are often utilized in steel bridge systems as an efficient and economical solution in a wide range of bridge applications. The exceptional strength-to-weight properties of steel provide desirable characteristics for bridge girders. The steel girders can be fabricated in shorter lengths, shipped to the site, spliced together, and quickly erected. However, the same properties can lead to slender elements and systems, which may cause difficulties during erection and other construction phases when the bracing conditions are highly variable. During construction stages, the steel section alone generally supports the full load. Construction stages are generally

critical for lateral-torsional buckling (LTB), a limit state that involves the lateral translation of the compression flange and twist of the section, as depicted in Figure 1-2. Stability of the finished bridge is rarely a concern due to the continuous bracing provided by the cured concrete deck to the composite system. The buckling occurs between bracing locations (unbraced length). Timoshenko (1961) derived the following exact elastic buckling solution for a simply supported, doubly-symmetric section with warping stiffness for the case of uniform moment loading:

$$M_{cr} = \frac{\pi}{L_b} \sqrt{EI_y GJ + \frac{\pi^2 E^2 C_w I_y}{L_b^2}} \quad 2.1$$

Where:

$M_{cr}$  is the buckling moment

$L_b$  is the unbraced length

E is the modulus of elasticity

$I_y$  is the weak-axis moment of inertia of a single girder

G is the shear modulus of elasticity

J is the torsional constant

$C_w$  is the torsional warping constant,  $\frac{I_y h_0^2}{4}$  for a doubly symmetric I-shaped sections

$h_0$  is the distance between flange centroids

In Equation 2.1, the first term under the radical is known as the St. Venant torsional resistance and is related to the uniform torsional stiffness. The second term under the radical is the warping torsional resistance and is related to the non-uniform torsional stiffness. In the original derivation of Equation 2.1, only the boundary condition of zero twist was enforced. Therefore, effective bracing against LTB can be achieved through solely restraining twist of the cross-section.

### 2.1.1.1. AASHTO Moment Gradient Factor

While Equation 2.1 was derived for the case of uniform moment loading, the buckling capacity of a beam with non-uniform moment may be significantly larger. Although solutions can be derived for specific load cases, the benefits of moment gradient in design are typically accounted for by using moment gradient factors ( $C_b$ ). There are a variety of  $C_b$  factors available to approximate the benefits of moment gradient. Expressions for  $C_b$  are provided in AASHTO LRFD (2020) and AISC LRFD (2017). The equation found in AASHTO LRFD Appendix A6 is shown in Equation 2.2.

$$C_{b,AASHTO} = 1.75 - 1.05 \left( \frac{M_1}{M_2} \right) + 0.3 \left( \frac{M_1}{M_2} \right)^2 \leq 2.3 \quad 2.2$$

Where:

$M_1$  is the smaller end moment

$M_2$  is the larger end moment

There are several rules provided in AASHTO for determining the value of  $M_1$  so that the expression can be used for “general” moment diagrams. As there is a great deal of work ongoing to incorporate more accurate  $C_b$  factors, these rules are not included in this dissertation. The AISC expression is one solution that is under consideration for inclusion in AASHTO. However, some work is looking at the impact of mono-symmetry and the effects of non-prismatic sections on the behavior (Reichenbach *et al.*, 2020).

### 2.1.1.2. AISC Moment Gradient Factor

The AASHTO specification in Equation 6.1 is only applicable to straight line moment diagrams, so its use becomes quite complicated when applying it to non-linear moment diagrams. As noted above, AASHTO includes several exceptions to the moments in an attempt to make the

expression applicable for general cases of moment gradient. In contrast, the specification provided in AISC LRFD Chapter F for  $C_b$  is rather straightforward and is independent of the shape of the moment diagram. This is shown as Equation 2.3. Of course, if a designer wishes to simplify the calculation, they may take  $C_b$  equal to 1.0, which is conservative for most cases.

$$C_{b,AISC} = \frac{12.5M_{max}}{2.5M_{max}+3M_A+4M_B+3M_C} \quad 2.3$$

Where:

$M_{max}$  is the absolute value of the maximum moment within the unbraced segment

(Lb)

$M_A$  is the absolute value of the moment at the quarter point of the unbraced segment

$M_B$  is the absolute value of the moment at the centerline of the unbraced segment

$M_C$  is the absolute value of the moment at the three-quarter point of the unbraced segment

### 2.1.2. System (Global) Lateral-Torsional Buckling

The system, or global, form of LTB has been investigated since the early 2000s. The studies in this area stemmed from issues encountered during the construction of a number of bridges. System LTB occurs when the girder system is interlinked by braces, such as cross-frames, and the overall system buckles as a unit. This mode often becomes more critical than conventional LTB (buckling between brace points) in narrow girder systems with larger span-to-width ratios. Yura et al. (2008) developed an expression for the elastic global buckling resistance of a doubly-symmetric twin I-girder system, which is shown in Equation 2.4:

$$M_g = \frac{\pi^2 SE}{L^2} \sqrt{I_y I_x} \quad 2.4$$

Where:

$M_g$  is the elastic global buckling resistance

$S$  is the girder spacing

$L$  is the span length

$I_x$  is the strong-axis moment of inertia of a single girder

This expression assumes a simply supported, prismatic system. Although Yura et al. (2008) included a slightly more complex solution which included both St. Venant and warping terms, the St. Venant term does not significantly impact the behavior. Neglecting this term produces the simple expression shown in Equation 2.4. Although the solution was derived for doubly-symmetric sections, when considering singly-symmetric sections,  $I_y$  in Equation 2.4 can be replaced with  $I_{eff}$  as defined by Equation 2.5 (Yura *et al.*, 2008):

$$I_{eff} = I_{yc} + \frac{t}{c} I_{yt} \quad 2.5$$

Where:

$I_{yc}$  is the lateral moment of inertia of the compression flange

$I_{yt}$  is the lateral moment of inertia of the tension flange

$t$  is the distance from the centroid of the tension flange to the neutral bending axis

$c$  is the distance from the centroid of the compression flange to the neutral bending axis

Equation 2.4 was originally introduced into the interim AASHTO specifications in 2015. An upper limit of 50% of the value given by Equation 2.4 was adopted into AASHTO (Sanchez

and White, 2012). For cases with moments exceeding 50% of  $M_g$ , changes in the girder sections or additional bracing were necessary. Subsequently, bridge owners found systems that had previously been constructed with no problems could not be constructed with the new provisions. Therefore, additional work was conducted by Han and Helwig (2016, 2020) considering the effects of girder continuity, imperfections and non-prismatic sections. Their work led to the following expression:

$$M_{gs} = C_{bs}M_g = C_{bs} \frac{\pi^2 SE}{L^2} \sqrt{I_{eff} I_x} \quad 2.6$$

Where:

$M_{gs}$  is the modified elastic global buckling resistance

$C_{bs}$  is the system mode moment gradient factor:

1.0 for simply supported or partially erected continuous girder systems

2.0 for fully erected continuous girder systems

To address the effects of imperfection, Han and Helwig suggest limiting the design moment ( $M_u$ ) to 70% of  $M_{gs}$ , which is the current limit in AASHTO LRFD (2020). Though the limit of 70% constituted an increase from the previous value of 50%, the increase was warranted because many bridge owners found that the original 50% reduction was perceived to be overly-conservative based upon field observations of previously constructed systems. The increase was justified in Han and Helwig (2016, 2020) based upon the assumed critical imperfection in comparison to the more likely value in erected girder systems with cross-frames fully installed. The critical shape is often assumed to include a lateral sweep of the compression flange with no sweep in the tension flange; however, such an imperfection would not generally be likely with cross-frames installed. The more



probable imperfection of a girder system with cross-frames installed consists of a “pure sweep” imperfection, which is much less sensitive to second-order amplification.

An update was proposed to the global buckling moment capacity by Fish et al. (2024). The updated expression is shown in Equation 2.7.

$$M_{gs,2024} = C_{bs} \frac{\pi^4 SE}{(KL)^2} \sqrt{I_{eff} I_x \frac{\alpha_x}{2n_g}} \quad 2.7$$

Where:

$K$  is an effective length factor used to account for warping restraint added by modifications to the bridge system such as lateral trusses

$\alpha_x$  is the system warping stiffness factor shown in Table 2-1

Table 2-1. System Warping Stiffness Factor Values

Number of Girders	System Warping Stiffness Factor
2	1
3	4
4	10
5	20
6	35
7	56
8	84
9	120
10	165

## 2.2. Stability Bracing

---

Now that the limit states for girder and system stability have been outlined, the following sections will discuss methods of improving system performance against LTB. These bracing types include lateral bracing, torsional bracing, and lean-on bracing.

### 2.2.1. Torsional Bracing

Torsional bracing directly restrains the rotation of the girder section in order to resist LTB. Torsional bracing systems include cross-frames, diaphragms, and composite concrete decks because they prevent twist of the girders (Yura, 2001). The most common form of bracing in steel bridge applications is the use of torsional braces consisting of cross-frames or diaphragms to ensure adequate LTB resistance. Cross-frames can be found in the form of X-shapes, Z-shapes, and K-shapes, as shown in Figure 2-1. X-type braces work well with deep girders, such as in built-up I-girder bridges, while K-type braces or diaphragms may be better suited for shallower girders. It is recommended that the angle of the diagonals is configured with a slope close to a 45-degree angle with the bottom strut. Significantly flatter or steeper slopes often reduce the effectiveness of the brace.

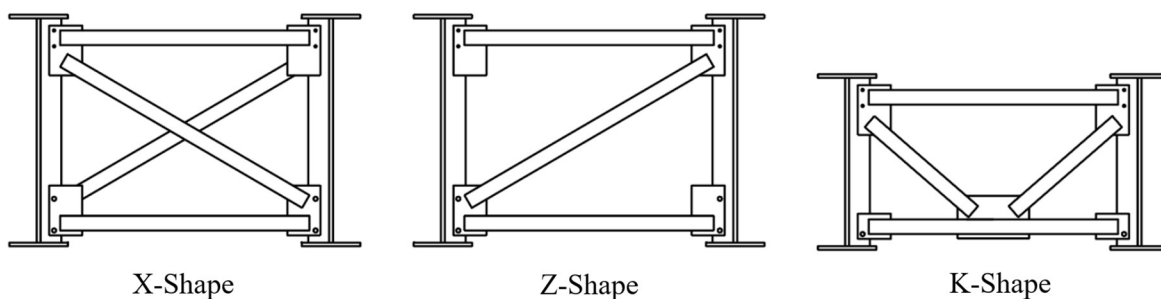


Figure 2-1. Various Forms of Cross-Frames

### **2.2.2. Lateral Bracing**

While torsional bracing directly restrains the rotation of the girder section, lateral bracing restrains translation of the compression flange of the girder in order to prevent rotation. Bracing against LTB can be achieved by restraining the lateral deformation of the compression flange of the bridge girder. This essentially prevents twist of the section, as the lateral deformation of the compression element generally leads to twist of the section. Methods of lateral bracing include continuous bracing, such as metal deck forms, as well as discrete braces, such as top and bottom struts. The lateral braces are most effective when placed where it best offsets the twist (Yura, 2001).

### **2.2.3. Lean-On Bracing**

Lean-on bracing is a method utilizing strategically placed torsional braces in combination with in-line lateral struts to stabilize bridge girders. This allows one or a few cross-frames to effectively brace the whole system due to the struts used to “lean” the girders off of each other. An example comparison of a bridge cross-section with lean-on bracing compared to conventional bracing was shown in Figure 1-2. The schematic demonstrated the lean-on concept of selectively replacing cross-frames in a given bracing line with top and bottom struts to provide a load path to support the girders with fewer cross-frames.

Lean-on bracing was introduced in the early 2000s as a way to address fatigue concerns in high-skew bridges (Helwig and Wang, 2003). The lean-on bracing system was first suggested for skewed bridges to help minimize the magnitudes of live load-induced forces, and was shown by Bechtel (2016) to decrease axial stresses in cross-frame members. Additionally, the reduction in the number of cross-frames can result in a significant reduction in material and fabrication costs, as these are typically the most expensive components per unit weight on steel bridges due to

complexities in fabrication and erection. Utilization of fewer cross-frames also generally corresponds to fewer complex details that must be inspected on routine bridge inspections, resulting in reduced inspection time, cost, and effort. The lean-on bracing applied in TxDOT Implementation Study 5-1772 is depicted in Figure 2-2.



Figure 2-2. Lean-on Bracing in Lubbock, Texas Implementation Study (TxDOT Project 5-1772)

As shown in the figure, torsional braces (i.e., cross-frames) provide the primary source of stability for the girders across the width of the bridge. In general terms, the top and bottom struts in the adjacent bays of a continuous bracing line effectively “lean” on the full torsional braces to stabilize these neighboring bridge girders. The top and bottom struts are then tasked with transferring the forces developed in the adjacent girders. This is analogous to the shear force that stabilizing columns in a frame must resist when adjacent columns lean on it for stability. Thus, the full cross-frames in a bracing line are subjected to increased demands for both stiffness and strength requirements to adequately stabilize more than two girders across the bridge width, as described in the next section.

Although lean-on concepts were initially proposed for systems with significant support skew, the approach can also be used for girder systems with normal supports. A typical bracing layout utilizing lean-on concepts is shown in Figure 2-3 and Figure 2-4 for a straight, three-span continuous bridge with normal supports. In skewed bridges, it has been shown to be advantageous to place the first cross-frame transversely in a given bracing line so as to position the brace as far from the support as possible (Romage, 2008). In these systems, cross-frames near the supports should be placed near the exterior girders that correspond to the acute angle of the skewed support. To maximize the in-plane stiffness of the girder system, the braces should be spread out across the full bridge width to fully engage the girder system. Near midspan, the use of a line of cross-frames across the full width of the system helps to engage all the girders for this purpose.

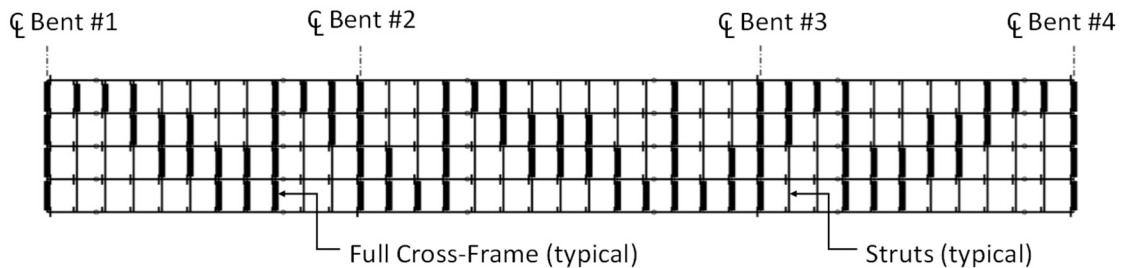


Figure 2-3. Typical Lean-On Bracing Layout

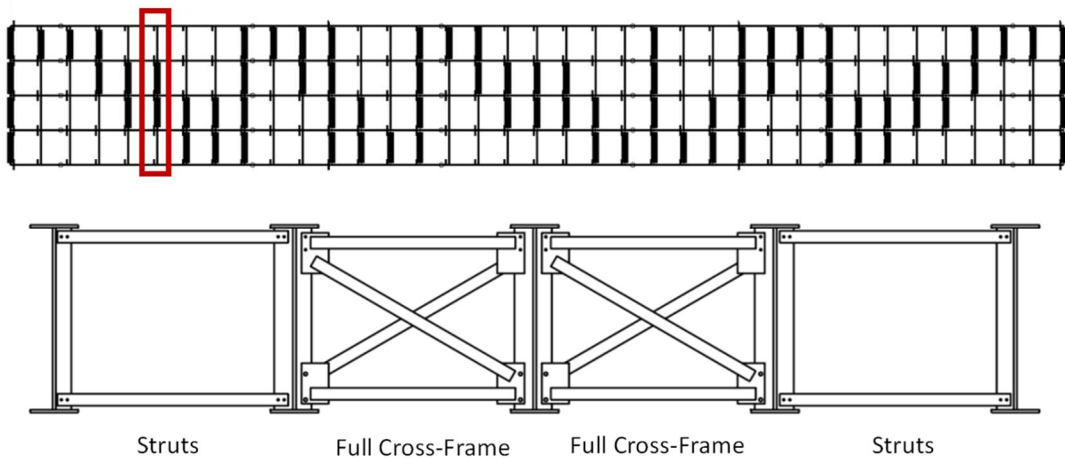


Figure 2-4. Lean-On Bracing Detailed Layout

Some research has investigated the use of “staggered” cross-frame placements in skewed bridges (Kamath, 2019). Such applications illustrate the benefit of strategic cross-frame placement within the bracing system, but do not include top and bottom lean-on struts to complete a full cross-frame line.

## **2.3. Torsional Bracing Stiffness Requirement**

---

Bracing systems are important structural elements in steel I-girder bridges. These systems provide resistance to lateral-torsional buckling (LTB) in straight girder systems by reducing the unbraced length of the girders. Although construction of the bridge deck is usually the most critical stage, the condition during erection may also be critical. During this time, not all of the bracing may be installed, leading to larger unbraced lengths as compared to the condition during deck construction. In both cases, the non-composite steel girders must resist all construction loading. Torsional braces, typically cross-frames, assist the girders in resisting torsion due to the eccentric loading of deck overhang construction and distribute any lateral loads across the structure. This section provides background information on the general bracing requirements of I-girder bracing systems.

### **2.3.1. Brace Stiffness Requirement**

Taylor and Ojalvo (1966) quantified the buckling capacity of a doubly-symmetric beam with continuous torsional bracing under uniform moment loading:

$$M_{cr} = \sqrt{M_0^2 + \bar{\beta}_b EI_y} \quad 2.8$$

Where:

$M_0$  is the buckling capacity of the unbraced beam (equivalent to  $M_{cr}$  in Equation 2.1)

$\bar{\beta}_b$  is the continuous torsional brace stiffness

Further research by Yura (1992, 2001) expanded the applicability of this equation to consider discrete torsional braces, moment gradient, load position, singly-symmetric sections, and the impact of cross-sectional distortion:

$$M_{cr} = \sqrt{C_{bu}^2 M_0^2 + \frac{C_{bb}^2}{C_T} \bar{\beta}_T E I_{eff}} \leq M_y \text{ or } M_{bp} \quad 2.9$$

Where:

$C_{bu}$  is the  $C_b$  factor corresponding to a beam with no intermediate braces

$C_{bb}$  is the  $C_b$  factor corresponding to a beam fully braced at intermediate brace locations

$C_T$  is the top flange loading modification factor:

1.0 for centroidal loading

1.2 for top flange loading

$\bar{\beta}_T$  is the equivalent effective continuous torsional brace stiffness =  $\beta_T \times \frac{n}{L}$

$\beta_T$  is the torsional stiffness provided by a single brace

$n$  is the number of intermediate braces

$L$  is the span length

$M_y$  is the yield moment (this can be replaced by the plastic moment capacity)

$M_{bp}$  is the buckling capacity of the girder when buckling occurs between the brace points

### 2.3.2. Ideal Stiffness

The ideal stiffness corresponds to the stiffness of the braces required to force the girders to buckle between the brace points, avoiding a system mode of buckling. In Figure 2-5, cases where the provided brace stiffness is less than the ideal stiffness (A) and greater than the ideal stiffness (B) are shown. The buckling mode shown in B, buckling between the brace points, results in a greater capacity of the system for equivalent girder geometries.

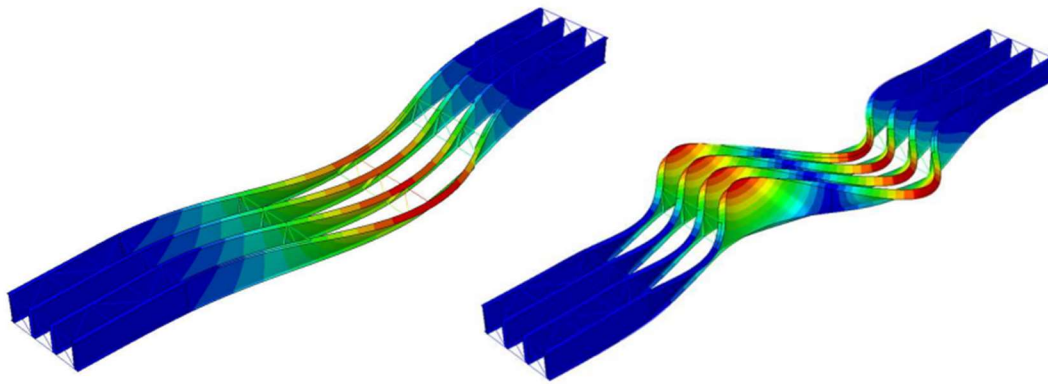


Figure 2-5. (A) Brace Stiffness Less than Ideal Stiffness and (B) Brace Stiffness Greater than Ideal Stiffness

The importance of sufficient brace stiffness was first demonstrated by Winter (1960). Winter utilized a model consisting of a column and lateral bracing system which was comprised of perfectly straight rigid links that were hinged at the points of bracing. The lateral bracing was represented as a spring with stiffness measured in units of force per unit displacement. Winter's model provided a simple means of determining the "ideal brace stiffness," which can be defined as the minimum required brace stiffness to force a perfectly straight member to buckle between its



braced locations. The ideal brace stiffness can be obtained by rearranging Equation 2.9 as shown in Equation 2.10.

$$\bar{\beta}_{Ti} = (M_{cr}^2 - C_{bu}^2 M_0^2) \frac{C_T}{C_{bb}^2 E I_{eff}} \quad 2.10$$

Adjusting for discrete torsional bracing, the ideal stiffness can now be written in terms of the continuous torsional bracing stiffness as shown in Equation 2.11

$$\beta_{Ti} = \frac{\bar{\beta}_{Ti} L}{n} \quad 2.11$$

In the bracing provisions of Appendix 6 AISC (2017), the buckling capacity of the unbraced beam ( $M_0$ ) is conservatively neglected. Taking this into account and substituting Equation 2.10 into Equation 2.11 results in Equation 2.12 for the ideal stiffness of a discrete torsional brace.

$$\beta_{Ti} = \frac{C_T L M_{cr}^2}{n E I_{eff} C_b^2} \quad 2.12$$

### 2.3.3. Initial Imperfection

Another benefit of Winter's model was that the effects of imperfection could be readily investigated. Winter's work demonstrated that when accounting for imperfections, the stiffness required to control brace forces and member deformations was higher than that of the ideal stiffness. Yura (2001) studied the effect of initial imperfection on braced columns, finding that two times the ideal stiffness was sufficient to restrain the initial imperfection, as shown in Figure 2-6. As a result, most bracing provisions currently recommend using two times the ideal stiffness. The assumption is that if twice the ideal stiffness is used, then deformations will be limited to the initial

imperfection imposed. Limiting the initial imperfection is important because the forces within the brace are directly related to its magnitude (Yura, 2001). Although Winter and Yura’s work focused on lateral bracing systems, the dual criteria of stiffness and strength are valid for all stability bracing systems, including torsional beam bracing.

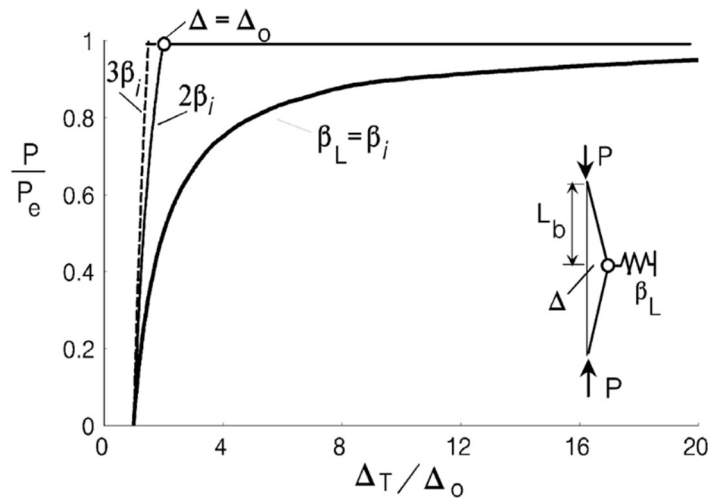


Figure 2-6. Braced Winter Column with Initial Out-of-Straightness (Yura, 2001)

The imperfection that produces the largest brace force, generally, will have one less “wave” than the unbraced section’s buckled shape. For example, with one intermediate brace, the critical imperfection would be a half-sine curve, for two intermediate braces the critical imperfection would be a sine curve, etc. (Helwig and Wang, 2003).

The initial imperfection assumed in the development of the current AISC design provision expressions is an assumption based on allowable fabrication and construction tolerances for girder out-of-straightness, as established by the AISC Code of Standard Practice (2017). The effect of initial imperfection on torsional bracing was studied by Wang and Helwig (2005). They demonstrated that in bridge girders the critical imperfection (i.e., the imperfection that maximizes force demands on the braces) usually involves a lateral sweep of the compression flange, with the

tension flange remaining straight (not displaced laterally). This effectively produces an initial twist of the cross-section. As a result of that research, the initial out of straightness of the compression flange is assumed to be  $\frac{L_b}{500}$ . The current assumed value for initial imperfection (twist), as defined in AISC (2017), is:

$$\theta_0 = \frac{L_b}{500h_0} \quad 2.13$$

Where:

$L_b$  is the unbraced length of the girder section

Finally, assuming top flange loading ( $C_T = 1.2$ ) and adjusting for twice the ideal stiffness by setting the buckling capacity ( $M_{cr}$ ) equal to the factored design moment ( $M_u$ ) results in the expression for required brace stiffness as shown in AISC (2017):

$$\beta_{T\ reqrd} = \frac{2.4LM_u^2}{\phi nEI_{eff}C_b^2} \quad 2.14$$

Where:

$\phi$  is 0.75 (LRFD)

Assuming that the brace stiffness is sufficient to limit the deformation to the initial twist, the relationship between the brace stiffness and brace moment can be described thus:

$$M_{br} = \beta_{T\ reqrd}\theta_0 = \frac{2.4LM_u^2}{\phi nEI_{eff}C_b^2} \frac{L_b}{500h_0} \quad 2.15$$

The use of twice the ideal stiffness works well for columns, but for beams stabilized by torsional braces, recent work by Liu and Helwig (2020) found that a higher stiffness was required to limit the deformation to that of the initial imperfection. The recommendation of their research

was to increase the stiffness requirement for torsional bracing to three times the ideal stiffness. The 2022 AISC Specification increased the required torsional brace stiffness to three times  $\beta_{ideal}$ , resulting in a constant of 3.6 instead of 2.4. The AASHTO bracing provisions permit two times  $\beta_{ideal}$  (resulting in expressions identical to Equations 2.14 and 2.15) provided the depth of the torsional brace is at least 80% of the beam depth.

Expressions based upon a moment equal to the stiffness times the initial imperfection such as that shown in Equation 2.15 are similar to past editions of AISC. In the 2017 AISC Specification, strength provisions for  $M_{br}$  were changed to two percent of the beam design moment based off of work by Prado (2015). However, this approach was recently found to be unconservative in many cases (Liu and Helwig, 2020). Therefore, the 2022 AISC strength provisions returned to a required torsional brace strength equal to the stiffness times the initial imperfection, similar to what was shown in Equation 2.15.

To summarize, the current 2022 AISC brace provisions require a stiffness equal to three times beta ideal (constant of 3.6 instead of 2.4 in Equation 2.13) and a strength requirement equal to the stiffness times the assumed initial imperfection ( $L_b/500h_0$ ). The 10<sup>th</sup> edition AASHTO bracing provisions for required strength and stiffness are identical to the AISC specification for torsional brace depths less than 80% of the beam web depth. Provided a brace depth of at least 80% of the beam depth is utilized, the 10<sup>th</sup> Ed. AASHTO bracing provisions require a stiffness of twice the ideal stiffness (constant of 2.4 in stiffness equation) and a strength equal to the stiffness times the assumed initial imperfection.

## 2.4. Lateral Bracing Stiffness Requirement

---

Much like torsional and lean-on braces, lateral braces must possess adequate strength and stiffness to provide a suitable brace point for a beam or girder. It is important to note that discrete lateral bracing is most effective when placed as close to the compression flange as possible, keeping in mind that in reverse-curvature bending, lateral bracing must be attached to both flanges. Largely based on the work of Winter (1960) that investigated column buckling, Yura (1992, 2001) developed a simple design approach to estimate these stiffness and strength requirements. As such, the required stiffness of a lateral beam brace is estimated using Equation 2.16, where  $P_f C_b$  can be approximated by  $\frac{M_f}{h_o}$  (AISC, 2022):

$$\beta_L^* = \frac{2N_i P_f C_b C_L C_d}{L_b} \text{ or } \frac{2N_i M_f C_L C_d}{h_o L_b} \quad 2.16$$

Where:

$N_i$  is  $4 - \frac{2}{n}$  or a coefficient depending on the number of braces within the span as provided in Table 2-2

$P_f$  is the equivalent elastic buckling capacity of the compression flange =  $\frac{\pi^2 E I_{yc}}{L_b^2}$

$C_L$  is the top flange factor, as defined in Equation 2.17

It was recognized that the required brace stiffness was a function of the number of intermediate braces provided along the length of the beam. Yura (1992, 2001) developed an accurate approximation of these effects (i.e., a definition for  $N_i$ ), which is given in Table 2-2. It is important to note that this equation is analogous to the ideal stiffness formulation developed for the lateral bracing of columns (Winter, 1960). In general, an increase in the number of braces results in an increase of the ideal brace stiffness.

Table 2-2. Brace Coefficient used in Equation 2.16

Number of Evenly Spaced Braces	Exact Value of $N_i$	Approximate Value of $N_i = 4 - \frac{2}{n}$
1	2	2
2	3	3
3	3.41	3.33
4	3.63	3.5
Many	4	4

Helwig et al. (1997) found that if certain circumstances mitigate the effects of load height (i.e., tipping restraint or benefits of intermediate bracing), then a flange loading modification of 1.0 may be used as in the case of centroidal or uniform moment loading. However, for top flange loading without mitigating factors,  $C_L$  is given as Equation 2.17 (Yura, 1992), and alternatively may be conservatively assumed to be 2.0 (AISC, 2022).

$$C_L = 1 + \frac{1.2}{n} \quad 2.17$$

## 2.5. Conventional Torsional Bracing System Stiffness

---

There are three stiffness components of a bracing system that generally contribute to the overall torsional bracing behavior: the brace stiffness, in-plane girder stiffness, and cross-section distortional stiffness. The overall stiffness of a torsional bracing system must be greater than the required stiffness and is given by the equation (Yura, 1992):

$$\frac{1}{\beta_T} = \frac{1}{\beta_{br}} + \frac{1}{\beta_g} + \frac{1}{\beta_{sec}} \quad 2.18$$

Where:

$\beta_T$  is the total brace stiffness of the torsional system

$\beta_{br}$  is the stiffness of the brace

$\beta_g$  is the in-plane girder stiffness

$\beta_{sec}$  is the stiffness of the cross section related to cross sectional distortion

Equation 2.18 indicates that  $\beta_T$  is less than the smallest of the three individual stiffness components, which are assumed to interact as springs in series. From this relationship, it is evident that an otherwise stiff cross-frame can be adversely affected by poor in-plane girder stiffness or significant distortional effects in the girder webs. Thus, the overall stiffness of a torsional brace is effectively limited by the most flexible component in Equation 2.18.

In design, the required torsional brace stiffness,  $\beta_{T req'd}$ , is found by using Equation 2.14. To serve as an adequate brace, the cross-frame and its connections shall be designed and detailed such that  $\beta_T$  exceeds  $\beta_{T req'd}$ . Satisfying this requirement, in addition to the corresponding strength requirements, ensures that a cross-frame or diaphragm can act as a suitable brace point and, in turn, enhance the LTB resistance of the girder.

### **2.5.1. In-Plane Girder Stiffness, $\beta_g$**

The in-plane (i.e., vertical) flexural stiffness of the bridge girders themselves contribute to the overall stiffness of the torsional bracing system. The stiffness contribution of the girders was first shown in twin-girder systems (Helwig, Yura and Frank, 1993). As shown in Figure 2-7, when the girders are subjected to a twist, the internal moment in the cross-frame is equilibrated by vertical shear forces acting at the ends of the brace. The vertical forces on the adjacent girders cause one girder to deflect upwards and the other to deflect downwards leading to a rigid body rotation. These deformations reduce the effectiveness of the brace. With a wider system, this displacement is reduced, as demonstrated by the four-girder system shown in the figure.

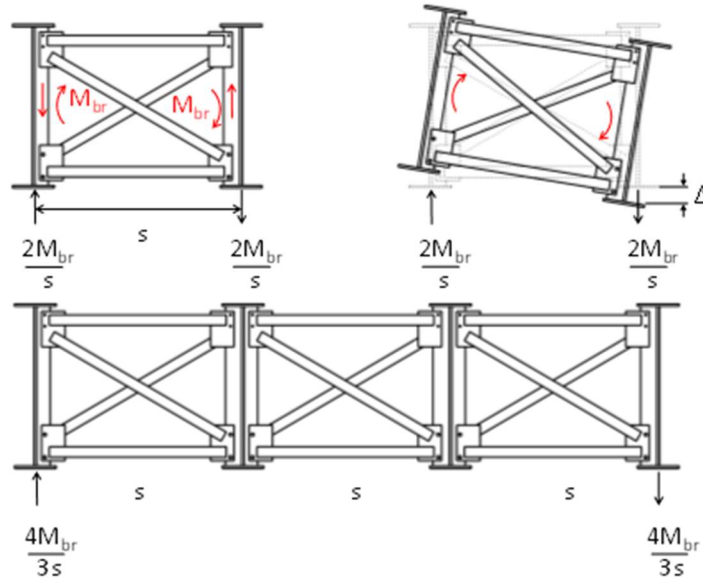


Figure 2-7. In-Plane Girder Stiffness

This behavior was quantified for a twin-girder system in Equation 2.19 (Helwig, Yura and Frank, 1993):

$$\beta_g = \frac{12S^2EI_x}{L^3} \quad 2.19$$

Where:

$I_x$  is the in-plane moment of inertia of the girder

For a framing system with more than two girders, Equation 2.20 is instead used (Yura, 2001; Helwig and Yura, 2015):

$$\beta_g = \frac{24(n_g-1)^2s^2EI_x}{n_gL^3} \quad 2.20$$

Where:

$n_g$  is the number of girders in the system



The in-plane girder stiffness contribution is most critical in narrow systems, such as two or three-girder bridges, and is tied to the system buckling mode, which was discussed in Section 2.1.2 (Yura *et al.*, 2008; Han and Helwig, 2016). If  $\beta_g$  is less than  $\beta_{Treq}$ , full bracing cannot be achieved regardless of the stiffness of the brace that is utilized. From a buckling perspective, the system mode will control over buckling between the brace points. As noted previously, design guidance for the system failure mode has been incorporated into AASHTO LRFD (2020). However, it is not currently included in AISC (2017) because narrow systems are not frequently found in building applications, such that this stiffness component is comparatively large relative to the other components identified in Equation 2.18. Consequently, the failure mode is not likely to govern bracing design applications in buildings, except in cases such as walkways or other narrow girder systems that mimic highway bridge applications.

Due to limitations related to quantifying the stiffness contribution of multiple girders and unconservative results produced with Equation 2.20, an update was proposed to the in-plane girder stiffness by Fish (2021). A final version was released by Fish *et al.* (2024) alongside an update to the global buckling moment capacity. The updated expression is shown in Equation 2.21, using the same variable definitions as in Equation 2.7.

$$\beta_{g,2024} = C_{bs}^2 \frac{\pi^4 E I_x S^2}{2n_g (KL)^3 (n_{CFL} + 1)} \alpha_x \quad 2.21$$

### 2.5.2. Torsional Brace Stiffness, $\beta_{br}$

The torsional brace stiffness, or the stiffness response of the brace when subjected to an in-plane moment, provides additional stiffness to the bridge girder system to help resist LTB. Without torsional brace stiffness, bridge girders will deform in a “racking” shape, as shown in Figure 2-8.

The torsional stiffness of the brace can be estimated based on an idealized truss model (Yura 2001; Helwig and Wang 2003). Equations have been derived for each brace type and the derivation process is discussed in the following sections.

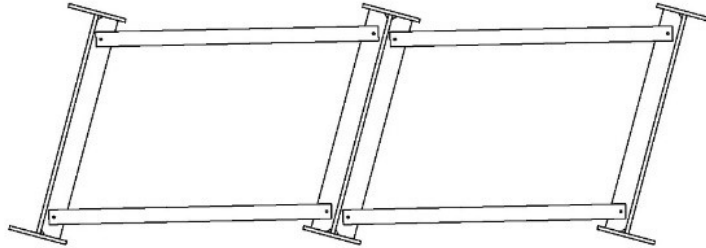


Figure 2-8. Girder Deformation with Zero Brace Stiffness

### 2.5.2.1. Twin Girder System Derivation for Tension Model

Yura (2001) developed an equation to estimate the torsional brace stiffness of a Z-type cross-frame, or a tension-only X-type cross-frame, for which the compression diagonal is conservatively neglected (assuming that member might buckle). In many cases, cross-frames are constructed with slender angle sections whose compression load-carrying capacity is relatively small and therefore neglected. Virtual work was used to derive the expression. The idealization of this system is shown in Figure 2-9.

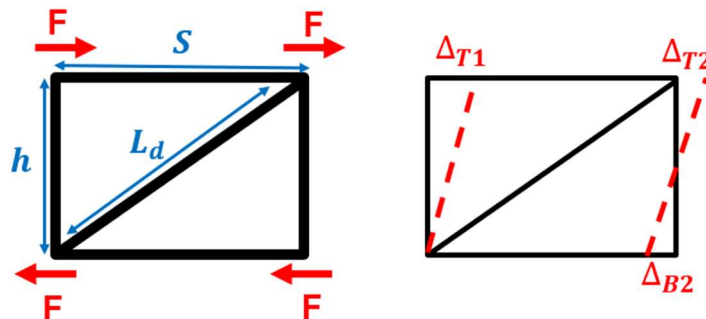


Figure 2-9. Twin Girder Tension Model Brace Stiffness Idealization

In this approach, Equations 2.22 and 2.23 are combined to result in Equation 2.24, indicating that the displacement of the critical girder is the basis for calculating the provided stiffness.

$$M = Fh \quad 2.22$$

$$\beta_{br} = \frac{M}{\theta} \quad 2.23$$

$$\beta_{br} = \frac{Fh^2}{\Delta_{crit}} \quad 2.24$$

Where:

$M$  is the moment applied to the system

$F$  is a unit load applied at the top and bottom of each girder in the directions shown

$h$  is the depth of the cross-frame

$\theta$  is the rotation of the girder

$\Delta_{crit}$  is the critical displacement of the girder (here,  $\Delta_{T2} + \Delta_{B2}$ ).

From the virtual work procedure,  $\Delta_{crit}$  is calculated, resulting in Equation 2.25 for  $\beta_{br}$ . This is the equation currently accepted for typical Z-frame bracing or a conservative X-frame design.

$$\beta_{br} = \frac{h^2 S^2 E}{\frac{2L_d^3}{A_d} + \frac{S^3}{A_s}} \quad 2.25$$

Where:

$L_d$  is the length of the line of action of the cross-frame diagonal members

$A_d$  is the cross-sectional area of the cross-frame diagonals

$A_h$  is the cross-sectional area of the cross-frame struts.

When all the cross-frame members are of equal size ( $A_d = A_h$ ), Equation 2.25 may be rewritten as shown in Equation 2.26.

$$\beta_{br} = \frac{A_d h^2 S^2 E}{2L_d^3 + S^3} \quad 2.26$$

### 2.5.2.2. Twin Girder System Derivation for Compression Model

Yura (2001) also derived a compression system stiffness model. In this model, the top and bottom struts of the cross-frame are not required, as shown in Figure 2-10. As in the tension model derivation,  $\Delta_{crit}$  is calculated from the virtual work procedure, resulting in Equation 2.27 for  $\beta_{br}$ .

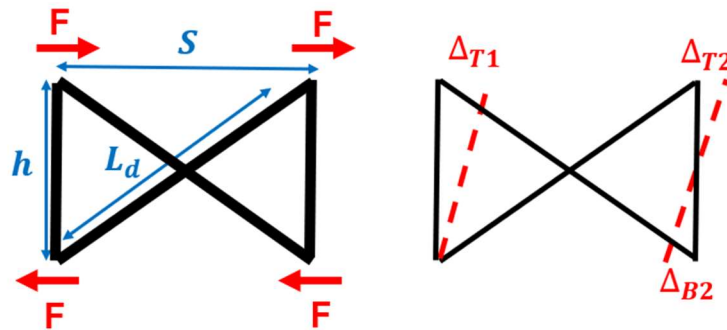


Figure 2-10. Twin Girder Compression Model Brace Stiffness Idealization

$$\beta_{br} = \frac{A_d h^2 S^2 E}{L_d^3} \quad 2.27$$

### 2.5.2.3. Twin Girder System Derivation for K-Frames

Yura (2001) additionally derived a stiffness equation for K-frames. In the K-frame system, the diagonals are designed for both tension and compression. As discussed previously, a virtual work method was applied to a system idealized as shown in Figure 2-11. The resulting stiffness equation is given by Equation 2.28.

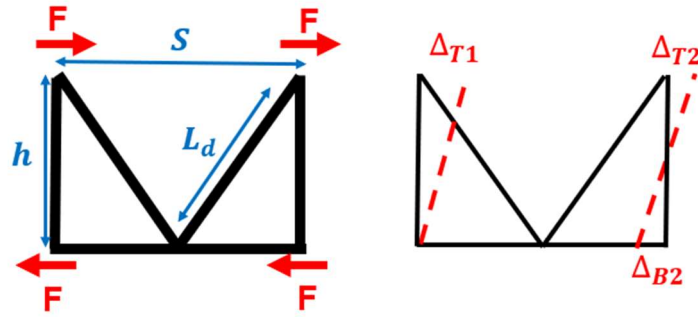


Figure 2-11. Twin Girder K-Frame Brace Stiffness Idealization

$$\beta_{br} = \frac{h^2 S^2 E}{\frac{2L_d^3 + S^3}{A_d} + A_s} \quad 2.28$$

### 2.5.3. Cross-Section Stiffness, $\beta_{sec}$

If the braces are shallow compared to the rest of the girder, the stiffness of the cross-section,  $\beta_{sec}$ , may have a significant effect. For full-depth web stiffeners, Yura derived the following equation (1992, 2001):

$$\beta_{sec} = \frac{3.3E}{h_0} \left( \frac{(N+1.5h_0)t_w^3}{12} + \frac{t_s b_s^3}{12} \right) \quad 2.29$$

Where:

$N$  is the contact length of the torsional brace

$h_w$  is the height of the web

$t_w$  is the thickness of the web

$t_s$  is the thickness of the stiffener

$b_s$  is the width of the stiffener

Since many bracing systems may not have “contact length,”  $N$ , Equation 2.29 may be rewritten as Equation 2.30 (Helwig and Yura, 2015). This form is included in AISC Appendix 6:

$$\beta_{sec} = \frac{3.3E}{h_0} \left( \frac{(1.5h_0)t_w^3}{12} + \frac{t_s b_s^3}{12} \right) \quad 2.30$$

The first term in the equation accounts for the effective moment of inertia for the part of the web assumed to participate in the distortion, and the second term accounts for the moment of inertia of the stiffener, taken about the centroid of the web. When the distance from the top cross-frame to the top of the girder is different than the distance from the bottom of the cross-frame to the bottom of the girder, then the below equations may be used to estimate  $\beta_{sec}$  (Yura, 2001):

$$\beta_{sec} = \frac{1}{\frac{1}{\beta_{top}} + \frac{1}{\beta_{bot}}} \quad 2.31$$

$$\beta_{top} = \frac{3.3E}{h_0} \left( \frac{h_0}{h_{top}} \right)^2 \left( \frac{1.5h_{top}t_w^3}{12} + \frac{t_s b_s^3}{12} \right) \quad 2.32$$

$$\beta_{bot} = \frac{3.3E}{h_0} \left( \frac{h_0}{h_{bot}} \right)^2 \left( \frac{1.5h_{bot}t_w^3}{12} + \frac{t_s b_s^3}{12} \right) \quad 2.33$$

Only the region outside of the brace depth contributes to the cross-sectional distortion. Because most cross-frames in bridge I-girder applications are relatively deep with respect to the girder depth, the cross-section stiffness component tends to be a large value, such that it is not usually a significant concern in Equation 2.18. Language in the 10<sup>th</sup> Edition of AASHTO (2024) for stability bracing will allow  $\beta_{sec}$  to be taken as infinity for braces deeper than 80% of the web depth. This provision recognizes the minimal impact of cross-sectional braces for relatively deep braces since the portion of the web above and below the brace is relatively small and doesn't distort significantly.

## 2.6. Lean-On Torsional Bracing System Stiffness

---

### 2.6.1. In-Plane Girder Stiffness, $\beta_g$

Helwig and Wang (2003) recommended the reduction of the in-plane girder stiffness by 50% when utilizing lean-on bracing as compared a system only utilizing traditional torsional bracing concepts, as expressed in Equation 2.19. It is assumed that a lean-on system would have an in-plane girder stiffness between that of a twin-girder system and of a traditional cross-frame layout, and finite element analysis solutions showed reasonable correlation with the 50% reduction.

$$\beta_{g,lean,2003} = \frac{12(n_g-1)^2 S^2 EI_x}{n_g L^3} \quad 2.34$$

However, as mentioned in the discussion of in-plane girder stiffness for conventional bracing, Equation 2.20, and thereby Equation 2.35, was derived based on a twin-girder system and did not account for the stiffness contribution of more than two girders. A modified version of Equation 2.21 was introduced as part of TxDOT Project 0-7093-1 to incorporate the effects of lean-on bracing on the in-plane girder stiffness (Bjelland, 2024; Helwig *et al.*, 2024).

$$\beta_{g,lean,2024} = C_{LO}^2 C_{BS}^2 \frac{\pi^4 EI_x S^2 \alpha_x}{2n_g (KL)^3 (n_{CFL}+1)} \quad 2.35$$

Where:

$C_{LO}$  is a lean-on layout factor, discussed in Section 8.2.3

### 2.6.2. Cross-Section Stiffness, $\beta_{sec}$

Equation 2.30 may be applied in lean-on cases as well as with conventional cases. However, as most lean-on configurations will use full-depth cross-frames, this term may also be taken as infinity, due to language in the 10<sup>th</sup> Edition of AASHTO (2020) for stability bracing allowing  $\beta_{sec}$  to be taken as infinity for braces deeper than 80% of the web depth.

### 2.6.3. Torsional Brace Stiffness, $\beta_{br}$

Helwig and Wang (2003) derived a generalized equation for the brace stiffness contribution in a lean-on bracing system based on the tension-system idealization developed by Yura (2001). Based on virtual work calculations of the displacement of the critical girder, they determined the generalized displacement equation shown:

$$\Delta_{crit} = n_{gc} \frac{FL_d^3}{EA_d S^2} + (n_{gc} - 1) \frac{FS}{EA_s} + (n_{gc} - 2)(n_{gc} - 1) \frac{FS}{EA_s} \quad 2.36$$

Where:

$n_{gc}$  is the number of girders per cross-frame

The first term corresponds to the displacement of the diagonal in the Z-frame, the second term corresponds to the displacement of the displacement of the top and bottom strut in the Z-frame, and the third term corresponds to the displacement of the lean-on top and bottom struts. The expression may be rewritten as:

$$\Delta_{crit} = n_{gc} \frac{FL_d^3}{EA_d S^2} + (n_{gc} - 1)^2 \frac{FS}{EA_d} \quad 2.37$$

To result in the stiffness expression proposed:

$$\beta_{br} = \frac{h^2 S^2 E}{\frac{n_{gc} L_d^3}{A_d} + \frac{S^3}{A_s} (n_{gc} - 1)^2} \quad 2.38$$

In this expression, the number of cross-frames per bracing line is assumed to be one, so  $n_{gc}$  is effectively the number of girders. As an example, the idealization of a four-girder system is shown in Figure 2-12. The free body diagram shows the accumulation of forces that develop across



the width of the bridge. The bracing demand from the girders results in force couples that lead to the forces indicated in the figure. Some designs that have made use of Equation 2.38 have included more than one brace in a given line, which results in an erroneous estimate of the stiffness demand since the resulting value of  $n_{gc}$  in those cases is not representative of the force distribution across the cross-frame line.

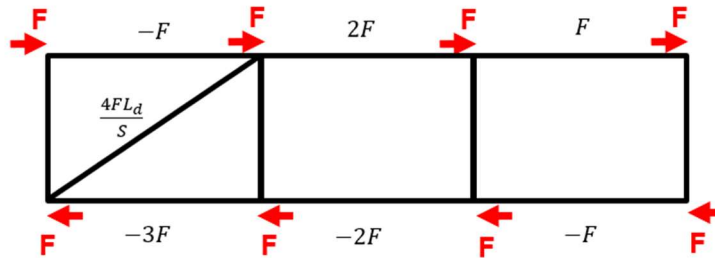


Figure 2-12. Force Distribution along Lean-On Bracing Line

## 2.7. R-Factors

From Equations 2.25 and 2.38, it is evident that the stiffness of the brace is a function of the axial stiffness of its individual members when the cross-frame is subjected to a moment. Although not explicitly presented, the inherent flexibility of the connections should also be considered in the evaluation of the overall brace stiffness, similar to what is done for cross-section distortional effects or in-plane girder flexibility.

For many cross-frame applications, single-angle or tee sections are attached to connection or gusset plates along only one leg or flange, respectively. This, in turn, introduces an eccentric load path through the connection that can significantly impact the stiffness of the brace. In lieu of a more refined assessment of these softening effects, AASHTO LRFD (2020) recommends a simple reduction factor based on experimental and analytical studies conducted by Battistini et al. (2013, 2016) and Wang (2013). For stability bracing applications, a fixed factor of 0.65 can be

applied to the cross-sectional area of the diagonals and struts in the calculation of the brace stiffness. This reduction factor was calibrated to represent these softening effects for a wide range of common cross-frame configurations, connections, and member sizes.

## 2.8. Torsional Bracing Strength Requirements

In addition to being designed for adequate stiffness, cross-frames must be designed with adequate strength. The current strength requirements for both conventional and lean-on bracing systems are discussed in the following sections.

### 2.8.1. Conventional Bracing

In addition to stiffness requirements, the bracing also must satisfy strength requirements to effectively prevent LTB of a bridge girder. The forces in the cross brace are found based on the required moment in the brace,  $M_{br}$ , that is calculated using the formulation shown in Equation 2.15. The brace moment can be idealized as a force couple so that forces in the cross-frame members can be determined. The relationship between the torsional brace moment and forces induced in cross-frames are depicted in Figure 2-13 for X-frames in either a tension only cross-frame or a compression system, as well as for K-frames.

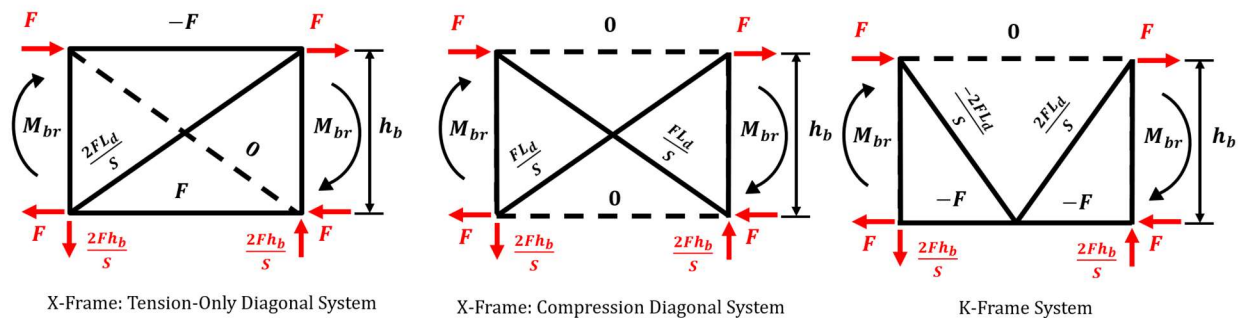


Figure 2-13. Idealized Cross-Frame Forces

As discussed previously, the AASHTO 10<sup>th</sup> Edition bracing provisions required twice the ideal stiffness for cross-frames at least equal to 80% of the girder depth, which will generally be the case. Provided that adequate stiffness is provided, the resulting girder twist is equal to the initial imperfection,  $\theta_0$ , and the resulting bracing moment is  $\beta_T\theta_0$ . This relationship is reflected by Equation 2.39.

$$M_{br} = \beta_T\theta_0 = F_{br}h_b \quad 2.39$$

The applied force couple in the brace results from the brace moment required to restrain girder twist. The couple is a linear function of the required stiffness and an assumed initial imperfection (Helwig and Wang, 2003):

$$F_{br} = \frac{M_{br}}{h_b} = \frac{0.0048LL_b}{nI_{eff}Eh_b} \left(\frac{M_u}{C_b}\right)^2 \quad 2.40$$

Where:

$F_{br}$  is the force in the brace

$\beta_T$  is the bracing system stiffness

From Equation 2.40, the force in each member can be estimated by evaluating the cross-frame as an idealized truss subjected to a moment, or a resolved force couple at the top and bottom nodes of the truss. As shown in Figure 2-13, for a tension-only system, the force in the struts is equal to  $F_{br}$  in compression, and the force in the tension diagonal is given by Equation 2.41 (Helwig and Wang, 2003):

$$F_d = \frac{2F_{br}L_d}{s} \quad 2.41$$

After the stability-related member forces are calculated in accordance with Figure 2-13, cross-frame members can be sized for adequate strength. Note that the stability bracing forces in cross-frames are to be treated as any other load case such as wind or live load force effects in cross-frames. As such, the stability bracing forces can and should be combined with other concurrently acting load cases via linear superposition.

### 2.8.2. Lean-On Bracing

Strength design for lean-on bracing is similar to conventional bracing. Helwig and Wang (2003) determined equations for the forces in lean-on bracing systems by conservatively utilizing the tension-model for cross-frames placed in exterior and interior bays. Equations 2.39 and 2.40 are used to determine  $F_{br}$ . In systems with the cross-frame placed in the exterior bay, the maximum force in the diagonals is:

$$F_d = \frac{n_{gc}F_{br}L_d}{s} \quad 2.42$$

The maximum force in the struts in compression is:

$$F_s = (n_{gc} - 1)F \quad 2.43$$

In systems with the cross-frame placed in the interior bay, the maximum force in the diagonals is:

$$F_d = \frac{n_{gc}F_{br}L_d}{s} \quad 2.44$$

The maximum force in the struts in compression is:

$$F_s = \frac{n_{gc}}{2}F \quad 2.45$$

## **Chapter 3. Lean-On Brace Stiffness Derivations for One Exterior X- or K-Frame**

In the previous lean-on bracing studies outlined in Chapter 2, analytical equations were developed for the brace stiffness of conventional cross-frame applications as well as for lean-on bracing lines with a single cross-frame in the exterior bay. These equations are limited in scope of application by the number, type, and position of the cross-frame. In order to provide solutions appropriate for a wider range of applications, expressions were developed for the brace stiffness of lean-on cross-frame lines that are valid for Z-, X-, or K-shaped cross-frame geometries with any number of cross-frames in varying positions along the bracing line.

### **3.1. Current Brace Stiffness Derivations**

---

This section begins with a detailed discussion of the stiffness expressions for conventional bracing as well as the lean-on applications overviewed in Chapter 2. Two particularly relevant derivations are provided for the brace stiffness: a single cross-frame, and a cross-frame line with a single exterior bay cross-frame and lean-on struts.

#### **3.1.1. Twin Girder System Derivation**

Yura (2001) developed expressions for the torsional brace stiffness of cross-frames with either Z-, X-, or K-shaped geometries. The Z-shaped cross-frame is also applicable to cross-frames with two diagonals, for which an engineer may conservatively neglect the compression diagonal due to the relatively low buckling strength of single-angle members that are frequently used for the braces. Such a cross-frame is often referred to as a tension-only diagonal system. The following discussion focuses on the derivation of the Z-shaped system. In the derivation, the cross-frame is idealized as a truss with axially loaded members. The method of virtual work can be used to derive

the expression. The idealization of this system is shown in Figure 3-1. The force demand on the cross-frame consists of a force couple on both ends, as shown in the figure.

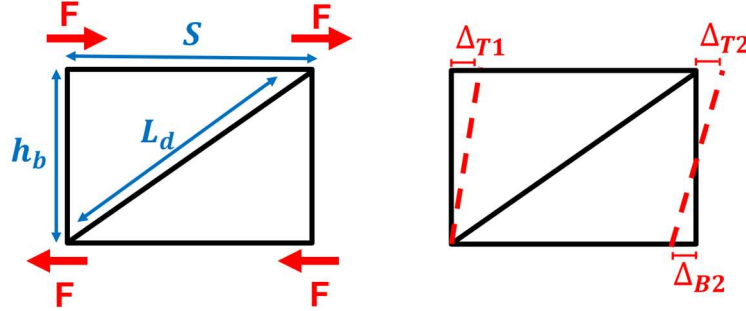


Figure 3-1. Twin Girder Brace Stiffness Idealization

In this approach, Equation 3.1 and Equation 3.2 are combined to result in Equation 3.3, indicating that the displacement of the critical girder is the basis for calculating the provided stiffness. The critical girder is the one with the largest total displacement of the top and bottom.

$$M = Fh_b \quad 3.1$$

$$\beta_{br} = \frac{M}{\theta} \quad 3.2$$

$$\beta_{br} = \frac{Fh_b^2}{\Delta_{crit}} \quad 3.3$$

Where:

$M$  is the moment applied to the system

$F$  is a unit load applied at the top and bottom of each girder in the directions shown

$h_b$  is the depth of the cross-frame

$\theta$  is the rotation of the girder

$\Delta_{crit}$  is the displacement of the critical girder (here,  $\Delta_{T2} + \Delta_{B2}$ )

From the virtual work procedure,  $\Delta_{crit}$  is calculated, resulting in Equation 3.4 for  $\beta_{brz}$ . This equation represents the stiffness of a Z-shaped cross-frame. Yura (2001) presented similar derivations for X-type and K-type cross-frames.

$$\beta_{brz} = \frac{h_b^2 S^2 E}{\frac{2L_d^3}{A_d} + \frac{S^3}{A_s}} \quad 3.4$$

Where:

$S$  is the girder spacing

$E$  is the modulus of elasticity

$L_d$  is the length of the cross-frame diagonal members

$A_d$  is the cross-sectional area of the cross-frame diagonals

$A_s$  is the cross-sectional area of the cross-frame struts

From Equation 3.4, it is evident that the stiffness of the brace is a function of the axial stiffness of the individual members when the cross-frame is subjected to equal force couples on either end. Although not explicitly presented, the inherent flexibility of the connections should also be considered in the evaluation of the overall brace stiffness, similar to what is done for cross-section distortional effects or in-plane girder flexibility.

As noted in Chapter 2, single-angle or tee sections are often used for cross-frames and are attached to connection or gusset plates with eccentric connections to the main member. These eccentricities lead to a reduction in stiffness, as covered in Battistini et al. (2013, 2016) and Wang (2013). The stiffness reduction is accounted for with a fixed reduction factor,  $R$ . The AASHTO LRFD (2020) recommends an  $R$ -value of 0.65 during construction and 0.75 in the completed bridge. The  $R$ -factor is applied to the cross-sectional area of the diagonals and struts in computer

analyses or stiffness equations. This reduction factor was calibrated to represent the softening effects for a wide range of common cross-frame configurations, connections, and member sizes.

### 3.1.2. Original Lean-On Bracing Derivation

Similar to the stiffness of a single cross-frame developed by Yura (2001), Helwig and Wang (2003) derived a generalized equation for the brace stiffness contribution in a lean-on bracing system that reflected the bracing load path of a series of adjacent girders restrained by top and bottom struts with a single cross-frame at one end of the bracing line. The expression is given by Equation 3.5.

$$\beta_{br,lean2003} = \frac{h_b^2 S^2 E}{\frac{n_{gc} L_d^3}{A_d} + \frac{S^3}{A_s} (n_{gc} - 1)^2} \quad 3.5$$

Where:

$n_{gc}$  is the number of girders per cross-frame

Based on the specific geometry that was considered in the derivation, the number of cross-frames per bracing line is assumed to be one, so  $n_{gc}$  is effectively the number of girders in this equation. The method of virtual work can be used to account for the axial shortening of the struts and diagonals based on the respective forces in the individual members. As an example, the idealization of a four-girder system is shown in Figure 3-2. The free-body diagram shows the accumulation of forces that develop across the width of the bridge. The bracing demand from the girders results in force couples that lead to the forces indicated in the figure.



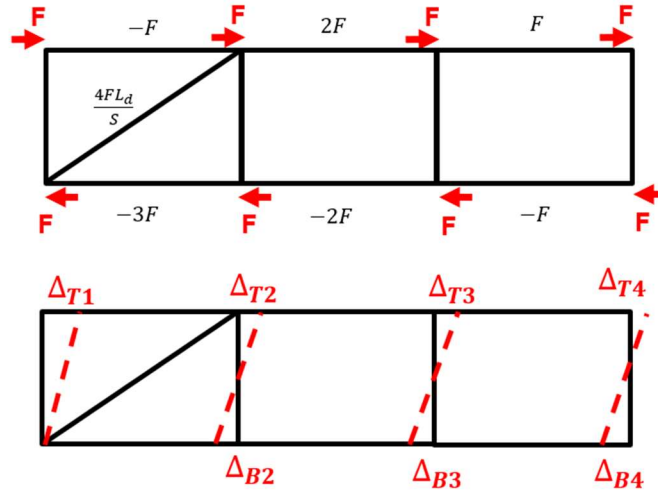


Figure 3-2. Lean-On Bracing Stiffness Idealization

The calculated brace stiffness of this system is shown in Equation 3.6.

$$\beta_{br,lean2003}(n_g = 4, n_c = 1) = \frac{h_b^2 S^2 E}{\frac{4L_d^3}{A_d} + \frac{9S^3}{A_s}} \quad 3.6$$

The expression in Equation 3.5 has been used in some designs for lean-on systems where more than one cross-frame in a given bracing line. Due to the definition for  $n_{gc}$  in Helwig and Wang (2003), which was the number of girders per cross-frame, designers simply divided the number of girders by the number of cross-frames. Although such an interpretation makes sense from the definition of the variable, the expression was not derived for such an application.

Another limitation of the lean-on bracing stiffness and strength from Helwig and Wang (2003) is that only the Z-shaped cross-frame was considered in the derivation. When this equation is applied to X-shaped cross-frames, it is referred to as the tension model. One diagonal is assumed to act in tension, like the Z-frame, and the second cross-frame is conservatively neglected. However, this idealization can be overly conservative in many situations. Derivations for X-type and K-type cross-frames will improve the applicability to a wider array of systems. In the following

sections, the model validation process, derivation, and validation of lean-on bracing stiffness equations for K-frames and full X-frames are discussed. These derivations implicitly assume a placement of a single cross-frame on the outside bay of the bracing system, to mirror the approach utilized in the derivation of lean-on stiffness with the tension model.

## 3.2. Derivations for Other Cross-Frame Shapes

---

This section presents derivations of the lean-on stiffness equations considering one full X-type or K-type cross-frame in an exterior bay of a cross-frame line. Modifications for lean-on applications with multiple cross-frames are discussed in Chapter 4.

### 3.2.1. Two-Dimensional Model Validation

In order to validate derived expressions, it was necessary to first develop models of cross-frame system sections with the same assumptions as previous derivations (Yura, 2001; Helwig and Wang, 2003). SAP2000 was used to model the cross-frame line as a two-dimensional truss system. The fundamental assumption for truss members is that elements are subjected to pure axial load. The girders were assumed to have infinite stiffness (which was later shown to be inconsequential), and the cross-frame line was simply supported with lateral unit loads applied at the top and bottom of each girder to create a force couple on both ends of the cross-frame, as shown in Figure 3-3.

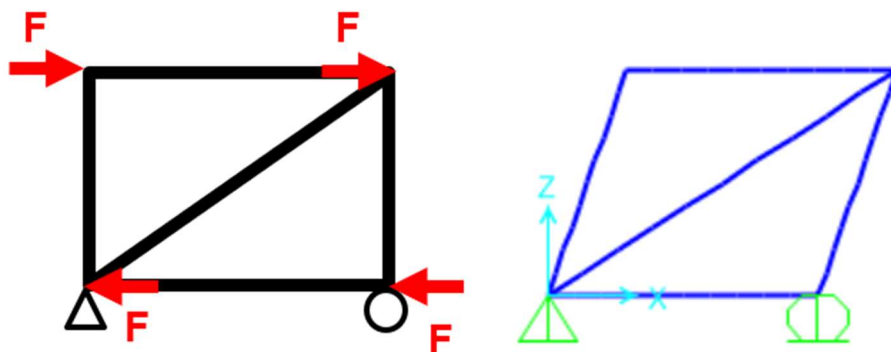


Figure 3-3. Twin Girder Tension Model Idealization and Deformed Shape

In order to validate the modeling procedure for an analysis of the brace stiffness ( $\beta_{br}$ ), the computer models were compared with analytical solutions. First, a twin-girder system was considered. The current equation for the brace stiffness based on the shown tension model is given by Equation 3.4 (Yura, 2001). In order to calculate the stiffness of the model, Equation 3.3 was used, with  $\Delta_{crit}$  indicating the sum of the respective displacements at the top and bottom of the right girder. Several cases were compared with an area of 6.45 in<sup>2</sup> for all members, girder spacing of 96 inches, and cross-frame depth of 76 inches. The stiffness of a tension-only diagonal system was 2,185,000 kip-in/rad, which agreed exactly with the Z-frame stiffness model given in Equation 3.4. The negligible error in the tension system SAP model relative to the tension system equation indicates the model is performing as expected.

A model including the second diagonal in the cross-frame was also analyzed. It was observed that the full cross-frame model was more than twice as stiff as the tension model, indicating that the addition of the second cross-frame diagonal significantly improves the stiffness of the brace.

### **3.2.2. Lean-On with K-Frames**

The derivation for lean-on with K-frames is based on Yura's (2001) derivation for a K-frame twin girder system. In this derivation, the diagonals are designed for tension and compression. The same assumptions as used for the tension model idealization apply, as shown in Figure 3-4.

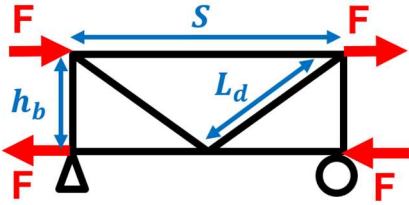


Figure 3-4. Twin Girder K-Frame Idealization

The real force distribution of the system is shown in Figure 3-5.

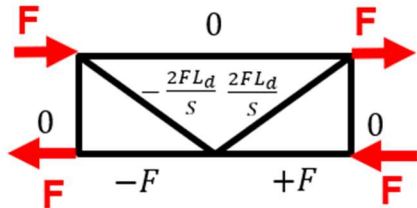


Figure 3-5. Twin Girder K-Frame Real Force Distribution

The virtual work force results for a unit force applied to the top of the right girder (T2) are shown in Figure 3-6.

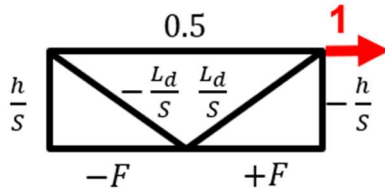


Figure 3-6. Twin Girder K-Frame Virtual T2 Force Distribution

The virtual work force results for a unit force applied to the bottom of the right girder (B2) are shown in Figure 3-7.

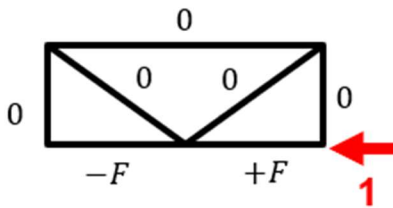


Figure 3-7. Twin Girder K-Frame Virtual B2 Force Distribution

The resulting displacement calculations are included in Table 3-1.

Table 3-1. Virtual Work Calculations for Two Girders and One K-Frame

Member	Length	Area	$F_{real}$	$F_{virtualT2}$	$F_{virtualB2}$	$\Delta_{T2}$	$\Delta_{B2}$
Top Strut	$S$	$A_s$	0	0	0	0	0
Left Bottom Strut	$S/2$	$A_s$	$F$	1	-1	$\frac{FS}{2A_sE}$	$-\frac{FS}{2A_sE}$
Right Bottom Strut	$S/2$	$A_s$	$-F$	0	-1	0	$\frac{FS}{2A_sE}$
Left Diagonal	$L_d$	$A_d$	$-\frac{2FL_d}{S}$	0	0	0	0
Right Diagonal	$L_d$	$A_d$	$\frac{2FL_d}{S}$	$\frac{2L}{S}$	0	$\frac{4FL_d^3}{S^2A_dE}$	0

From this, the total displacement of the critical girder is given by:

$$\Delta_{crit} = \Delta_{T2} + \Delta_{B2} = \frac{4FL_d^3}{S^2A_dE} + \frac{FS}{2A_sE} \quad 3.7$$

This critical displacement can be used in Equation 3.3 to determine the stiffness of the system, as given by Equation 2.28.

### 3.2.2.1. Lean-On Real Force Distribution

It was necessary to develop a generalized force distribution for lean-on bracing with one K-frame. In order to accomplish this, the internal forces in systems with one K-frame and varying numbers of lean-on bays were compared. The forces vary based on the number of girders (effectively the number of lean-on bays) in the system. The distribution for one K-frame and one lean-on bay is shown in Figure 3-8.

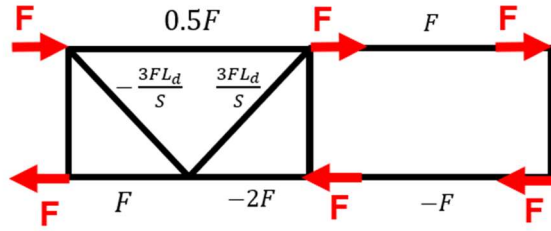


Figure 3-8. Force Distribution for One K-Frame and Three Girders

The distribution for one K-frame and two lean-on bays is shown in Figure 3-9.

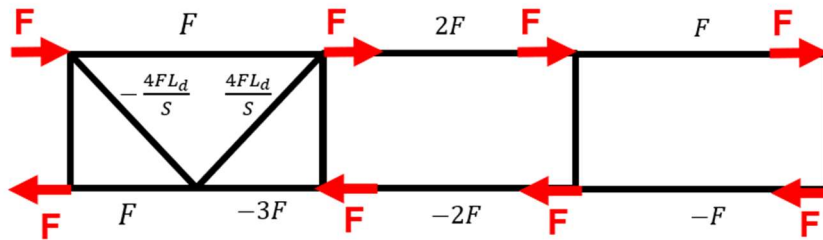


Figure 3-9. Force Distribution for One K-Frame and Four Girders

A general form of the force distribution is shown in Figure 3-10.

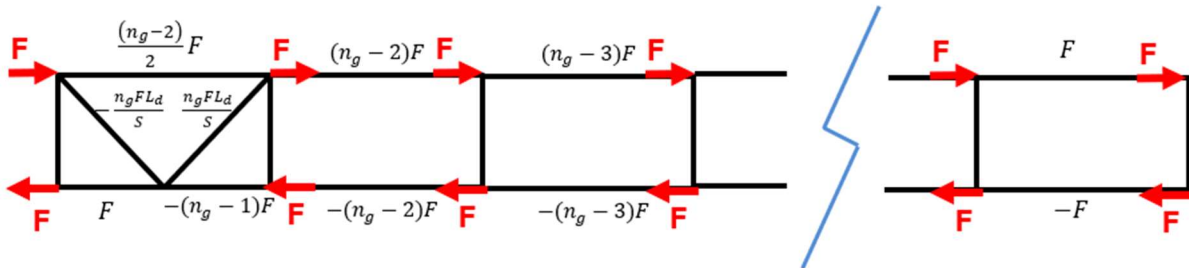


Figure 3-10. Generalized Lean-On K-Frame Force Distribution

### 3.2.2.2. Lean-On Virtual Work Calculations

Virtual work calculations were completed for systems with one K-frame and three or four girders. The forces in the girders are neglected because the modulus of the girders is assumed to be infinite. In SAP models with a girder modulus of 29,000 ksi as opposed to 29,000,000 ksi (multiplier of 1000), the difference in displacement was less than 1%, indicating that  $\beta_{br}$  is

essentially the only stiffness component contributing. The calculations are shown in Table 3-2 and Table 3-3.

Table 3-2. Virtual Work Calculations for Three Girders and One K-Frame

Member	Length	Area	$F_{real}$	$F_{virtualT3}$	$F_{virtualB3}$	$\Delta_{T2}$	$\Delta_{B2}$
Top Strut	$S$	$A_s$	$0.5F$	$0.5$	$0$	$\frac{FS}{4A_sE}$	$0$
Left Bottom Strut	$S/2$	$A_s$	$F$	$1$	$-1$	$\frac{FS}{2A_sE}$	$-\frac{FS}{2A_sE}$
Right Bottom Strut	$S/2$	$A_s$	$-2F$	$0$	$-1$	$0$	$\frac{FS}{A_sE}$
Left Diagonal	$L_d$	$A_d$	$-\frac{3FL}{S}$	$-\frac{L}{S}$	$0$	$\frac{3FL_d^3}{S^2A_dE}$	$0$
Right Diagonal	$L_d$	$A_d$	$\frac{3FL}{S}$	$\frac{L}{S}$	$0$	$\frac{3FL_d^3}{S^2A_dE}$	$0$
Lean-On Bottom Strut 1	$S$	$A_s$	$-F$	$0$	$-1$	$0$	$\frac{FS}{A_sE}$
Lean-On Top Strut 1	$S$	$A_s$	$F$	$1$	$0$	$\frac{FS}{A_sE}$	$0$

The total displacement of the critical girder in a three-girder system is given by Equation 3.8.

$$\Delta_{crit} = \Delta_{T3} + \Delta_{B3} = 6 \frac{FL_d^3}{S^2A_dE} + \frac{16}{4} \frac{FS}{A_sE} \quad 3.8$$

Table 3-3. Virtual Work Calculations for Four Girders and One K-Frame

Member	Length	Area	$F_{real}$	$F_{virtualT4}$	$F_{virtualB4}$	$\Delta_{T2}$	$\Delta_{B2}$
Top Strut	$S$	$A_s$	$F$	0.5	0	$\frac{FS}{2A_sE}$	0
Left Bottom Strut	$S/2$	$A_s$	$F$	1	-1	$\frac{FS}{2A_sE}$	$-\frac{FS}{2A_sE}$
Right Bottom Strut	$S/2$	$A_s$	$-3F$	0	-1	0	$\frac{3FS}{A_sE}$
Left Diagonal	$L_d$	$A_d$	$-\frac{4FL_d}{S}$	$-\frac{L_d}{S}$	0	$\frac{4FL_d^3}{S^2A_dE}$	0
Right Diagonal	$L_d$	$A_d$	$\frac{4FL_d}{S}$	$\frac{L_d}{S}$	0	$\frac{4FL_d^3}{S^2A_dE}$	0
Lean-On Bottom Strut 1	$S$	$A_s$	$-2F$	0	-1	0	$\frac{2FS}{A_sE}$
Lean-On Top Strut 1	$S$	$A_s$	$2F$	1	0	$\frac{2FS}{A_sE}$	0
Lean-On Bottom Strut 2	$S$	$A_s$	$-F$	0	-1	0	$\frac{FS}{A_sE}$
Lean-On Top Strut 2	$S$	$A_s$	$F$	1	0	$\frac{FS}{A_sE}$	0

The total displacement of the critical girder in a four-girder system is given by Equation 3.9.

$$\Delta_{crit} = \Delta_{T4} + \Delta_{B4} = 8 \frac{FL_d^3}{S^2A_dE} + 8 \frac{FS}{A_sE} \quad 3.9$$

### 3.2.2.3. Generalized Lean-On Stiffness Equation with One K-Frame

A generalized displacement equation was determined for lean-on with one K-frame based on the virtual work calculations discussed previously. This expression is given by Equation 3.10.

$$\Delta_{crit} = 2n_g \left( \frac{FL_d^3}{S^2A_dE} \right) + \left[ \frac{1}{4}(n_g - 2) + \frac{n_g - 1}{2} + (n_g - 1)(n_g - 2) \right] \left( \frac{FS}{A_sE} \right) \quad 3.10$$

Where the first term corresponds to the displacements of the diagonals in the K-frame, the second term corresponds to the displacement of the top strut of the cross-frame, the third term corresponds to the displacement of the bottom strut of the cross-frame, and the last term corresponds to the



cumulative displacements of the top and bottom struts in lean-on bays. The equation may be further simplified to the form shown in Equation 3.11.

$$\Delta_{crit} = 2n_g \left( \frac{FL_d^3}{S^2 A_d E} \right) + \left[ n_g^2 - \frac{9}{4} n_g + 1 \right] \left( \frac{FS}{A_s E} \right) \quad 3.11$$

This equation was validated against a model with six girders and one K-frame, with both the equation and the model computing a critical displacement of 0.0149 inches for the values included in Section 3.2. The resulting generalized stiffness equation for lean-on bracing with one exterior bay K-frame is given by Equation 3.12.

$$\beta_{br,leanK1} = \frac{ES^2 h_b^2}{2n_g \frac{L_d^3}{A_d} + (n_g^2 - \frac{9}{4} n_g + 1) \frac{S^3}{A_s}} \quad 3.12$$

### 3.2.3. Lean-On with Full X-Frames

Based on preliminary comparisons between the “full X-frame” and “tension model” SAP models discussed in Section 3.2, it was apparent that the tension model assumption was underpredicting the stiffness of the full cross-frame system by at least 50%. From these findings, it is necessary to include the contribution of the second diagonal member to accurately quantify the stiffness of the brace. Yura (2001) developed a “compression system” model which accounted for both X-frame diagonals, but assumed the top and bottom struts were zero-force members. When this model is applied to a lean-on bracing system, the system is unstable because the deflection of the cross-frame diagonals is not restrained laterally. Based on these observations, a new approach was developed to consider both of the diagonals, as well as the top and bottom struts of the X-frame for lean-on bracing lines.

### 3.2.3.1. Lean-On Real Force Distribution

The idealization of a lean-on bracing line with one X-frame is an indeterminate system, so the derivation for a precise expression is reliant on pattern recognition in comparisons between models. Similar force paths as the Z-frame and K-frame were observed, with slightly different proportions. The distribution for one X-frame and one lean-on bay is shown in Figure 3-11.

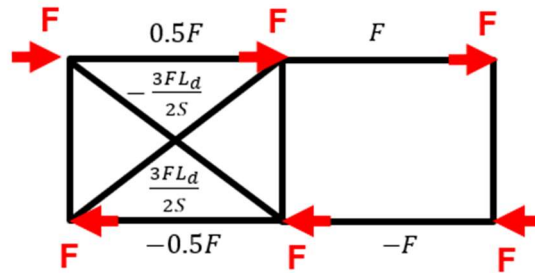


Figure 3-11. Force Distribution for One X-Frame and Three Girders

The distribution for one X-frame and two lean-on bays is shown in Figure 3-12.

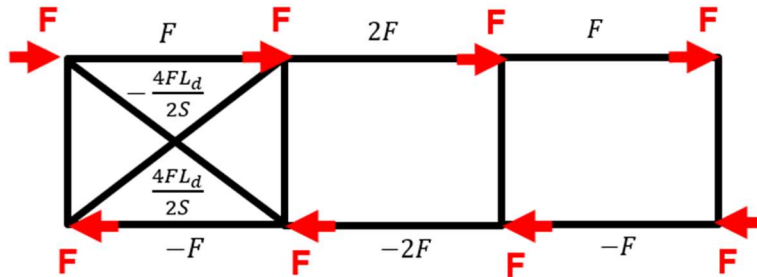


Figure 3-12. Force Distribution for One X-Frame and Four Girders

The general form of the X-frame force distribution is shown in Figure 3-13.

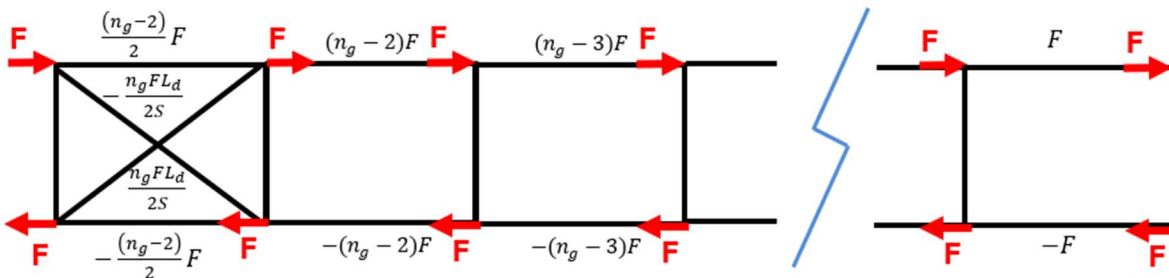


Figure 3-13. Generalized Lean-On X-Frame Distribution

### 3.2.3.2. Lean-On Virtual Work Calculations

Virtual work calculations were completed for systems with one X-frame and three or four girders. The member axial forces for the virtual force cases were obtained by applying a unit load to the appropriate model, and the values were converted into ratios of  $L$ ,  $S$ ,  $A_d$ , and  $A_s$ . As in previous derivations, the forces in the girders are neglected because the modulus of the girders is assumed to be infinite. The calculations for a three-girder system are shown in Table 3-4, and the calculations for a four-girder system are shown in Table 3-5.

Table 3-4. Virtual Work Calculations for Three Girders and One X-Frame

Member	Length	Area	$F_{real}$	$F_{virtualT3}$	$F_{virtualB3}$	$\Delta_{T2}$	$\Delta_{B2}$
Top Strut	$S$	$A_s$	$\frac{1}{2}F$	$\frac{1}{3}$	$\frac{1}{6}$	$\frac{1}{6} \frac{FS}{A_s E}$	$\frac{1}{12} \frac{FS}{A_s E}$
Bottom Strut	$S$	$A_s$	$-\frac{1}{2}F$	$\frac{1}{3}$	$-\frac{5}{6}$	$-\frac{1}{6} \frac{FS}{A_s E}$	$\frac{5}{12} \frac{FS}{A_s E}$
Top Diagonal	$L_d$	$A_d$	$-\frac{3FL_d}{2S}$	$-\frac{1}{3} \frac{L_d}{S}$	$-\frac{1}{6} \frac{L_d}{S}$	$\frac{1}{2} \frac{FL_d^3}{S^2 A_d E}$	$\frac{1}{4} \frac{FL_d^3}{S^2 A_d E}$
Bottom Diagonal	$L_d$	$A_d$	$\frac{3FL_d}{2S}$	$\frac{2}{3} \frac{L_d}{S}$	$-\frac{1}{6} \frac{L_d}{S}$	$\frac{FL_d^3}{S^2 A_d E}$	$-\frac{1}{4} \frac{FL_d^3}{S^2 A_d E}$
Lean-On Bottom Strut 1	$S$	$A_s$	$-F$	0	-1	0	$\frac{FS}{A_s E}$
Lean-On Top Strut 1	$S$	$A_s$	$F$	1	0	$\frac{FS}{A_s E}$	0

The total displacement of the critical girder in a three-girder system is given by Equation 3.13.

$$\Delta_{crit} = \Delta_{T3} + \Delta_{B3} = \frac{3}{2} \frac{FL_d^3}{S^2 A_d E} + \frac{5}{2} \frac{FS}{A_s E} \quad 3.13$$

Table 3-5. Virtual Work Calculations for Four Girders and One X-Frame

Member	Length	Area	$F_{real}$	$F_{virtualT3}$	$F_{virtualB3}$	$\Delta_{T2}$	$\Delta_{B2}$
Top Strut	$S$	$A_s$	$F$	$\frac{1}{3}$	$\frac{1}{6}$	$\frac{1}{3} \frac{FS}{A_s E}$	$\frac{1}{6} \frac{FS}{A_s E}$
Bottom Strut	$S$	$A_s$	$-F$	$\frac{1}{3}$	$-\frac{5}{6}$	$-\frac{1}{3} \frac{FS}{A_s E}$	$\frac{5}{6} \frac{FS}{A_s E}$
Top Diagonal	$L_d$	$A_d$	$-2 \frac{FL_d}{S}$	$-\frac{1}{3} \frac{L_d}{S}$	$-\frac{1}{6} \frac{L_d}{S}$	$\frac{2}{3} \frac{FL_d^3}{S^2 A_d E}$	$\frac{2}{6} \frac{FL_d^3}{S^2 A_d E}$
Bottom Diagonal	$L_d$	$A_d$	$2 \frac{FL_d}{S}$	$\frac{2}{3} \frac{L_d}{S}$	$-\frac{1}{6} \frac{L_d}{S}$	$\frac{4}{3} \frac{FL_d^3}{S^2 A_d E}$	$-\frac{2}{6} \frac{FL_d^3}{S^2 A_d E}$
Lean-On Bottom Strut 1	$S$	$A_s$	$-2F$	0	-1	0	$2 \frac{FS}{A_s E}$
Lean-On Top Strut 1	$S$	$A_s$	$2F$	1	0	$2 \frac{FS}{A_s E}$	0
Lean-On Bottom Strut 2	$S$	$A_s$	$-F$	0	-1	0	$\frac{FS}{A_s E}$
Lean-On Top Strut 2	$S$	$A_s$	$F$	1	0	$\frac{FS}{A_s E}$	0

The total displacement of the critical girder in a four-girder system is given by Equation 3.14.

$$\Delta_{crit} = \Delta_{T3} + \Delta_{B3} = 2 \frac{FL_d^3}{S^2 A_d E} + 7 \frac{FS}{A_s E} \quad 3.14$$

### 3.2.3.3. Generalized Lean-On Stiffness Equation with One X-Frame

A generalized displacement equation was determined for lean-on with one X-frame based on the virtual work calculations discussed previously. This expression is given by Equation 3.15.

$$\Delta_{crit} = \frac{1}{2} n_g \left( \frac{FL_d^3}{S^2 A_d E} \right) + \left[ \frac{1}{2} (n_g - 2) + \frac{n_g - 1}{2} + (n_g - 1)(n_g - 2) \right] \left( \frac{FS}{A_s E} \right) \quad 3.15$$

Where the first term corresponds to the displacements of the diagonals in the X-frame, the second term corresponds to the displacement of the top strut of the cross-frame, the third term corresponds to the displacement of the bottom strut of the cross-frame, and the last term corresponds to the cumulative displacements of the top and bottom struts in lean-on bays. The equation may be further simplified to the form shown in Equation 3.16.

$$\Delta_{crit} = \frac{1}{2}n_g \left( \frac{FL_d^3}{S^2A_dE} \right) + \left[ n_g^2 - \frac{5}{2}n_g + 1 \right] \left( \frac{FS}{A_sE} \right) \quad 3.16$$

This equation was validated against a model with six girders and one K-frame, with both the equation and the model computing a critical displacement of 0.0145 inches for the values included in Section 3.2. The resulting brace stiffness equation for lean-on bracing lines with one exterior bay X-frame is given by Equation 3.17.

$$\beta_{br,leanX1} = \frac{ES^2h_b^2}{\frac{1}{2}n_g \frac{L_d^3}{A_d} + (n_g^2 - \frac{5}{2}n_g + 1) \frac{S^3}{A_s}} \quad 3.17$$

## Chapter 4. Lean-On Brace Stiffness Equation Modifications for Multiple Cross-Frames

Helwig and Wang (2003) derived a generalized equation for the brace stiffness contribution in a lean-on bracing system based on the tension model idealization developed by Yura (2001). In this expression, the number of cross-frames per bracing line is implicitly assumed to be one, so  $n_{gc}$  is effectively the number of girders. As an example, the idealization of a four-girder system is shown in Figure 4-1. The corresponding value of  $n_{gc}$  is four.



Figure 4-1. Four Girder, One Z-Frame Lean-On Bracing Stiffness Idealization

Some designs that have made use of Equation 3.5 have included more than one brace in a given line, which results in an erroneous estimate of the stiffness demand since the resulting value of  $n_{gc}$  in those cases is not representative of the force distribution across the cross-frame line. In these cases,  $n_{gc}$  is calculated as the ratio of girders to cross-frames. For example, as shown in Figure 4-2, a bracing line with four girders and two Z-frames would be reduced to the same stiffness as a system with two girders and one Z-frame since both have a girder to cross-frame ratio of 2:1.

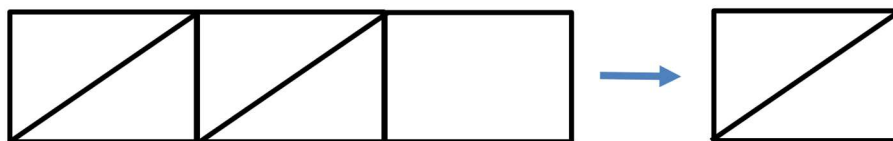


Figure 4-2. Four Girder, Two Z-Frame Lean-On Bracing Stiffness Idealization

Currently, designers that have utilized lean-on bracing concepts often make use of more than one cross-frame in each line in their application of lean-on bracing. More than one brace per line is used in an attempt to reduce the demand on the cross-frame. However, the resulting  $n_{gc}$  that is used is not representative of the stiffness derivation for Equation 3.5. Therefore, it is necessary to develop an expression for the brace stiffness that accounts for the additional cross-frame relative to the Helwig and Wang expression in Equation 3.5. Four potential alternative approaches are described in the following sections in the context of a four-girder system with two Z-frames. As discussed in Gasser (2023), all four approaches were compared preliminarily, and the most promising approach was generalized to account for varying numbers of girders and configurations of cross-frames. A detailed parametric study was conducted to finalize the best approach and was validated for K and X-frames as well.

## **4.1. Approaches for Multiple Cross-Frames**

---

### **4.1.1. Cross-Section Slice Approach**

The first method is called a “Cross-Section Slice Approach,” where a redundant cross-frame is essentially ignored. This is shown for a four-girder system with two cross-frames in Figure 4-3, where the left cross-frame is not considered in determining the brace stiffness. This results in  $\Delta_{crit}$  equal to the sum of  $\Delta_{T3}$ ,  $\Delta_{T4}$ ,  $\Delta_{B3}$ , and  $\Delta_{B4}$ . The brace stiffness of the configuration is then calculated using Equation 3.5 or virtual work for a three-girder system, resulting in Equation 4.1.

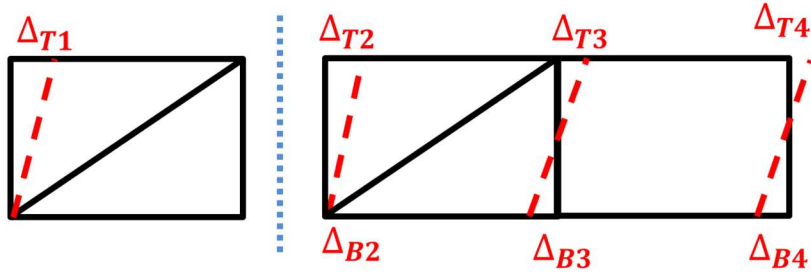


Figure 4-3. Cross-Section Slice Approach

$$\beta_{br} = \frac{Fh^2}{\Delta_{crit}} = \frac{Fh^2}{\frac{3FL_d^3}{5^2 A_d E} + \frac{4FS}{A_s E}} \quad 4.1$$

#### 4.1.2. Displacement Combination Approach

A second method is called the “Displacement Combination Approach,” which is similar to the “Cross-Section Slice Approach,” but the displacement of the second girder is accounted for differently. In the “Cross-Section Slice Approach,” the displacement is ignored, whereas in “Displacement Combination Approach,” the displacement is accounted for by adding the second girder from the first cross-frame to the result obtained in the “Cross-Section Slice Approach.” This is shown in Figure 4-4, and the resulting stiffness is Equation 4.2. In this approach,  $\Delta_{crit}$  is equal to the sum of  $\Delta_{T2}$ ,  $\Delta_{T3}$ ,  $\Delta_{T4}$ ,  $\Delta_{B2}$ ,  $\Delta_{B3}$ , and  $\Delta_{B4}$ .

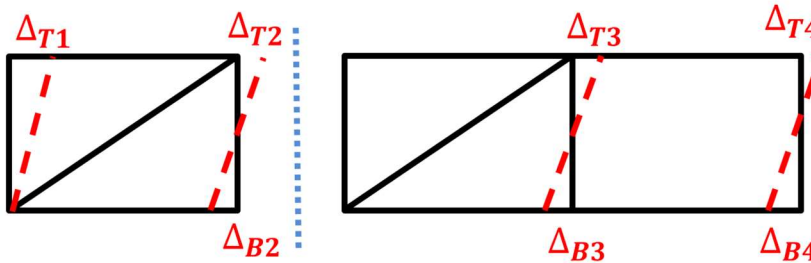


Figure 4-4. Displacement Combination Approach



$$\beta_{br} = \frac{Fh^2}{\Delta_{crit}} = \frac{Fh^2}{\frac{5FL_d^3}{S^2A_dE} + \frac{5FS}{A_sE}} \quad 4.2$$

### 4.1.3. Stiffness Superposition Approach

The third method is called the “Stiffness Superposition Approach” and is the least conservative of the four approaches. In this idealization, the cross-frame line is essentially broken into two single-cross-frame systems, and the respective stiffness values of each system are added together. This is shown for the four-girder, two-cross-frame system in Figure 4-5, with the resulting brace stiffness equation shown in Equation 4.3.

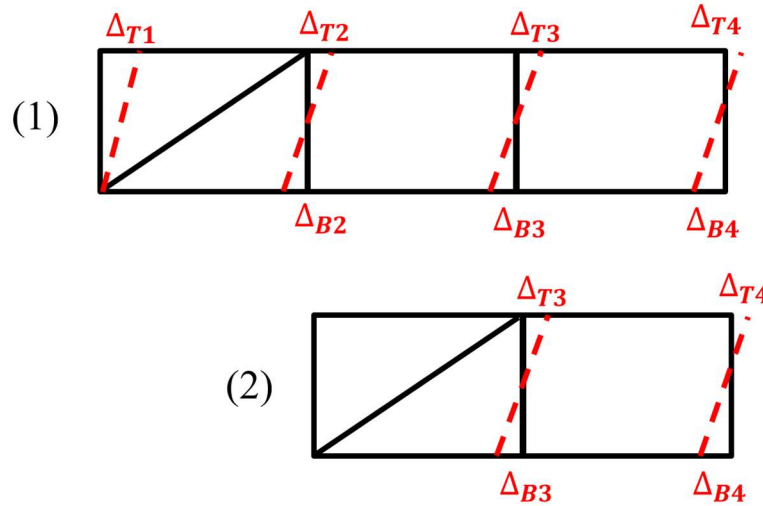


Figure 4-5. Stiffness Superposition Approach

$$\beta_{br} = \beta_{br1} + \beta_{br2} = \frac{Fh^2}{\frac{4FL_d^3}{S^2A_dE} + \frac{9FS}{A_sE}} + \frac{Fh^2}{\frac{3FL_d^3}{S^2A_dE} + \frac{4FS}{A_sE}} \quad 4.3$$

### 4.1.4. Cross-Frame Coefficient Approach

The fourth method is called the “Cross-Frame Coefficient Approach.” In this idealization, the system is idealized as a cross-frame line with the same number of girders as the real system with a single exterior cross-frame and the remaining bays lean-on. The stiffness of that cross-frame

line is then multiplied by the number of cross-frames present. This is shown for the four-girder, two-cross-frame system in Figure 4-7, with the resulting brace stiffness equation shown in Equation 4.4.

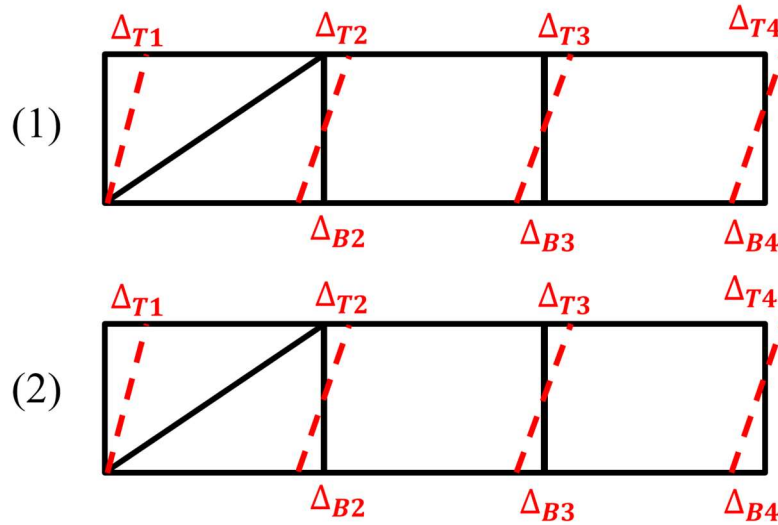


Figure 4-6. Cross-Frame Coefficient Approach

$$\beta_{br} = 2 \times \beta_{br1} = 2 \times \frac{Fh^2}{\frac{4FL_d^3}{S^2 A_d E} + \frac{9FS}{A_s E}} \quad 4.4$$

## 4.2. Comparison of Approaches

Given that the equation variability from the model is insensitive to the geometry of the system, the same representative dimensions were used to run additional preliminary models in order to narrow down the approaches to include in a parametric study. In addition to the four-girder system with two cross-frames, the stiffnesses of six-girder systems with two and three cross-frames were calculated based on the four approaches and compared against the respective full cross-frame model. Results are shown in Table 4-1. The “Cross-Section Slice” approach was shown to be conservative in all cases without being excessively conservative, and thus was selected for further study.

Table 4-1. Preliminary Comparison of Approaches:  $\beta_{br,approach}/\beta_{br,SAP\ model}$

	4G 2 CF	6G 2CF	6G 3CF
<b>SAP Model - Tension System</b>	1.0	1.0	1.0
<b>Helwig and Wang (1 CF)</b>	0.5	0.6	0.4
<b>Lean-On Guide Interpretation (Holt <i>et al.</i>, 2022)</b>	1.6	2.3	2.8
<b>Cross-Section Slice</b>	0.8	0.9	0.8
<b>Displacement Combination</b>	0.6	0.7	0.4
<b>Stiffness Superposition</b>	1.3	1.5	1.5
<b>Cross-Frame Coefficient</b>	1.0	1.2	1.2

### 4.3. Generalized Equation for Cross-Section Slice Approach

The method selected to account for multiple cross-frames in the lean-on brace stiffness equation is the “Cross-Section Slice” (CSS) approach, where a redundant cross-frame is essentially ignored. In order to construct a universally applicable equation, the cross-section slice approach was applied to Equation 3.5, to result in Equation 4.5. The  $n_{gc}$  term was substituted for separate terms representing the number of girders and the number of cross-frames separately.

$$\beta_{br,leanZ,CSS} = \frac{ES^2 h_b^2}{\frac{(n_g - n_c + 1)L_d^3}{A_d} + \frac{(n_g - n_c)^2 S^3}{A_s}} \quad 4.5$$

Where:

$n_g$  is the number of girders

$n_c$  is the number of cross-frames in the bracing line

### 4.4. Detailed Validation of CSS Approach for Z-Frames

A parametric study was conducted utilizing the representative cross-frame geometry discussed above. As discussed previously, the accuracy of the approach was found to be insensitive to the girder spacing, cross-frame height, and area of the cross-frame members. The remaining variable was the positioning of the cross-frame and lean-on struts along a cross-frame line. Various

cross-frame positions in girder systems ranging from two to sixteen girders were investigated. The results from the generalized CSS equation (Equation 4.5) were compared with finite element analysis results for varied cross-frame layouts. The stiffness obtained from the CSS equation was divided by the stiffness obtained from the SAP model to obtain a ratio where a value greater than one indicated the CSS equation was unconservative. Values less than or equal to one indicate an accurate or conservative expression. In all configurations, the equation was found to be exact or conservative. The analysis sets are discussed in detail below for a modulus of 29,000 ksi, an area of 6.45 in<sup>2</sup> for all members, girder spacing of 96 inches, and cross-frame depth of 76 inches. A discussion of the CSS validation is available in Gasser et al. (2024).

The exterior cross-frame position aligned to the left was studied first. One to nine cross-frames were positioned next to each other on one side of two to ten girder systems. The stiffnesses resulting from each of the three calculations were normalized against the model stiffness, such that a value greater than 1.0 would indicate the equation giving a larger stiffness than the model, which is unconservative. In this configuration, the CSS approach was always conservative. For layouts with exactly one cross-frame, the equation predicted the exact same stiffness as the model. For cross-frame lines with more cross-frames, the conservatism of the equation relative to the model increased to a maximum of 25%. The results are depicted in Figure 4-7. Example cross-sections for six-girder bridges are shown to the left of the plot. Note that the right plot includes results for layouts with two to ten girders.

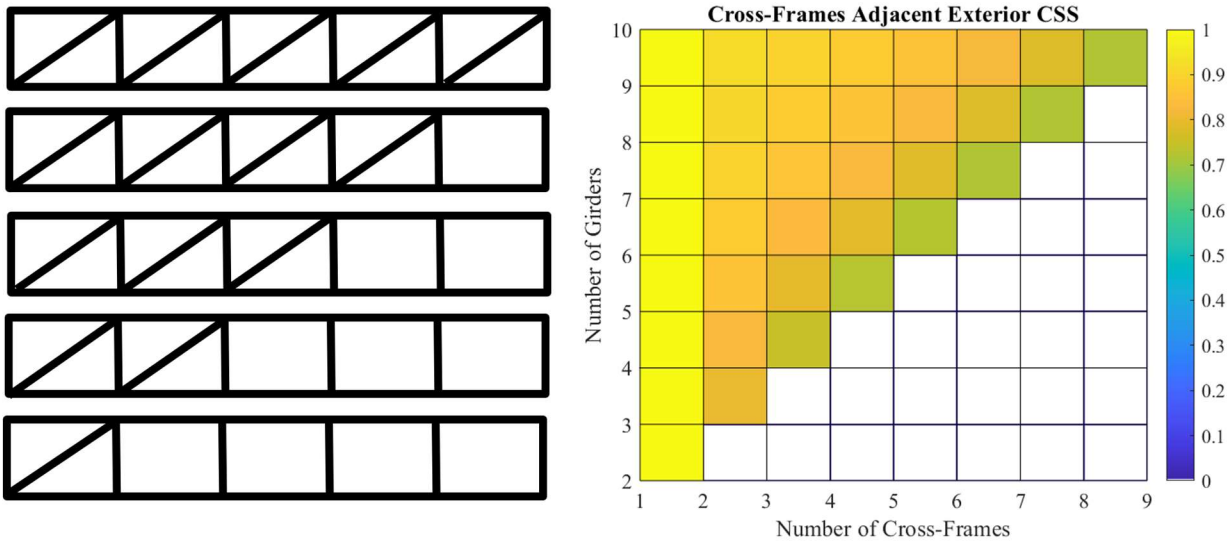


Figure 4-7.  $\beta_{br,leanZ,CSS} / \beta_{br,SAP\ model}$  for Exterior Z-Frames

Next, a similar approach was applied to a checkerboard pattern, with the cross-frame line bays alternating cross-frames and lean-on struts. In this layout, the least conservative configuration is an even number of girders missing cross-frames on ends. However, the equation was conservative for all layouts. The equation became increasingly more conservative with more girders, as shown in Figure 4-8. The left side of the figure illustrates six-girder layouts, and the right plot provides the result for layouts with two to eleven girders.

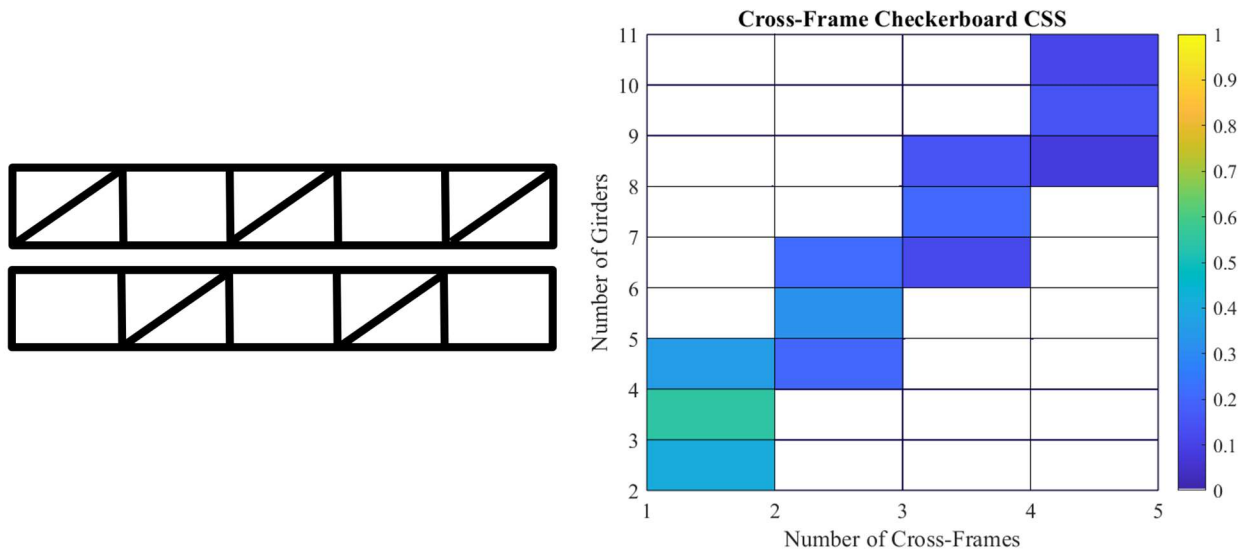


Figure 4-8.  $\beta_{br,leanZ,CSS}/\beta_{br,SAP model}$  for Checkerboard Z-Frames

Cross-frame placements for interior and exterior bays were compared, as depicted in Figure 4-9. Interestingly, the equation was most conservative for layouts with cross-frames placed in the two exterior bays, even compared to layouts with the same number of girders and more cross-frames placed in interior bays.

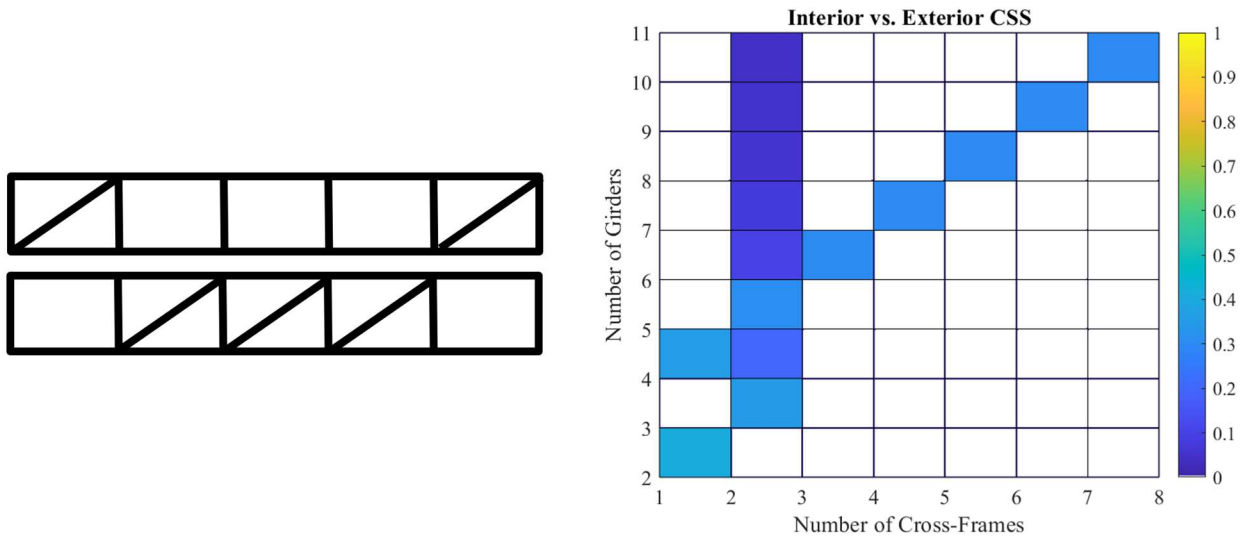


Figure 4-9.  $\beta_{br,leanZ,CSS}/\beta_{br,SAP model}$  for Interior and Exterior Z-Frames

In the next set of models, the number of cross-frames was kept constant, but the position of the cross-frame was changed. In the charts, the cross-frame axis was changed from the number of cross-frames to the position (or bay) of the first cross-frame in the line. In the case of the single cross-frame, the layouts with one cross-frame in the leftmost bay resulted in perfect agreement with the model, as this is the layout with which the equation was first derived. Results for cross-frame lines with one, two, and three cross-frames are shown in Figure 4-10, Figure 4-11, and Figure 4-12, respectively. The equation was more conservative for cross-frames placed in interior bays, and most conservative for cross-frames placed furthest from the pin support. This confirms that the limiting cross-section pattern is cross-frames aligned to one side, near the pin support.

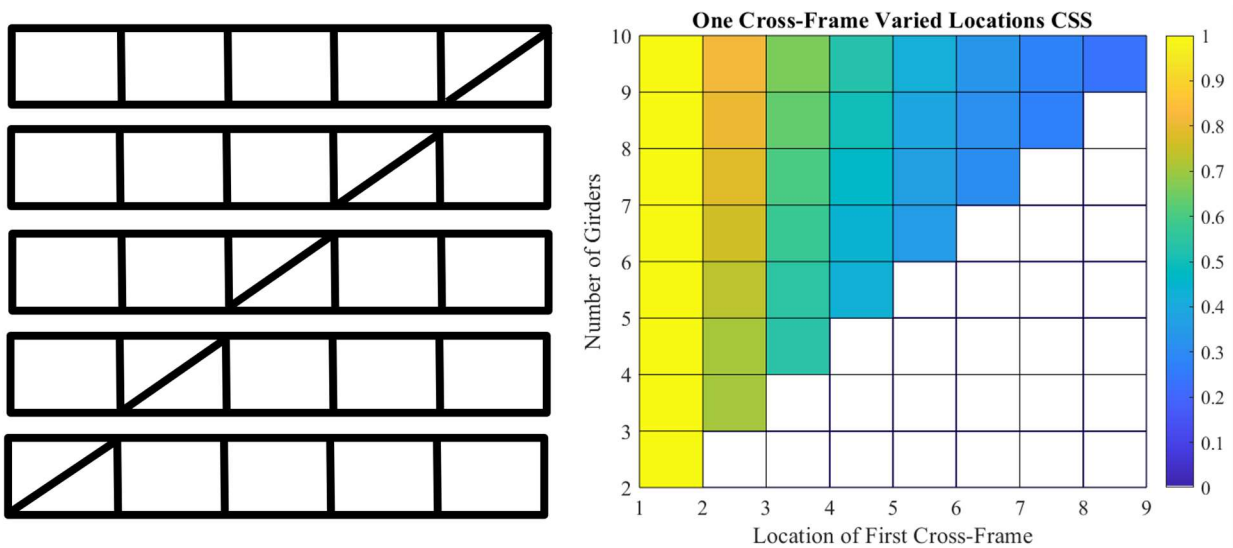


Figure 4-10.  $\beta_{br,leanZ,CSS}/\beta_{br,SAP\ model}$  for One Z-Frame Varied Location

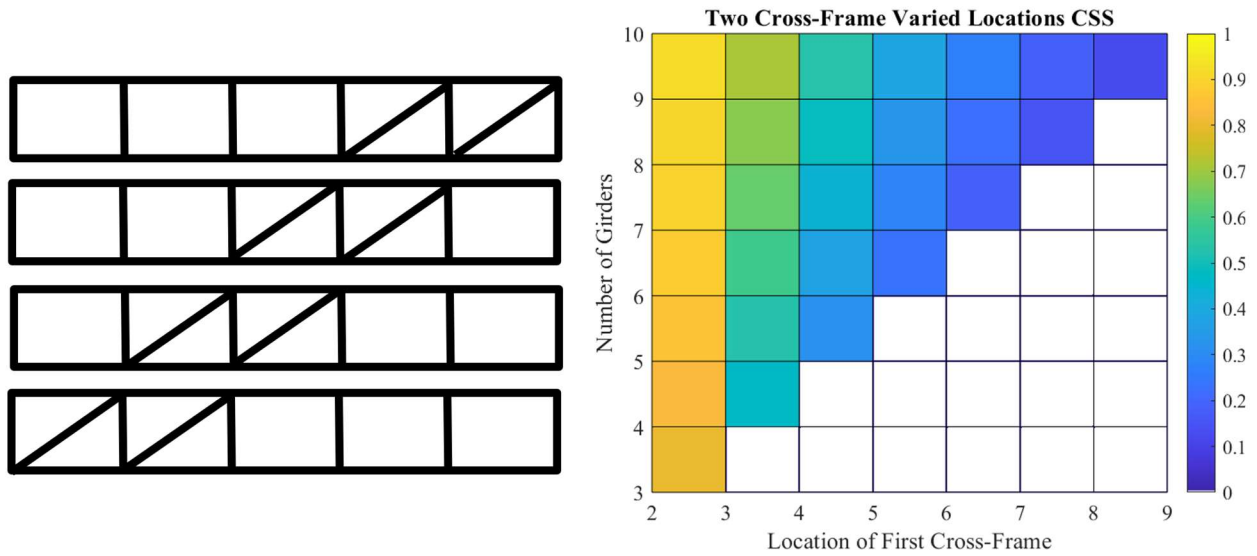


Figure 4-11  $\beta_{br,leanZ,CSS}/\beta_{br,SAP model}$  for Two Z-Frames Varied Location

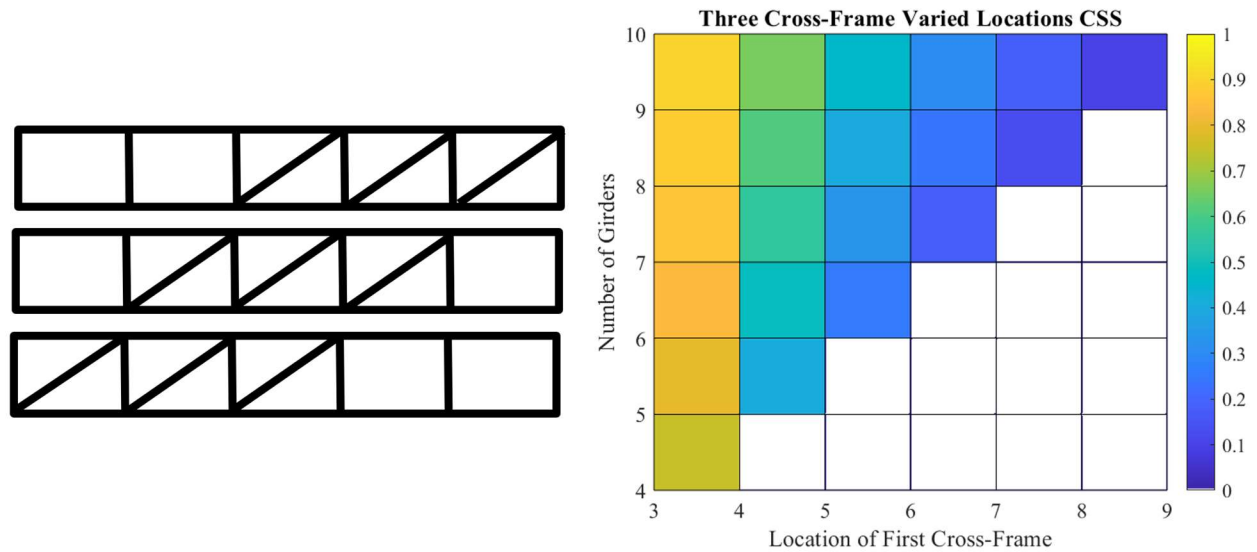


Figure 4-12.  $\beta_{br,leanZ,CSS}/\beta_{br,SAP model}$  for Z-Frames Three Cross-Frames Varied Location

Overall, the CSS equation results in perfect agreement with the SAP model for systems with only one exterior cross-frame and becomes increasingly conservative for systems approaching conventional bracing. The CSS approach results in the same stiffness value regardless



of cross-frame placement within the cross-frame line, as it is only dependent on the number of cross-frames and girders.

The limiting cross-frame placement was found to be “cross-frames aligned exterior” (Figure 4-7), which is where all of the cross-frames were placed in adjacent exterior bays. This results in the largest possible number of adjacent lean-on bays. In other configurations, the model predicted greater stiffness values, indicating that the CSS equation is even more conservative for cross-frames positioned near the interior or spaced out along the cross-frame line. Quantification of these stiffness increases is discussed in Chapter 5.

## 4.5. Validation of CSS Approach for Other Cross-Frame Shapes

---

The CSS approach was validated for X-frames and K-frames in addition to the Z-frame shape. The equations derived in the previous section were modified and generalized to account for the CSS approach, and the procedure comparing SAP models with the equations used for Z-frames was applied.

### 4.5.1. Lean-On K-Frames

In the K-frame lean-on derivation, the generalized displacement of the critical girder is given by Equation 4.6.

$$\Delta_{crit} = 2n_g \left( \frac{FL^3}{S^2 A_d E} \right) + \left[ \frac{1}{4} (n_g - 2) + \frac{n_g - 1}{2} + (n_g - 1)(n_g - 2) \right] \left( \frac{FS}{A_s E} \right) \quad 4.6$$

In order to apply the CSS approach and remove the implicit assumption of one cross-frame, the expression may be rewritten as Equation 4.7

$$\Delta_{crit} = 2(n_g - n_c + 1) \left( \frac{FL^3}{S^2 A_d E} \right) + \left[ \frac{1}{4} (n_g - n_c - 1) + \frac{n_g - n_c}{2} + (n_g - n_c)(n_g - n_c - 1) \right] \left( \frac{FS}{A_s E} \right) \quad 4.7$$

Which can be reduced to the form of Equation 4.8.

$$\Delta_{crit} = 2n_g \left( \frac{FL^3}{S^2 A_d E} \right) + \left[ n_g^2 + n_c^2 - 2n_g n_c - \frac{n_g}{4} + \frac{n_c}{4} - \frac{1}{4} \right] \left( \frac{FS}{A_s E} \right) \quad 4.8$$

This form can be used to determine the stiffness as Equation 4.9.

$$\beta_{br,leanK,CSS} = \frac{ES^2 h_b^2}{2(n_g - n_c + 1) \frac{L_d^3}{A_d} + \left( n_g^2 + n_c^2 - 2n_g n_c - \frac{n_g}{4} + \frac{n_c}{4} - \frac{1}{4} \right) \frac{S^3}{A_s}} \quad 4.9$$

The result when the stiffness given by Equation 4.9 is divided by the stiffnesses from a K-frame SAP model with the same cross-frames aligned exterior configuration is shown in Figure 4-13. The agreement between the equation and the SAP model is better than with the Z-frames, likely due to the ability of K-frame members to carry compression as well as tension to better distribute the forces across the adjacent cross-frames. There is perfect agreement in systems with just one cross-frame, and the minimum value in the plot is 0.83.

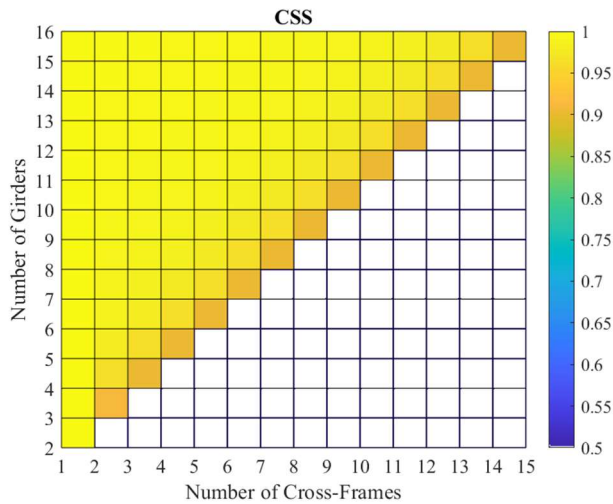


Figure 4-13.  $\beta_{br,leanK,CSS}/\beta_{br,SAP model}$  for K-Frames Cross-Frames Aligned Exterior

The expression in Equation 4.9 contains many terms, so for the purposes of simpler application, an alternative form of the expression where the last three values in the second term of the denominator are neglected is given by:

$$\beta_{br,leanK,CSS,reduced} = \frac{ES^2h_b^2}{2(n_g-n_c+1)\frac{L_d^3}{A_d}+(n_g-n_c)\frac{2S^3}{A_s}} \quad 4.10$$

The result for when the stiffness given by Equation 4.10 is divided by the stiffnesses from a K-frame SAP model with the same cross-frames aligned exterior configuration is shown in Figure 4-14. Similar trends are observed as for Equation 4.9, but the equation is more conservative, particularly for cross-frame lines with more cross-frames than lean-on bays. The maximum value in the plot is 0.98, and the minimum is 0.68.

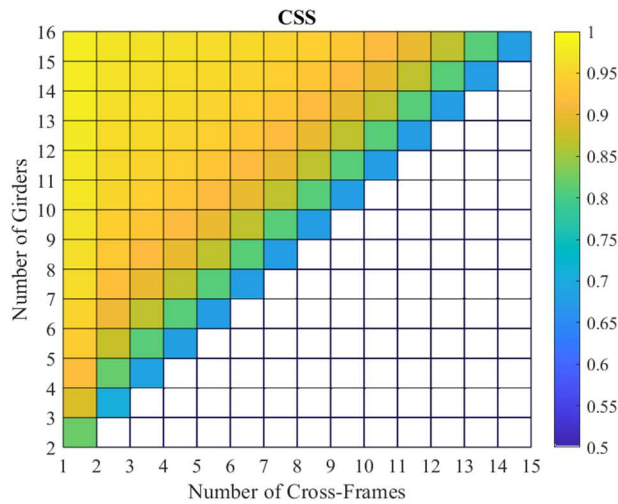


Figure 4-14.  $\beta_{br,leanK,CSS,reduced}/\beta_{br,SAP\ model}$  for Simplified K-Frame Equation Cross-Frames Aligned Exterior

### 4.5.2. Lean-On X-Frames

In a similar fashion to the K-frame equation, in the X-frame lean-on derivation, the generalized displacement of the critical girder is given by Equation 4.11

$$\Delta_{crit} = \frac{1}{2}n_g \left( \frac{FL^3}{S^2A_dE} \right) + \left[ \frac{1}{2}(n_g - 2) + \frac{n_g - 1}{2} + (n_g - 1)(n_g - 2) \right] \left( \frac{FS}{A_sE} \right) \quad 4.11$$

In order to apply the CSS approach and remove the implicit assumption of one cross-frame, the expression may be rewritten as Equation 4.12.

$$\Delta_{crit} = \frac{1}{2}(n_g - n_c + 1) \left( \frac{FL^3}{S^2A_dE} \right) + \left[ \frac{1}{2}(n_g - n_c - 1) + (n_g - n_c)(n_g - n_c - 1) \right] \left( \frac{FS}{A_sE} \right) \quad 4.12$$

Which can be reduced to the form of Equation 4.13.

$$\Delta_{crit} = \frac{1}{2}(n_g - n_c + 1) \left( \frac{FL^3}{S^2A_dE} \right) + \left[ n_g^2 + n_c^2 - 2n_gn_c - \frac{n_g}{2} + \frac{n_c}{2} - \frac{1}{2} \right] \left( \frac{FS}{A_sE} \right) \quad 4.13$$

This form can be used to determine the stiffness as Equation 4.14.

$$\beta_{br,leanX,CSS} = \frac{ES^2h_b^2}{\frac{1}{2}(n_g - n_c + 1) \frac{L_d^3}{A_d} + \left( n_g^2 + n_c^2 - 2n_gn_c - \frac{n_g}{2} + \frac{n_c}{2} - \frac{1}{2} \right) \frac{S^3}{A_s}} \quad 4.14$$

The result for when the stiffness given by Equation 4.14 is divided by the stiffnesses from an X-frame SAP model with the same cross-frames aligned exterior configuration is shown in Figure 4-15. The agreement between the equation and SAP model is again better than with the Z-frames, likely due to the X-frame members ability to carry compression as well as tension to better distribute the forces across the adjacent cross-frames. There is perfect agreement in systems with just one cross-frame, and the minimum value in the plot is 0.85.

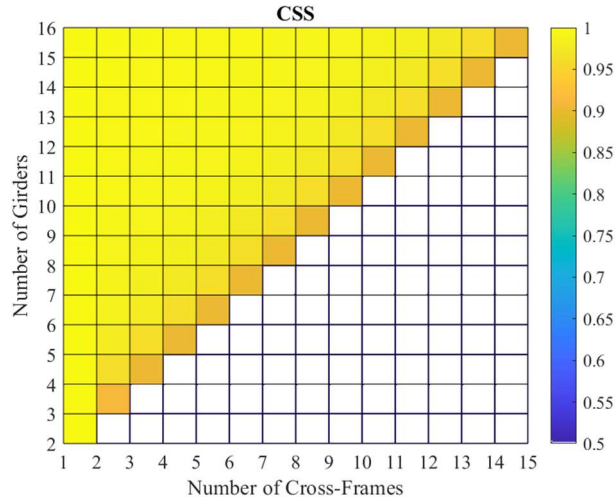


Figure 4-15.  $\beta_{br,leanX,CSS}/\beta_{br,SAP\ model}$  for X-Frames Cross-Frames Aligned Exterior

The expression in Equation 4.14 contains many terms, so for the purposes of simpler application, an alternative form of the expression where the last three values in the second term of the denominator are neglected is given by:

$$\beta_{br,leanX,CSS,reduced} = \frac{ES^2 h_b^2}{\frac{1}{2}(n_g - n_c + 1) \frac{L_d^3}{A_d} + (n_g - n_c) \frac{2S^3}{A_s}} \quad 4.15$$

The result for when the stiffness given by Equation 4.15 is divided by the stiffnesses from an X-frame SAP model with the same cross-frames aligned exterior configuration is shown in Figure 4-16. Similar trends are observed as for Equation 4.14, but the equation is more conservative. The maximum value in the plot is 0.97, and the minimum is 0.57.

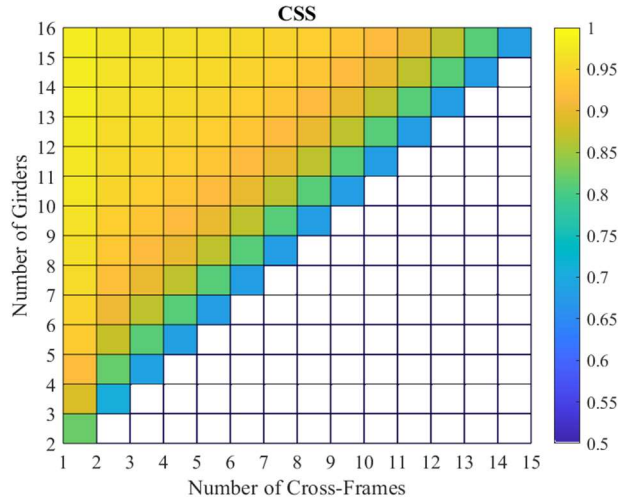


Figure 4-16.  $\beta_{br,leanX,CSS,reduced}/\beta_{br,SAP\ model}$  for Simplified X-Frame Equation Cross-Frames  
Aligned Exterior

#### 4.6. Summary of CSS Equation

The reduced expressions for all three cross-frame types are similar in form. Therefore, it is possible to write the generalized brace stiffness equation given by Equation 5.2, which accounts for any shape and number of cross-frames. The varying coefficients for each cross-frame type are implemented with the cross-frame type coefficient  $C_{CF}$ .

$$\beta_{br,lean,CSS} = R \frac{ES^2 h_b^2}{C_{CF}(n_g - n_c + 1) \frac{L_d^3}{A_d} + (n_g - n_c) \frac{2S^3}{A_s}} \quad 4.16$$

Where:

$R$  is the stiffness reduction factor for connection eccentricity, 0.65

$C_{CF}$  is the cross-frame type coefficient: 1.0 for Z-Frames, 0.5 for X-Frames, and 2.0 for K-Frames

$n_g$  is the number of girders

$n_c$  is the number of cross-frames in a given bracing line

## **Chapter 5. Lean-On Brace Stiffness Equation Modifications for Interior Bay Cross-Frames**

The appropriate modification to the brace stiffness equation to account for the inclusion of more than one cross-frame in a given bracing line was discussed in the previous chapter. While the cross-section slice equations significantly decreased the excessive conservatism in the equations for multiple Z, X, and K-frames, the location of the cross-frame in the line was not precisely accounted for. The cross-frames were conservatively assumed to be located in adjacent exterior bays. The impact of this assumption and appropriate adjustments to the expression for the placement of the cross-frames are discussed in the following sections.

### **5.1. Performance of Cross-Section Slice with Interior Cross-Frame Placement**

When a single cross-frame is placed near the middle bay of the cross-frame line, as opposed to in an exterior bay, the forces in several of the top and bottom struts are reduced. This reduction in the force distribution results in an increased stiffness of the system. However, the equations derived in Sections 3.1 and 3.2 and with the CSS approach do not take this into account. A comparison of stiffness results from SAP models with the equation for constant cross-frame dimensions is shown in Figure 5-1 for one, two, and three Z, X, or K-frames positioned in the middle of the cross-frame line. As shown, in some cases, the equation indicates as low as one-third of the stiffness of the model due to only changing the location of the cross-frame(s) in the bracing line. The different cross-frame shapes are shown to behave similarly, but the equation is consistently most conservative for X-Frames and least conservative for Z-frames.

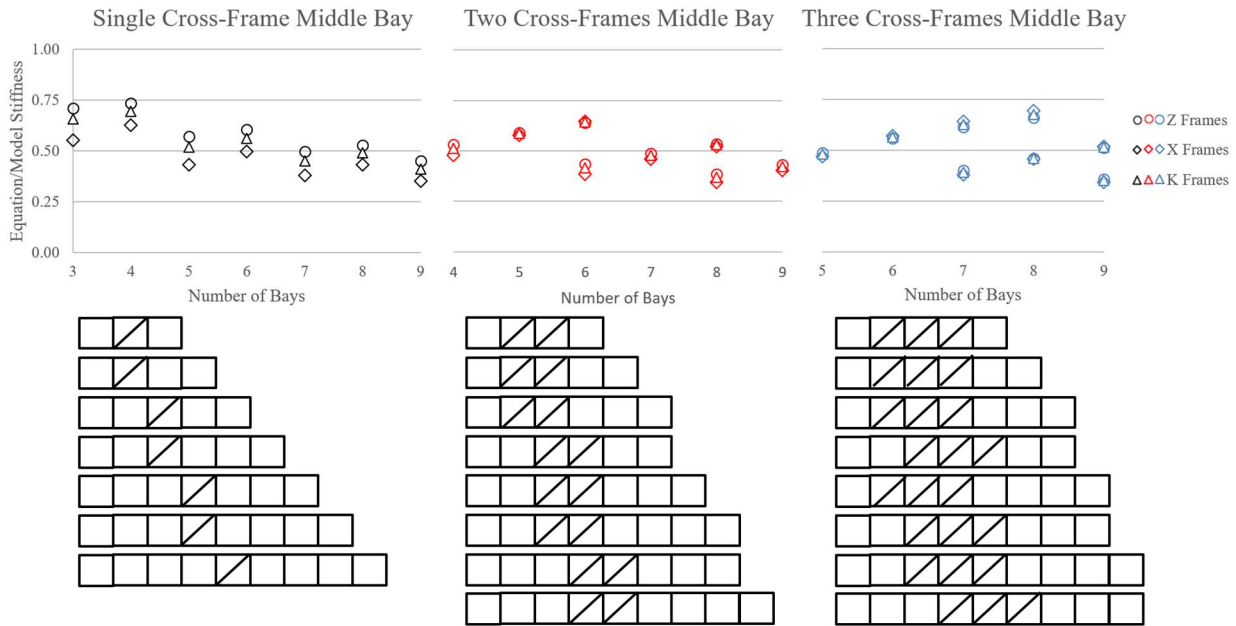


Figure 5-1. Brace Stiffness Increase due to Interior Cross-Frame Placement

The plots in Figure 5-1 are superimposed in Figure 5-2 to compare the significance of the number of cross-frames on the stiffness of the system. Overall, the equation predicts 34 to 73% of the stiffness indicated by the model. The results vary depending on the number of bays in the system. For systems with an even number of bays, systems with two cross-frames have the highest stiffness relative to the equation, while systems with an odd number of bays have the highest stiffness relative to the equation for one or three cross-frames. These are configurations where the cross-frames are perfectly centered in the bracing line. Additional study was conducted in order to reduce the variation in performance of the equation and reduce the level of conservatism to a more reasonable level.



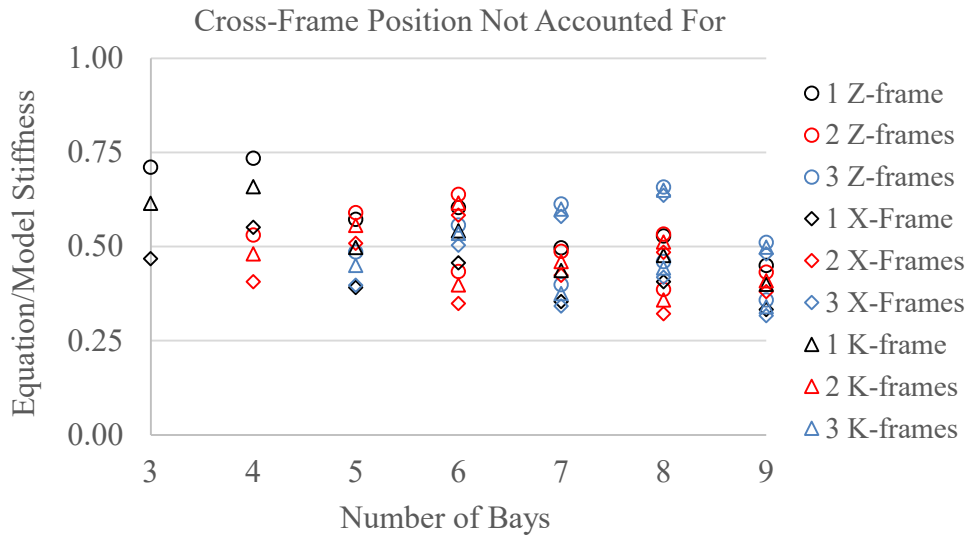


Figure 5-2. Overlay of Brace Stiffness Increase due to Interior Cross-Frame Placement

### 5.1.1. Revised Idealizations and Equation

An updated idealization of the cross-frame line was proposed in order to account for the stiffness variance depending on the cross-frame position. Examples are shown in Table 5-3. A revised equation reflecting these changes is given by Equation 5.1. An  $n_{lean}$  term was introduced in the denominator of the equation in the term corresponding to the lean-on struts. This value is defined as the maximum number of adjacent lean-on bays in the cross-frame line and helps account for the stiffness increase (reduced number of adjacent lean-on bays) provided by an interior cross-frame placement. The coefficient of the second term in the denominator of the CSS equation was  $n_g - n_c$ . When all of the cross-frames are aligned to one side, this is equal to  $n_{lean} + 1$ . When the cross-frames are moved to an interior bay,  $n_{lean}$  is reduced, unlike the coefficient  $n_g - n_c$ . This allows the expression to account for the effect of cross-frame placement along the bracing line.

Table 5-1. Revised CSS Idealization

Real System	$n_g$	$n_c$	CSS Equation Idealization	$n_{lean}$	Revised CSS Idealization
	8	7		0	
	8	2		5	
	8	1		3	
	8	2		3	
	8	3		2	

$$\beta_{br,lean} = \frac{ES^2 h_b^2}{C_{CF}(n_g - n_c + 1) \frac{L_d^3}{A_d} + (n_{lean} + 1) \frac{2S^3}{A_s}} \quad 5.1$$

Where:

$n_{lean}$  is the maximum number of adjacent lean-on bays (or leaning girders)

### 5.1.2. Modified Equation Performance

The revised expression substantially reduces the error relative to the model for Z, X, and K-frames, while still maintaining a conservative value. The revised equation predicts 66 to 100% of the value indicated by the model, which is a significant improvement in performance. Layouts that have perfectly centered cross-frames are most conservative, while layouts with off-center cross-frames approach the same value as the model. Additionally, some of the conservatism is due to the simplification of the expression for X- and K-frames.

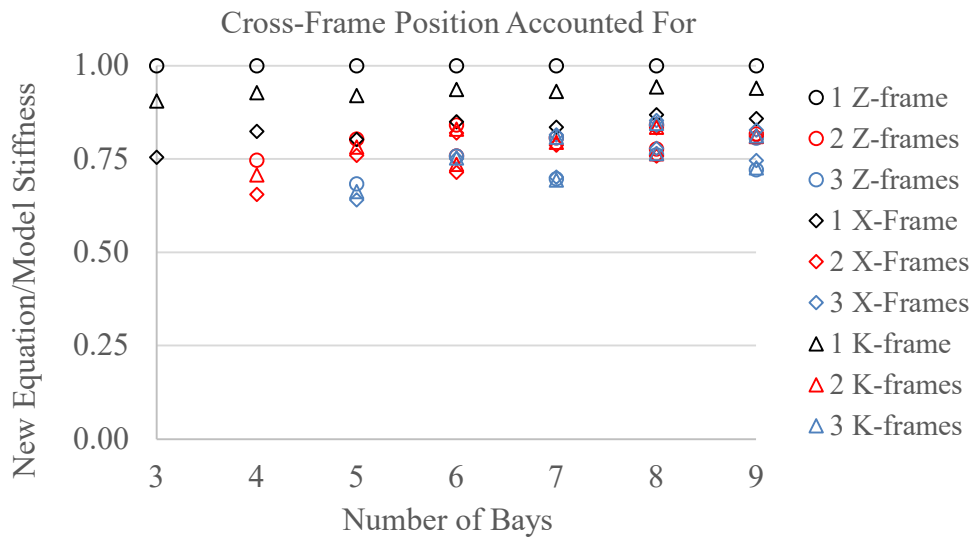


Figure 5-3. Modified Brace Stiffness Equation with Interior Cross-Frames

## 5.2. Adjustments for Nonadjacent Cross-Frames

The cross-section slice approach was observed to be excessively conservative for cross-frame lines with nonadjacent cross-frames, such as in the checkerboard and X layouts (discussed in Chapter 8). The equation was studied and adjusted to increase precision without compromising the simplicity of the equation application.

### 5.2.1. Checkerboard Layouts

Cross-frame patterns that would be included in a Checkerboard layout using Z-, X-, or K-frames were modeled. The respective stiffnesses were calculated using the displacement of the critical girder, which is consistent with the method used previously. These values are shown in Figure 5-4, where the cross-frame line patterns are indicated using “0” to designate lean-on bays and “1” to designate cross-frames. The stiffnesses of the models of the full cross-frame lines were compared with the stiffnesses of models of a single cross-frame.



Figure 5-4. Model Stiffness of Checkerboard Bracing Lines

A significant reduction in stiffness can be observed for cross-frame lines with lean-on bays on both exterior bays. With this distinction, checkerboard cross-frame lines can be split into two groups: (1) lines with cross-frames in one or both of the exterior bays, or (2) lines with lean-on struts in both of the exterior bays. The cross-frame lines in the first group may be idealized as a single cross-frame, while the lines in the second group may be idealized as a single cross-frame with a lean-on bay on each side. To confirm this, the SAP model stiffnesses were divided by the idealized stiffness equation and plotted, as shown in Figure 5-5. Values in the plot that are less than or equal to 1.0 indicate the equation predicts a lower stiffness than the model, and the two values greater than 1.0 are within 10%.

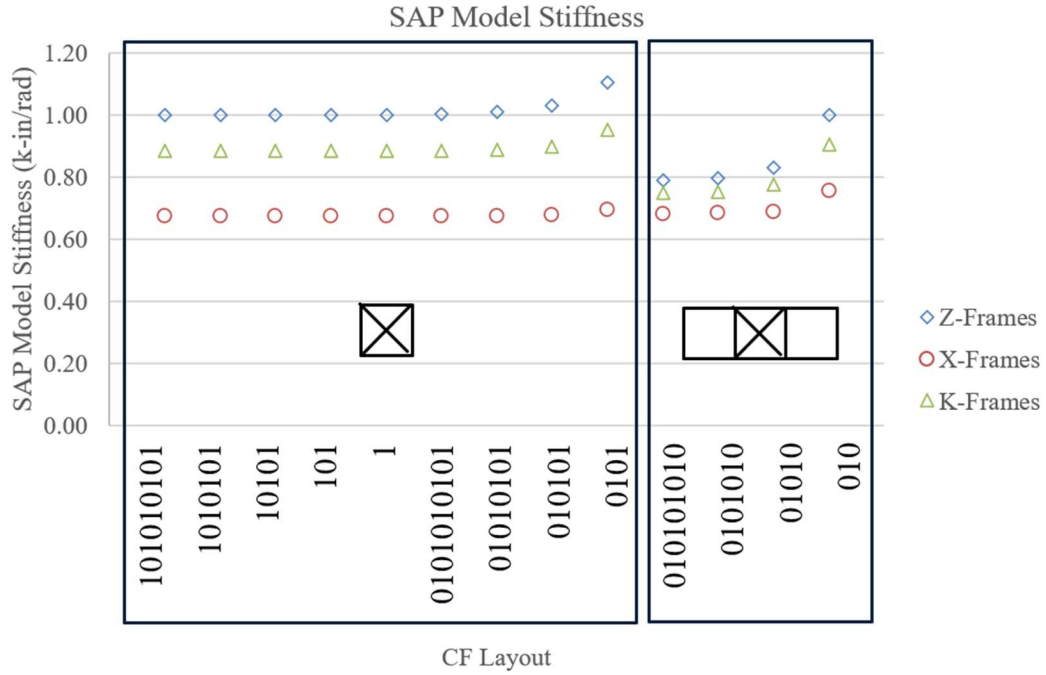


Figure 5-5. Checkerboard Model Stiffness/Idealized Stiffness

As a result, it is appropriate to use “effective” values of  $n_{g,eff} = 2$ ,  $n_{c,eff} = 1$ , and  $n_{lean,eff} = 0$  for checkerboard cross-frame lines with at least one exterior bay with a cross-frame. For lines with two lean-on exterior bays,  $n_{g,eff} = 4$ ,  $n_{c,eff} = 1$ , and  $n_{lean,eff} = 1$  are the effective values. These findings are summarized in Table 5-2.

Table 5-2. Effective Values for Checkerboard Patterns

Number of Bays	Exterior Bay Cross-Frames	Example Patterns	Appropriate Idealization	Equation Values
Odd	2 Cross-Frames			$n_{g,eff} = 2$ $n_{c,eff} = 1$ $n_{lean,eff} = 0$
Even	1 Cross-Frame, 1 Lean-On			$n_{g,eff} = 2$ $n_{c,eff} = 1$ $n_{lean,eff} = 0$
Odd	2 Lean-On			$n_{g,eff} = 4$ $n_{c,eff} = 1$ $n_{lean,eff} = 1$

### **5.2.2. Other Nonadjacent Cross-Frame Patterns**

A similar analysis was conducted for other nonadjacent cross-frame patterns. These remaining instances are grouped into cross-frame lines where greater than 50% of bays contain cross-frames and both exterior cross-frames contain cross-frames, cross-frame lines where less than 50% of bays contain cross-frames and both exterior cross-frames contain cross-frames, and instances where one or both exterior bays are lean-on. For cross-frame lines where greater than 50% of bays and both exterior bays contain cross-frames, the twin girder idealization may be used. When less than 50% of bays contain cross-frames, and both exterior bays contain cross-frames, the effective number of adjacent lean-on bays in the system may be reduced to reflect the governing section, meaning that the maximum number of adjacent lean-on bays may be divided by two, and rounded up to the nearest whole number. When an exterior bay contains lean-on with any percentage of cross-frames, the effective numbers of girders and cross-frames may not be reduced, but the effective number of adjacent lean-on bays may be treated as in the previous case if adjacent lean-on bays are bounded on both sides by cross-frames. Examples of these three cases are shown in Table 5-3.

Table 5-3. Example Idealizations for Non-Checkerboard Nonadjacent Cross-Frame Patterns

% Cross-Frames in Brace Line	Exterior Bay Cross-Frames	Example Pattern	Example Idealization	Equation Values
> 50%	2 Cross-Frames			$n_{g,eff} = 2$ $n_{c,eff} = 1$ $n_{lean,eff} = 0$
				$n_{g,eff} = 2$ $n_{c,eff} = 1$ $n_{lean,eff} = 0$
≤ 50%	2 Cross-Frames			$n_{g,eff} = 8$ $n_{c,eff} = 3$ $n_{lean,eff} = 2$
				$n_{g,eff} = 8$ $n_{c,eff} = 3$ $n_{lean,eff} = 2$
Any	1 or 2 Lean-On			$n_{g,eff} = 8$ $n_{c,eff} = 3$ $n_{lean,eff} = 2$
				$n_{g,eff} = 8$ $n_{c,eff} = 4$ $n_{lean,eff} = 2$

### 5.3. Summary of Brace Stiffness Equation

With the adjustment for effective numbers of girders, cross-frames, and lean-on bays, the final generalized brace stiffness equation is given by Equation 5.2.

$$\beta_{br,lean} = R \frac{ES^2 h_b^2}{C_{CF}(n_{g,eff} - n_{c,eff} + 1) \frac{L_d^3}{A_d} + (n_{lean,eff} + 1)^2 \frac{S^3}{A_s}} \quad 5.2$$

Where:

$R$  is the stiffness reduction factor for connection eccentricity, 0.65

$C_{CF}$  is 1.0 for Z-Frames, 0.5 for X-Frames, and 2.0 for K-Frames

$n_{g,eff}$  is the effective number of girders

$n_{c,eff}$  is the effective number of cross-frames in a given bracing line

$n_{lean,eff}$  is the effective number lean-on bays

It is important to note that in lean-on systems, even when a full cross-frame line is present, the  $C_{nc}$  factor for conventional bracing cannot be used. Examples of correct  $n_{g,eff}$ ,  $n_{c,eff}$ , and  $n_{lean,eff}$  values for given bracing lines are shown in Table 5-4.

Table 5-4. Correct Values for Brace Stiffness Equation

Cross-Frame Line Pattern Category	Example Cross-Frame Line	$n_{g,eff}$	$n_{c,eff}$	$n_{lean,eff}$
Adjacent: Exterior Bay Cross-Frame		8	3	4
Adjacent: Interior Bay Cross-Frame		8	2	3
Checkerboard: $\geq 1$ Exterior Cross-Frame		2	1	0
Checkerboard: No Exterior Cross-Frame		4	1	1
Nonadjacent: 2 Exterior Cross-Frames and $> 50\%$ Cross-Frames		2	1	0
Nonadjacent: 2 Exterior Cross-Frames and $\leq 50\%$ Cross-Frames		8	3	2
Nonadjacent: $\leq 1$ Exterior Lean-On		8	3	3



## **Chapter 6. Field Instrumentation**

With revised brace stiffness equations validated for individual cross-frames, the next step was to develop detailed models of complete bridge systems to assess the performance of the brace stiffness in combination with the in-plane girder stiffness. This chapter includes detailed descriptions of the instrumentation and field assessment of three bridges utilizing lean-on bracing, with the validation of detailed ABAQUS models for each included in Chapter 7.

### **6.1. Identification of Existing Lean-On Bridges**

---

In an effort to identify existing bridge designs utilizing lean-on bracing, as well as to gather information about the experiences of bridge engineers with existing design guidance, the research team conducted interviews and released an electronic survey in 2021. Three Texas Bridges utilizing lean-on bracing were identified in addition to the Lubbock bridges, of which the research team was already familiar.

Engineers who were engaged in recent lean-on design applications provided information regarding the issues with interpreting and applying existing lean-on expressions in the design of a bridge over the Brazos River on SH 105. The lean-on system was designed primarily using the existing design expressions as developed by Helwig and Wang (2003). As a result of discussions with the engineers involved in the design, there were a few specific points of difficulty (specifically regarding the application of the current design expressions):

1. The role/implementation of multiple cross-frames within a given bracing line
2. Impact of girder continuity
3. Effect of non-prismatic girder cross-sections

Based upon uncertainties in the potential behavior of the bridge during construction, the design team revisited their original analysis and design. During this process, concerns were raised about the stability of the system during deck casting. Due to the girders and cross-frames having already been fabricated, coupled with the simplistic nature of the existing design expressions, the design team conducted detailed finite element analyses (FEA) of the system to confirm that the bridge would be sufficiently stable.

Another application of lean-on bracing was a bridge on Chisholm Trail Parkway at FM 1902B, south of Fort Worth, Texas. The designer provided information from an electronic survey documenting the experience with lean-on bracing. The bridge was designed using the FEA program LARSA. Lean-on bracing was chosen for the purpose of handling heavy skew and minimizing fatigue effects. The designer utilized the Steel Bridge Design Handbook (Helwig and Yura, 2015) and previous project documents to complete the design.

Lean-on bracing was also used on an overpass to IH35 E south of downtown Dallas. The lean-on system was designed primarily using finite element analysis. With proper modeling decisions, a 3D model inherently accounts for the impact of many of the parameters not yet fully accounted for in the original design expressions as developed by Helwig and Wang (2003). The existing design expressions, however, were used as a “check” of the FEA results.

The survey received responses from several states, including engineers from Alaska, Arkansas, Connecticut, Florida, Illinois, Kentucky North Carolina, Pennsylvania, Tennessee Texas, Virginia, and Wisconsin. Of these responses, only a few had completed lean-on bracing projects, and fewer still had designed bridges while primarily utilizing the existing design

expressions. Concerns were raised by those who had completed lean-on bracing projects about how to appropriately calculate the brace stiffness at various locations within the structure.

In response to a question about the reason for choosing lean-on bracing for their project, the primary reason identified was the benefit in heavy skew scenarios, followed by economy and facilitating erection, and the lowest priority was general fatigue performance. There were other reasons mentioned, including bridge widening and controlling deflection differentials. Designers utilized TxDOT Report 0-1772 (Helwig and Wang, 2003), the Steel Bridge Design Handbook (Helwig and Yura, 2015), previous project documents, and class notes to aid in the design process, but survey respondents noted that designing lean-on bracing required similar or more effort relative to conventional bracing.

Regarding the responses from those who had not been a part of a lean-on bracing design project, all desired additional insight into lean-on bracing design concepts. However, many of the respondents noted the lack of confidence in lean-on bracing from government DOTs and practicing engineers due to the following reasons:

1. A formal procedure for designing all types of bracing
2. A dependence on knowing a contractor's erection plan and the discrepancies between an assumed and desired erection sequence
3. Lack of coverage in the AASHTO Bridge Design Specifications

Although the research team continued the effort to identify a lean-on bridge currently in the construction phases, no active projects were identified that coincided with the duration of the research project. As such, the team moved forward with the field instrumentation of two completed Texas bridges. A brief background on prior instrumentation of a lean-on bracing system and the

instrumentation of the SH 105 Brazos River Bridge and the Chisholm Trail bridge are provided in the next sections. The research team had access to data from TxDOT Project 5-1772 on bridges in Lubbock, Texas, a field monitoring study on the first lean-on bridges constructed in Texas. Data gathered from the field instrumentations was used to validate models to be utilized in parametric studies on lean-on bracing, and findings are discussed in Chapter 7.

## **6.2. Lubbock Bridge**

---

### **6.2.1. Background**

The 19<sup>th</sup> Street West Bound Bridge in Lubbock, TX (referred to as the Lubbock bridge), was instrumented as part of TxDOT Project 5-1772, which was the implementation study for TxDOT Project 0-1772, Cross-Frame and Diaphragm Behavior in Bridges with Skewed Supports. Romage (2008) provides a detailed discussion of the sensor layout for the project, where the instrumented cross-frames were chosen based on the critical design cases. The critical locations were the intermediate brace near the support and the braces closest to midspan, due to the girder moments and bracing layout. The lean-on equations discussed in Chapter 2 were used to size the cross-frame members, and the controlling angle size was used throughout the structure. It is important to note that this bridge has a 60-degree skew, resulting in different critical cases compared to a non-skewed bridge.

These governing cases resulted in the instrumentation of the cross-frames designated in Figure 6-1. Because a given bracing line consists of bays with cross-frames and bays with only top and bottom struts, it is necessary to use specific designations to present the bracing layout. The cross-frames (designated X#), struts (designated S#), and girders (designated G#) were instrumented with strain gages, as shown in Figure 6-2 and Figure 6-3. The # following each member designator provides an indication of the strut or cross-frame number. Tilt sensors were

used to measure girder rotations at locations labeled “TS,” and laser distance meters were used to measure global deflections at locations designated A through K. “M” and “D” are used to designate multiplexers and dataloggers used for data acquisition. The laser distance meters provide distance measurements used to estimate girder deflections with a reading accurate to 1/32 in. Readings at each location are taken with the bridge unloaded and with the trucks in position, and the girder deflection is determined from the difference. Three readings are taken and averaged to obtain each measurement. The elastic strain readings from the sensors were used to determine the stresses/forces in the cross-frames during deck placement and during a live load test after the deck had cured.

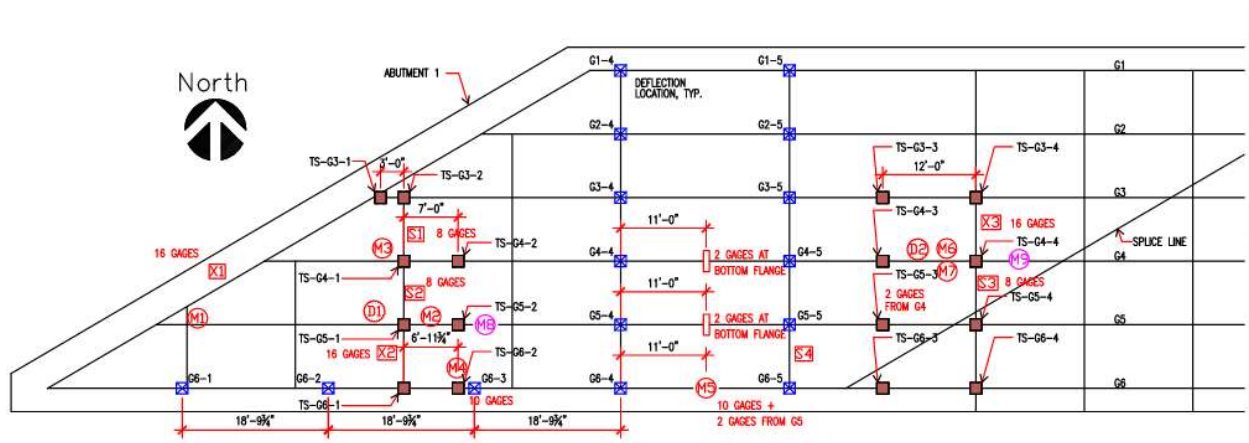


Figure 6-1. Lubbock Bridge Instrumentation Plan (Romage, 2008)

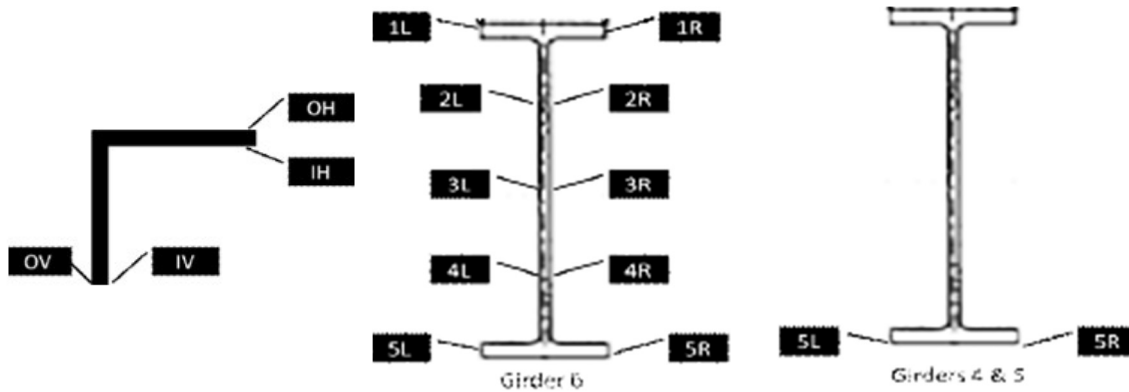


Figure 6-2. Lubbock Bridge (a) Brace Angle and (b) Girder Gage Locations (Romage, 2008)

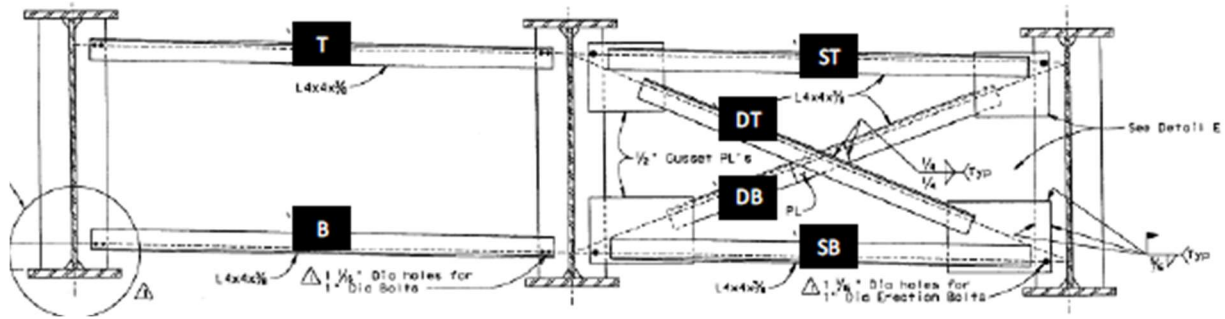


Figure 6-3. Lubbock Bridge Strut and Cross-Frame Strain Gage Locations (Romage, 2008)

### 6.2.2. Data Archive

Two cross-frame lines (CFL) were instrumented on the Lubbock Bridge: CFL #3 and CFL #7. Construction and live load data were collected for these cross-frames (Romage, 2008). During construction, a timeline for the pour is estimated based on field notes, and the assumed rate is 48 feet per hour over approximately 6 hours. Strain data was collected during the pour, but deflections were not.

Live load testing occurred in several stages due to the substantial number of cases tested, which can be subdivided by gridline number and truck positioning. The gridlines were positioned every 20 feet perpendicular to the longitudinal axis of the bridge, as shown in Figure 6-4. In total, there were 24 gridlines. The trucks were positioned in 6 different configurations with schematics provided in Appendix A.

- Staggered ahead station
- Staggered behind station
- Side-by-side south
- Side-by-side north
- End-to-end south
- End-to-end central

For a preliminary analysis, the research team on this project focused on the gridline subset with the largest axial forces, Grid #7.

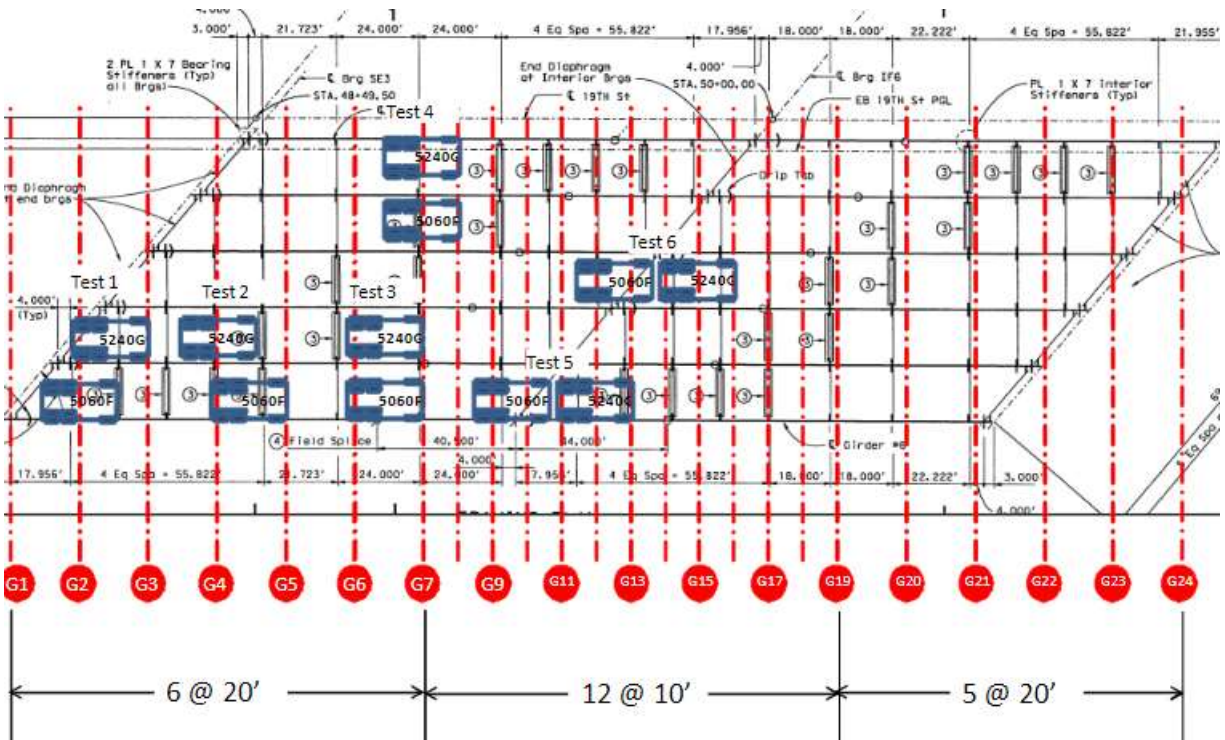


Figure 6-4. Lubbock Bridge Truck Positions (Romage, 2008)

### 6.3. SH 105 Bridge at Brazos River

#### 6.3.1. Overview

The bridge on SH 105 at the Brazos River is a three-span steel plate girder structure utilizing lean-on bracing, with prestressed concrete girder approach spans. A plan view of the three steel spans (denoted 6, 7, and 8) are shown in the framing plan in Figure 6-5, and a typical transverse section is shown in Figure 6-6. The spans are 234 feet, 300 feet, and 234 feet, respectively. The bridge is a five-girder system, with each bay braced by a full cross-frame

(denoted by a thicker line in the framing plan) or struts (denoted by a thinner line). The bracing layout of span 8 is a mirror image of span 6.

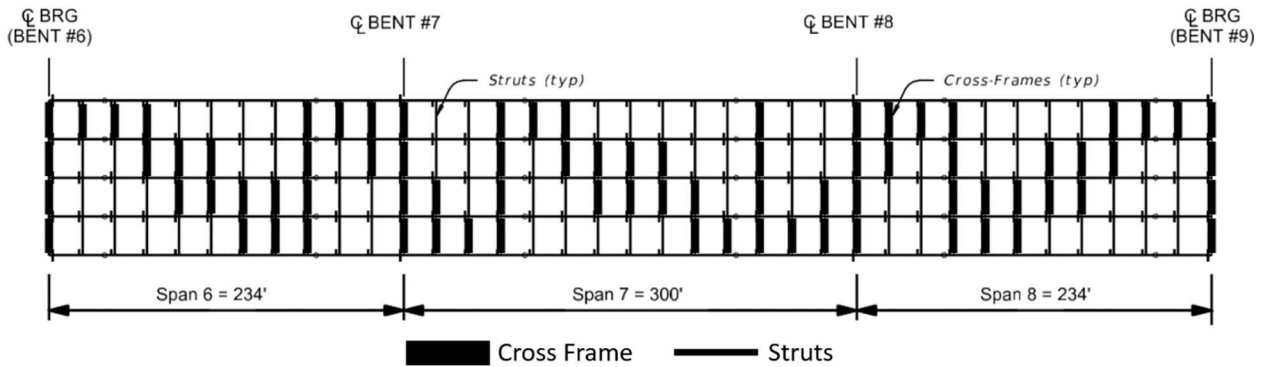


Figure 6-5. SH 105 Bridge Framing Plan

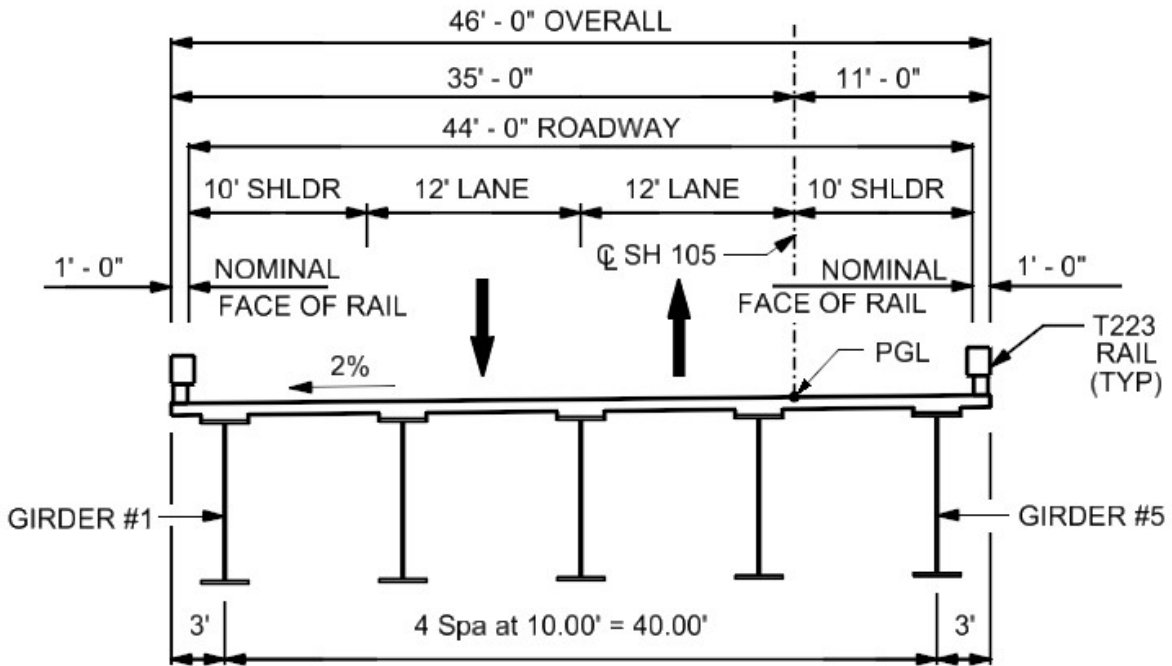


Figure 6-6. Typical Transverse Section on SH 105 Bridge

Prior to instrumentation, the research team visited the SH 105 bridge to inspect the site for accessibility. Figure 6-7 and Figure 6-8 are photographs taken by the research team on September



24, 2020. As shown in the pictures, Spans 7 and 8 cross over the Brazos River, and as such, are not conveniently accessible. Span 6, however, extends over a flat grassland, which allowed for a simpler method of accessing the bridge members for instrumentation.



Figure 6-7. SH 105 Bridge Span 7-8



Figure 6-8. SH 105 Bridge Span 6

**6.3.2. Sensor Layout**

The purpose and scheme for the instrumentation of the bridge on SH 105 at the Brazos River is similar to that of the 19<sup>th</sup> Street Westbound Bridge discussed in the previous section.

Measurements from strain gages were utilized for determining the force distribution in select girders, cross-frames, and struts. Girder displacements were also measured in order to quantify global behavior.

To determine an efficient placement of the strain gages, a preliminary analysis to estimate the girder moments and global displacements was considered, as differential vertical movement of the girders induces cross-frame and strut forces. As a result, locations of relatively high positive bending moment were selected. For this continuous end span, relatively large positive moments (and vertical deflections) occur approximately in the range of 25-55% of the span length from the exterior support. Therefore, bridge cross-sections within this portion of the span were selected. Other motivating factors for the instrumentation locations included the number and position of the cross-frames. The finalized strain gauge layout for Span 6 of the SH 105 bridge is shown in Figure 6-9, and the layout for the girder displacement readings is shown in Figure 6-10. Girder deflections were determined with a laser distance meter using the same method applied in the Lubbock Bridge load testing discussed in the last section. Cross-frame line 5 was chosen because it is close to midspan, while line 3 was selected to compare the behavior of cross-frames centered in the cross-section as compared to near the edge.

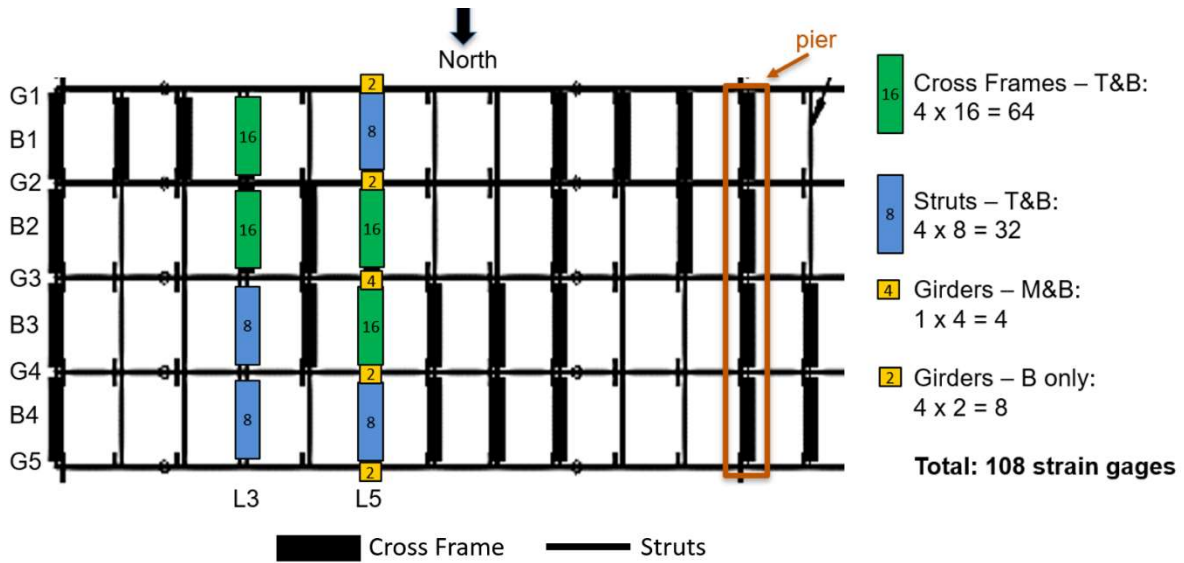


Figure 6-9. SH 105 Bridge Span 6 Strain Gauge Layout

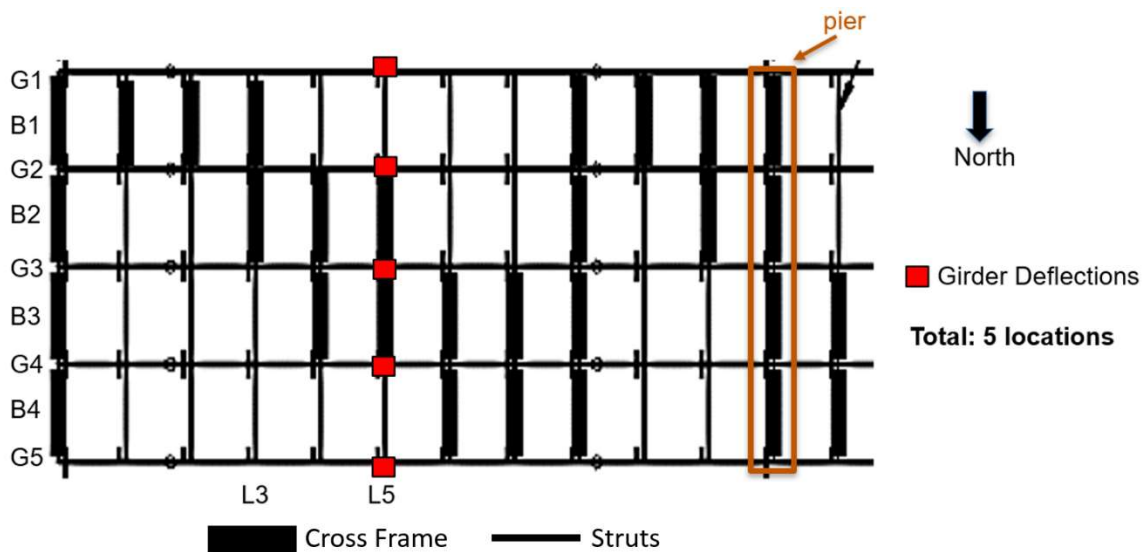


Figure 6-10. SH 105 Bridge Span 6 Girder Displacement Layout

A more granular look at the sensor layout for each member type is provided below. These sensor placements are again similar to the locations used on the 19<sup>th</sup> Street Westbound Bridge discussed in the last section. Each cross-frame is composed of angles, so four strain gauges were required to accurately capture out-of-plane behavior and twist for each member cross section. As such, the conventions “OH” for outer horizontal, “IH” for inner horizontal, “OV” for outer vertical,

and “IV” for inner vertical describe the sensor placement on each angle. A visual representation of the location of the four strain gauges on each angle is shown in Figure 6-11.

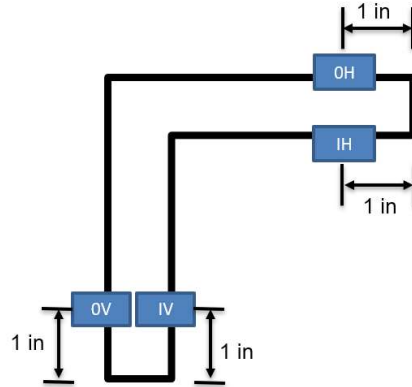


Figure 6-11. Strain Gage Placement on Angles

During field instrumentation, a slight revision was made to the sensor positioning on the top struts. With the deck in place, access to the top of the top strut was excessively difficult. Instead of placing the OH strain gauge as indicated in Figure 6-11, this sensor was placed as indicated in Figure 6-12 for all top struts.

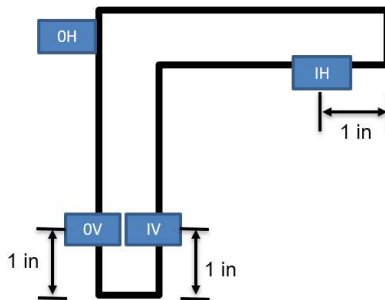


Figure 6-12. Revised Strain Gauge Placement on Top Struts

The top struts were instrumented to obtain a measure of the role of the composite bridge deck, and to observe the lateral force distribution between the cross-frames and lean-on bays. The composite bridge deck represents a relatively rigid element, and the forces in the top struts should

be small. This meant each instrumented cross-frame required 16 strain gauges, while each instrumented lean-on bay required eight strain gauges. The labeling convention is shown in Figure 6-13, where “ST” denotes strut, top; “SB” denotes strut, bottom; “XT” denotes cross-frame, top; and “XB” denotes cross-frame, bottom.

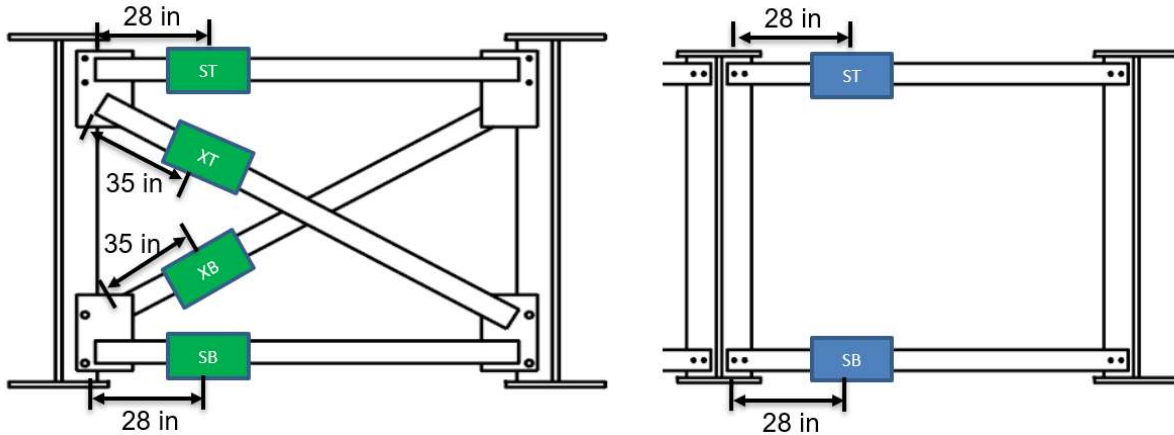


Figure 6-13. Strain Gage Placement on Cross-Frames and Struts

To capture global behavior, each girder was instrumented with two strain gages at the bottom flange, with the center girder instrumented with two additional strain gauges at mid-height. Although this girder instrumentation was not as extensive as on the 19<sup>th</sup> Street bridge, the SH 105 bridge is not skewed, and thus out-of-plane bending and distortion of the girders were not the primary concerns. As shown in Figure 6-14, N and S were used to denote the North and South sides of the girder, with the number 1 designating a flange location and 2 designating a web location.

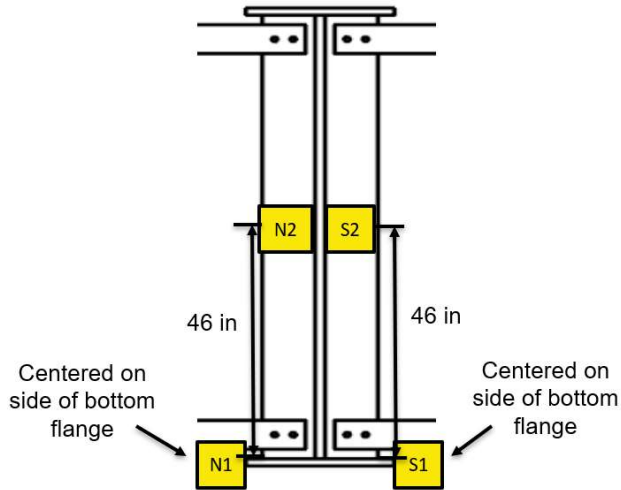


Figure 6-14. Strain Gage Placement on Center Girder

All sensor list conventions are provided in Appendix B, while the full sensor list is located in Appendix C.

### 6.3.3. Data Acquisition

Two Campbell Scientific CR6 dataloggers (DAQ) and seven Campbell Scientific AM16/32B multiplexers (MUX) were used to collect data from the 108 strain gauges specified in the layout. Each DAQ was coded and powered independently, with DAQ 1 collecting data from MUX 1-4 for cross-frame line 5, and DAQ 2 collecting data from MUX 5-7 for cross-frame line 3. The wiring diagram is shown in Figure 6-15.

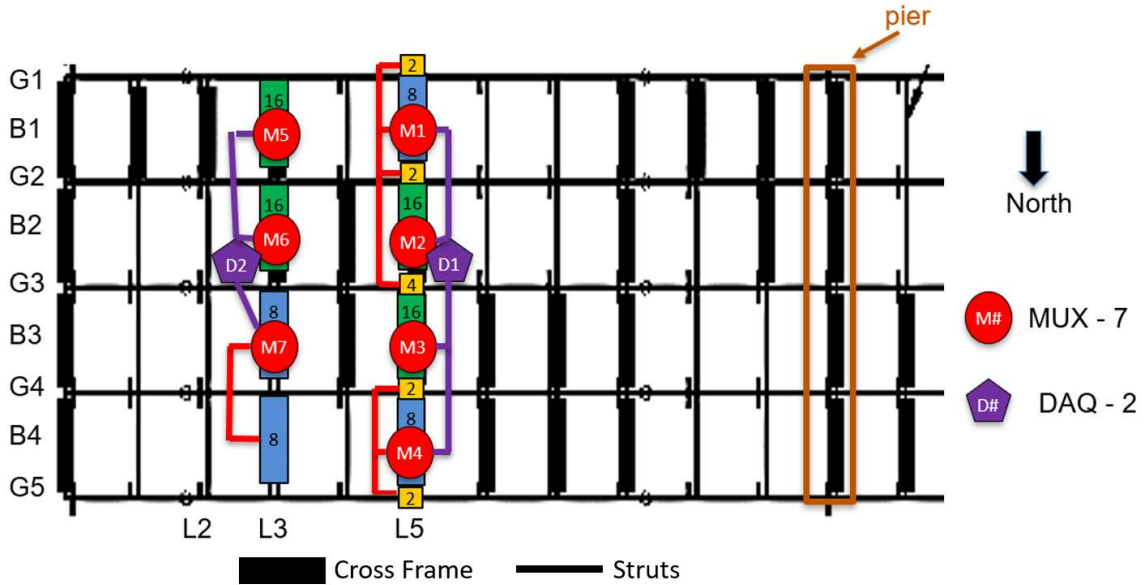


Figure 6-15. SH 105 Bridge Wiring Diagram

Both DAQs were programmed to sample data at 30-second intervals, and timestamps were manually recorded at the start of each load case to allow for continuous data collection as trucks were moved to specific locations and paused to collect data. The data was sampled a minimum of 5 times for each loading and unloading position to allow for stable readings to be taken, and select sensors were monitored throughout the test to ensure values were properly recorded (Figure 6-16).



Figure 6-16. Sensor Monitoring During Loading

### 6.3.4. Live Loading

Before live load testing could occur, load case patterns were determined based on the position of the cross-frame lines instrumented. Identifiers were provided on the deck using spray paint and duct tape to assist in positioning the trucks into the proper position for each load case. The load case patterns are provided in Appendix D, along with actual truck positions during these load cases.

Truck loading was conducted on July 13, 2021, using four trucks loaded with sand/gravel. Prior to testing, each truck was measured and weighed using two vehicle scales. The scales provided a measure of the wheel loads and were positioned in front of each select wheel, and the truck drove onto the scale. Measurements for each truck are shown in Figure 6-17, while the axle weights are listed in Table 6-1.

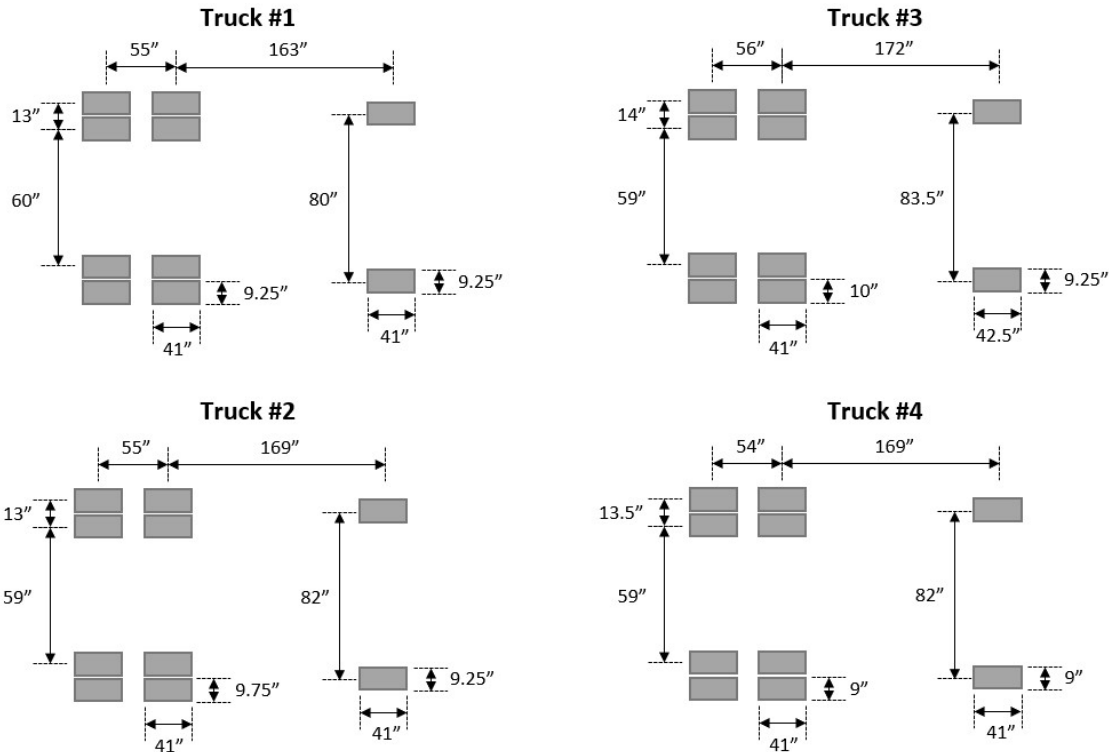


Figure 6-17. SH 105 Bridge Truck Dimensions for Live Load Testing



Table 6-1 SH 105 Bridge Measured Truck Weights

Truck #	Steer Axle (lb)	Forward Drive Axle (lb)	Backward Drive Axle (lb)	Gross Vehicle Weight (lb)
1	11250	16800	16000	44050
2	12050	20450	19900	52400
3	12200	19850	19900	51950
4	12650	21650	20600	54700

Each truck was labeled with a number to keep track of the position of each truck during each test. The numbers were attached on the rear of each truck and also on the front bumper, as shown in Figure 6-18.



Figure 6-18. Truck Setup for SH 105 Bridge Load Case #1

During testing, the following four-step process was followed for the nine load cases tested:

1. Collect unloaded deflection at midspan and strain measurements for five minutes.
2. Position trucks into desired load case.
3. Collect loaded deflection at midspan and strain measurements for five minutes. Collect truck distances from the ideal location using measure tape (Figure 6-19).
4. Remove trucks from the span.

After testing was complete, the duct tape markers for positioning trucks were removed from the deck, and all trucks were cleared of any markings.

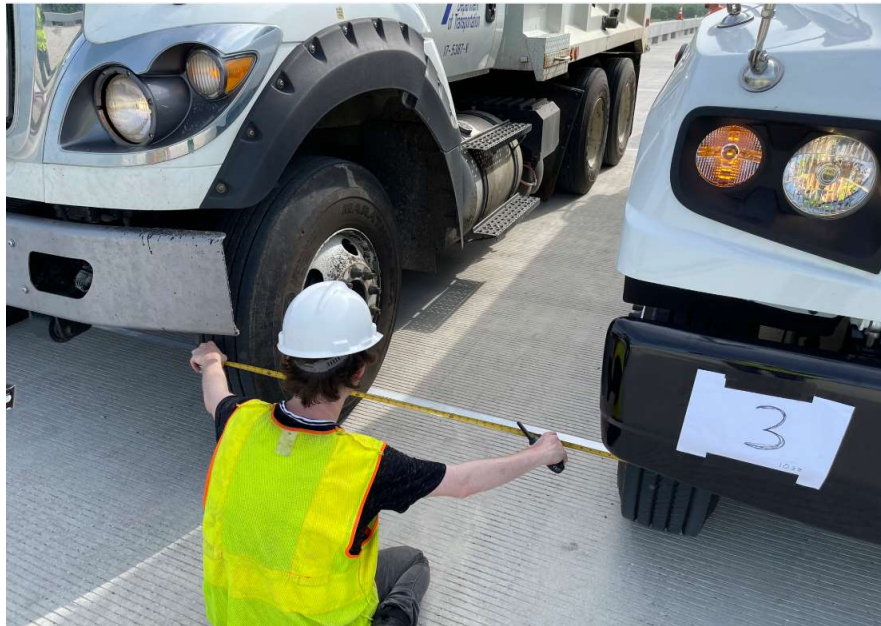


Figure 6-19. Measuring the Distance Between Trucks

## **6.4. Chisholm Trail Bridge at FM1902**

---

### **6.4.1. Overview**

The FM 1902B Overpass at Chisholm Trail Parkway is a six-girder bridge located in Johnson County, Texas, south of Fort Worth, which is in use for the Chisholm Trail Parkway toll road. The girders are spaced at 10 feet, and each side of the bridge has a 4-foot overhang. The bridge consists of three spans of 180.5 feet, 235 feet, and 195 feet for a total length of 611 feet. The bridge has a width of 58 feet and has a 45-degree skew at the supports. The use of lean-on bracing resulted in a replacement of 155 of the 203 intermediate cross-frames with lean-on struts, a reduction of approximately 76% cross-frames. The cross-frames are spread out across the width, as shown in Figure 6-20.

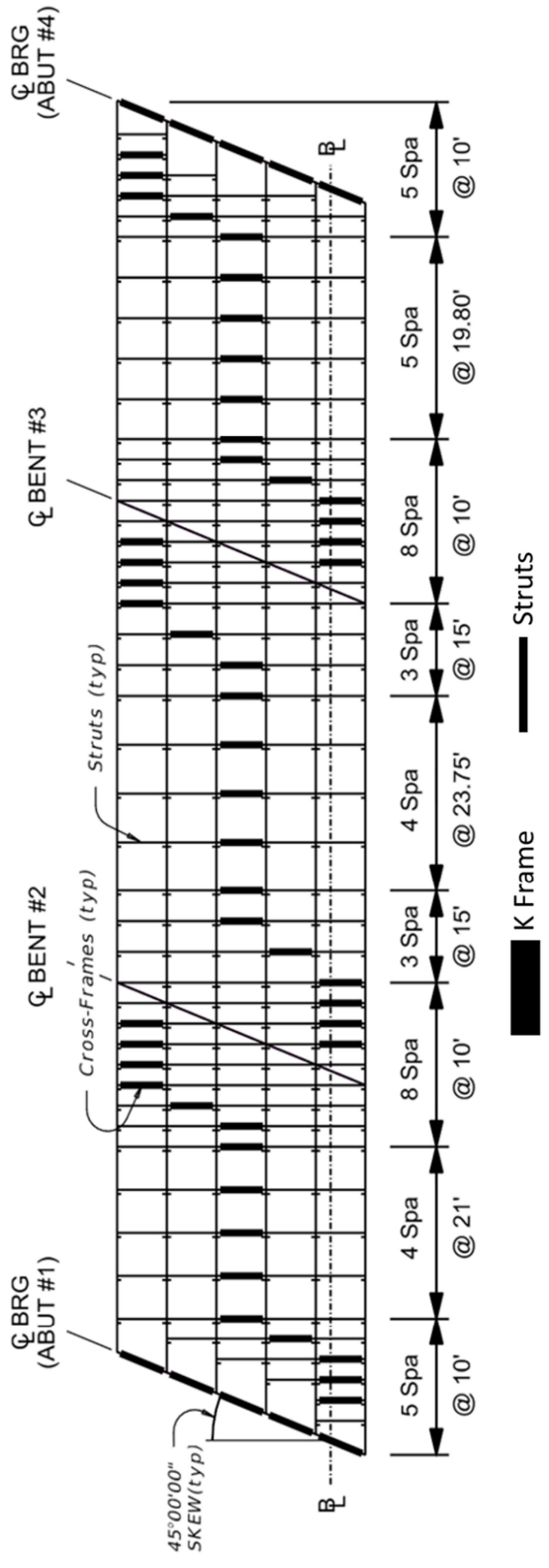


Figure 6-20. Chisholm Trail Bridge Framing Plan

A typical transverse section of the bridge is shown in Figure 6-21. The Chisholm Trail bridge has an interior barrier that separates north and southbound traffic, which was recognized by the researchers as a factor impacting live load testing by limiting load cases across the width of the bridge.

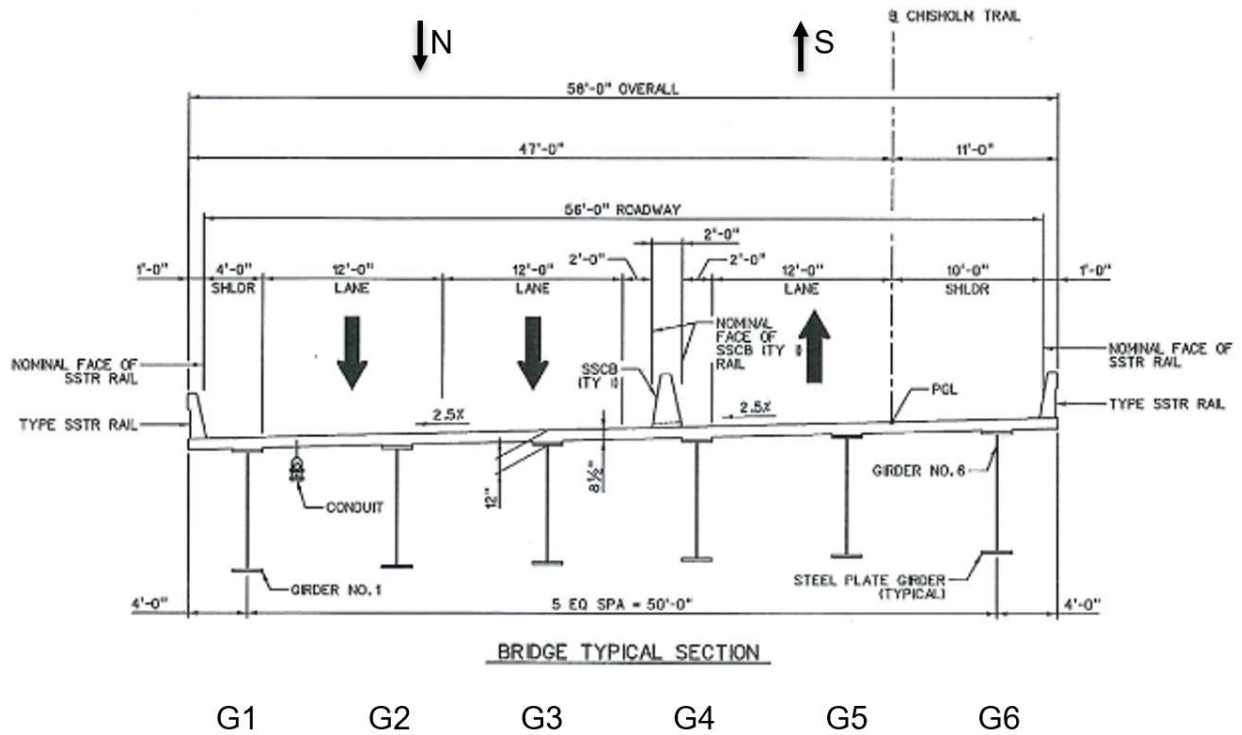


Figure 6-21. Chisholm Trail Bridge Typical Transverse Section

During a site visit, the research team was able to determine that both Spans 1 and 3 were accessible to instrumentation from beneath the bridge without the need for traffic closures. The flat grass areas under these spans are ideal for access during instrumentation and are shown in Figure 6-22. The research team selected Span 1.



Figure 6-22. Chisholm Trail Bridge Spans

#### 6.4.2. Sensor Layout

The instrumentation plan of the Chisholm Trail bridge was focused on monitoring two key locations: midspan and near the interior pier. Similar to the data collection for the SH 105 and the 19<sup>th</sup> Street Westbound Bridges, strain gauges were placed and deflections were measured near midspan to capture the effect of the high positive bending moment and maximum bridge deflection. Strain gauges placed at the interior pier were used to collect data related to the effect of the system's skew and cross-frame detailing on the pier.

The research team used 128 strain gauges. The final strain gauge layout for the Chisholm Trail bridge is illustrated in Figure 6-23, while the locations for deflection measurements are shown in Figure 6-24. The deflection readings were determined with the laser distance meter in the same way as for the Lubbock and SH 105 Bridges.

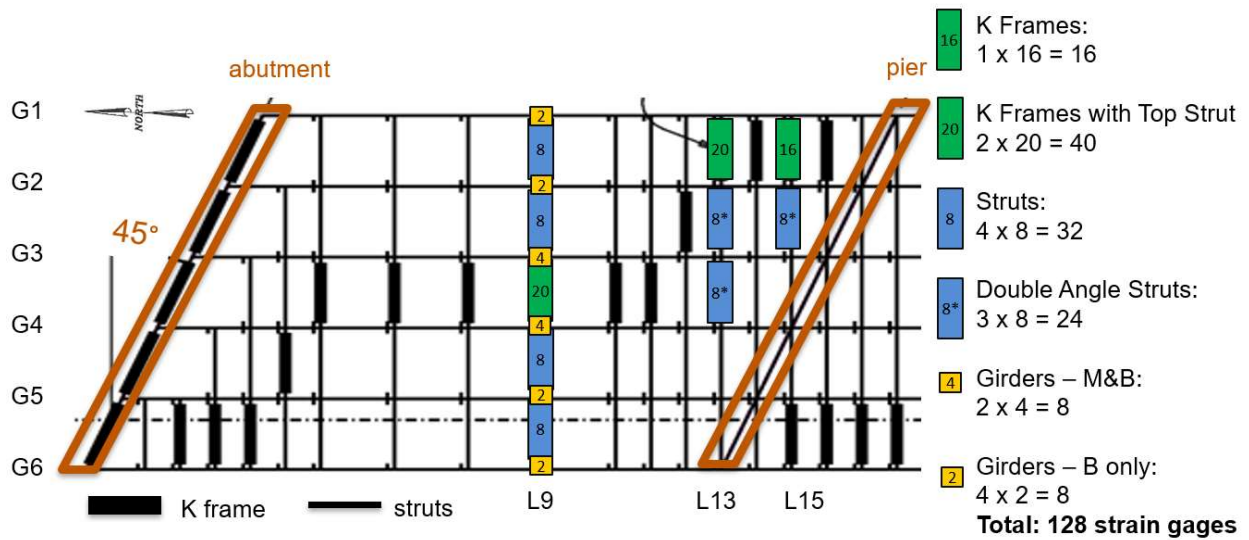


Figure 6-23. Chisholm Trail Bridge Span 1 Strain Gauge Layout

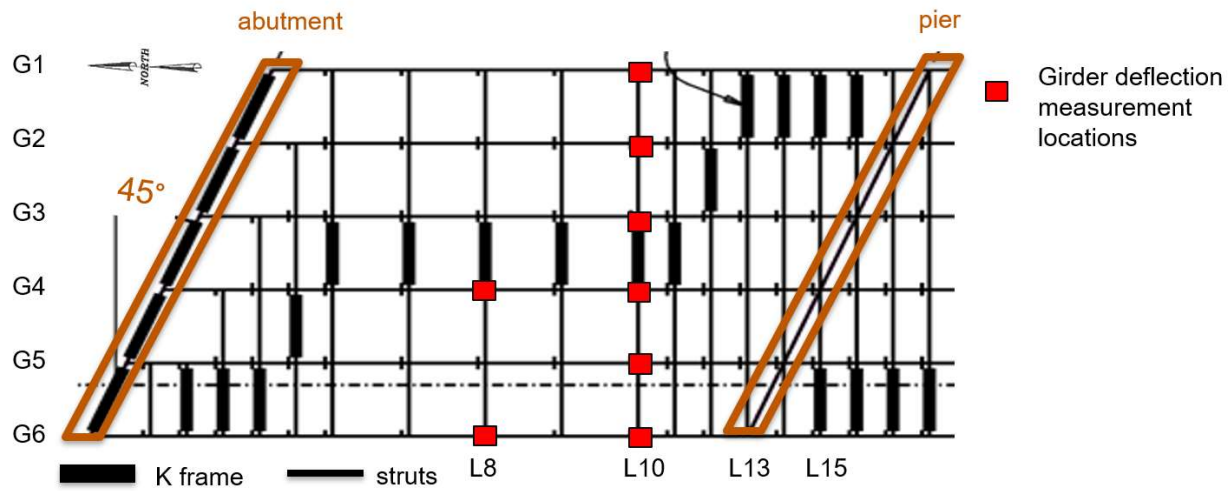


Figure 6-24. Chisholm Trail Span 1 Girder Displacement Layout

As discussed in the section outlining the instrumentation plan for the SH 105 bridge, the typical convention for each sensor is “OH” for the outer horizontal, “IH” for the inner horizontal, “OV” for the outer vertical, and “IV” for the inner vertical. Numbers are added to the double angle members to further distinguish sensor locations.

The sensor locations on the double-angle top and bottom struts are displayed in Figure 6-25. Due to the detailing on these members, the double angle members are assumed to function as a built-up member with a concentric connection, and only four total sensors were used. The sensor location on the horizontal was selected based on accessibility.

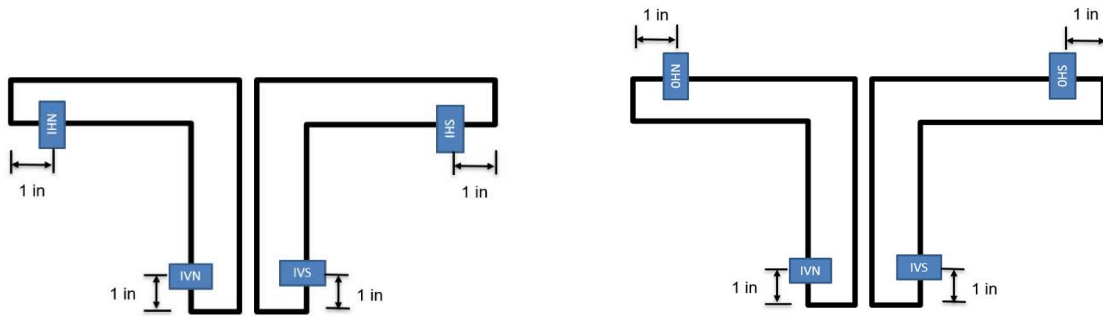


Figure 6-25. Chisholm Trail Double Angle Top and Bottom Strut Strain Gauge Placement

Figure 6-26 displays the sensor locations on single-angle top and bottom struts. The sensor location on the horizontal was based on accessibility and was similar to the selected locations used for the SH 105 Bridge.

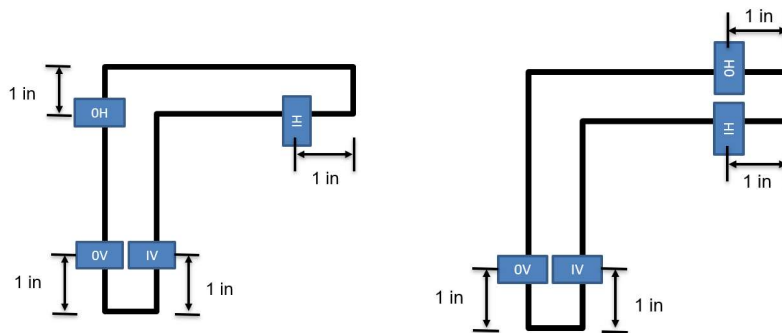


Figure 6-26. Chisholm Trail Single Angle Top and Bottom Strut Strain Gauge Placement

Similar to the SH 105 Bridge, the labeling convention is shown in Figure 6-27, where “ST” denotes strut, top; “SBE” denotes strut, bottom east; “SBW” denotes strut, bottom west; “XT” denotes cross-frame, top; and “XB” denotes cross-frame, bottom. Two of the three instrumented K-frames include a top strut sensor set for a total of 20 sensors (16 for the third K-frame). Each

lean-on bay has eight sensors. Girder sensor placements remained unchanged from Section 6.3.2. All labeling conventions can be found in Appendix D, while the full sensor list is given in Appendix E.

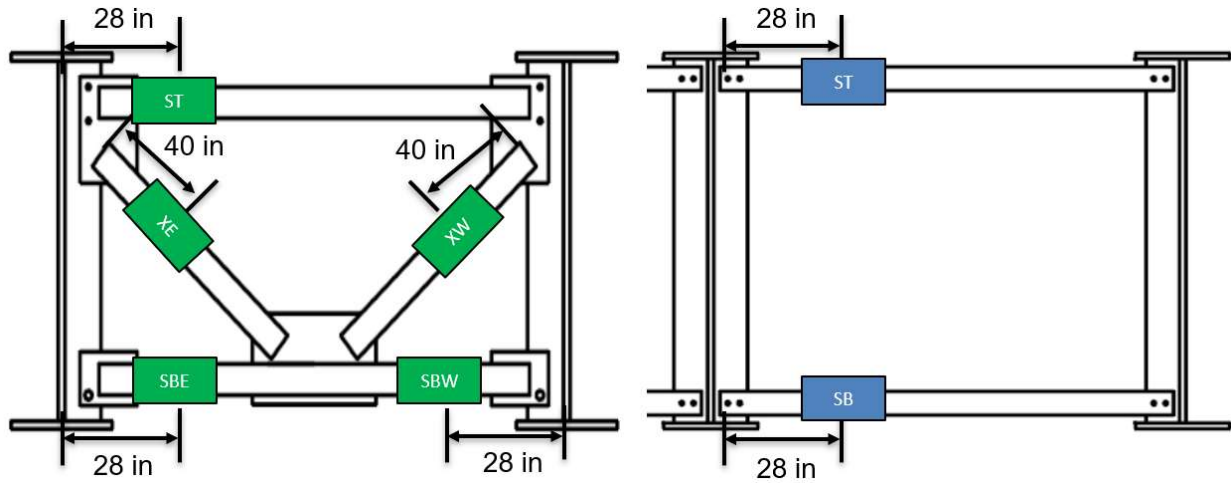


Figure 6-27. Chisholm Trail Strain Gauge Placement on Cross-Frames and Struts

### 6.4.3. Data Acquisition

Data acquisition for the Chisholm Trail bridge was similar to the systems used for collecting data from the SH 105 Bridge. Two Campbell Scientific CR6 dataloggers (DAQ) and eight Campbell Scientific AM16/32B multiplexers (MUX) were used to collect data from the 128 strain gauges specified in the layout. Each DAQ was coded and powered independently, with DAQ 1 collecting data from MUX 1-4 (cross-frame line 8), and DAQ 2 collecting data from MUX 5-8 (primarily cross-frame lines 13 and 15). The wiring diagram is shown in Figure 6-28.



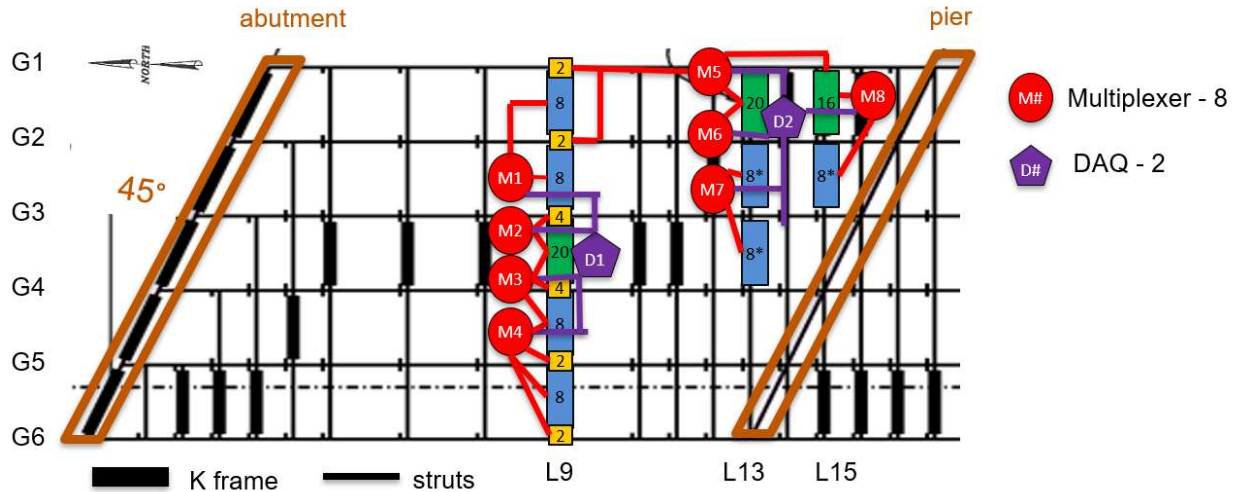


Figure 6-28. Chisholm Trail Strain Gauge Placement on Cross-Frames and Struts

#### 6.4.4. Live Loading

The live load cases for the Chisholm Trail Bridge were selected based on preliminary Finite Element Analyses (FEA), data collected during the testing of the Lubbock bridge, and the position of the instrumented cross-frame lines. All live load cases for the Chisholm Trail Bridge are included in Appendix F.

Live load testing was conducted on November 14, 2021, utilizing four trucks supplied by TxDOT. Trucks were measured via tape measure and weighed using two vehicle scales. Measurements are displayed in Figure 6-29, and axle weights are listed in Table 6-2. To avoid data contamination from other bridge traffic, the researchers worked with the toll authority to have the bridge shut down to traffic for approximately three hours. The traffic was diverted from the toll road via detour.

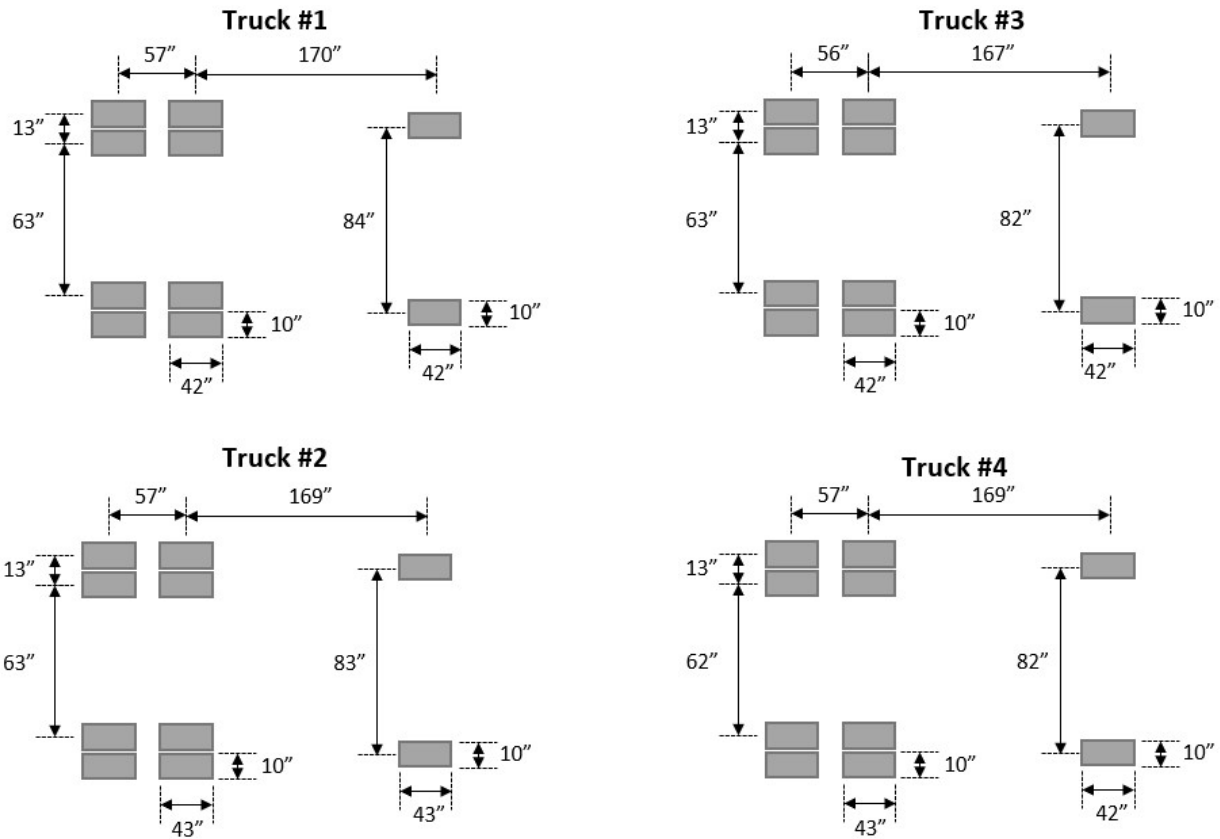


Figure 6-29. Chisholm Trail Bridge Truck Dimensions for Live Load Testing

Table 6-2 Truck Weights for Live Load Testing of the Chisholm Trail Bridge

Truck #	Steer Axle (lb)	Forward Drive Axle (lb)	Backward Drive Axle (lb)	Gross Vehicle Weight (lb)
1	11000	15800	16050	42850
2	11750	14200	14800	40750
3	11200	14700	15100	41000
4	11100	14500	14650	40250



Figure 6-30. Chisholm Trail Bridge Load Case 4

After labeling the trucks to keep track of their positions, live load testing occurred using the same four-step procedure previously discussed:

1. Collect unloaded deflection at midspan and strain measurements for five minutes.
2. Position trucks into desired load case.
3. Collect loaded deflection at midspan and strain measurements for five minutes. Collect truck distances from the ideal location using measure tape.
4. Remove trucks from the span.

In total, six load cases were completed for the Chisholm Trail Bridge. Upon completion of the testing, all markings and duct tape were removed from the bridge.

## 6.5. Data Processing

---

### 6.5.1. Strain Gauge Readings to Axial Forces

In order to convert the measured strains from the cross-frames into axial forces and stresses, a linear regression procedure outlined in Helwig and Fan (2000) Appendix B was used. The cross-frames were made up of angle sections. According to the mechanics of thin-walled structures, no warping stresses are induced in these cross-sections when members are subjected to torsional moments. Therefore, longitudinal stresses are caused exclusively by axial force and bending moment and are distributed linearly along the cross-section of the bracing members. The longitudinal stress distribution is described by the following equation:

$$f = a + bx + cy \quad 6.1$$

Where:

$f$  is the longitudinal stress (determined from Hooke's Law as the measured strain multiplied by the modulus of elasticity  $E$ )

$x, y$  are locations on the coordinate system of the cross-section

$a, b, c$  are constants

The Regression Method is used to determine constants  $b$  and  $c$  using the following equations:

$$I_{11}b + I_{12}c = I_{10} \quad 6.2$$

$$I_{21}b + I_{22}c = I_{20} \quad 6.3$$

Where:

$$I_{11} = \sum_{i=1}^n (x_i - \bar{x})^2$$

$$I_{22} = \sum_{i=1}^n (y_i - \bar{y})^2$$

$$I_{12} = I_{21} = \sum_{i=1}^n (x_i - \bar{x})(y_i - \bar{y})$$

$$I_{10} = \sum_{i=1}^n (x_i - \bar{x})(f_i - \bar{f})$$

$$I_{20} = \sum_{i=1}^n (y_i - \bar{y})(f_i - \bar{f})$$

$$\bar{x} = \frac{1}{n} \sum_{i=1}^n x_i$$

$$\bar{y} = \frac{1}{n} \sum_{i=1}^n y_i$$

$$\bar{f} = \frac{1}{n} \sum_{i=1}^n f_i$$

The constant  $a$  from Equation 6.1 is then calculated using:

$$a = \bar{f} - b\bar{x} - c\bar{y} \quad 6.4$$

The axial force in the member can be derived using beam-column theory after the constants in Equation 6.1, are determined. If the origin of the x-y coordinate system passes through the centroid of the cross-section, the axial force is given by:

$$N = aA \quad 6.5$$

Where:

$N$  is the axial force

$A$  is the cross-sectional area of the member

Detailed sample calculations for this method are included in Appendix H. Calculated axial forces based on strain measurements for Lubbock Bridge, SH 105 Bridge, and Chisholm Trail Bridge are included in Appendices I, J, and K.

### **6.5.2. Deflection Measurements**

Deflection readings were measured using laser distance meters from ground level beneath the span. Quick-setting Hydrostone was used to create a level surface in holes dug directly below the reading locations. The laser distance meters were positioned on the hardened Hydrostone surface next to a marked location to ensure consistency in the readings. Upon taking a measurement, the meters collected three rounds of data from each position. Readings were taken with each bridge loaded and unloaded between each truck position. During post-processing, these three data points were averaged and rounded to the nearest unit able to be collected by the strain gauge. After all data points were averaged, the deflection measured during a load case was subtracted by the deflection measured during the last zeroth case (no load on bridge). The difference in these quantities signified the deflection of the bridge. Deflection measurements for the SH 105 Bridge and Chisholm Trail Bridge are included in Appendices J and K.

## Chapter 7. Bridge Model Validation

Parametric finite element models were used in the study to develop an understanding of the system behavior and provide comprehensive results that could be used to establish consistent design guidance for a broad range of lean-on bracing applications. Therefore, accurate modeling methods are crucial for the development of correct guidance. The data from the field monitoring of bridges under construction (Lubbock Bridge) and the completed bridges (SH105 and Chisholm Trail Bridges) were used for validation of the modeling procedures.

The model validation process consists of modeling the subject of the experimental data in a finite element analysis program, identifying key validation parameters affecting the results, and determining the minimum complexity of the model required to get representative results of the real system. The SH 105, Chisholm Trail, and Lubbock bridges were modeled using ABAQUS 2022 based on design drawings and field measurements. The key validation parameters affecting the results were identified as the support conditions, the deck and barrier stiffnesses, as well as the R-factors for the cross-frame members. The identification of these parameters led to adjustments to the model's element structure, mass distribution, and material properties. With accurate values for these parameters, high-fidelity models of SH 105, Chisholm Trail, and Lubbock bridges were developed.

This dissertation includes the validation of the three bridge models. This work was conducted in collaboration with Aidan Bjelland. In order to test the variables described previously, a Python script was developed by Bjelland to efficiently build and analyze hundreds of detailed models with varied parameters in Abaqus. The models were compared with field instrumentation

data in an objective function produced and processed by the author. Details regarding the Abaqus modeling procedures and Python scripting logic may be found in TxDOT Report 0-7093-1 (Helwig *et al.*, 2024) and Bjelland (2024).

## 7.1. Objective Functions

---

The data points from the models were compared with measured values of the girder displacements in order to validate the support conditions and concrete modulus of elasticity. Models of each bridge were built and analyzed using ranges of values for the stiffness of the support conditions and the modulus of elasticity. In order to determine the most accurate combination of values for the support conditions and modulus, the displacement of the girders in the model was compared with the measured values for several truckload cases. In order to effectively compare these values, an equation for a square root sum of squares objective function was used, as shown in Equation 7.1. The resulting value represents the total sum of the error from every data point measured in inches.

$$obj = \sqrt{\sum_{t=1}^T \sum_{n=1}^{n_g} (\Delta_{exp_{tn}} - \Delta_{model_{tn}})^2} \quad 7.1$$

Where:

T is the number of load cases considered

$n_g$  is the number of girders

$\Delta_{exp}$  is the experimental girder deflection (in)

$\Delta_{model}$  is the model girder deflection (in)



## 7.2. SH 105 Bridge Model Validation

---

The geometry of the SH 105 at the Brazos River bridge and the layout of instrumentation were discussed in Section 6.3. This section provides the steps that were utilized to validate the FEA model based on the field data. In order to validate an Abaqus model of the SH 105 bridge, emphasis was placed on the spring and deck stiffness parameters. Parametric studies were run in order to determine the effect of the elastic modulus of the deck, elastic modulus of the bridge rails, and the support conditions. The test range of the elastic modulus was 1000 ksi to 5000 ksi in increments of 100 ksi. The bearing stiffness was adjusted based on a normalization of the default values in increments of 10% of the base value within a range of 80% to 120%. After analysis of the results, the models were determined to be insensitive to the modulus of the barrier and insensitive to the spring stiffness value. Overall, the displacement results were primarily affected by the deck modulus. The range of objective function values can be seen in Figure 7-1, with an optimum deck modulus of 5200 ksi and 100% spring stiffness. Plots of the girder deflections for this model are shown in Figure 7-2 through Figure 7-5. The agreement between measured and predicted values is reasonable and well within the resolution of the laser distance meter used to measure displacement, which was 1/16".

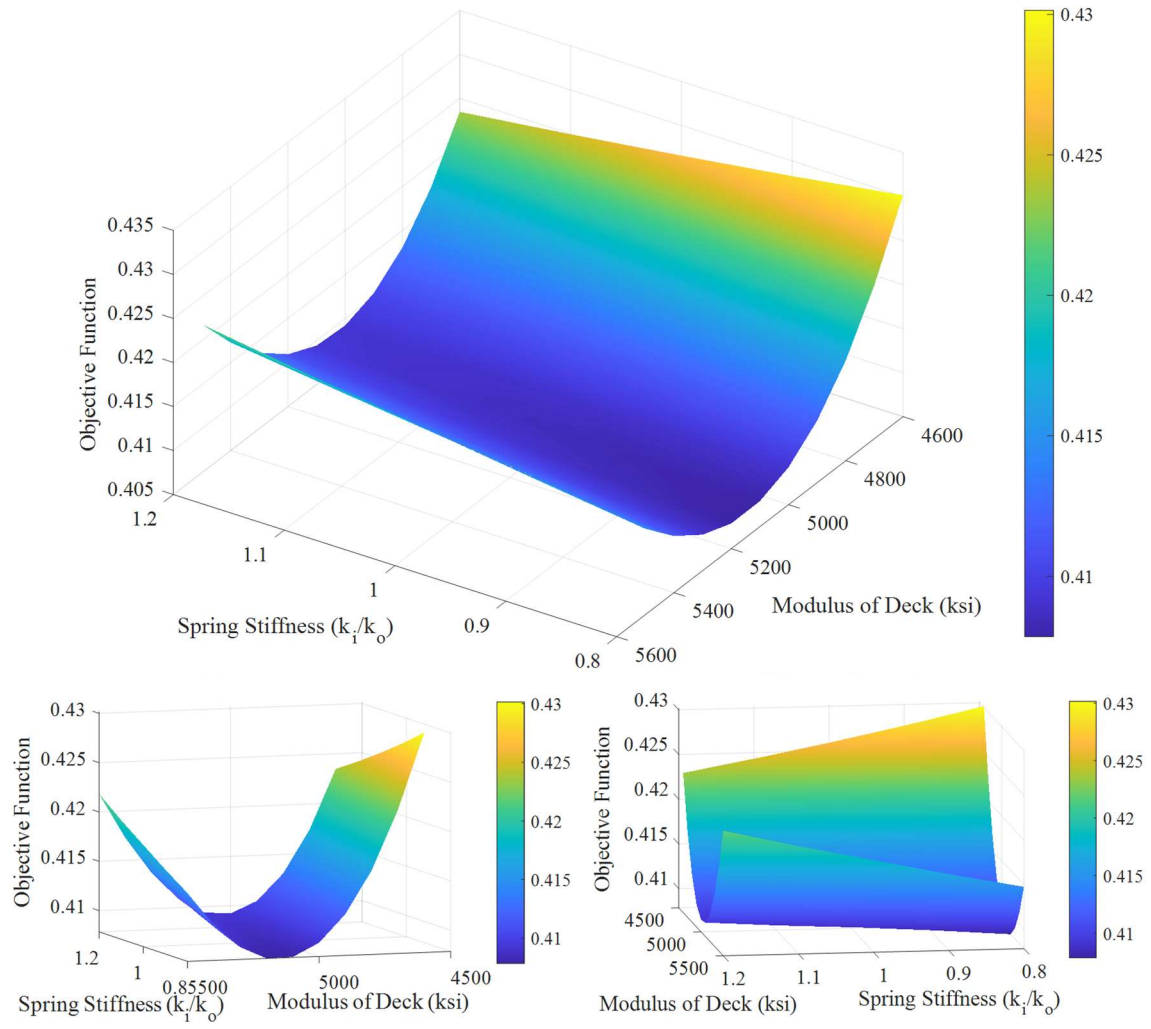
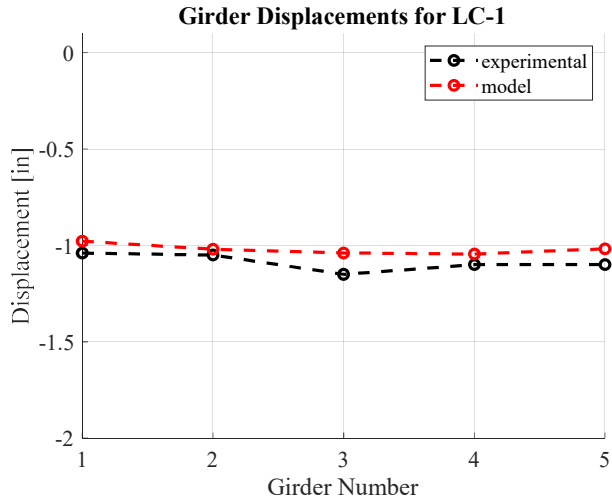
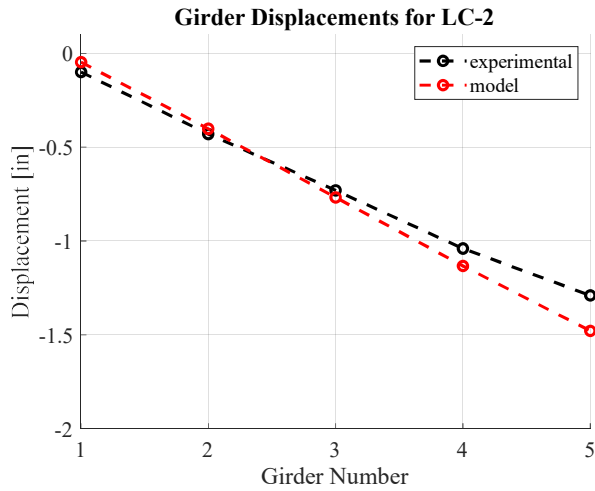


Figure 7-1. SH 105 Spring and Deck Stiffness Objective Function



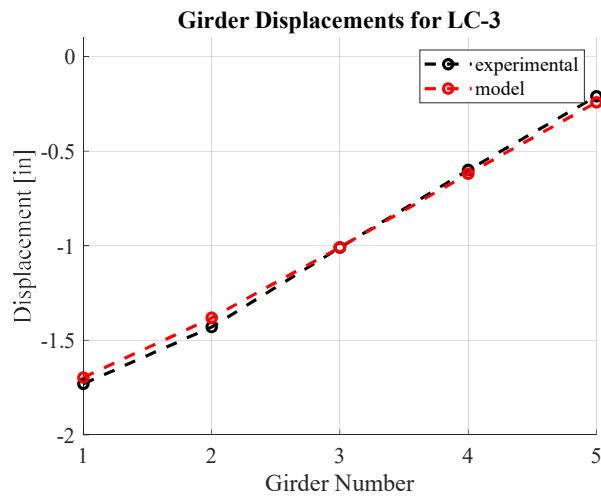
Load Case 1 Displacements [in]			
G	Experimental	Model	Exp/Model Difference
1	-1.04	-0.98	0.06
2	-1.05	-1.02	0.03
3	-1.15	-1.04	0.11
4	-1.10	-1.04	0.06
5	-1.10	-1.02	0.08
		Average	0.07

Figure 7-2. SH 105 Bridge Girder Displacements Load Case 1



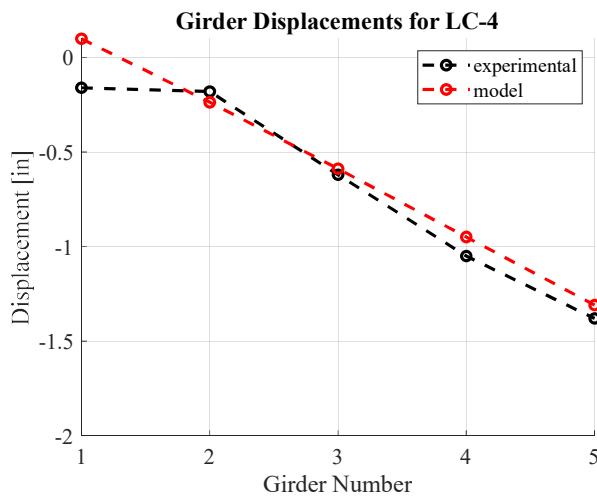
Load Case 2 Displacements [in]			
G	Experimental	Model	Exp/Model Difference
1	-0.10	-0.05	0.05
2	-0.43	-0.40	0.03
3	-0.73	-0.77	0.04
4	-1.04	-1.13	0.09
5	-1.29	-1.48	0.19
		Average	0.08

Figure 7-3. SH 105 Bridge Girder Displacements Load Case 2



Load Case 3 Displacements [in]			
G	Experimental	Model	Exp/Model Difference
1	-1.73	-1.70	0.03
2	-1.43	-1.38	0.05
3	-1.01	-1.01	0.00
4	-0.60	-0.62	0.02
5	-0.21	-0.24	0.03
		Average	0.03

Figure 7-4. SH 105 Bridge Girder Displacements Load Case 3



Load Case 4 Displacements [in]			
G	Experimental	Model	Exp/Model Difference
1	-0.16	0.10	0.26
2	-0.18	-0.24	0.06
3	-0.62	-0.59	0.03
4	-1.05	-0.95	0.10
5	-1.38	-1.31	0.07
		Average	0.10

Figure 7-5. SH 105 Bridge Girder Displacements Load Case 4

### 7.3. Chisholm Trail Bridge Model Validation

The Chisholm Trail Parkway overpass at FM 1902B is a completely constructed six-girder bridge located in Johnson County, Texas, south of Ft. Worth. The bridge geometry and instrumentation were discussed in Section 6.4. The validation of the Chisholm Trail bridge was conducted similarly to the SH 105 bridge model. However, there are two key differences between the two bridges. The Chisholm Trail bridge has a large barrier in the middle of the deck and utilizes some double-angle members, while SH 105 does not. The interior barrier greatly affected the

stiffness of the system and thus was a significant focus in the stiffness validation. The parametric studies varied the elastic modulus of the deck, the elastic modulus of the barrier, and the stiffness of the support conditions. The range of the elastic modulus evaluated was 1000 ksi to 5000 ksi. The spring stiffness was adjusted based on a normalization of the default values in increments of 10% of the base value from 80% to 120%. Similar to the findings from SH 105, the behavior of the model was found to be insensitive to the spring stiffness value, and the base approximation was acceptable. Unlike the SH 105 model, however, both the modulus of the deck and barrier influenced system performance. The analysis of the system was conducted with variations of the modulus of the deck and barrier/rails from 2000 to 5000 ksi in increments of 750 ksi. The objective function results are provided in Figure 7-6. The modulus of the deck with the best correlation is shown to be 4250 ksi, and the modulus of the barrier and rails is 5000 ksi. The resolution of the laser distance meter used to measure displacement is 1/16", and many of the model values are within or close to that tolerance.

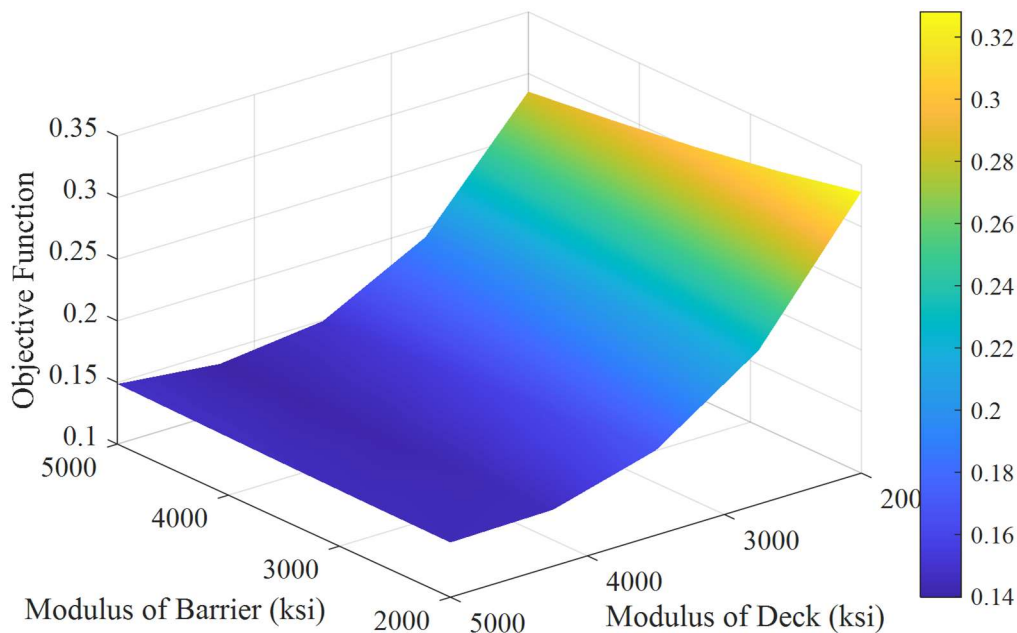
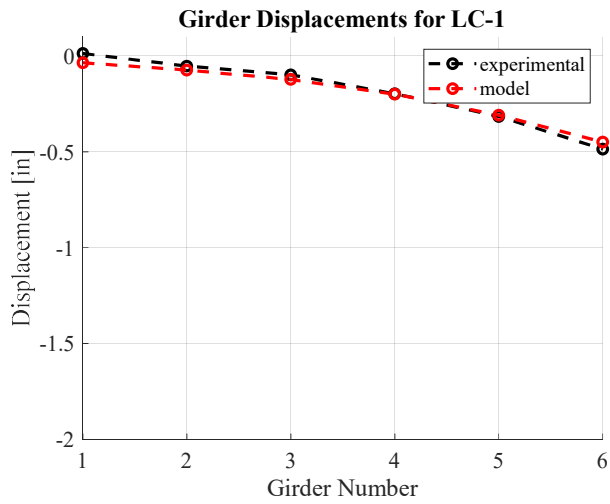
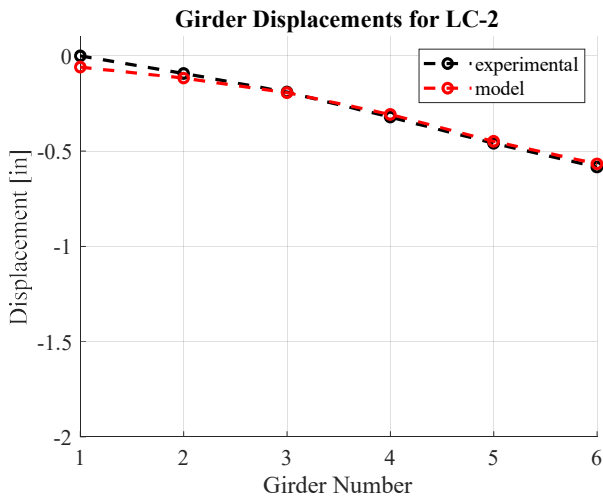


Figure 7-6. Chisholm Trail Deck and Barrier Stiffness Objective Function



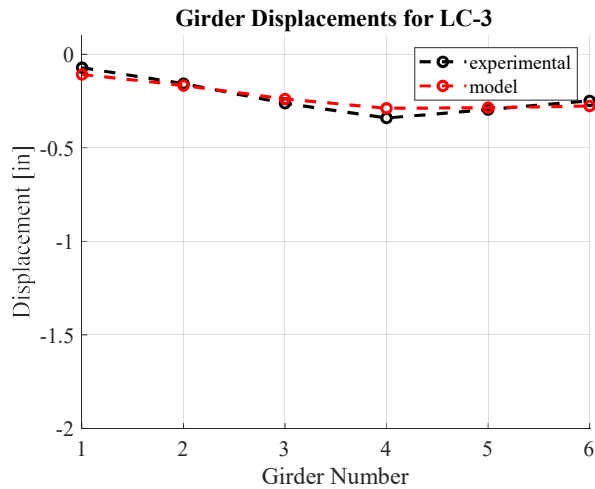
Load Case 1 Displacements [in]			
G	Experimental	Model	Exp/Model Difference
1	0.01	-0.04	0.05
2	-0.05	-0.07	0.02
3	-0.10	-0.12	0.02
4	-0.20	-0.20	0.00
5	-0.31	-0.31	0.01
6	-0.49	-0.45	0.04
		Average	0.02

Figure 7-7. Chisholm Trail Girder Displacements Load Case 1



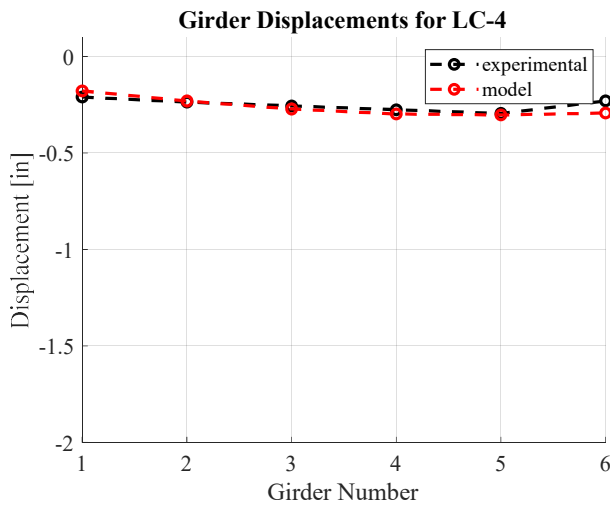
Load Case 2 Displacements [in]			
G	Experimental	Model	Exp/Model Difference
1	0.00	-0.06	0.06
2	-0.09	-0.12	0.02
3	-0.19	-0.19	0.00
4	-0.32	-0.31	0.01
5	-0.46	-0.45	0.01
6	-0.58	-0.57	0.02
		Average	0.02

Figure 7-8. Chisholm Trail Girder Displacements Load Case 2



Load Case 3 Displacements [in]			
G	Experimental	Model	Exp/Model Difference
1	-0.07	-0.11	0.04
2	-0.16	-0.17	0.01
3	-0.26	-0.24	0.02
4	-0.34	-0.29	0.05
5	-0.30	-0.29	0.01
6	-0.25	-0.28	0.03
		Average	0.03

Figure 7-9. Chisholm Trail Girder Displacements Load Case 3



Load Case 4 Displacements [in]			
G	Experimental	Model	Exp/model Difference
1	-0.21	-0.18	0.03
2	-0.24	-0.23	0.01
3	-0.26	-0.27	0.02
4	-0.28	-0.30	0.02
5	-0.30	-0.30	0.01
6	-0.23	-0.29	0.06
		Average	0.02

Figure 7-10. Chisholm Trail Girder Displacements Load Case 4

## 7.4. Lubbock Bridge Model Validation

### 7.4.1. Overview of Lubbock Bridge

The 19<sup>th</sup> Street West Bound Bridge in Lubbock, TX, was instrumented as part of TxDOT Project 0-1772. The bridge has a 60-degree skew, resulting in different critical cases compared to a non-skewed bridge. The bridge has three spans and six girders across the width. Data for this bridge was recorded for the lean-on bracing during the deck pour, as reported by Romage (2008). The data from this bridge is valuable to the present study because no bridges with lean-on bracing

under construction during the duration of this study. Romage (2008) provides a detailed discussion of the sensor layout for the project, and a summary is provided in Section 6.2. Sensor readings from the deck pour were used for model validation.

#### **7.4.2. Field Instrumentation and Testing**

The instrumentation plan utilized for assessment of the Lubbock bridge is discussed in Section 6.2. Two cross-frame lines were instrumented: one in the support region and one at the midspan of the bridge. Three sets of lean-on struts and two cross-frames were instrumented with strain gauges.

As previously stated, the Lubbock data is currently the only data set available for lean-on bracing during construction. The data includes several hours of deck pour, which was the focus of the validation. Unlike SH 105 and the Chisholm Trail bridge, modeling construction phases requires the consideration of the loads applied by overhangs, screed, scaffolding bridges, and concrete. Figure 7-11 is a picture taken during the deck pour highlighting these construction components.



Figure 7-11. Lubbock Bridge During Deck Pour (Romage, 2008)



Based upon the field notes (Romage, 2008), a deck pour timeline was constructed and is shown in Figure 7-12. Gaps in the field notes prevented a full timeline from being prepared. There was some uncertainty in the timeline; however, the focus of the validation readings is based on the readings with no concrete and the changes when all of the concrete was placed on the bridge. Therefore, the timeline is not a major factor in the resulting data. An overview of the deck casting sequence is provided in Figure 7-12. The concrete placement started on the West end of the bridge and progressed across the positive moment region close to 7am. Concrete was placed on the support region at the East end of the bridge to prevent uplift. The casting then proceeded from the span on the West end of the bridge towards the East end with a continuous deck casting sequence.

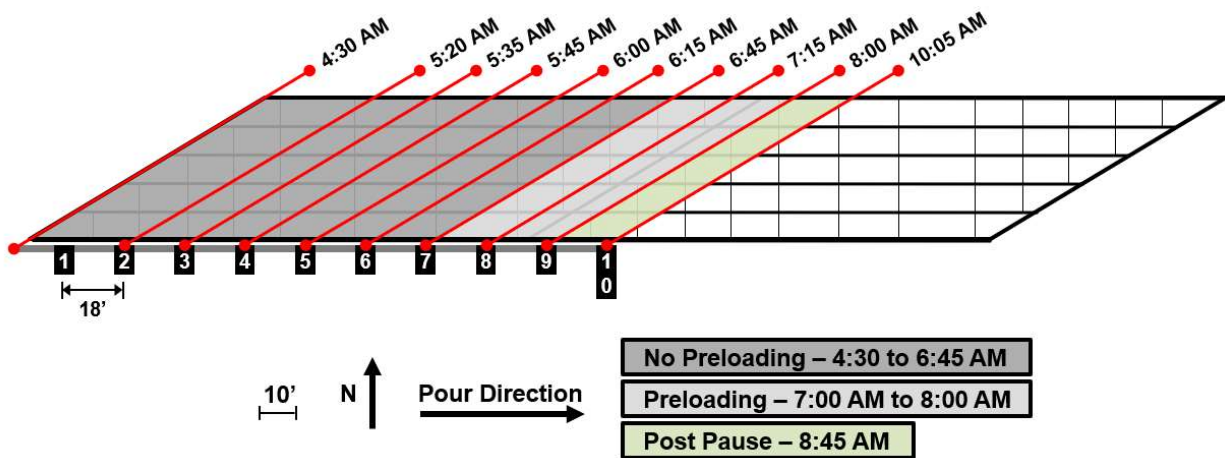


Figure 7-12. Lubbock Bridge Deck Pour Sequence Timeline (Helwig *et al.*, 2024)

A mockup of the applied loads for the construction condition is shown in Figure 7-13 based on the field notes from the instrumentation and typical construction values. The overhangs were placed every 72".

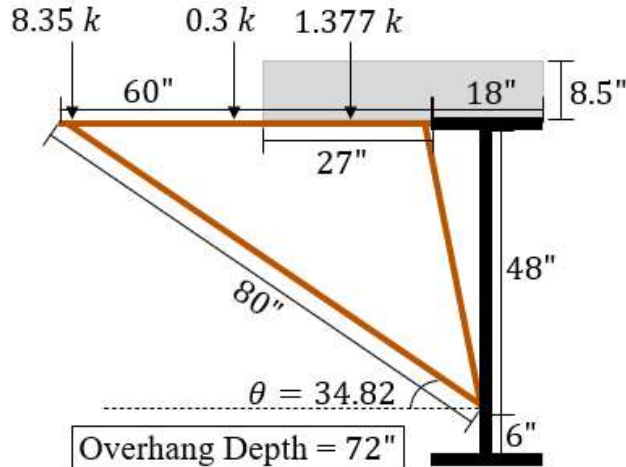


Figure 7-13. Lubbock Overhang Loading During Construction (Helwig *et al.*, 2024)

The horizontal loads applied to the girders at each overhang brace can be categorized by the source of the load:

- The concrete (C) contributed 0.5 kips.
- The screed (S) contributed 12.5 kips.
- The first bridge (B1) contributed 6.2 kips.
- The second bridge (B2) contributed 3.3 kips.

Based upon the field notes, these loads were applied at the following positions relative to each other and to the skew of the system, as shown in Figure 7-14. The exact position of these components was not measured throughout the deck pour. As such, the research team used the estimated rate of the deck pour and consistent spacing based on the initial few hours of field notes.

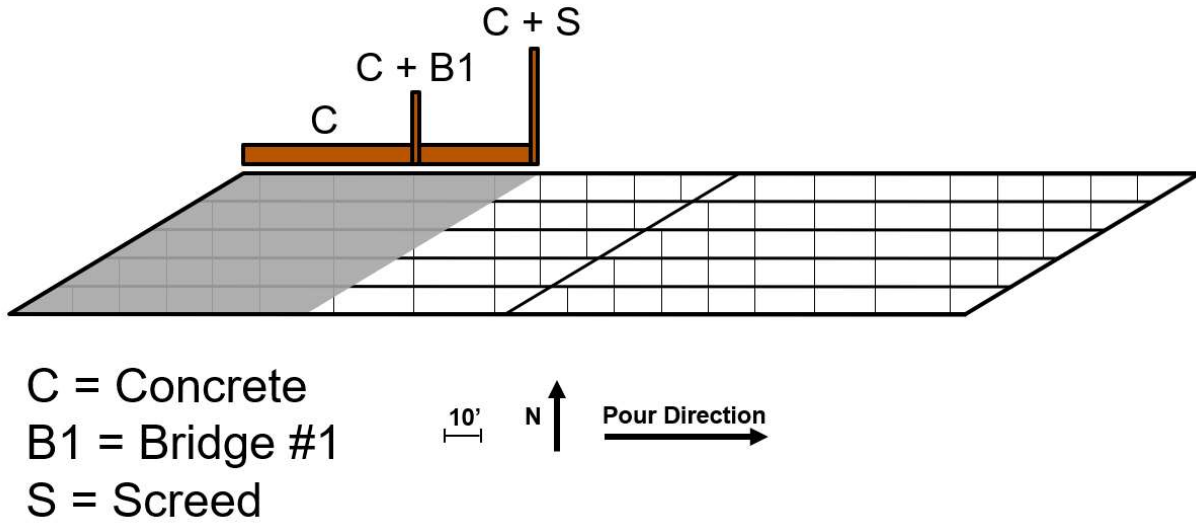


Figure 7-14. Lubbock Overhang Load Positions of Screed and Deck Pour (Helwig *et al.*, 2024)

The Lubbock model was designed to fit the 6:00 AM deck pour condition based upon the previously stated modeling assumptions and can be seen in Figure 7-15. The figure illustrates all of the potential locations for the overhang forces based on the overhang bracket positions. However, only brackets in the deck pour region were given load magnitudes. The self-weight of the concrete was included in the concrete properties.

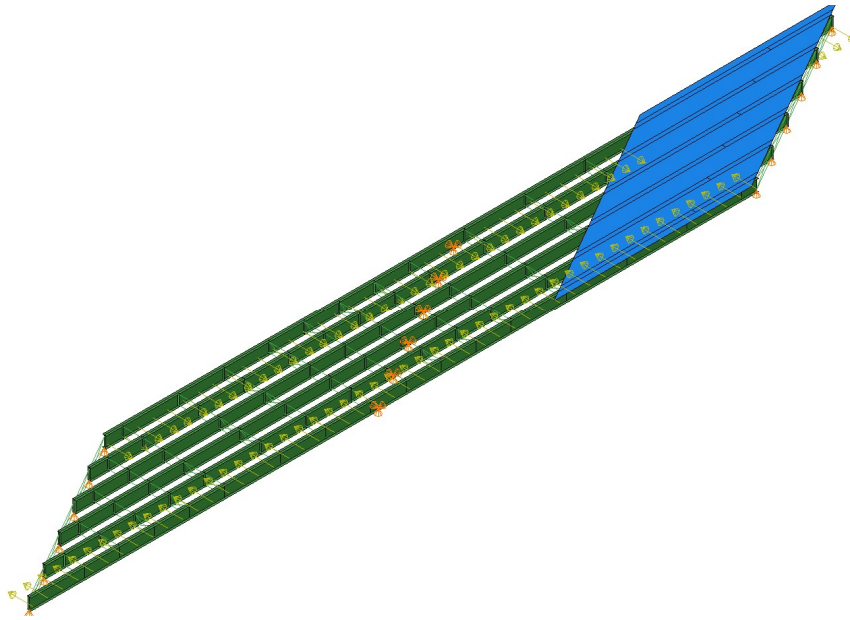


Figure 7-15. Lubbock Model used for Validation (Bjelland, 2024)

#### 7.4.3. Validated Model Results

The research team conducted a parametric study varying the R-factor for lean-on bracing from 0.4 to 0.6 for both the lean-on struts and full cross-frames, and the modulus of the deck (0 to 200 ksi). The results demonstrated the best settings involved a lower stiffness of 36 ksi was preferred, but the results were generally insensitive to the R-factor.

However, the reason the results were indifferent to the R-factor was due to the conflicting behavior of the two cross-frames instrumented in the model. When the results of one cross-frame line improved, the results of the other cross-frame line strayed further from the experimental results. Figure 7-16 highlights this by showing relatively comparable results in CFL #7 at the loss of comparable results in CFL #3.

**Experimental vs. FEA Model Brace Axial Forces (Tension vs. Compression)**

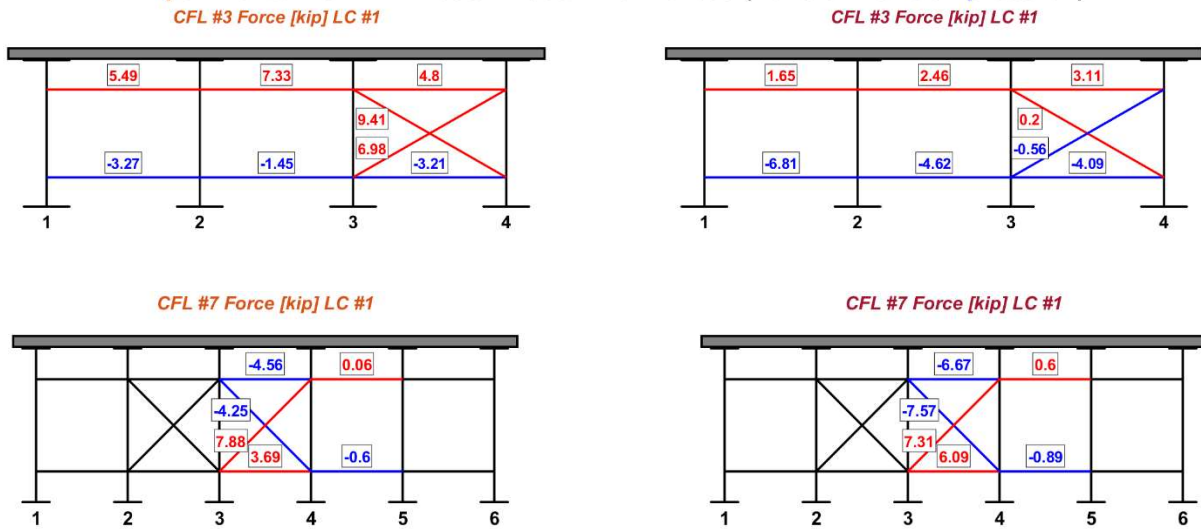


Figure 7-16. Results from 6:00 AM Model (created in collaboration with Aidan Bjelland)

The research team attempted to adjust the model by introducing a linear concrete stiffness distribution and manipulating the support conditions. These alterations did little to change the conflicting results. Based on the validation of SH 105 and Chisholm, the research team concluded that the uncertainty in the loading and deck pour timeline was likely the cause of the discrepancy and was not something the research team could overcome by altering the model.

## Chapter 8. Study of Bridge Models

With FEA modeling procedures validated for the SH 105, Chisholm Trail, and Lubbock bridges, additional models were analyzed to evaluate the live-load response of lean-on compared to conventional bracing, as well as to determine optimal cross-frame layouts for lean-on systems. The additional Abaqus models were constructed utilizing a Python script developed by Bjelland (2024) to ensure consistent modeling techniques. Findings from these studies are summarized in the following sections.

### 8.1. Live Load Stress Response of Lean-on Systems

---

Historically, cross-frames have been members affected by fatigue concerns. In AASHTO LRFD BDS (2020), bridge details are categorized for allowable constant-amplitude fatigue thresholds. An  $E'$  detail category was introduced in the 9<sup>th</sup> edition, which applies to welded cross-frame members and lean-on struts.  $E'$  details have a threshold of 2.6 ksi for infinite life. For this reason, it is necessary to assess the live-load stress performance of lean-on bracing as compared to conventional bracing.

Models were created for the SH 105 and Chisholm Trail bridges with conventional bracing. They were loaded with the same truck cases used during live loading of the system, and the resulting forces in the bracing members were compared with the forces from the lean-on models. In order to facilitate equitable comparison between the systems, the maximum tensile force value for each cross-frame line was determined, including cross-frames and lean-on struts. The lean-on value was subtracted from the conventional value, such that a positive value indicates that conventional bracing had a higher maximum bracing line force, and a negative value indicates that

the lean-on bracing had a higher maximum bracing line force. This eliminated the issue of not being able to directly compare member-to-member, due to the varying numbers of cross-frames. However, this also dismisses an intrinsic benefit of lean-on bracing, which is the reduced number of cross-frames in the bracing line. The maximum member force for each bridge and load case is generally close to 10-15 kips. Percent differences were not used because for some cases, the maximum cross-frame line member force was less than one kip.

### **8.1.1. SH 105 Bridge**

Load cases one, two, and four were analyzed for span six of SH-105, which is the span instrumented during field testing. Bridge layout information for the SH 105 bridge is discussed in section 6.3, while truck placement information is included in Appendix D. Load case one included four trucks lined up side-to-side between cross-frame lines five and six. The results of the comparison between conventional and lean-on bracing are shown in Figure 8-1. For this load case, lean-on bracing resulted in lower maximum brace forces for seven of the eleven cross-frame lines in span six. The maximum brace force was higher for lean-on bracing in four of the cross-frame lines. Overall, the maximum difference between conventional and lean-on bracing for load case one is less than three kips.

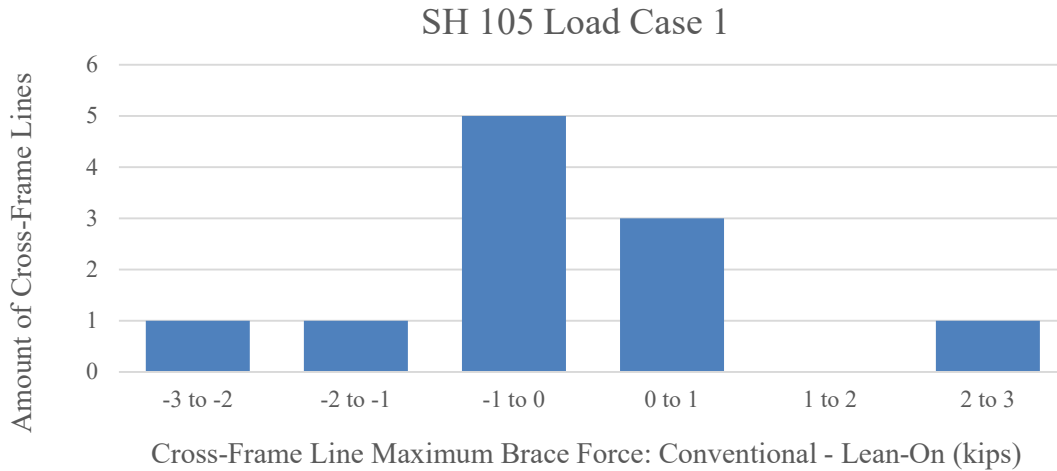


Figure 8-1. SH 105 Load Case One Conventional vs. Lean-On Bracing Line Forces

Load case two consisted of the four trucks clustered in a two-by-two configuration over cross-frame line three. The trucks were directly above the cross-frames in the lean-on bracing configuration. The comparison results for load case two are shown in Figure 8-2. The difference between the maximum brace force for lean-on compared to conventional bracing in eight of the eleven cross-frame lines is within one kip. Two cross-frame lines had a reduction in maximum brace force between two and three kips for lean-on bracing. However, one cross-frame line had a maximum member force increase of over eight kips for lean-on. The maximum brace force in cross-frame line four was 7.9 kips for conventional bracing and 16.4 kips for lean-on bracing.



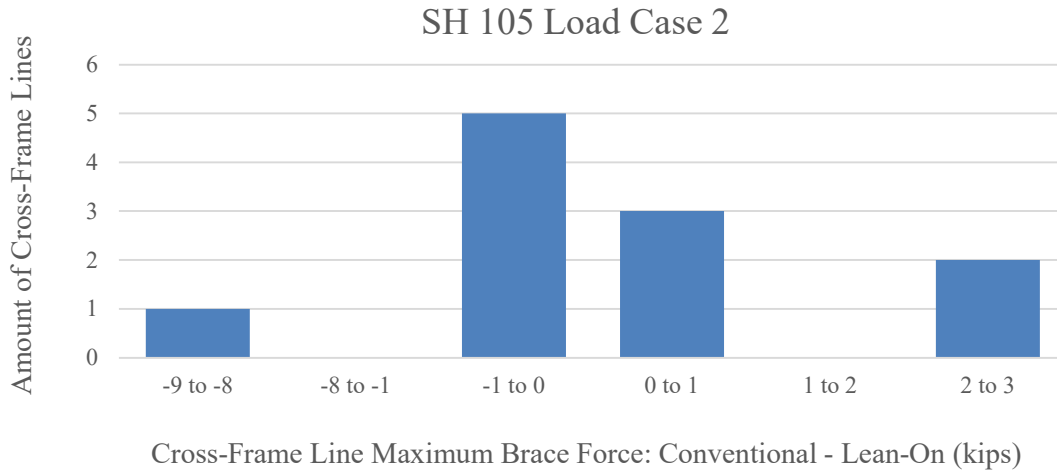


Figure 8-2. SH 105 Load Case Two Conventional vs. Lean-On Bracing Line Forces

Load case four is similar to load case two, except the trucks were placed over the lean-on bays of cross-frame three. The results are shown in Figure 8-3. In contrast to load case two, in load case four, the difference between the maximum brace force for lean-on compared to conventional bracing is within one kip for ten of the eleven cross-frame lines. One cross-frame line has a difference slightly greater than one kip, indicating the maximum force in the lean-on cross-frame line is less than the maximum force in the conventional bracing. From the comparison between load-cases two and four, it seems that the position of the truck along the cross-frame line, as well as the span, will have an impact on live-load induced brace forces.

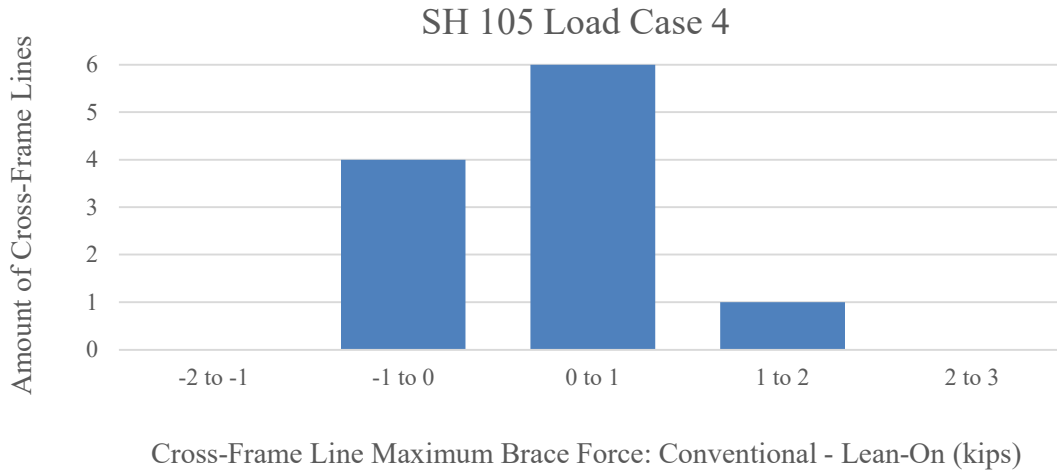


Figure 8-3. SH 105 Load Case Four Conventional vs. Lean-On Bracing Line Forces

### 8.1.2. Chisholm Trail Bridge

Comparisons of the maximum cross-frame line member forces were conducted with load cases three, two, and five for conventional and lean-on bracing models of the Chisholm Trail bridge. Bridge layout information for the Chisholm Trail bridge is discussed in section 6.4, while truck placement information is included in Appendix G. Load case three consisted of four trucks aligned front-to-back over bay three, centered along the cross-section. The trucks were centered over cross-frame line nine along the span. The results of comparing the maximum cross-frame member forces are shown in Figure 8-4. The maximum bracing line forces between the conventional and lean-on bracing are similar. Six of the seventeen bracing lines have higher maximum forces for lean-on bracing, but still within two kips. The remaining eleven cross-frame lines have higher maximum forces for conventional bracing, within three kips of the lean-on maximums.

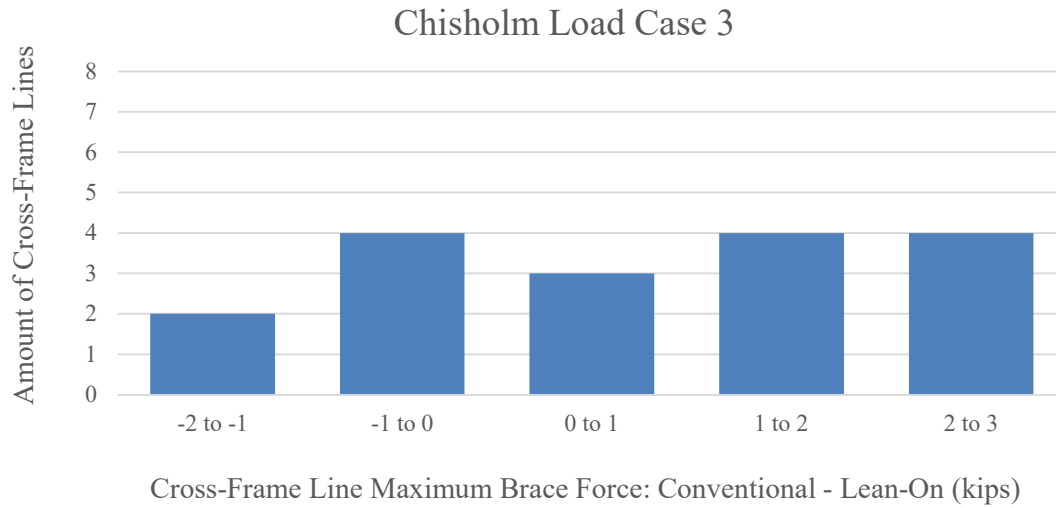


Figure 8-4. Chisholm Trail Load Case Three Conventional vs. Lean-On Bracing Line Forces

Load case two consisted of four trucks in a two-by-two configuration over cross-frame lines nine through eleven. The trucks were slightly closer to the pier than they were to the abutment, with the trucks on the side of the bridge with the skew region. The results are shown in Figure 8-5. The maximum cross-frame member forces tended to be reduced for the lean-on model, with twelve cross-frame lines, and five cross-frame lines had reduced maximum cross-frame member forces for conventional bracing.

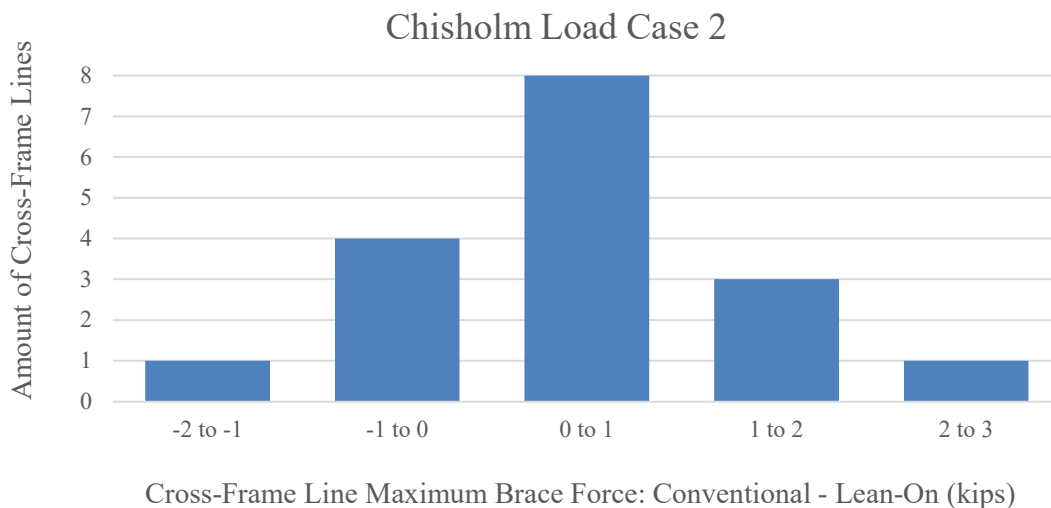


Figure 8-5. Chisholm Trail Load Case Two Conventional vs. Lean-On Bracing Line Forces

Load case five is similar to load case two. The four trucks were again positioned in a two-by-two configuration, but over bays four and five of cross-frame lines seven, eight, and nine. The trucks were slightly closer to the abutment than the pier. With the bridge layout and truck position essentially symmetrical to load case two, similar performance is expected. As shown in Figure 8-6, the distribution of the differences in the maximum cross-frame force between the lean-on and conventional models is similar to what was observed for load case three. However, a few more cross-frame lines have lower forces than the conventional layout.

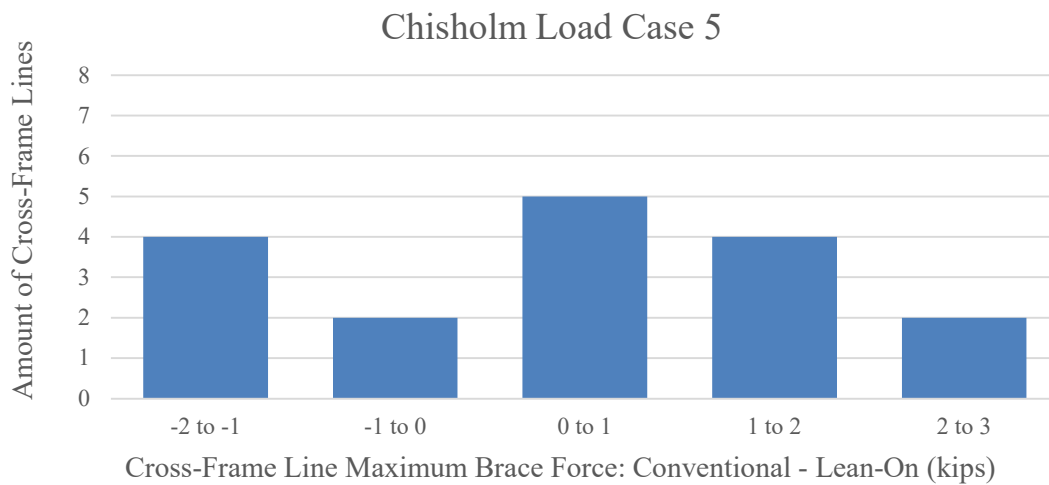


Figure 8-6. Chisholm Trail Load Case Five Conventional vs. Lean-On Bracing Line Forces

Overall, the live-load force study shows that the maximum tensile member forces in lean-on bridges are generally comparable to the maximum member forces in equivalent bridges with conventional bracing. Additionally, lean-on bracing has the added benefit of fewer brace members required for installation and inspection. However, the position of the truck on the cross-section of the bridge may play a significant role in determining governing load cases for fatigue in lean-on bridges.

## 8.2. Cross-Frame Layout Study

A parametric study was conducted by Bjelland (2024) as part of TxDOT Project 0-7093 (Helwig *et al.*, 2024) to determine ideal cross-frame layouts for lean-on systems. The study was conducted in three phases:

- 1) Initial Layout Study
- 2) Layout Effect Study with Isolated Brace Stiffness
- 3) Layout Effect Study with Isolated In-Plane Girder Stiffness

### 8.2.1. Findings From Phase 1: Initial Layout Study

The research team considered several possible bracing configurations and compared the relative performance of each layout. Plan view schematics for the initial cross-frame layouts tested are shown in Figure 8-7, where cross-frames are represented by solid lines and lean-on struts are represented by dashed lines. Single and two-span continuous bridges were studied with unbraced lengths of either 25 or 40 feet. Bridge systems were considered with 4 or 5 girders spaced at 10 or 12 feet. The spans were non-skew, with lengths of 150 or 250 feet, with span-to-depth ratios of 25 for single-span bridges and 35 for continuous systems. Girder sections with a girder-to-flange width ratio ranging from four to six were considered.

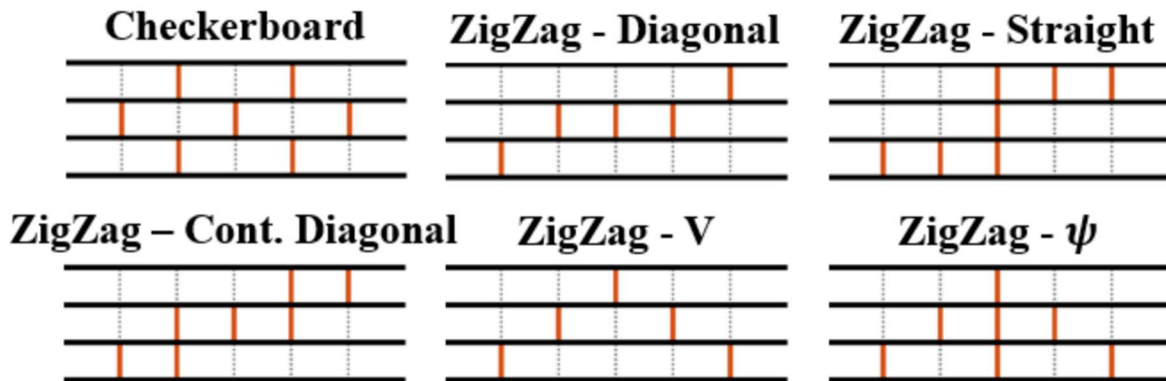


Figure 8-7. Phase 1 Lean-On Layouts (Bjelland, 2024)

The effectiveness of the lean-on bracing configurations was evaluated based on the performance relative to the conventional bracing configurations (no lean-on bracing). These comparisons were conducted by examining the maximum moment capacity and the minimum brace area required to cause buckling between the brace points with uniformly distributed loads for the lean-on systems relative to the conventional bracing configuration. The primary metric used to compare the configurations is the average minimum brace area obtained from the eigenvalue buckling analyses, where a lower required brace area indicated a more efficient system. From the preliminary study, ZigZag- $\psi$  and Checkerboard patterns were shown to require the lowest average brace area.

### **8.2.2. Findings From Phase 2: Layout Effect with Isolated Brace Stiffness**

As noted in Chapter 2, the total system stiffness is a function of the stiffness of the brace, the in-plane stiffness of the girders, and the cross-sectional stiffness to control distortion. Phase 1 of the study was insufficient for the identification of governing factors behind the system behavior, so it was necessary to perform additional studies isolating the system behavior due to a particular component. In Phase 2, the brace stiffness was isolated for study. To accomplish this, the cross-sectional distortion component,  $\beta_{sec}$ , and in-plane stiffness component,  $\beta_g$ , were modeled so that they could be taken as infinite. To eliminate the effects of the cross-sectional distortion component, full-depth cross-frames were used. To eliminate the effects of the in-plane stiffness, extremely wide girder spacings of 40 and 80 feet were used. By analyzing systems governed by the brace stiffness,  $\beta_{br}$ , the effectiveness of the cross-frames and struts layouts could be the focus of the study. The performance of a layout was assessed based on the buckling behavior of the girder system. As a result, five general recommendations were made as to guidelines for optimal cross-frame placement:

- 1) Ensure that cross-frames are equally distributed about the bridge centerlines, along the span, and along the cross-section.
- 2) Ensure all cross-frame lines are linked with girder pairs to allow for a direct lateral load path.
- 3) Ensure a cross-frame is included in every bay such that no bay is fully leaning along the span.
- 4) Ensure the number of adjacent leaning girders never exceeds a maximum of three in each cross-frame line.
- 5) Ensure a full cross-frame line is installed at the midspan of the bridge in order to facilitate erection and maximize the vertical warping stiffness of the girders. Diaphragms should be included at the supports.

### **8.2.3. Findings from Phase 3: Layout Effect with Isolated In-Plane Girder Stiffness**

In Phase 3, a complementary study to Phase 2 was conducted to assess the impact of the in-plane girder stiffness,  $\beta_g$ . To accomplish this, the cross-sectional distortion component,  $\beta_{sec}$ , and brace stiffness component,  $\beta_{br}$ , were modeled so that they could be taken as infinity. To eliminate the effects of the cross-sectional distortion component, full-depth cross-frames were used. To eliminate the effects of the brace stiffness, the area of the bracing components was increased beyond typical sizing to provide at least 10 times the ideal stiffness.

As discussed in section 2.6.1, the in-plane girder stiffness had previously been shown to be reduced compared to conventional bracing when lean-on bays were introduced to the system (Helwig and Wang, 2003). However, Fish (2021) showed that the original in-plane girder stiffness expression led to increasing errors for larger numbers of cross-frame lines relative to FEA solutions. The updated expression derived by Fish (2021) and later verified by Fish et al. (2024),

considered the effects of multiple girders and the stiffness of multiple inline cross-frames. The formulation of the new  $\beta_g$  expression from Fish et al. (2024) is directly related to the derivation of the new  $M_g$  equation discussed in section 2.5.1. As such, a layout factor, referred to as  $C_{LO}$ , that encompasses the effects of cross-frame configurations on  $M_g$ , can be squared and applied to  $\beta_g$ . The use of such a factor allows the intricate complexities of layout effects to be represented by a reduction that provides good accuracy with FEA solutions.  $C_{LO}$  is defined by Equation 8.1.

$$C_{LO,FEA} = \frac{M_{g,lean}}{M_{g,conventional}} \quad 8.1$$

Where:

$M_{g,lean}$  is the global lateral torsional buckling capacity of the lean-on system analyzed

$M_{g,conventional}$  is the global lateral torsional buckling capacity of the conventional system analyzed

In skewed systems, the bracing lines adjacent girders at varying locations along the length of the girder. The stability of the system is improved because many of the bracing lines frame directly into the support, so the distance of a bracing line from a support is reduced, compared to a nonskew span of identical length. The bracing lines in skew systems provide similar performance benefits as flange-level lateral trusses. Both increase the system warping stiffness, which is quantified by an effective length factor,  $K$ . The appropriate values for  $C_{LO}$  and  $K$ , depending on the cross-frame layout and skew, are shown in Table 8-1. The equations for system buckling moment and in-plane girder stiffness are given by Equations 8.2 and 8.3.



Table 8-1. Lean-on  $\beta_g$  and  $M_g$  Recommendations adapted from Bjelland (2024)

Skew Angle ( $\theta$ ) in Degrees	Layout	$C_{LO}$	$K$	Effective $M_g$	Effective $\beta_g$
$\theta < 20$	Conventional	1.00	1.0	1.00	1.00
	Lean-On	0.95		0.95	0.90
$20 \leq \theta < 30$	Conventional	1.00	0.8	1.56	1.95
	Lean-On	0.85		1.33	1.41
$\theta \geq 30$	Conventional	1.00	0.7	2.04	2.92
	Lean-On	0.85		1.73	2.11

$$M_{gs,2024} = C_{LO} C_{bs} \frac{\pi^4 s E}{(KL)^2} \sqrt{I_{eff} I_x \frac{\alpha_x}{2n_g}} \quad 8.2$$

$$\beta_{g,2024} = C_{LO}^2 C_{bs}^2 \frac{\pi^4 E I_x s^2}{2n_g (KL)^3 (n+1)} \alpha_x \quad 8.3$$

General recommendations as a result of the in-plane girder stiffness isolation study include:

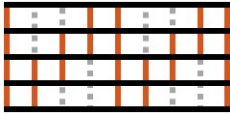

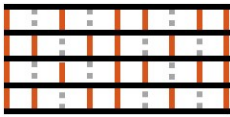
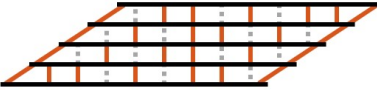
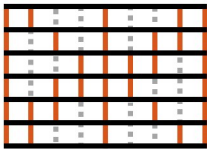
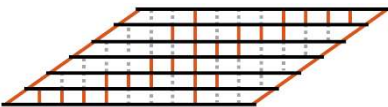
- 1) As a general rule, lean-on bracing should not be used with bridges with only three girders since there is very little savings in eliminating braces. An exception to this would be the removal of individual cross-frames near a support in a heavily skewed bridge.
- 2) The checkerboard layout should be limited to cases with 4 or 5 girders since wider systems become dominated by local layout effects.
- 3) The diagonal layout should not be utilized for bridges with nonskewed supports, ZigZag should be used instead.
- 4) The X-layout should not be used for systems with less than six girders, as using the layout would lead to situations that either include too many cross-frames (effectively

conventional) or too few cross-frames (poor distribution of cross-frames to maximize lean-on bracing).

### 8.2.4. Summary of Recommended Layouts

A summary of the recommended cross-frame layouts is shown in Table 8-2 for varying skew angle, number of girders, and additional span length and erection considerations.

Table 8-2. Recommended Lean-On Layout Summary adapted from Bjelland (2024) and Helwig (2024)

Layout Name	Nonskew (< 20°)	Skew (≥ 20°)	# of Girders	# of CFL	Additional Notes
ZigZag		Not Recommended	4-5	7+	Optional layout for nonskew
Diagonal	Not Recommended		4-5	Any	Preferred layout for skew
Checkerboard			4-5	Any	Preferred layout for nonskew Optional layout for skew
X			6+	5+	Position cross-frames of second diagonal to minimize clusters of leaning girders

## Chapter 9. System Stiffness Equation Performance Comparison with 3D Models

The final step for validating the revised lean-on brace stiffness equation was to perform comparisons between full bridge models and the calculated system stiffness using the revised brace stiffness and in-plane girder stiffness expressions. Data for the full bridge system models was provided by Aidan Bjelland and comparisons were made by the author. Differences between the brace system equation derivation and the full system behavior, the system performance resulting from the worst lean-on cross-frame layouts, mitigation strategies to improve cross-frame placements, equation accuracy with the recommended layouts, and considerations for the design of ideal lean-on systems are discussed in the following sections.

### 9.1. Differences Between Brace Stiffness Derivation and 3D Bridge System Models

---

The derivation of the previous  $\beta_{br,lean2003}$  equation and new  $\beta_{br,lean}$  equation assume an idealization of the cross-frame line behavior. The idealization includes vertical supports at each girder, preventing any vertical displacement of the girders. The deformed shape and loading of the cross-frame line is shown in Figure 9-1.

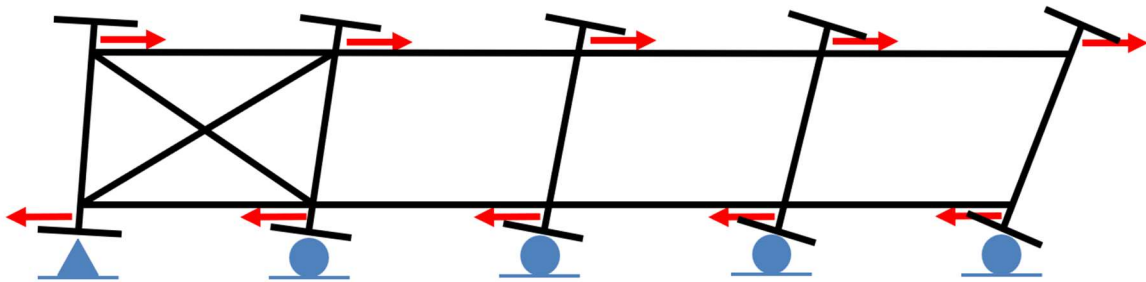


Figure 9-1. Bridge Cross-Frame Line Displacement with Supports Under Each Girder

However, in a full bridge system, the idealization of zero vertical displacements at each cross-frame line is not true. The girders are supported at the ends of the span, which allows the section of the cross-frame line to deflect vertically. An example displacement profile of a span with a single cross-frame line is illustrated in Figure 9-2. This disjointed behavior is mitigated by distributing cross-frames in different bays along the length of the span.

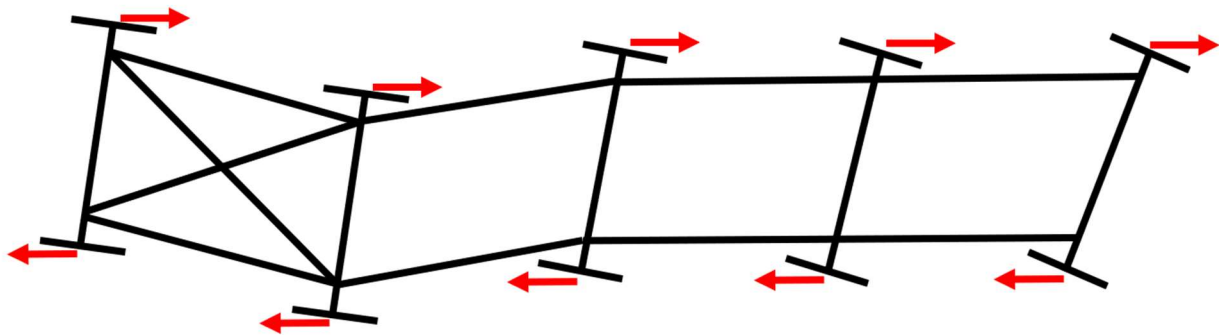


Figure 9-2. Bridge Cross-Frame Line Displacement with Supports at Ends of Span

Mechanisms of poor system performance, referred to as layout effects, can be mitigated by distributing cross-frames equally along the cross-frame line and opposite along the span, as well as linking cross-frame lines together, as discussed in section 8.2. In the cases where these layout effects are minimized, the idealized cross-frame line assumption is accurate.

Additionally, layout effects can have a negative impact on the assumptions behind the derivations for the in-plane girder stiffness,  $\beta_g$ . The research behind the revised  $\beta_g$  equations applied a similar cross-frame line assumption regarding rigid rotation. If a layout is extremely ineffective (poorly distributed cross-frame layout), the fundamental assumptions behind the  $\beta_{br,lean}$  and  $\beta_g$  expressions may not be applicable. With the recommended layouts, the equations will perform as intended to calculate the total system stiffness. Validation of this assertion is discussed in the following sections.

## 9.2. Equation Validation for Constant Cross-Frame Placements

---

One way to invalidate the fundamental cross-frame line behavior assumptions is to maximize the number of leaning girders along the span and minimize the distribution of cross-frames. A study was conducted to show the impacts of this behavior using a single cross-frame line. FEA was used to determine an applicable  $C_{LO}$  value using the same method discussed in section 8.2.3. Pairs of models were analyzed for each girder system in order to compare the global buckling moment capacity for a given lean-on system was compared with the moment capacity of an identical system with conventional bracing, as shown in Equation 8.1. The  $C_{LO}^2$  value was used to calculate  $\beta_g$  by use of Equation 8.3. The minimum brace area corresponding to buckling between the brace points was obtained using a genetic algorithm (Bjelland, 2024). In these tests, standard-sized girders for a span length of 50 feet were spaced at 10 feet. There was only one line of lean-on bracing, resulting in an unbraced length of 25 feet. A single cross-frame was provided on one side of the cross-frame line, with additional adjacent lean-on bays added with additional girders. The data is included in Table 9-1, with layouts indicated using “1” for cross-frame locations and “0” for lean-on bays.

Table 9-1. Results for 1 CFL with 10 Foot Girder Spacing

CFL Layout	$A_{br}$	$\beta_{br,lean}$	$C_{LO}^2$	$\beta_g$	$\beta_T$	$\frac{\beta_T}{\beta_{ideal}}$
1 CFL	$(in^2)$	$\left(\frac{kip - in}{rad}\right)$	FEA Results	$\left(\frac{kip - in}{rad}\right)$	$\left(\frac{kip - in}{rad}\right)$	$\beta_{ideal}$
[1]	1.1	253,000	1.00	1,617,000	219,000	0.99
[1,0]	2.1	222,000	0.26	1,130,000	186,000	0.84
[1,0,0]	3.8	224,000	0.11	872,000	178,000	0.81
[1,0,0,0]	6.3	239,000	0.05	712,000	179,000	0.81
[1,0,0,0,0]	10.2	265,000	0.03	603,000	184,000	0.84
[1,0,0,0,0,0]	15.9	303,000	0.02	525,000	192,000	0.87
[1,0,0,0,0,0,0]	24.6	356,000	0.01	466,000	202,000	0.92
[1,0,0,0,0,0,0,0]	38.3	435,000	0.01	419,000	213,000	0.97
[1,0,0,0,0,0,0,0,0]	61.3	562,000	0.01	382,000	227,000	1.03

$$*\beta_{ideal} = 220,000 \frac{kip-i}{rad}$$

The brace stiffness is directly affected by the brace area, so despite the increase in the number of adjacent leaning girders,  $\beta_{br,lean}$  increases due to the unreasonable brace area required for the system to achieve  $\beta_{ideal}$ . As indicated by the  $C_{LO}^2$  values in Table 9-1, the lean-on system is unable to benefit from the warping stiffness provided by additional girders. Instead, the leaning girders become parasitic to the stiffness of the system, as they effectively pull on the system without contributing substantial stiffness, which results in a significant reduction of  $\beta_g$ . Additionally, the  $\beta_{br,lean}$  equation is limited by the assumption that the girders and cross-frames do not deflect downward vertically.

### 9.3. Performance Improvement for Staggered Layouts

To further highlight the impact of poor layouts, bridge systems with three cross-frame lines were studied. Each of the three cross-frame lines had the same pattern of cross-frames and lean-on bays. The girders were extended to 100 feet in length and spaced at 80 feet in order to maximize

$\beta_g$  after observing the previous results. The unbraced length of 25 feet stayed the same for each of the three cross-frame lines. The results from these models are shown in Table 9-2.

The data in Table 9-2 indicates that the calculated system stiffness is conservative relative to the ideal stiffness.  $\beta_{br,lean}$  for the layouts with three cross-frame lines is less than in the layouts with one cross-frame line. The distance of the midspan from the supports increases the difference in vertical deflection along the cross-frame lines, which appears to increase the effective stiffness of the single brace. The effectively infinite  $\beta_g$  value is reduced by the leaning girders such that  $\beta_g$  influences system behavior.

Table 9-2. Results for 3 CFL with 80 Foot Girder Spacing

CFL Layout	$A_{br}$	$\beta_{br,lean}$	$C_{LO}^2$	$\beta_g$	$\beta_T$	$\frac{\beta_T}{\beta_{ideal}^*}$
3 CFL (no stagger)	( $in^2$ )	( $\frac{kip-in}{rad}$ )	FEA Results	( $\frac{kip-in}{rad}$ )	( $\frac{kip-in}{rad}$ )	$\beta_{ideal}^*$
[1]	6.2	224,000	1.00	6,467,000	216,000	0.98
[1,0]	11.3	175,000	0.26	4,518,000	169,000	0.77
[1,0,0]	19.0	159,000	0.11	3,486,000	152,000	0.69
[1,0,0,0]	29.3	151,000	0.05	2,848,000	144,000	0.65
[1,0,0,0,0]	42.5	149,000	0.03	2,414,000	140,000	0.64
[1,0,0,0,0,0]	59.5	150,000	0.02	2,100,000	140,000	0.64
[1,0,0,0,0,0,0]	80.1	153,000	0.01	1,862,000	141,000	0.64
[1,0,0,0,0,0,0,0]	104.3	155,000	0.01	1,676,000	142,000	0.65
[1,0,0,0,0,0,0,0,0]	132.5	158,000	0.01	1,526,000	143,000	0.65

$$*\beta_{ideal} = 220,000 \frac{kip-in}{rad}$$

Based on the layout recommendations provided in section 8.2.2, a “staggered” layout, meaning the placement of the cross-frame in the second cross-frame line is opposite the first and third lines, is likely to improve the overall system behavior by improving the girder connectivity and reducing the global layout effect. A schematic of staggered layouts is shown in Figure 9-3. For girder systems with more than three girders, local layout effects may still be present due to the

interior girders not being connected by cross-frames. The results for staggering the same layouts used in Table 9-2, by reversing the middle cross-frame line, are listed in Table 9-3.

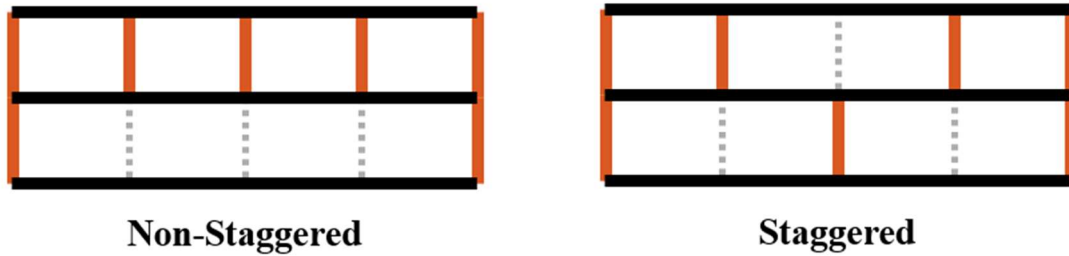


Figure 9-3. Schematic of Non-Staggered vs. Staggered Lean-On Layouts

Table 9-3. Results from 3 staggered CFL parametric study on leaning girders

CFL Layout	$A_{br}$	$\beta_{br,lean}$	$C_{LO}^2$	$\beta_g$	$\beta_T$	$\frac{\beta_T}{\beta_{ideal}^*}$
3 CFL (stagger)	( $in^2$ )	( $\frac{kip - in}{rad}$ )	FEA Results	( $\frac{kip - in}{rad}$ )	( $\frac{kip - in}{rad}$ )	
[1]	6.2	224,000	1.00	6,467,000	216,000	0.98
[1,0]	11.5	179,000	0.71	8,731,000	175,000	0.80
[1,0,0]	19.4	162,000	0.44	6,365,000	158,000	0.72
[1,0,0,0]	30.4	157,000	0.32	5,229,000	153,000	0.69
[1,0,0,0,0]	44.6	156,000	0.24	4,442,000	151,000	0.69
[1,0,0,0,0,0]	61.9	156,000	0.19	3,866,000	150,000	0.68
[1,0,0,0,0,0,0]	82.6	157,000	0.16	3,425,000	150,000	0.68
[1,0,0,0,0,0,0,0]	106.6	159,000	0.13	3,078,000	151,000	0.69
[1,0,0,0,0,0,0,0,0]	134.2	160,000	0.11	2,797,000	152,000	0.69

$$*\beta_{ideal} = 220,000 \frac{kip-in}{rad}$$


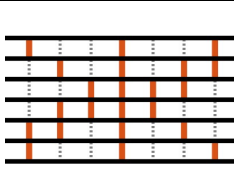
The calculated  $\beta_{br,lean}$  is the same for the staggered and unstaggered layouts, as regardless of the orientation, all of the cross-frame lines contain the same  $n_{g,eff}$ ,  $n_{c,eff}$ , and  $n_{lean,eff}$ . As a result, the staggering of the cross-frames had minimal impact on the minimum brace areas needed to obtain buckling between the brace points. However, the corresponding layout factors and, thus, the  $\beta_g$  of the staggered layouts were greatly increased.



## 9.4. Performance of Recommended Layouts

Although examining the effects of extreme systems often leads to discoveries with system behavior, practical applications often will never encounter these extreme scenarios. As such, the new  $\beta_{br,lean}$  expression was examined using models with optimized cross-frame line brace areas. Two recommended layouts were tested, covering a wide array of typical cross-frame lines. The results for these two layouts are shown in Table 9-4. For simplicity, lateral trusses were included due to insufficient  $\beta_g$  provided by the girder geometry and covered 25% of the span length. Due to the length covered by the lateral trusses and thus the large amount of warping restraint provided, the K value is assumed to be  $\sim 0.5$  instead of the design recommendation of 0.7 (Fish *et al.*, 2024).

Table 9-4. Results from recommended layout study

Layout	CFL	$A_{br}$	$\beta_{br,lean}$	$C_{LO}^2$	$\beta_g$	$\beta_T$	$\frac{\beta_T}{\beta_{ideal}^*}$
Lateral Trusses Included ( $K = 0.5$ )		( $in^2$ )	( $\frac{kip-in}{rad}$ )	FEA Resu lt	( $\frac{kip-in}{rad}$ )	( $\frac{kip-in}{rad}$ )	
	[1,1,0,0]	7.5	445,000	0.99	406,000	212,000	0.97
	[0,1,1,0]	5.5	497,000	0.99	406,000	224,000	1.02
	[1,1,1,1]	1.3	287,000	0.99	406,000	168,000	0.76
	[1,1,0,0,0,1]	3.3	258,000	0.99	813,000	196,000	0.89
	[0,1,1,0,1,0]	5.0	396,000	0.99	813,000	288,000	1.21
	[0,0,1,1,0,0]	7.6	381,000	0.99	813,000	260,000	1.18
	[1,1,1,1,1,1]	4.5	1,032,000	0.99	813,000	455,000	2.07

$$*\beta_{ideal} = 220,000 \frac{kip-in}{rad}$$

The results in Table 9-4 highlight the behavioral differences between narrow and wide bridge systems. Note that  $\beta_{br,lean}$  is conservative for bracing lines that approach conventional bracing. The narrow zigzag system produced results that were in accord with expected values. However, the full cross-frame line at midspan in the wider X system requires nearly two times the

expected stiffness value. The reason for this increased stiffness requirement can be better understood by examining the buckled shape in Figure 9-4.

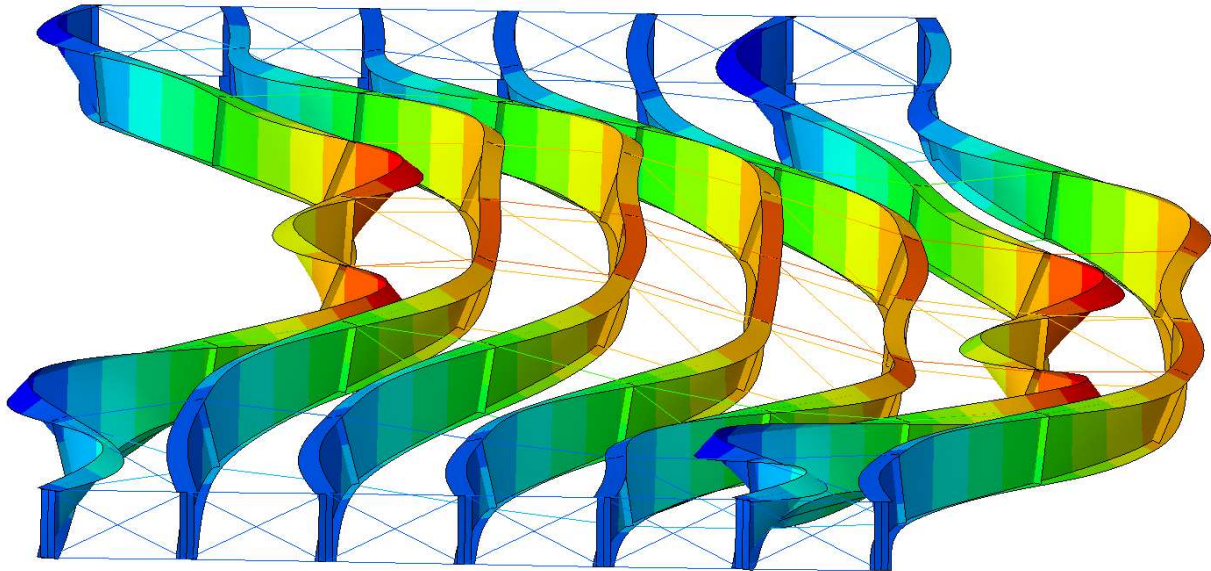


Figure 9-4. Buckled Shape of Optimized X Bridge System (Bjelland, 2024)

The buckled shape in Figure 9-4 illustrates how the full cross-frame line at midspan preserves the system stiffness by being rigid enough to maintain the vertical system warping stiffness needed for  $\beta_g$ . Due to the nonlinear behavior of the system and the optimization algorithm, the resulting optimized system minimized the brace stiffness of the cross-frame lines with lean-on bays at the expense of increasing the stiffness requirement of the full cross-frame line. As such, in this permutation of the system, the full cross-frame line at midspan is forced to effectively be the sole contributor to the vertical system warping stiffness, maintaining the girder pairs. For typical bridge systems, this likely will not be an issue as the moment distribution is less critical (non-uniform), and the moment corresponding to buckling between the brace point will generally exceed the deck pour loading. Overall, these results emphasize that designers will need

to be cognizant of nonlinear behavior of these systems and how the full cross-frame line at midspan is vital in preserving  $\beta_g$ .

## 9.5. Relationship of $\beta_g$ and $\beta_{br}$ for Design

---

A plot of the springs-in-series relationship of the minimum brace stiffness and in-plane girder stiffness is highlighted in Figure 9-5. The total system stiffness in the models discussed in this chapter needed to satisfy exactly the ideal stiffness, and in design must satisfy two times the ideal stiffness.  $\beta_{br,lean}$  and  $\beta_g$  both play a vital role in determining the system stiffness.

If the brace stiffness and in-plane girder stiffness are similar in quantity to each other and the ideal stiffness, the minimum stiffness for both is approximately two times the ideal ( $\sim 4$  times with imperfection). If one component is much greater than the ideal stiffness, for example, the in-plane girder stiffness for wide systems or the brace stiffness for conventional systems, the other component requirement reduces to the ideal stiffness. This is relevant for design, since the  $2\beta_{ideal}$  design requirement may lead to a design being insufficient due to an individual stiffness component.

In the application of the equations in the design process, this principle is essential to understand, as an insufficient girder stiffness ( $\beta_g$ ) will result in a negative or impossible brace area requirement with lean-on, or even conventional bracing.

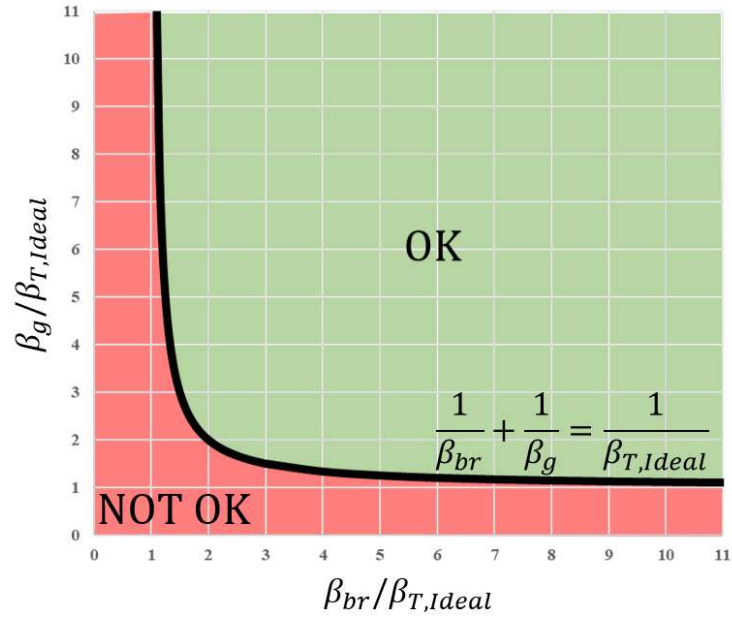


Figure 9-5. Relationship Between Stiffness Components Relative to the Ideal Stiffness (Bjelland, 2024)

## Chapter 10. Revised Expressions for Brace Strength Design

Stability bracing must satisfy both stiffness and strength requirements, so it was necessary to update the form of the strength design equations to reflect the layouts permitted by the revised stiffness equations. Updated strength design equations were derived based on the models used to derive the stiffness equations for lean-on bracing with Z-, X-, or K-frames discussed in Chapter 3, Chapter 4, and Chapter 5. The following sections provide an overview of the previous equations and the rationale for the revised expressions. As discussed in section 2.8, all force requirement equations include the total brace force, denoted by  $F$  or  $F_{br}$ .  $F$  is calculated using the brace moment,  $M_{br}$ , which is given by Equation 10.1 as a simplified version of Equation 2.15.

$$M_{br} = \frac{0.0048LL_b}{nI_{eff}Eh_0} \left( \frac{M_u}{C_b} \right)^2 \quad 10.1$$

Where:

$L$  is the span length

$L_b$  is the length of a diagonal brace member

$n_{CFL}$  is the number of cross-frame lines

$I_{eff}$  is the effective moment of inertia about the y-axis

$E$  is the modulus of elasticity

$h_0$  is the distance between flange centroids

$M_u$  is the applied moment

$C_b$  is the moment gradient factor

$F$  is calculated using Equation 10.2.

$$F = \frac{M_{br}}{h_b} \quad 10.2$$

Where:

$h_b$  is the height of the brace

## 10.1. Previous Strength Requirement Equations

Helwig and Wang (2003) developed strength equations for lean-on bracing lines with a single Z-frame. Like the stiffness equations developed at the same time, the strength equations included the term  $n_{gc}$ , which limited the application to lines with a single cross-frame, as shown in Figure 10-1.

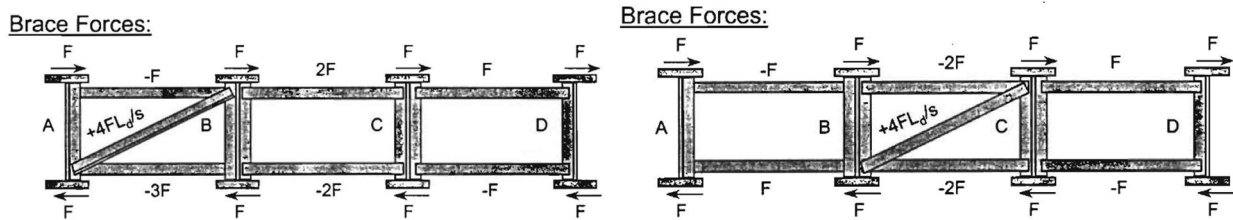


Figure 10-1. Brace Forces (Helwig and Wang, 2003)

Equations for the maximum force demand in a diagonal,  $F_d$ , and the maximum force demand in the top and bottom struts,  $F_s$ , are given by Equations 10.3 and 10.4, respectively.

$$F_{d,2003} = \frac{n_{gc}L_d F}{s} \quad 10.3$$

$$F_{s,2003} = (n_{gc} - 1)F \quad 10.4$$

Where:

$n_{gc}$  is the number of girders per cross-frame

$L_d$  is the length of the diagonal member

$S$  is the girder spacing

## 10.2. Z-Frame Revised Strength Equations

In the revised equations, the coefficients are defined in terms of the same values used in the refined stiffness equation: the effective number of girders,  $n_{g,eff}$ , the effective number of cross-frames,  $n_{c,eff}$ , and the effective number of adjacent lean-on bays,  $n_{lean,eff}$ . The maximum forces are induced when the cross-frame is positioned in the exterior bay, as shown in Figure 10-2. The forces for a bracing line with a single exterior cross-frame were derived using static analysis, and were verified using the modeling software SAP2000, utilizing modeling practices validated previously for stiffness analysis.

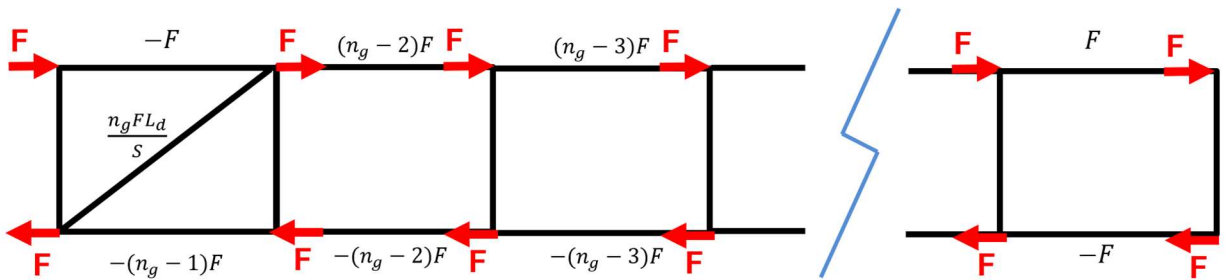


Figure 10-2. Z-Frame Single Brace Forces Exterior Bay

The models were used to develop member forces in more complex bracing layouts. For bracing lines with more than one cross-frame, the diagonal force is reduced and distributed between them. The diagonal forces shown in Figure 10-3 are conservative bounds, as the proportion of force in each cross-frame varies depending on the number and geometry of the cross-frames.

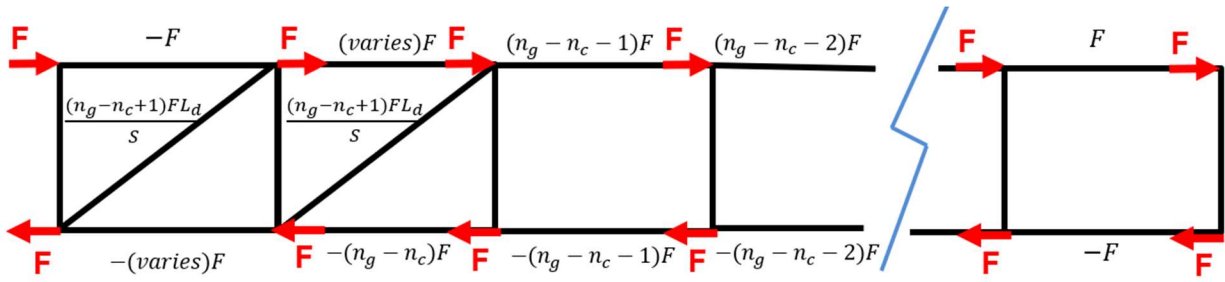


Figure 10-3. Z-Frame Brace Forces Multiple Cross-Frames

When the cross-frame(s) are moved to an interior bay, the maximum force in the struts is reduced, and the maximum force in the diagonal remains constant, as shown in Figure 10-4.

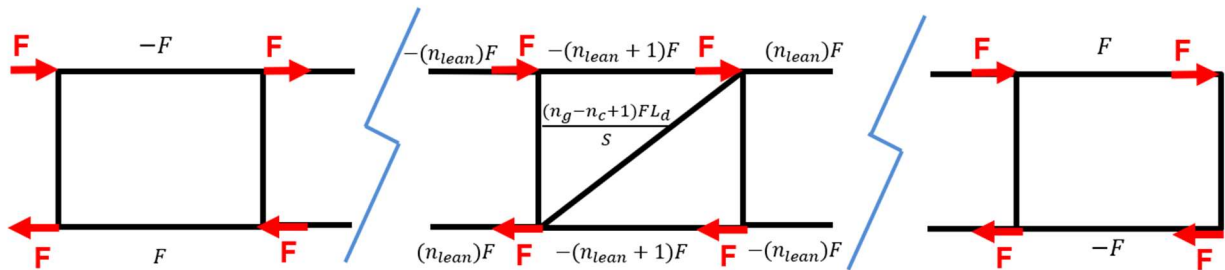


Figure 10-4. Z-Frame Brace Forces Interior Bay

By incorporating together all of these considerations, the force requirements for Z-Frames are given by Equations 10.5 and 10.6.

$$F_{dZ} = \frac{(n_{g,eff} - n_{c,eff} + 1)L_d F}{s} \quad 10.5$$

$$F_{sZ} = (n_{lean,eff} + 1)F \quad 10.6$$

### 10.3. X-Frame Revised Strength Equations

Strength equations were developed for X-shaped cross-frames by following a process similar to that used for Z-frames. The governing cross-frame position is again a single cross-frame in an exterior bay. The force path for this configuration is shown in Figure 10-5



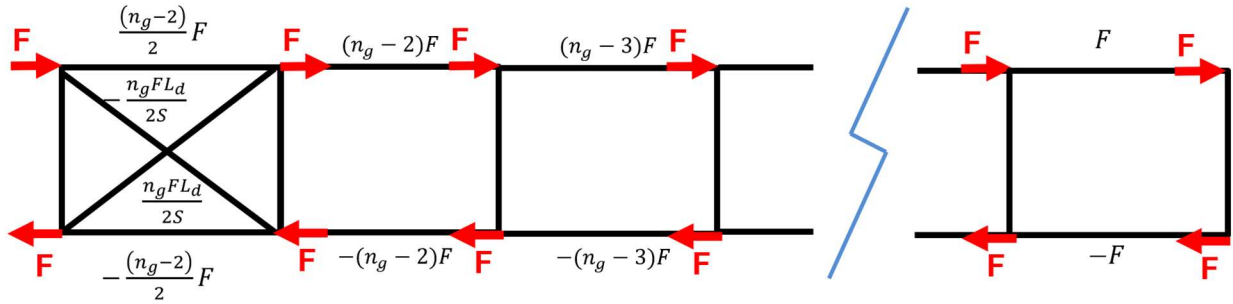


Figure 10-5. X-Frame Single Brace Forces

In order to account for the reduction in member forces due to multiple cross-frames and interior cross-frame placement, the cross-frame forces were rewritten as shown in Figure 10-6

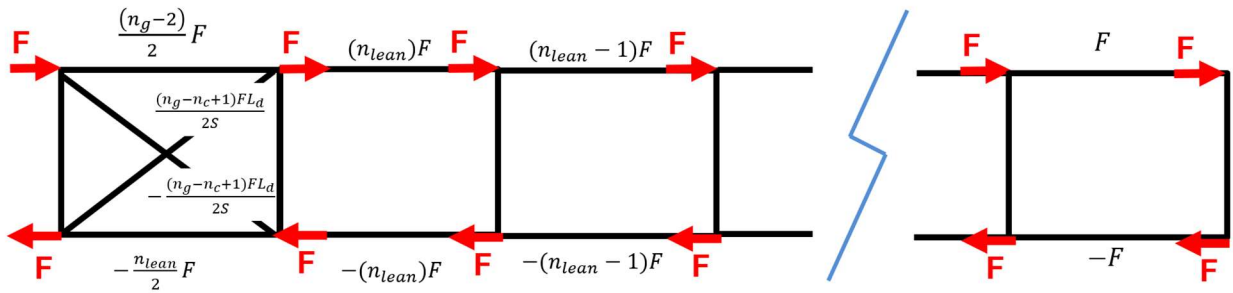


Figure 10-6. X-Frame Generalized Brace Forces

By taking the maximum force for the diagonals and struts, respectively, the force requirements for X-Frames are given by Equations 10.7 and 10.8.

$$F_{dX} = \frac{(n_{g,eff} - n_{c,eff} + 1)L_d F}{2S} \quad 10.7$$

$$F_{sX} = (n_{lean,eff})F \quad 10.8$$

#### 10.4. K-Frame Revised Strength Equations

Like Z- and X-frames, the maximum forces for K-frames are induced in a cross-frame line with a singular cross-frame in an exterior bay, as shown in Figure 10-7

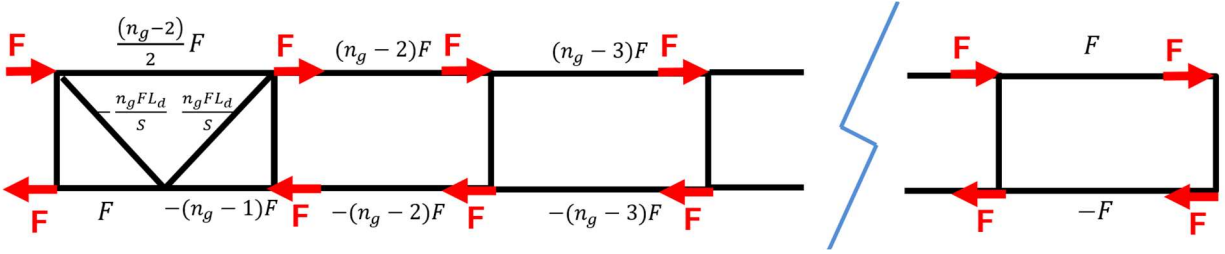


Figure 10-7. K-Frame Single Brace Forces

In order to account for reduced member forces with the presence of multiple K-frames, or K-frame positioning in interior bays, the force terms may be rewritten as shown in Figure 10-8.

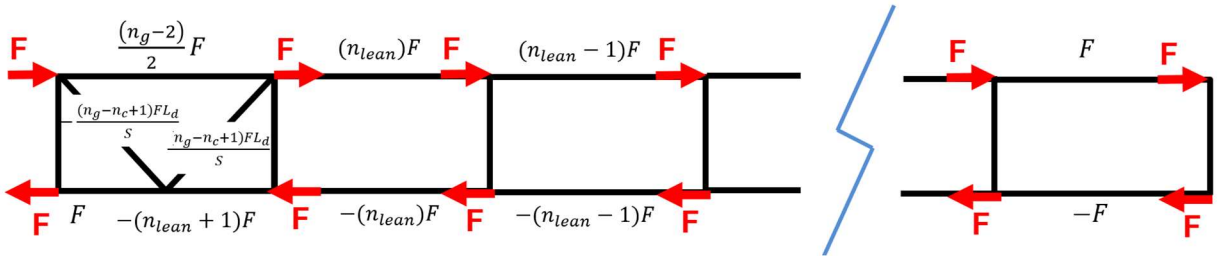


Figure 10-8. K-Frame Generalized Brace Forces

The maximum forces for the diagonals and struts in K-frame lines are given by Equations 10.9 and 10.10.

$$F_{dK} = \frac{(n_{g,eff} - n_{c,eff} + 1)L_d F}{s} \quad 10.9$$

$$F_{sK} = (n_{lean,eff} + 1)F \quad 10.10$$

## 10.5. Summary of Brace Force Equations

The lean-on member force equations for Z-, X-, and K-frames are similar, but not exactly the same for all cross-frame shapes. The correct expressions for the forces in Z- and K-frame members are given by Equations 10.11 and 10.12.

$$F_{d,leanZK} = \frac{(n_{g,eff} - n_{c,eff} + 1)L_d F}{s} \quad 10.11$$

$$F_{s,leanZK} = (n_{lean,eff} + 1)F \quad 10.12$$

The correct expressions for the forces in X-frame members are given by Equations 10.13 and 10.14.

$$F_{d,leanX} = \frac{(n_{g,eff} - n_{c,eff} + 1)L_d F}{2S} \quad 10.13$$

$$F_{s,leanX} = (n_{lean,eff})F \quad 10.14$$

## Chapter 11. Refined Design Methodology for Lean-On Bracing

The design process for a lean-on bracing system subject to vertical loading during construction is outlined and discussed in the following sections. An approach utilizing derived expressions is intended for direct application by design engineers. Numerical design examples for each methodology are included in Chapter 12.

### 11.1. Determine Girder Layout and Geometry

---

First, the girder design must be completed. This design should follow the AASHTO LRFD BDS. For a given girder with stepped flanges (also called a nonprismatic section), effective girder dimensions may be used in the design of the bracing system. An approach for the calculation of effective flange thickness is provided by Reichenbach et al. (2020) and is shown in Equation 11.1. The effective flange width can be calculated using the same equation and substituting  $t$  values for  $b$  values.

$$t_{eff} = t_{small}[1 - (1 - x_{small})^2] + t_2(1 - x_{small})^2 \quad 11.1$$

Where:

$t_{eff}$  is the effective flange thickness

$t_{small}$  is the smallest flange thickness

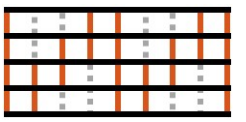

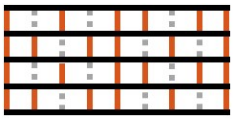
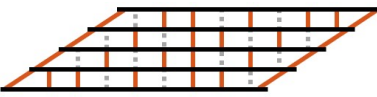
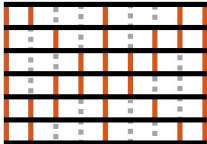
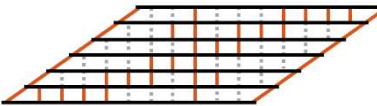
$x_{small}$  is the fraction of the span with smallest flange thickness

$t_2$  is the second smallest flange thickness

## 11.2. Determine Cross-Frame Locations Based on Recommended Layouts

To ensure the optimal placement of cross-frames in layouts, the research team has outlined four lean-on layouts for designers as the most effective options. These layouts and their appropriate application are shown in Table 11-1.

Table 11-1. Recommended Lean-On Layout Summary

Layout Name	Nonskew ( $< 20^\circ$ )	Skew ( $\geq 20^\circ$ )	# of Girders	# of CFL	Additional Notes
ZigZag		---	4-5	7+	Optional layout for nonskew
Diagonal	---		4-5	---	Preferred layout for skew
Checker-board			4-5	---	Preferred layout for nonskew Optional layout for skew
X			6+	5+	Position cross-frames of second diagonal to minimize clusters of leaning girders

## 11.3. Determine Moment Demands at Each Brace Line

The next step is to calculate the moment demand at each brace line. This should be known in advance from the girder design process. The maximum applied moment needs to be checked against the maximum system global buckling moment, as well as the braced buckling moment.

### 11.3.1. Calculate the Moment Loading at Each Cross-Frame Line

The applied moment at each brace line is determined using load tables or other software for construction loads.

### 11.3.2. Check System Global Buckling Moment

The global system buckling moment defines the capacity of the full system, assuming sufficient bracing between the girders. It is impossible for the full bridge to exceed this capacity, even with additional bracing, so the global system buckling moment must be greater than the maximum applied moment.  $M_{gs}$  is given by Equation 11.2.

$$M_{gs} = C_{LO} C_{bs} \frac{\pi^2 SE}{(KL)^2} \sqrt{I_y I_x \left( \frac{\alpha_x}{2n_g} \right)} \quad 11.2$$

Where:

$C_{LO}$  is 0.95 for nonskew bridges or 0.85 for skew bridges

$C_{bs}$  is 1.1 for single span, 2.0 for continuous span

$S$  is the girder spacing

$E$  is the modulus of elasticity of the girders

$K$  is 1.0 for systems without lateral trusses, 0.7 for single span systems with lateral trusses

$L$  is the span length

$I_y$  is the effective moment of inertia of the girder about the y-axis

$I_x$  is the effective moment of inertia of the girder about the x-axis

$n_g$  is the number of girders

$\alpha_x$  is the system warping stiffness factor shown in Table 11-2.

Table 11-2. System Warping Stiffness Factor ( $\alpha_x$ ) Values

Number of Girders $n_g$	System Warping Stiffness Factor $\alpha_x$
2	1
3	4
4	10
5	20
6	35
7	56
8	84
9	120
10	165

Check  $M_u < 0.7M_{gs}$  as discussed in Section 2.1.2.

### 11.3.3. Check the Conventional Lateral-Torsional Buckling Moment

Another limit on the maximum moment capacity is the conventional lateral-torsional buckling moment of the braced girder. Therefore, the maximum applied load cannot exceed the  $M_0$  capacity given by Equation 11.3.

$$M_0 = \frac{\pi}{L_b} \sqrt{EI_y GJ + \frac{\pi^2 E^2 I_y C_w}{L_b^2}} \quad 11.3$$

Where:

$L_b$  is the unbraced length of the girder (maximum distance between cross-frame lines)

$G$  is the shear modulus of elasticity

$J$  is the torsional constant

$C_w$  is the torsional warping constant:  $I_{cf} \frac{h_0^2}{2} \cong \frac{I_y h_0^2}{2}$  for a doubly symmetric I-shaped section

$h_0$  is the distance between flange centroids

$I_{cf}$  is the local strong-axis moment of inertia of the compression flange

Check  $M_u < 1.0M_0$

## 11.4. Determine Minimum Brace Area for Each Bracing Line

---

Now that the demand is known and the girders meet the global and lateral-torsional buckling criteria, the bracing system can be designed.

### 11.4.1. Determine Required System Stiffness

The required system stiffness is calculated using Equation 11.4.

$$\beta_{T,req} = \frac{2.4LM_u^2}{\phi C_b^2 n_{CFL} I_{y,eff} E} \quad 11.4$$

Where:

$\phi$  is the LRFD reduction factor (0.8)

$C_b$  is the moment gradient modifier

$n_{CFL}$  is the number of bracing lines in the span

$I_{y,eff}$  is the effective moment of inertia about the y-axis

### 11.4.2. Calculate In-Plane Girder Stiffness

The provided in-plane girder stiffness is calculated using Equation 11.5.

$$\beta_g = C_{LO}^2 C_{bs}^2 \frac{\pi^4 E I_x S^2 \alpha_x}{2n_g (KL)^3 (n_{CFL} + 1)} \quad 11.5$$



### 11.4.3. Calculate Cross-Sectional Stiffness

Language in the draft AASHTO ballot for stability bracing suggests that  $\beta_{sec}$  can be taken as infinity for braces deeper than 80% of the web depth.

If the braces are shallow compared to the rest of the girder, the stiffness of the cross-section,  $\beta_{sec}$ , may have a significant effect. The provided cross-section stiffness for shallow braces may be calculated using Equation 11.6 (Helwig and Yura, 2015).

$$\beta_{sec} = \frac{3.3E}{h_0} \left( \frac{(1.5h_0)t_w^3}{12} + \frac{t_s b_s^3}{12} \right) \quad 11.6$$

Where:

$h_0$  is the height of the web

$t_w$  is the thickness of the web

$t_s$  is the thickness of the stiffener

$b_s$  is the width of the stiffener

When the distance from the top cross-frame to the top of the girder is different than the distance from the bottom of the cross-frame to the bottom of the girder, then Equations 11.7, 11.8, and 11.9 may be used to estimate  $\beta_{sec}$  (Yura, 2001):

$$\beta_{sec} = \frac{1}{\frac{1}{\beta_{top}} + \frac{1}{\beta_{bot}}} \quad 11.7$$

$$\beta_{top} = \frac{3.3E}{h_0} \left( \frac{h_0}{h_{top}} \right)^2 \left( \frac{1.5h_{top}t_w^3}{12} + \frac{t_s b_s^3}{12} \right) \quad 11.8$$

$$\beta_{bot} = \frac{3.3E}{h_0} \left( \frac{h_0}{h_{bot}} \right)^2 \left( \frac{1.5h_{bot}t_w^3}{12} + \frac{t_s b_s^3}{12} \right) \quad 11.9$$

#### 11.4.4. Use Brace Stiffness Equation to Determine Minimum Brace Area

The required system stiffness is calculated using a variation of Equation 11.10

$$\beta_{br,lean} = R \frac{ES^2h^2}{C_{cf}(n_{g,eff}-n_{c,eff}+1)\frac{L_d^3}{A_d}+(n_{lean,eff}+1)\frac{2S^3}{A_s}} \quad 11.10$$

Where:

$R$  is a factor accounting for connection eccentricity (0.65)

$h$  is the height of the brace

$C_{cf}$  is 1.0 for Z-frames, 0.5 for X-frames, and 2.0 for K-frames

$n_{c,eff}$  is the effective number of cross-frames in the bracing line

$n_{g,eff}$  is the effective number of girders in the bracing line

$n_{lean,eff}$  is the effective number of lean-on bays in the bracing line

$A_d$  is the area of the diagonal braces

$A_s$  is the area of the top and bottom struts

$L_d$  is the length of a diagonal brace

The total provided brace stiffness of the system is given by Equation 11.11

$$\beta_{T,prov} = \left( \frac{1}{\beta_g} + \frac{1}{\beta_{br,lean}} + \frac{1}{\beta_{sec}} \right)^{-1} \quad 11.11$$

For a given in-plane girder stiffness, a required brace stiffness can be determined with Equation 11.12. If  $\beta_{br,req}$  is negative,  $\beta_g$  is insufficient and not even conventional bracing will pass. The girders must be redesigned with a larger  $I_x$ .

$$\beta_{br,req} = \left( \frac{1}{\beta_{T,req}} - \frac{1}{\beta_g} - \frac{1}{\beta_{sec}} \right)^{-1} \quad 11.12$$

When the provided brace stiffness is set equal to the required brace stiffness, and assuming the area of the diagonals and struts are equal, the result is Equation 11.13, which can be used to calculate the minimum brace area for each cross-frame line.

$$A_{b,min} = \frac{\beta_{br,req}(C_{cf}(n_{g,eff}-n_{c,eff}+1)L_d^3+(n_{lean,eff}+1)^2S^3)}{RES^2h^2} \quad 11.13$$

#### 11.4.5. Select Brace Member Size

Select a member size such that  $A_{b,prov} > A_{b,min}$ .

### 11.5. Check Strength Requirements

---

The strength of the brace members must be sufficient for each bracing line.

#### 11.5.1. Determine the Total Brace Force Demand in Diagonals and Struts

The moment in the brace,  $M_{br}$ , is calculated with Equation 11.14.

$$M_{br} = \frac{0.0048LL_b}{nI_{yeff}Eh_b} \left( \frac{M_u}{C_b} \right)^2 \quad 11.14$$

Where:

$L$  is the span length

$L_b$  is the length of a diagonal brace member

$n_{CFL}$  is the number of brace lines

$I_{yeff}$  is the effective moment of inertia about the y-axis

$E$  is the modulus of elasticity

$h_0$  is the effective depth

$M_u$  is the applied moment

$C_b$  is the moment gradient factor

The total brace force,  $F$ , is calculated using Equation 11.15.

$$F = \frac{M_{br}}{h_b} \quad 11.15$$

Where:

$h_b$  is the height of the brace

The maximum force in the cross-frame diagonals and struts is calculated using Equations 11.16 and 11.17, respectively, for Z or K-shaped braces. Equations 11.18 and 11.19 are used with X-shaped cross-frames.

$$F_{d,leanZK} = \frac{(n_{g,eff} - n_{c,eff} + 1)L_d F}{s} \quad 11.16$$

$$F_{s,leanZK} = (n_{lean,eff} + 1)F \quad 11.17$$

$$F_{d,leanX} = \frac{(n_{g,eff} - n_{c,eff} + 1)L_d F}{2s} \quad 11.18$$

$$F_{s,leanX} = (n_{lean,eff})F \quad 11.19$$

## 11.5.2. Check Strength Capacity

The tensile and compressive capacity of each member should be determined with standard design procedures to ensure it is sufficient.

### 11.5.2.1. Tensile Capacity of Diagonals and Struts

#### 11.5.2.1.1. Gross Section Yield

The yield capacity of the bracing members must be greater than the forces calculated using Equations 11.16 and 11.17. The yield capacity is given by Equation 11.20.

$$\varphi_y P_{ny} = \varphi_y F_y A_{b,prov} \quad 11.20$$

Where:

$\varphi_y$  is the resistance factor for yielding (0.95)

$F_y$  is the yield strength of the brace members

#### 11.5.2.1.2. Net Section Fracture

The fracture capacity of the bracing members must be greater than the forces calculated using Equations 11.16 and 11.17. The yield capacity is given by Equation 11.21.

$$\varphi_u P_{nu} = \varphi_u F_u A_n R_p U \quad 11.21$$

Where:

$\varphi_u$  is the resistance factor for fracture (0.8)

$R_p$  is the reduction factor for holes (1.0)

$U$  is the shear lag reduction factor

$A_n$  is the nominal area of the brace member

#### 11.5.2.2. Compressive Capacity of Cross-Frame Diagonals and Struts

The compressive capacity of the bracing members must exceed the member forces calculated using Equations 11.16 and 11.17. The effective slenderness ratio should be calculated per AASHTO LRFD (2020) Article 6.9.4.4. The factored compressive resistance of a single angle should be calculated using the provisions in AASHTO LRFD Section 6.9.4.1.

#### 11.5.3. Other Design Requirements

The system must be checked to ensure that it satisfies all other applicable design requirements including but not limited to connection designs, varied load conditions, construction phasing, etc.

## Chapter 12. Design Examples

### 12.1. Design Example 1

An application of lean-on bracing for a nonskew, single span, five-girder bridge and checkerboard cross-frame layout is illustrated in this example. The girder sections are shown in Figure 12-1.

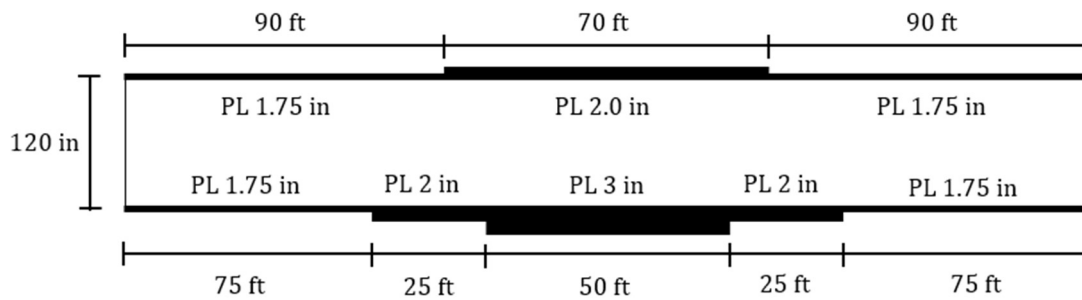


Figure 12-1. Example 1 Girder Elevation View

#### 12.1.1. Determine Girder Layout and Geometry

##### Span Information

$n_g = 5$	Number of girders
$S = 10.5 \text{ ft}$	Girder spacing
$L = 250 \text{ ft}$	Span length
$E = 29,000 \text{ ksi}$	Modulus of elasticity
$\theta = 0^\circ$	Skew angle

##### Web Information

$t_w = 1.5 \text{ in}$	Thickness of girder web
$h_w = 120 \text{ in}$	Height of girder web

### Bottom Flange Information

$$b_{bf} = 36 \text{ in}$$

Width of bottom flange

$$t_{bsmall} = 1.75 \text{ in}$$

Thickness of thinnest section of girder flange

$$t_{b2} = 2 \text{ in}$$

Thickness of second thinnest section of girder flange

$$x_{bsmall} = \frac{75 \text{ ft} + 75 \text{ ft}}{250 \text{ ft}} = 0.6$$

Fraction of span with  $t_{bsmall}$

### Top Flange Information

$$b_{tf} = 36 \text{ in}$$

Width of top flange

$$t_{tsmall} = 1.75 \text{ in}$$

Thickness of thinnest section of girder flange

$$t_{t2} = 2.0 \text{ in}$$

Thickness of second thinnest section of girder flange

$$x_{tsmall} = \frac{90 \text{ ft} + 90 \text{ ft}}{250 \text{ ft}} = 0.72$$

Fraction of span with  $t_{bsmall}$

### Calculated Girder Section Properties, as defined in AASHTO LRFD BDS

$$t_{beff} = t_{bsmall}(1 - 1 - x_{bsmall})^2 + t_{b2}(1 - x_{bsmall})^2 = 1.79 \text{ in}$$

$$t_{teff} = t_{tsmall}(1 - 1 - x_{tsmall})^2 + t_{t2}(1 - x_{tsmall})^2 = 1.77 \text{ in}$$

Bottom Flange	Top Flange	Web
$y_{bf} = \frac{t_{beff}}{2} = 0.9 \text{ in}$	$y_{tf} = \frac{t_{teff}}{2} = 122.7 \text{ in}$	$y_w = t_{beff} + \frac{h_w}{2} = 61.8 \text{ in}$
$A_{bf} = b_{bf}t_{beff} = 64.4 \text{ in}^2$	$A_{tf} = b_{tf}t_{teff} = 63.7 \text{ in}^2$	$A_w = b_w t_w = 180 \text{ in}^2$
$I_{xbf} = \frac{b_{bf}t_{beff}^3}{12} = 17.2 \text{ in}^4$	$I_{xtf} = \frac{b_{tf}t_{teff}^3}{12} = 16.6 \text{ in}^4$	$I_{xw} = \frac{b_w t_w^3}{12} = 216000 \text{ in}^4$
$I_{ybf} = \frac{t_{beff}b_{bf}^3}{12} = 6960 \text{ in}^4$	$I_{ytf} = \frac{t_{teff}b_{tf}^3}{12} = 6880 \text{ in}^4$	$I_{yw} = \frac{t_w b_w^3}{12} = 33.8 \text{ in}^4$

$$d_{bot} = \frac{A_{bf}y_{bf} + A_w y_w + A_{tf}y_{tf}}{A_{bf} + A_w + A_{tf}} = 61.6 \text{ in}$$

$$d_{top} = t_{beff} + h_w + t_{teff} - d_{bot} = 61.9 \text{ in}$$

$$I_x = I_{xbf} + A_{bf}(d_{bot} - y_{bf})^2 + I_{xw} + A_w(d_{bot} - y_w)^2 + I_{xtf} + A_{tf}(d_{bot} - y_{tf})^2 = 690,980 \text{ in}^4$$

$$I_y = I_{ybf} + I_{yw} + I_{ytf} = 13,870 \text{ in}^4$$

$$c = d_{top} - \frac{t_{eff}}{2} = 61.0 \text{ in}$$

$$t = d_{bot} - y_{bf} = 60.7 \text{ in}$$

$$I_{yeff} = I_{ytf} + \left(\frac{t}{c}\right) I_{ybf} = 13,800 \text{ in}^4$$

$$J = \frac{b_{bf}t_{beff}^3}{3} + \frac{b_{tf}t_{teff}^3}{3} + \frac{h_w t_w^3}{3} = 270 \text{ in}^4$$

### 12.1.2. Determine Cross-Frame Locations Based on Recommended Layouts

Because the bridge is nonskew with five girders, checkerboard is a recommended cross-frame layout. X-frames are used because the web depth is greater than 75% of the girder spacing. Nine cross-frame lines are used to keep the spacing close to 25 feet. In Figure 12-2 and following calculations, CFL represents “cross-frame line,” dashed lines represent lean-on struts, and thick lines represent cross-frames. A cross-section view of CFL 1 is shown in Figure 12-3. Lateral trusses were implemented in order to increase the in-plane girder stiffness of the relatively slender girder system.



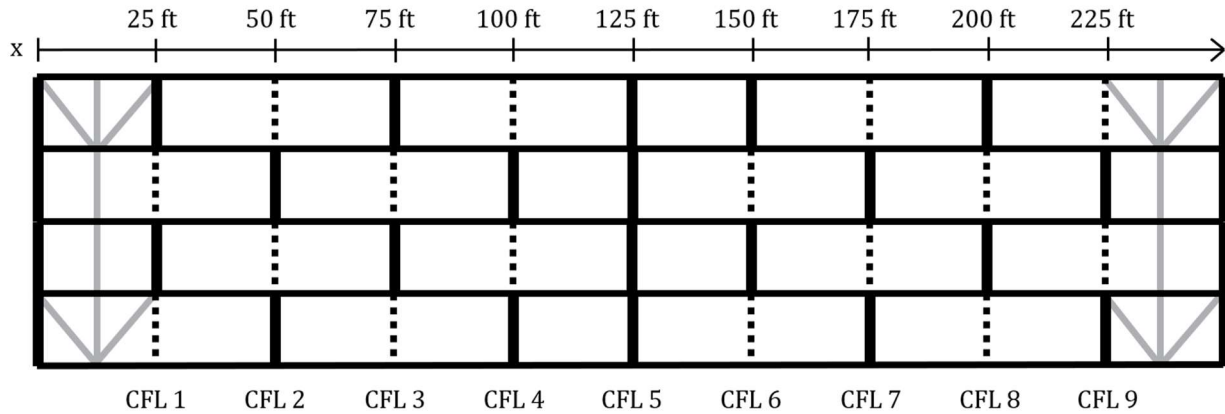


Figure 12-2. Example 1 Cross-Frame Layout

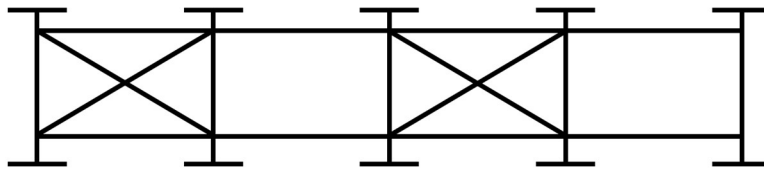


Figure 12-3. Example 1 CFL 1 Section View

### Connection Plate Information

$$b_s = 9 \text{ in}$$

Width of connection plate

$$h_i = 11 \text{ in}$$

Distance from top of cross-frame to bottom of top flange

$$t_s = 0.5 \text{ in}$$

Thickness of connection plate

### Brace Information

$$n_{CFL} = 9$$

Number of intermediate cross-frame lines in the span

$$L_b = \frac{L}{n_{CFL} + 1} = 25 \text{ ft}$$

Unbraced length (cross-frame spacing)

$$h_b = h_w - 2h_i = 98 \text{ in}$$

Height of cross-frame

$$L_d = \sqrt{(S - 2b_s)^2 + h_b^2} = 146 \text{ in}$$

Length of diagonal braces

$$L_s = S - 2b_s = 108 \text{ in}$$

Length of top and bottom struts

### 12.1.3. Check Moment Demands

#### 12.1.3.1. Calculate the Moment Loading at Each Cross-Frame Line

##### Loading Information

$$\rho_{concrete} = 150 \frac{lb}{ft^3} \quad \text{Unit weight of concrete}$$

$$t_{deck} = 10 \text{ in} \quad \text{Thickness of deck}$$

$$\rho_{steel} = 490 \frac{lb}{ft^3} \quad \text{Density of steel}$$

$$DL_{form} = 5 \frac{lb}{ft^2} \quad \text{Load of formwork}$$

$$w_{deck} = \rho_{concrete} + t_{deck} * S = 1310 \frac{lb}{ft} \quad \text{Self-weight of fresh concrete}$$

$$w_{girder} = (A_{bf} + A_{tf} + A_w) * \rho_{steel} = 1050 \frac{lb}{ft} \quad \text{Self-weight of girder}$$

$$w_{form} = DL_{form} * S = 53 \frac{lb}{ft} \quad \text{Self-weight of formwork}$$

$$w_{CLL} = 150 \frac{lb}{ft} \quad \text{Construction live load}$$

$$w_{total} = 1.4(w_{deck} + w_{girder} + w_{form} + w_{CLL}) = 3590 \frac{lb}{ft} \quad \text{Total line load (factored)}$$

The maximum moment for a single span with uniformly distributed load is:

$$M_u = \frac{w_{total}L^2}{8} = 28,000 \text{ kip} - ft$$

The moment at each cross-frame line for a uniformly distributed load is:

$$M = \frac{w_{total}x(L-x)}{2} \text{ [kip} - ft]$$

	$x$	$M_u$
<b>CFL 1</b>	25 ft	10,100 kip – ft
<b>CFL 2</b>	50 ft	18,000 kip – ft
<b>CFL 3</b>	75 ft	23,600 kip – ft
<b>CFL 4</b>	100 ft	27,000 kip – ft
<b>CFL 5</b>	125 ft	28,000 kip – ft
<b>CFL 6</b>	150 ft	27,000 kip – ft
<b>CFL 7</b>	175 ft	23,600 kip – ft
<b>CFL 8</b>	200 ft	18,000 kip – ft
<b>CFL 9</b>	225 ft	10,100 kip – ft

### 12.1.3.2. Check System Global Buckling Moment

$C_{LO} = 0.95$  Lean-On Factor - 0.95 for bridges with less than 30° skew and 0.85 greater than or equal to 30° skew

$C_{bs} = 1.1$  1.1 for single span, 2.0 for continuous span

$\alpha_x = 20$  System warping stiffness factor from Table 11-2

$K = 0.7$  1.0 if lateral trusses are not used, 0.7 if lateral trusses are used

$$0.7M_{gs} = 0.7C_{LO}C_{BS} \frac{\pi^2 SE}{(KL)^2} \sqrt{I_y I_x \left( \frac{\alpha_x}{2n_g} \right)} = 69,000 \text{ kip – ft}$$

$$M_u < 0.7M_{gs} \text{ OK}$$

NOTE: In the event  $M_u > 0.7M_{gs}$ , no number of cross-frames will be satisfactory. The girders must be resized or spacing increased to resist the system mode of buckling.

### 12.1.3.3. Check Conventional Lateral-Torsional Buckling Moment

$C_b = 1$  LTB moment gradient factor

$C_w = \frac{I_{y,eff}}{2} * \frac{h_w^2}{2} = 24,768,700 \text{ in}^6$  Torsional warping constant

$$G = 11150 \text{ ksi}$$

Shear modulus

$$M_0 = C_b \frac{\pi}{L_b} \sqrt{EI_{yeff}GJ + \frac{\pi^2 E^2 I_{yeff} C_w}{L_b^2}} = 157,900 \text{ kip-ft}$$

$$M_u < M_0 \text{ OK}$$

#### 12.1.4. Determine Minimum Brace Area for Each Bracing Line

##### 12.1.4.1. Determine Required System Stiffness at Each Bracing Line

$$\varphi_{sb} = 0.8$$

Resistance factor for stability bracing

The required stiffness at each bracing line is given by:

$$\beta_{Treq,max} = \frac{2.4L}{\varphi_{sb} C_b^2 n_{CFL} I_{yeff} E} M_u^2 = 282,800 \frac{\text{kip-in}}{\text{rad}}$$

	$\beta_{T,req}$
<b>CFL 1</b>	36,600 $\frac{\text{kip-in}}{\text{rad}}$
<b>CFL 2</b>	115,800 $\frac{\text{kip-in}}{\text{rad}}$
<b>CFL 3</b>	199,500 $\frac{\text{kip-in}}{\text{rad}}$
<b>CFL 4</b>	260,600 $\frac{\text{kip-in}}{\text{rad}}$
<b>CFL 5</b>	282,800 $\frac{\text{kip-in}}{\text{rad}}$
<b>CFL 6</b>	260,600 $\frac{\text{kip-in}}{\text{rad}}$
<b>CFL 7</b>	199,500 $\frac{\text{kip-in}}{\text{rad}}$
<b>CFL 8</b>	115,800 $\frac{\text{kip-in}}{\text{rad}}$
<b>CFL 9</b>	36,600 $\frac{\text{kip-in}}{\text{rad}}$

##### 12.1.4.2. Calculate In-Plane Girder Stiffness (Constant)

$$\beta_g = C_{LO}^2 C_{BS}^2 \frac{\pi^4 E I_x S^2 \alpha_x}{2n_g (KL)^3 (n_{CFL} + 1)} = 699,300 \frac{\text{kip-in}}{\text{rad}}$$

### 12.1.4.3. Calculate Cross-Sectional Stiffness (Constant)

The cross-frames are greater than 80% of the web depth, so the cross-sectional stiffness may be taken as infinite.

$$\beta_{sec} = \infty \frac{\text{kip-in}}{\text{rad}}$$

### 12.1.4.4. Use the Brace Stiffness Equation to Determine the Minimum Brace Area for Each Line

$C_{CF} = 0.5$  Cross-frame coefficient: 1.0 for Z-frames, 0.5 for X-frames, 2.0 for K-frames

$R = 0.65$  Connection eccentricity factor

Use these equations to determine the minimum area requirement for each cross-frame line:

$$\beta_{br,req} = \frac{1}{\beta_{T,req}} - \left( \frac{1}{\beta_g} + \frac{1}{\beta_{sec}} \right)$$

$$A_{br,req} = \frac{\beta_{br,req}(C_{CF}(n_{g,eff} - n_{c,eff} + 1)L_d^3 + (n_{lean,eff} + 1)^2 S^3)}{RES^2 h_b^2}$$

	$n_{g,eff}$	$n_{c,eff}$	$n_{lean,eff}$	$\beta_{br,req}$	$A_{br,req}$
<b>CFL 1</b>	2	1	0	$38,700 \frac{\text{kip-in}}{\text{rad}}$	$0.19 \text{ in}^2$
<b>CFL 2</b>	2	1	0	$138,800 \frac{\text{kip-in}}{\text{rad}}$	$0.69 \text{ in}^2$
<b>CFL 3</b>	2	1	0	$279,100 \frac{\text{kip-in}}{\text{rad}}$	$1.38 \text{ in}^2$
<b>CFL 4</b>	2	1	0	$415,300 \frac{\text{kip-in}}{\text{rad}}$	$2.05 \text{ in}^2$
<b>CFL 5</b>	5	4	0	$474,600 \frac{\text{kip-in}}{\text{rad}}$	$0.84 \text{ in}^2$
<b>CFL 6</b>	2	1	0	$415,300 \frac{\text{kip-in}}{\text{rad}}$	$2.05 \text{ in}^2$
<b>CFL 7</b>	2	1	0	$279,100 \frac{\text{kip-in}}{\text{rad}}$	$1.38 \text{ in}^2$
<b>CFL 8</b>	2	1	0	$138,800 \frac{\text{kip-in}}{\text{rad}}$	$0.69 \text{ in}^2$
<b>CFL 9</b>	2	1	0	$38,700 \frac{\text{kip-in}}{\text{rad}}$	$0.19 \text{ in}^2$

The minimum brace area is dictated by CFL 4 and 6.  $A_{br,req} = 2.05 \text{ in}^2$ .

#### 12.1.4.5. Select Brace Member Size

An L5x5x1/2 angle is selected for all brace lines, resulting in  $A_{br,prov} = 4.79 \text{ in}^2$ .

#### 12.1.5. Check Strength Requirements for Each Bracing Line

##### 12.1.5.1. Determine the Force Demand in Diagonals and Struts for Each Cross-Frame Line

It is simplest to use the maximum moment in the span to check all brace lines.

$$M_{br,max} = \frac{0.0048LL_b}{n_{CFL}EI_{yeff}h_b} \left( \frac{M_u}{C_b} \right)^2 = 2,300 \text{ kip-in}$$

$$F_{br,max} = \frac{M_{br}}{h_b} = 24 \text{ kip}$$

The force in the struts and diagonals is dependent on  $n_c$  and  $n_{lean}$ , so it will vary depending on the cross-frame pattern in each bracing line. The force equations for X-frames are:

$$F_{d,leanX} = \frac{(n_{g,eff} - n_{c,eff} + 1)F_{br}L_d}{2S}$$

$$F_{s,leanX} = n_{lean,eff}F_{br}$$

	$n_{g,eff}$	$n_{c,eff}$	$n_{lean,eff}$	$F_d$	$F_s$
<b>CFL 1</b>	2	1	0	54.5 kip	23.6 kip
<b>CFL 2</b>	2	1	0	54.5 kip	23.6 kip
<b>CFL 3</b>	2	1	0	54.5 kip	23.6 kip
<b>CFL 4</b>	2	1	0	54.5 kip	23.6 kip
<b>CFL 5</b>	5	4	0	27.3 kip	0 kip
<b>CFL 6</b>	2	1	0	54.5 kip	23.6 kip
<b>CFL 7</b>	2	1	0	54.5 kip	23.6 kip
<b>CFL 8</b>	2	1	0	54.5 kip	23.6 kip
<b>CFL 9</b>	2	1	0	54.5 kip	23.6 kip

The maximum force in the diagonals is  $F_d = 54.5 \text{ kip}$  and the maximum force in the struts is  $F_s = 23.6 \text{ kip}$ .

### 12.1.5.2. Check Strength Capacity

#### Brace Angle Information

$F_u = 70 \text{ ksi}$  Tensile strength

$F_y = 50 \text{ ksi}$  Yield strength

$\bar{x} = 1.42 \text{ in}$  Centroid of angle

$r_x = 1.53 \text{ in}$  Radius of gyration

$t_{leg} = \frac{1}{2} \text{ in}$  Thickness of leg

#### Brace Connection Information

$d_b = 1 \text{ in}$  Bolt diameter

$F_{ub} = 120 \text{ ksi}$  Tensile strength of bolt

$F_{yb} = 70 \text{ ksi}$  Yield strength of bolt

$L_{bolt} = 3 \text{ in}$  Bolt spacing

$A_b = \frac{\pi}{4} d_b^2 = 0.785 \text{ in}^2$  Area of bolt

#### 12.1.5.2.1. Tensile Capacity of Diagonals and Struts

##### Gross Section Yield

$\phi_y = 0.95$  Resistance factor for yielding

$\phi_y P_{ny} = \phi_y F_y A_{b,prov} = 228 \text{ kip}$

$\phi_y P_{ny} > F_d \text{ OK}, \phi_y P_{ny} > F_s \text{ OK}$

### Net Section Fracture

$$\phi_u = 0.8 \quad \text{Resistance factor for fracture}$$

$$R_p = 1.0 \quad \text{Reduction factor for holes}$$

$$U = 1 - \frac{\bar{x}}{L_{bolt}} = 0.5 \quad \text{Shear lag reduction factor}$$

$$A_n = A_{b,prov} - 1 \left( d_b + \frac{1}{8} in \right) t_{leg} = 4.2 in^2 \quad \text{Nominal area of brace member}$$

$$\phi_u P_{nu} = \phi_u F_u A_n R_p U = 125 kip$$

$$\phi_u P_{nu} > F_d \text{ OK, } \phi_u P_{nu} > F_s \text{ OK}$$

### 12.1.5.2.2. Compressive Capacity of Cross-Frame Diagonals

As per AASHTO LRFD Article 6.9.4.4:

$$\frac{L_d}{r_x} = 95.3$$

Hence, effective slenderness ratio is calculated as:

AASHTO LRFD Eqn. 6.9.4.4-1:

$$\left( \frac{KL_d}{r_x} \right)_{eff} = 72 + 0.75 \frac{L_d}{r_x} = 143.5$$

Elastic critical buckling resistance of single angle is calculated as:

AASHTO LRFD Eqn. 6.9.4.1.2-1:

$$P_e = \frac{\pi^2 E}{\left( \frac{KL_d}{r_x} \right)_{eff}^2} A_g = 67 kip$$

Nominal yield resistance:

AASHTO LRFD Article 6.9.4.1

$$P_0 = F_y A_{b,prov} = 239 kip$$

As per AASHTO LRFD Article 6.9.4.1:



$$\frac{P_o}{P_e} = 3.6 > 2.25$$

Hence, nominal compressive resistance of a single angle is:

AASHTO LRFD Eqn. 6.9.4.1-2

$$P_n = 0.877P_e = 58.4 \text{ kip}$$

Factored compressive resistance of a single angle is:

$$\varphi_c = 0.95 \qquad \text{Resistance factor for compression}$$

$$\varphi_c P_n = 55.5 \text{ kip} > F_d \text{ OK}$$

### 12.1.5.2.3. Compressive Capacity of Top and Bottom Struts

As per AASHTO LRFD Article 6.9.4.4:

$$\frac{L_s}{r_x} = 70.6$$

Hence, effective slenderness ratio is calculated as:

AASHTO LRFD Eqn. 6.9.4.4-1:

$$\left(\frac{KL_s}{r_x}\right)_{eff} = 72 + 0.75 \frac{L_s}{r_x} = 125$$

Elastic critical buckling resistance of single angle is calculated as:

AASHTO LRFD Eqn. 6.9.4.1.2-1:

$$P_e = \frac{\pi^2 E}{\left(\frac{KL_s}{r_x}\right)_{eff}^2} A_g = 87.8 \text{ kip}$$

Nominal yield resistance:

AASHTO LRFD Article 6.9.4.1

$$P_o = F_y A_{b,prov} = 240 \text{ kip}$$

As per AASHTO LRFD Article 6.9.4.1:

$$\frac{P_o}{P_e} = 2.7 > 2.25$$

Hence, nominal compressive resistance of a single angle is:

AASHTO LRFD Eqn. 6.9.4.1-2

$$P_n = 0.877P_e = 77 \text{ kip}$$

Factored compressive resistance of a single angle is:

$$\phi_c P_n = 73.2 \text{ kip} > F_s \text{ OK}$$

#### 12.1.5.2.4. Limiting Slenderness Ratio Check

$$\frac{KL_s}{r_x} = 70.6 < 140 \text{ OK}$$

## 12.2. Design Example 2

An application of lean-on bracing for a  $56^\circ$  skew, single span, seven-girder bridge with a cross-frame layout resembling an X is illustrated in this example. The girder sections are shown in Figure 12-4.

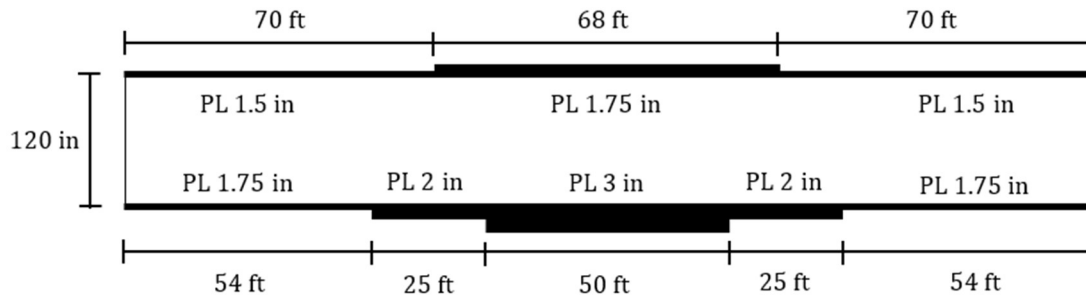


Figure 12-4. Example 2 Girder Elevation View

### 12.2.1. Determine Girder Layout and Geometry

#### Span Information

$n_g = 7$	Number of girders
$S = 12 \text{ ft}$	Girder spacing
$L = 208 \text{ ft}$	Span length
$E = 29,000 \text{ ksi}$	Modulus of elasticity
$\theta = 56^\circ$	Skew angle

#### Web Information

$t_w = 1 \text{ in}$	Thickness of girder web
$h_w = 120 \text{ in}$	Height of girder web

#### Bottom Flange Information

$b_{bf} = 30 \text{ in}$	Width of bottom flange
--------------------------	------------------------

$t_{b_{small}} = 1.75 \text{ in}$	Thickness of thinnest section of girder flange
$t_{b_2} = 2 \text{ in}$	Thickness of second thinnest section of girder flange
$x_{b_{small}} = \frac{54 \text{ ft} + 54 \text{ ft}}{208 \text{ ft}} = 0.52$	Fraction of span with $t_{b_{small}}$

**Top Flange Information**

$b_{tf} = 30 \text{ in}$	Width of top flange
$t_{t_{small}} = 1.5 \text{ in}$	Thickness of thinnest section of girder flange
$t_{t_2} = 1.75 \text{ in}$	Thickness of second thinnest section of girder flange
$x_{t_{small}} = \frac{70 \text{ ft} + 70 \text{ ft}}{208 \text{ ft}} = 0.67$	Fraction of span with $t_{b_{small}}$

**Calculated Girder Section Properties, as defined in AASHTO LRFD BDS**

$$t_{beff} = t_{b_{small}}(1 - 1 - x_{b_{small}})^2 + t_{b_2}(1 - x_{b_{small}})^2 = 1.81 \text{ in}$$

$$t_{teff} = t_{t_{small}}(1 - 1 - x_{t_{small}})^2 + t_{t_2}(1 - x_{t_{small}})^2 = 1.55 \text{ in}$$

Bottom Flange	Top Flange	Web
$y_{bf} = \frac{t_{beff}}{2} = 0.9 \text{ in}$	$y_{tf} = \frac{t_{teff}}{2} = 122.3 \text{ in}$	$y_w = t_{beff} + \frac{h_w}{2} = 61.8 \text{ in}$
$A_{bf} = b_{bf}t_{beff} = 54.2 \text{ in}^2$	$A_{tf} = b_{tf}t_{teff} = 46.6 \text{ in}^2$	$A_w = b_w t_w = 120 \text{ in}^2$
$I_{x_{bf}} = \frac{b_{bf}t_{beff}^3}{12} = 14.8 \text{ in}^4$	$I_{x_{tf}} = \frac{b_{tf}t_{teff}^3}{12} = 9.4 \text{ in}^4$	$I_{x_w} = \frac{b_w t_w^3}{12} = 144000 \text{ in}^4$
$I_{y_{bf}} = \frac{t_{beff}b_{bf}^3}{12} = 4068 \text{ in}^4$	$I_{y_{tf}} = \frac{t_{teff}b_{tf}^3}{12} = 3495 \text{ in}^4$	$I_{y_w} = \frac{t_w b_w^3}{12} = 10 \text{ in}^4$

$$d_{bot} = \frac{A_{bf}y_{bf} + A_w y_w + A_{tf}y_{tf}}{A_{bf} + A_w + A_{tf}} = 59.6 \text{ in}$$

$$d_{top} = t_{beff} + h_w + t_{teff} - d_{bot} = 63.7 \text{ in}$$

$$I_x = I_{x_{bf}} + A_{bf}(d_{bot} - y_{bf})^2 + I_{x_w} + A_w(d_{bot} - y_w)^2 + I_{x_{tf}} + A_{tf}(d_{bot} - y_{tf})^2 = 514,843 \text{ in}^4$$

$$I_y = I_{ybf} + I_{yw} + I_{ytf} = 7573 \text{ in}^4$$

$$c = d_{top} - \frac{t_{eff}}{2} = 63.0 \text{ in}$$

$$t = d_{bot} - y_{bf} = 58.7 \text{ in}$$

$$I_{yeff} = I_{ytf} + \left(\frac{t}{c}\right) I_{ybf} = 7289 \text{ in}^4$$

$$J = \frac{b_{bf}t_{beff}^3}{3} + \frac{b_{tf}t_{teff}^3}{3} + \frac{h_w t_w^3}{3} = 137 \text{ in}^4$$

### 12.2.2. Determine Cross-Frame Locations Based on Recommended Layouts

Because the bridge is skewed with seven girders, the X-layout is recommended. X-frames are used because the web depth is greater than 75% of the girder spacing. Eight cross-frame lines are used to keep the maximum spacing close to 25 feet. In Figure 12-5 and following calculations, CFL represents “cross-frame line,” dashed lines represent lean-on struts, and thick lines represent cross-frames. A cross-section view of CFL 1 is shown in Figure 12-6.

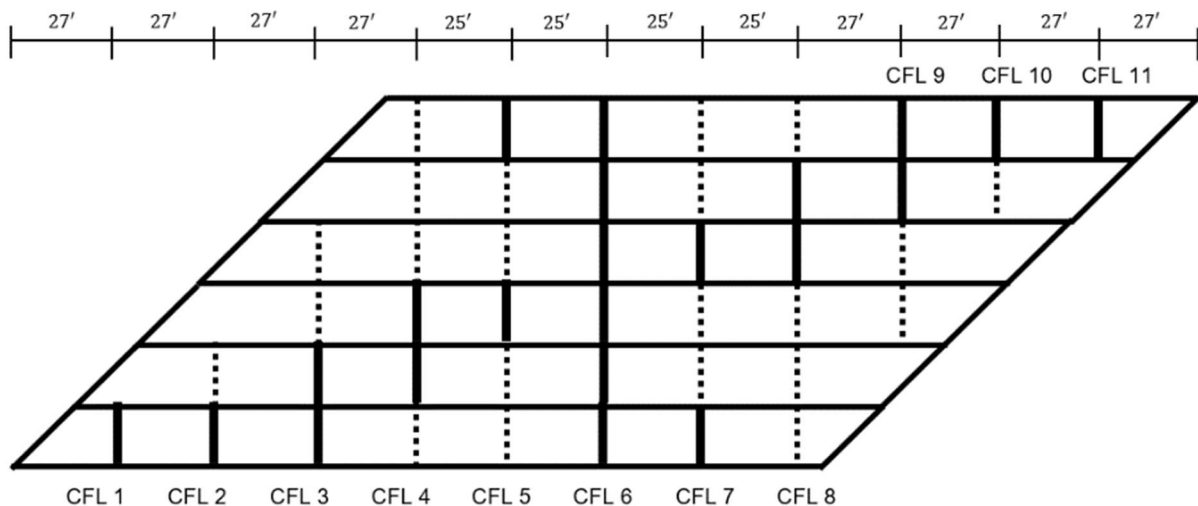


Figure 12-5. Example 2 Cross-Frame Layout

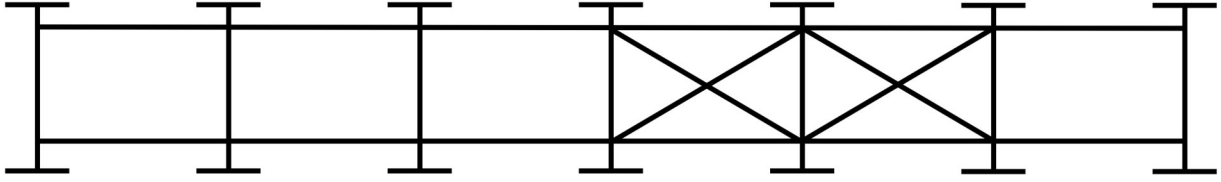


Figure 12-6. Example 2 CFL 4 Section View

### Connection Plate Information

$b_s = 9 \text{ in}$	Width of connection plate
$h_i = 11 \text{ in}$	Distance from top of cross-frame to bottom of top flange
$t_s = 0.5 \text{ in}$	Thickness of connection plate

### Brace Information

$n_{CFL} = 8$	Number of intermediate cross-frame lines in the span
$L_b = 27 \text{ ft}$	Unbraced length (maximum cross-frame spacing)
$h_b = h_w - 2h_i = 98 \text{ in}$	Height of cross-frame
$L_d = \sqrt{(S - 2b_s)^2 + h_b^2} = 160 \text{ in}$	Length of diagonal braces
$L_s = S - 2b_s = 126 \text{ in}$	Length of top and bottom struts

## 12.2.3. Check Moment Demands

### 12.2.3.1. Calculate the Moment Loading at Each Cross-Frame Line

#### Loading Information

$\rho_{concrete} = 150 \frac{\text{lb}}{\text{ft}^3}$	Unit weight of concrete
$t_{deck} = 10 \text{ in}$	Thickness of deck
$\rho_{steel} = 490 \frac{\text{lb}}{\text{ft}^3}$	Density of steel

$$DL_{form} = 5 \frac{lb}{ft^2}$$

Load of formwork

$$w_{deck} = \rho_{concrete} + t_{deck} * S = 1500 \frac{lb}{ft}$$

Self-weight of fresh concrete

$$w_{girder} = (A_{bf} + A_{tf} + A_w) * \rho_{steel} = 751 \frac{lb}{ft}$$

Self-weight of girder

$$w_{form} = DL_{form} * S = 60 \frac{lb}{ft}$$

Self-weight of formwork

$$w_{CLL} = 150 \frac{lb}{ft}$$

Construction live load

$$w_{total} = 1.4(w_{deck} + w_{girder} + w_{form} + w_{CLL}) = 3466 \frac{lb}{ft}$$

Total line load (factored)

Each bracing line must be designed for the maximum moment demand along the bracing line. For a simply supported skew bridge, these locations may be grouped as support regions and midspan regions, as shown in Figure 12-7. The girder locations with the maximum moment demand for each cross-frame line are indicated by stars.

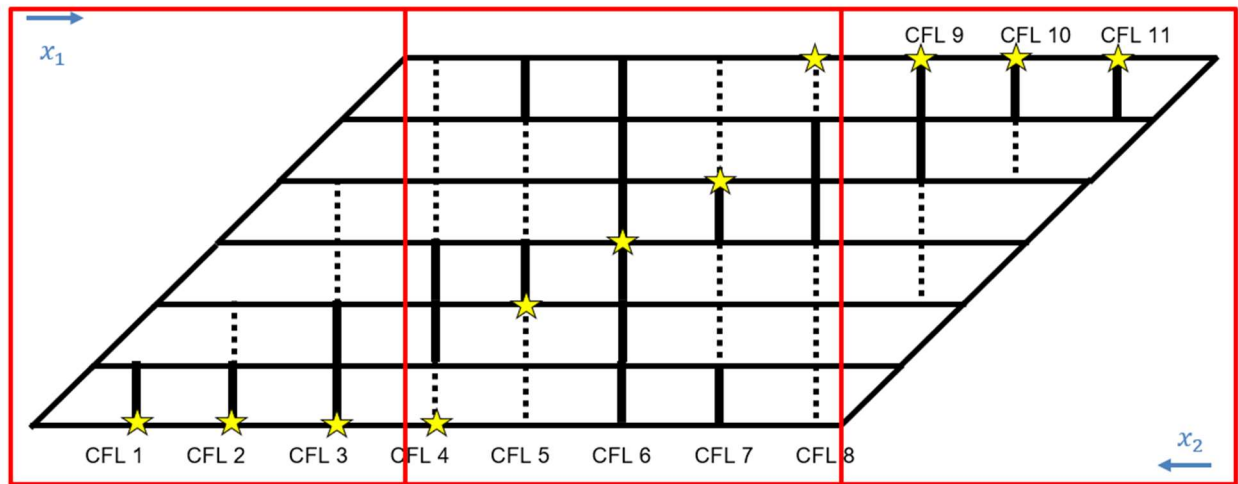


Figure 12-7. Example 2 Maximum Moment Locations

The maximum moment in the support regions is governed by the girder closest to the skew. This is given by:

$$M = \frac{w_{total}x(L-x)}{2} [kip - ft]$$

For the midspan region, the governing moment is  $M_u$ . The maximum moment for a single girder with uniformly distributed load is:

$$M_u = \frac{w_{total}L^2}{8} = 18,600 \text{ kip} - \text{ft}$$

	Support 1 $x_1$	Midspan	Support 2 $x_2$	$M_{CFL}$
<b>CFL 1</b>	27 ft			8,400 kip - ft
<b>CFL 2</b>	54 ft			14,300 kip - ft
<b>CFL 3</b>	81 ft			17,700 kip - ft
<b>CFL 4</b>		$M_u$		18,600 kip - ft
<b>CFL 5</b>		$M_u$		18,600 kip - ft
<b>CFL 6</b>		$M_u$		18,600 kip - ft
<b>CFL 7</b>		$M_u$		18,600 kip - ft
<b>CFL 8</b>		$M_u$		18,600 kip - ft
<b>CFL 9</b>			81 ft	17,700 kip - ft
<b>CFL 10</b>			54 ft	14,300 kip - ft
<b>CFL 11</b>			27 ft	8,400 kip - ft

### 12.2.3.2. Check System Global Buckling Moment

$C_{LO} = 0.85$  Lean-On Factor - 0.95 for bridges with less than 30° skew and 0.85 greater than or equal to 30° skew

$C_{BS} = 1.1$  1.1 for single span, 2.0 for continuous span

$\alpha_x = 56$  System warping stiffness factor from Table 11-2

$K = 0.7$  1.0 if lateral trusses are not used, 0.7 if lateral trusses are used or skew  $\geq 30^\circ$

$$0.7M_{gs} = 0.7C_{LO}C_{BS} \frac{\pi^2 SE}{(KL)^2} \sqrt{I_y I_x \left( \frac{\alpha_x}{2n_g} \right)} = 91,960 \text{ kip} - \text{ft}$$



$$M_u < 0.7M_{gs} \text{ OK}$$

NOTE: there is no additional stiffness benefit of adding lateral trusses to this bridge, since  $K$  is equal to 0.7 for bridges with  $\geq 30^\circ$  skew.

### 12.2.3.3. Check Conventional Lateral-Torsional Buckling Moment

$$C_b = 1 \quad \text{LTB modification factor}$$

$$C_w = \frac{I_{ytf}}{2} * \frac{h_w^2}{2} = 26,239,000 \text{ in}^6 \quad \text{Torsional warping constant}$$

$$G = 11150 \text{ ksi} \quad \text{Shear modulus}$$

$$M_0 = C_b \frac{\pi}{L_b} \sqrt{EI_{yeff}GJ + \frac{\pi^2 E^2 I_{yeff} C_w}{L_b^2}} = 100,400 \text{ kip-ft}$$

$$M_u < M_0 \text{ OK}$$

### 12.2.4. Determine Minimum Brace Area for Each Bracing Line

#### 12.2.4.1. Determine Required System Stiffness at Each Bracing Line

$$\varphi_{sb} = 0.8 \quad \text{Resistance factor for stability bracing}$$

The required stiffness at each bracing line is given by:

$$\beta_{Treq,max} = \frac{2.4L}{\varphi C_b^2 n_{CFL} I_{yeff} E} M_u^2 = 221,500 \frac{\text{kip-in}}{\text{rad}}$$

	$\beta_{T,req}$
<b>CFL 1</b>	45,200 $\frac{kip-in}{rad}$
<b>CFL 2</b>	131,000 $\frac{kip-in}{rad}$
<b>CFL 3</b>	200,300 $\frac{kip-in}{rad}$
<b>CFL 4</b>	221,500 $\frac{kip-in}{rad}$
<b>CFL 5</b>	221,500 $\frac{kip-in}{rad}$
<b>CFL 6</b>	221,500 $\frac{kip-in}{rad}$
<b>CFL 7</b>	221,500 $\frac{kip-in}{rad}$
<b>CFL 8</b>	221,500 $\frac{kip-in}{rad}$
<b>CFL 9</b>	200,300 $\frac{kip-in}{rad}$
<b>CFL 10</b>	131,000 $\frac{kip-in}{rad}$
<b>CFL 11</b>	45,200 $\frac{kip-in}{rad}$

#### 12.2.4.2. Calculate In-Plane Girder Stiffness (Constant)

$$\beta_g = C_{LO}^2 C_{BS}^2 \frac{\pi^4 E I_x S^2 \alpha_x}{2n_g (KL)^3 (n_{CFL} + 1)} = 2,196,900 \frac{kip-in}{rad}$$

#### 12.2.4.3. Calculate Cross-Sectional Stiffness (Constant)

The cross-frames are greater than 80% of the web depth, so the cross-sectional stiffness may be taken as infinite.

$$\beta_{sec} = \infty \frac{kip-in}{rad}$$

#### 12.2.4.4. Use the Brace Stiffness Equation to Determine the Minimum Brace Area for Each Line

$C_{CF} = 0.5$  Cross-frame coefficient: 1.0 for Z-frames, 0.5 for X-frames, 2.0 for K-frames

$R = 0.65$  Connection eccentricity factor

Use these equations to determine the minimum area requirement for each cross-frame line:

$$\beta_{br,req} = \frac{1}{\beta_{T,req}} - \left( \frac{1}{\beta_g} + \frac{1}{\beta_{sec}} \right)$$

$$A_{br,req} = \frac{\beta_{br,req}(C_{CF}(n_{g,eff} - n_{c,eff} + 1)L_d^3 + (n_{lean,eff} + 1)^2 S^3)}{RES^2 h_b^2}$$

	$n_{g,eff}$	$n_{c,eff}$	$n_{lean,eff}$	$\beta_{br,req}$	$A_{br,req}$
<b>CFL 1</b>	7	1	0	46,100 $\frac{kip-in}{rad}$	0.21 $in^2$
<b>CFL 2</b>	7	1	1	139,200 $\frac{kip-in}{rad}$	0.97 $in^2$
<b>CFL 3</b>	7	2	2	220,400 $\frac{kip-in}{rad}$	2.29 $in^2$
<b>CFL 4</b>	7	2	3	246,300 $\frac{kip-in}{rad}$	3.94 $in^2$
<b>CFL 5</b>	7	2	2	246,300 $\frac{kip-in}{rad}$	2.56 $in^2$
<b>CFL 6</b>	7	6	0	246,300 $\frac{kip-in}{rad}$	0.46 $in^2$
<b>CFL 7</b>	7	2	2	246,300 $\frac{kip-in}{rad}$	2.56 $in^2$
<b>CFL 8</b>	7	2	3	246,300 $\frac{kip-in}{rad}$	3.94 $in^2$
<b>CFL 9</b>	7	2	2	220,400 $\frac{kip-in}{rad}$	2.29 $in^2$
<b>CFL 10</b>	7	1	1	139,200 $\frac{kip-in}{rad}$	0.97 $in^2$
<b>CFL 11</b>	7	1	0	46,100 $\frac{kip-in}{rad}$	0.21 $in^2$

The minimum brace area is dictated by CFL 4 and 8.  $A_{br,req} = 3.94 in^2$ .

#### 12.2.4.5. Select Brace Member Size

A L5x5x1/2 angle is selected for all brace lines, resulting in  $A_{br,prov} = 4.79 in^2$ .

#### 12.2.5. Check Strength Requirements for Each Bracing Line

##### 12.2.5.1. Determine the Force Demand in Diagonals and Struts for Each Cross-Frame Line

It is simplest to use the maximum moment in the span to check all brace lines.

$$M_{br} = \frac{0.0048LL_b}{n_{CFL}EI_{yeff}h_b} \left( \frac{M_u}{C_b} \right)^2 = 1172 kip - in$$

$$F_{br} = \frac{M_{br}}{h_b} = 12 \text{ kip}$$

The force in the struts and diagonals is dependent on  $n_c$  and  $n_{lean}$ , so it will vary depending on the cross-frame pattern in each bracing line. The force equations for X-frames are:

$$F_{d,leanX} = \frac{(n_{g,eff} - n_{c,eff} + 1)F_{br}L_d}{2S}$$

$$F_{s,leanX} = n_{lean,eff}F_{br}$$

	$n_{g,eff}$	$n_{c,eff}$	$n_{lean,eff}$	$F_d$	$F_s$
<b>CFL 1</b>	7	1	0	46.4 kip	0 kip
<b>CFL 2</b>	7	1	1	46.4 kip	12 kip
<b>CFL 3</b>	7	2	2	39.8 kip	23.9 kip
<b>CFL 4</b>	7	2	3	39.8 kip	35.9 kip
<b>CFL 5</b>	7	2	2	39.8 kip	23.9 kip
<b>CFL 6</b>	7	6	0	13.3 kip	0 kip
<b>CFL 7</b>	7	2	2	39.8 kip	23.9 kip
<b>CFL 8</b>	7	2	3	39.8 kip	35.9 kip
<b>CFL 9</b>	7	2	2	39.8 kip	23.9 kip
<b>CFL 10</b>	7	1	1	46.4 kip	12 kip
<b>CFL 11</b>	7	1	0	46.4 kip	0 kip

The maximum force in the diagonals is  $F_d = 46.4 \text{ kip}$  and the maximum force in the struts is  $F_s = 35.9 \text{ kip}$ .

### 12.2.5.2. Check Strength Capacity

#### Brace Angle Information

$$F_u = 70 \text{ ksi}$$

Tensile strength

$$F_y = 50 \text{ ksi}$$

Yield strength

$$\bar{x} = 1.42 \text{ in}$$

Centroid of angle

$$r_x = 1.53 \text{ in}$$

Radius of gyration

$$t_{leg} = \frac{1}{2} \text{ in}$$

Thickness of leg

### Brace Connection Information

$$d_b = 1 \text{ in}$$

Bolt diameter

$$F_{ub} = 120 \text{ ksi}$$

Tensile strength of bolt

$$F_{yb} = 70 \text{ ksi}$$

Yield strength of bolt

$$L_{bolt} = 3 \text{ in}$$

Bolt spacing

$$A_b = \frac{\pi}{4} d_b^2 = 0.785 \text{ in}^2$$

Area of bolt

### 12.2.5.2.1. Tensile Capacity of Diagonals and Struts

#### Gross Section Yield

$$\phi_y = 0.95$$

Resistance factor for yielding

$$\phi_y P_{ny} = \phi_y F_y A_{b,prov} = 228 \text{ kip}$$

$$\phi_y P_{ny} > F_d \text{ OK}, \phi_y P_{ny} > F_s \text{ OK}$$

#### Net Section Fracture

$$\phi_u = 0.8$$

Resistance factor for fracture

$$R_p = 1.0$$

Reduction factor for holes

$$U = 1 - \frac{\bar{x}}{L_{bolt}} = 0.5$$

Shear lag reduction factor

$$A_n = A_{b,prov} - 1 \left( d_b + \frac{1}{8} \text{ in} \right) t_{leg} = 4.2 \text{ in}^2$$

Nominal area of brace member

$$\phi_u P_{nu} = \phi_u F_u A_n R_p U = 125 \text{ kip}$$

$$\phi_u P_{nu} > F_d \text{ OK, } \phi_u P_{nu} > F_s \text{ OK}$$

### 12.2.5.2.2. Compressive Capacity of Cross-Frame Diagonals

As per AASHTO LRFD Article 6.9.4.4:

$$\frac{L_d}{r_x} = 104$$

Hence, effective slenderness ratio is calculated as:

AASHTO LRFD Eqn. 6.9.4.4-1:

$$\left(\frac{KL_d}{r_x}\right)_{eff} = 72 + 0.75 \frac{L_d}{r_x} = 150$$

Elastic critical buckling resistance of single angle is calculated as:

AASHTO LRFD Eqn. 6.9.4.1.2-1:

$$P_e = \frac{\pi^2 E}{\left(\frac{KL_d}{r_x}\right)_{eff}^2} A_g = 61 \text{ kip}$$

Nominal yield resistance:

AASHTO LRFD Article 6.9.4.1

$$P_0 = F_y A_{b,prov} = 240 \text{ kip}$$

As per AASHTO LRFD Article 6.9.4.1:

$$\frac{P_0}{P_e} = 3.9 > 2.25$$

Hence, nominal compressive resistance of a single angle is:

AASHTO LRFD Eqn. 6.9.4.1-2

$$P_n = 0.877 P_e = 53 \text{ kip}$$

Factored compressive resistance of a single angle is:

$$\phi_c = 0.95$$

Resistance factor for compression

$$\phi_c P_n = 50.6 \text{ kip} > F_d \text{ OK}$$

### 12.2.5.2.3. Compressive Capacity of Top and Bottom Struts

As per AASHTO LRFD Article 6.9.4.4:

$$\frac{L_s}{r_x} = 82.4$$

Hence, effective slenderness ratio is calculated as:

AASHTO LRFD Eqn. 6.9.4.4-1:

$$\left(\frac{KL_s}{r_x}\right)_{eff} = 72 + 0.75 \frac{L_s}{r_x} = 134$$

Elastic critical buckling resistance of single angle is calculated as:

AASHTO LRFD Eqn. 6.9.4.1.2-1:

$$P_e = \frac{\pi^2 E}{\left(\frac{KL_s}{r_x}\right)_{eff}^2} A_g = 77 \text{ kip}$$

Nominal yield resistance:

AASHTO LRFD Article 6.9.4.1

$$P_o = F_y A_{b,prov} = 239.5 \text{ kip}$$

As per AASHTO LRFD Article 6.9.4.1:

$$\frac{P_o}{P_e} = 3.1 > 2.25$$

Hence, nominal compressive resistance of a single angle is:

AASHTO LRFD Eqn. 6.9.4.1-2

$$P_n = 0.877 P_e = 67.2 \text{ kip}$$

Factored compressive resistance of a single angle is:

$$\varphi_c P_n = 63.8 \text{ kip} > F_s \text{ OK}$$

#### 12.2.5.2.4. Limiting Slenderness Ratio Check

$$\frac{KL_s}{r_x} = 82.4 < 140 \text{ OK}$$



## Chapter 13. Conclusions

The project successfully addressed many of the previous limitations of design methods for lean-on bracing. At the outset of the study, a comprehensive literature review was performed to capture the current state of knowledge. Detailed derivations for expanded application of the brace stiffness equation for lean-on systems were completed and revised. Then, field instrumentation and live-load testing of two Texas bridges with lean-on bracing were conducted, and corresponding finite element analysis models were developed and validated based on the recorded data. These models were used to determine relationships between bracing components for optimal lean-on bridge system stiffness behavior. Revised strength equations for lean-on bracing were developed, along with a detailed lean-on bracing design methodology.

### 13.1. Research Contributions

---

The primary research contributions were in five areas, which are summarized below.

- 1) Lean-on brace stiffness equation ( $\beta_{br,lean}$ ): Prior lean-on stiffness equations were limited to a single exterior cross-frame in every cross-frame line. These equations also assumed only one diagonal was active (tension-only model) and ignored the contribution of a second diagonal (X frames). As part of this study, a revised equation was derived for the brace stiffness, which now can account for any number, position, or shape of cross-frames.
- 2) Lean-on strength equations: The original strength equations for lean-on systems had similar limitations to the brace stiffness equations, as previously mentioned. Revised cross-frame diagonal ( $F_{d,leanZK}$  or  $F_{d,leanX}$ ) and strut ( $F_{s,leanZK}$  or  $F_{s,leanX}$ ) strength design equations were developed to correspond with the brace stiffness expression. These strength equations

were updated for varied cross-frame geometry, number, and position along the cross-frame line.

- 3) Data and behavior analysis from field testing: Prior field testing of lean-on bracing systems only included data from one bridge during construction. Field testing of two additional lean-on bridges added to the collection of data, and processed data was used to validate models and confirm the performance of lean-on bracing systems.
- 4) Relationship between stiffness components: The relationship between the brace stiffness and in-plane girder stiffness was not previously well understood. Advancements were made in identifying how varying cross-frame patterns (and potentially brace stiffnesses) along the span affect the system behavior.
- 5) Detailed design methodology and examples: Practical contributions were included for the application of the revised design expressions. A detailed design methodology was provided, as well as two design examples to convey a conventional nonskew and skew lean-on bracing design using the equation-based methodology.

## **13.2. Future Work**

---

The project resulted in several significant contributions to lean-on bracing design. The resulting design equations and procedures are applicable to straight bridges with any skew angle. In order to expand the application of lean-on bracing and remove some built-in conservatism of the approach, there are several avenues that should be pursued as part of future research:

- The scope of this research did not include curved bridges. Lean-on bracing is a viable concept for curved bridges, but additional study is recommended to quantify additional considerations induced by the curvature of bridge girders.

- Connection eccentricity factors (R-factors) were studied in detail for conventional bracing systems (Reichenbach *et al.*, 2021). These recommendations were applied directly for lean-on bracing. An additional study is recommended to refine connection eccentricity factors for lean-on bracing.
- In calculating the brace stiffness for bracing lines for skew systems,  $n_{g,eff}$  and  $n_{lean,eff}$  may be able to be reduced, as there are realistically fewer girders being braced by that cross-frame line. This would increase the calculated stiffness provided by these cross-frame lines due to the reduction in the number of leaning girders. These bracing lines typically do not govern for single spans, but this may be consequential for the design of continuous spans.
- It has been suggested that it is inconsequential to remove approximately 10% or less of the cross-frames in a conventional bracing system. Further study in quantifying a maximum value of cross-frames that may be removed without the application of lean-on equations is worthwhile.
- Finally, the girder erection process may be streamlined with additional study of construction phasing for the recommended lean-on layouts.

## References

- AASHTO (2020) *LRFD Bridge Design Specifications*. 9th edn. Washington, DC: American Association of State Highway and Transportation Officials.
- AASHTO (2024) *LRFD Bridge Design Specifications*. 10th edn. Washington, DC: American Association of State Highway and Transportation Officials.
- AISC (2017) *Manual of Steel Construction*. 15th edn. Chicago, IL: American Institute of Steel Construction.
- AISC (2022) *Specification for Structural Steel Buildings*. Chicago, IL: American Institute of Steel Construction.
- Battistini, A., Wang, W., Donahue, S., Helwig, T., Engelhardt, M., and Frank, K. (2013) "Improved Cross Frame Details." TxDOT Research Report 0-6564.
- Battistini, A. Wang, W., Helwig, T., Engelhardt, M., and Frank, K. (2016) "Stiffness Behavior of Cross Frames in Steel Bridge Systems," *Journal of Bridge Engineering*, 21(6): 04016024-1-11.
- Bechtel, A. (2016) "Effect of Implementing Lean-On Bracing in Skewed Steel I-Girder Bridges." The College of New Jersey, University Transportation Research Center.
- Bjelland, A. (2024) "Impact of Lean-On Bracing Layouts on System Stiffness Behavior." Dissertation. University of Texas at Austin.
- Fish, D. (2021) "Refined Design Expressions for In-Plane Girder Stiffness and System Buckling Capacity." Thesis. University of Texas at Austin.
- Fish, D., Bjelland, A., Helwig, T., Engelhardt, M., and Park, S. (2024) "Torsional Beam Bracing Design for Straight I-Shaped Girder Systems." In Review.
- Gasser, C., Bjelland, A., Fish, D., Park, S., Yarnold, M., Helwig, T., Hurlebaus, S., Williamson, E., Engelhardt, M., and Hebdon, M. (2023) "Brace Stiffness Quantification for Lean-on Bracing," *Structural Stability Research Council Conference*. Charlotte, NC.
- Gasser, C., Bjelland, A., Yarnold, M., Helwig, T., Hurlebaus, S., Engelhardt, M., and Hebdon, M. (2024) "Identification of Critical Bracing Lines in Lean-on Bracing Systems and Corresponding Stiffness/Strength Expressions," *Structural Stability Research Council Conference*. San Antonio, TX.
- Han, L. and Helwig, T. (2016) "Effect of Girder Continuity and Imperfections on System Buckling of Narrow I-Girder Systems," *Structural Stability Research Council Conference*. Orlando, FL.

- Han, L. and Helwig, T. (2020) "Elastic Global Lateral-Torsional Buckling of Straight I-Shaped Girder Systems," *Journal of Structural Engineering*, 146(No .4).
- Helwig, T. and Yura, J. (2015) "Bracing System Design," *Steel Bridge Design Handbook*. US DOT, Federal Highway Administration (Publication No. FHWA-HIF-16- 002).
- Helwig, T., Yura, J. and Frank, K. (1993) "Bracing Forces in Diaphragms and Cross Frames," in *Structural Stability Research Council Conference "Is Your Structure Suitably Braced?"*, 129–140.
- Helwig, T., Yarnold, M., Gasser, C., Bjelland, A., Fish, D., Park, S., Patel, S., Hurlebaus, S., Hebdon, M., Engelhardt, M., and Williamson, E. (2024) "Refined Design Methods for Lean-On Bracing." Research Report 0-7093. Texas Department of Transportation.
- Helwig, T. and Fan, Z. (2000) "Field and Computational Studies of Steel Trapezoidal Box Girder Bridges." Research Report 1395-3. Texas Department of Transportation.
- Helwig, T., Frank, K. and Yura, J. (1997) "Lateral-Torsional Buckling of Singly Symmetric I-Beams," *Journal of Structural Engineering*, 123(9), pp. 1172–1179.
- Helwig, T.A. and Wang, L. (2003) "Cross-Frame and Diaphragm Behavior for Steel Bridges with Skewed Supports." Research Report 1772–1. Texas Department of Transportation.
- Holt, J., Romage-Chambers, M., Clancy, C., Panchal, D., and Wasserman, E. (2022) *Lean-On Bracing Reference Guide*, AISC.
- Kamath, A. (2019) "Behavior of Straight Skewed I-Girder Bridges with Skew Index Approaching 0.3." Dissertation. Georgia Institute of Technology.
- Liu, Y. and Helwig, T. (2020) "Torsional Brace Strength Requirements for Steel I-Girder Systems," *Journal of Structural Engineering*, 146(1).
- Prado, E. (2015) "Assessment of Basic Steel I-Section Beam Bracing Requirements by Test Simulation." Thesis. Georgia Institute of Technology.
- Reichenbach, M. et al. (2020) "Lateral-Torsional Buckling of Singly Symmetric I-Girders with Stepped Flanges," *Journal of Structural Engineering*, 146(10), pp. 04020203-1–15.
- Reichenbach, M., White, J., Park, S., Zecchin, E., Moore, M., Liu, Y., Liang, C, Kovesdi, B., Helwig, T., Engelhardt, M., Connor, R., and Grubb, M. (2021) "Proposed Modification to AASHTO Cross-Frame Analysis and Design." Final Report NCHRP 962.
- Romage, M. (2008) "Field Measurements on Lean-On-Bracing for Steel Girder Bridges with Skewed Supports." Thesis. University of Texas at Austin.
- Sanchez, T. and White, D. (2012) "Stability of Curved Steel I-Girder Bridges during Construction," *Transportation Research Record: Journal of the Transportation Research Board*, 2268(1), pp. 122–129.

- Taylor, A.C. and Ojalvo, M. (1966) "Torsional Restraint of Lateral Buckling," *Journal of the Structural Division*, ASCE, ST2, pp. 115–129.
- Timoshenko, S. and Gere, J. (1961) *Theory of Elastic Stability*. New York: McGraw-Hill.
- Wang, L. and Helwig, T. (2005) "Critical Imperfections for Beam Bracing Systems," *Journal of Structural Engineering*, 131(6), pp. 933–940.
- Wang, W. (2013) "A Study of Stiffness of Steel Bridge Cross Frames," Dissertation. University of Texas at Austin.
- Winter, G. (1960) "Lateral Bracing of Columns and Beams," *ASCE Transactions*, 125, pp. 809–825.
- Yura, J., Helwig, T., Herman, R., and Shou, C. (2008) "Global Lateral Buckling of I-Shaped Girder Systems," *Journal of Structural Engineering*, 134(9), pp. 1487–1494.
- Yura, J. (1992) "Bracing of Steel Beams in Bridges." Research Report FHWA/TX-93+1239-4F. Texas Department of Transportation.
- Yura, J. (2001) "Fundamentals of Beam Bracing," *Engineering Journal*, (1) 11-26.

## Appendix A. Lubbock Bridge Live Load Testing Layouts

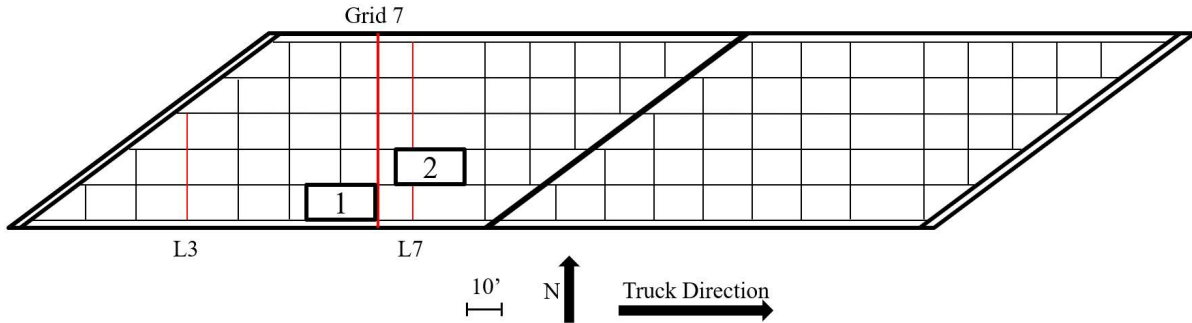


Figure A-1. Lubbock Bridge Load Case 1: Staggered Ahead Station

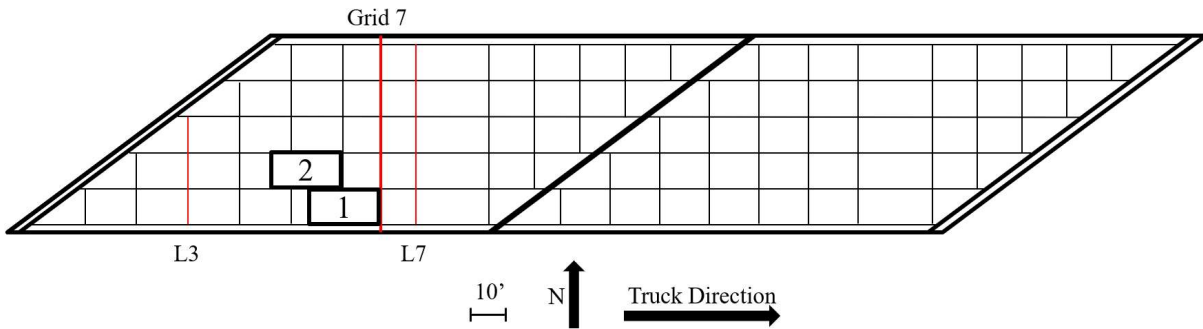


Figure A-2. Lubbock Bridge Load Case 2: Staggered Behind Station

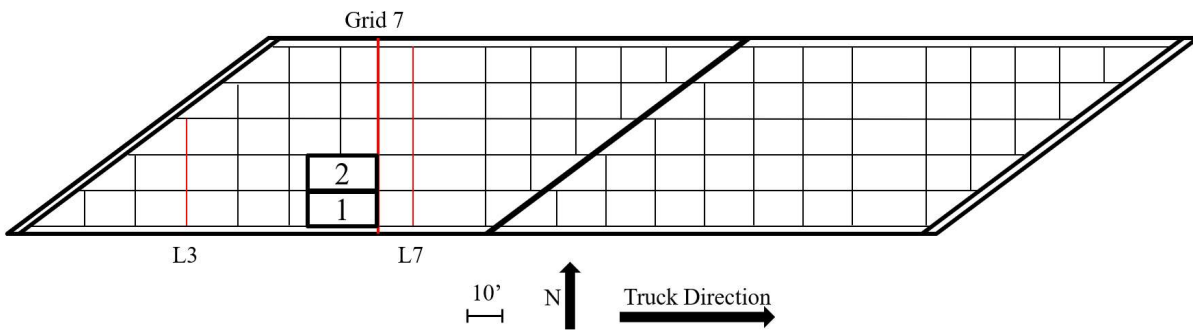


Figure A-3. Lubbock Bridge Load Case 3: Side-by-Side South

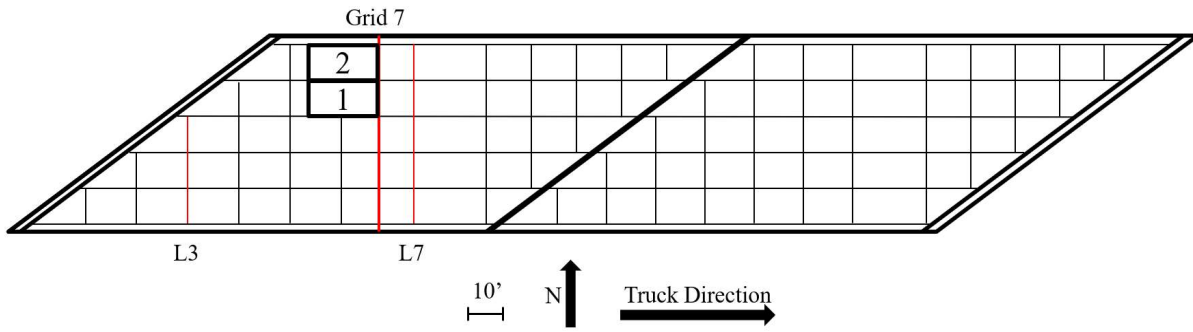


Figure A-4. Lubbock Bridge Load Case 4: Side-by-Side North

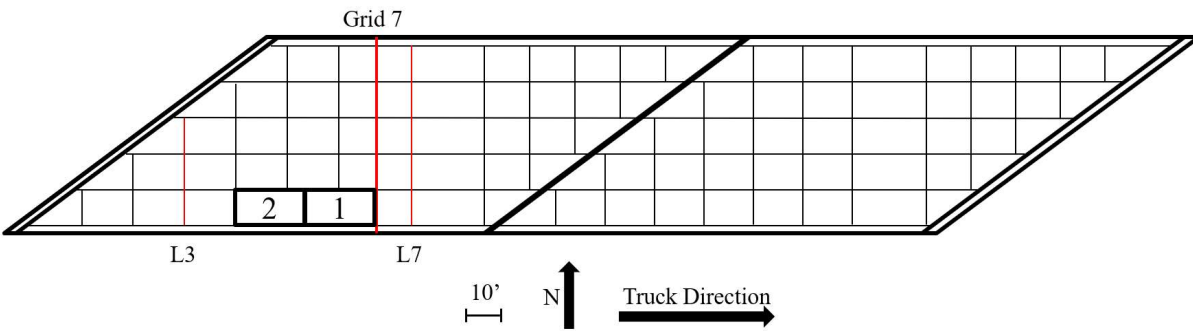


Figure A-5. Lubbock Bridge Load Case 5: End-to-End South

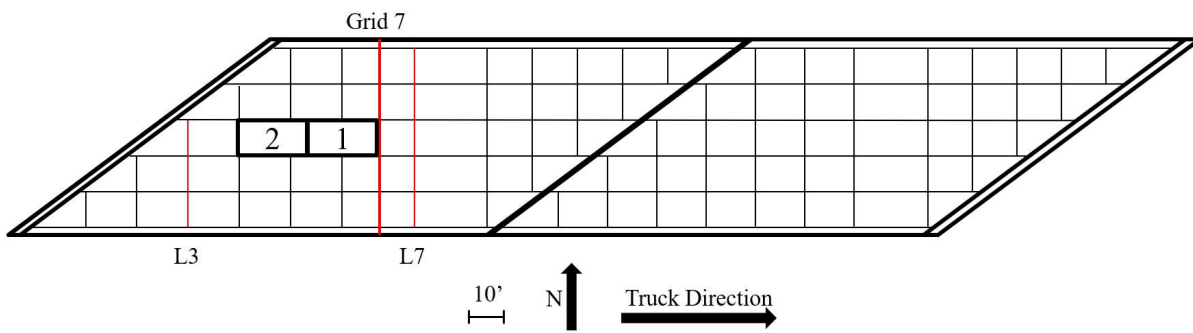


Figure A-6. Lubbock Bridge Load Case 6: End-to-End Central



## Appendix B. SH 105 Bridge Sensor List Conventions

Table B-1. SH 105 Bridge Sensor List Conventions

<b>Sensor List Conventions</b>		
Bay/ Girder #	G#	girder #
	B#	bay #
Member Type	GR	girder
	ST	strut, top
	SB	strut, bottom
	XT	cross-frame, top
	XB	cross-frame, bottom
Location on Member: Girders	N1	north bottom
	S1	south bottom
	N2	north middle
	S2	south middle
Location on Member: Angle	OH	outer horizontal
	IH	inner horizontal
	OV	outer vertical
	IV	inner vertical

## Appendix C. SH 105 Bridge Sensor List

Table C-1. SH 105 Bridge Sensor List

Strain Gauge	Datalogger	Multiplexer	Channel	Cross-frame Line	Bay/ Girder Number	Member Type	Location on Member	Label
1	D1	M1	C01	L5	G1	GR	N1	D1M1C01-L5G1-GR-N1
2	D1	M1	C03	L5	G1	GR	S1	D1M1C03-L5G1-GR-S1
3	D1	M1	C05	L5	B1	ST	OH	D1M1C05-L5B1-ST-OH
4	D1	M1	C07	L5	B1	ST	IH	D1M1C07-L5B1-ST-IH
5	D1	M1	C09	L5	B1	ST	OV	D1M1C09-L5B1-ST-OV
6	D1	M1	C11	L5	B1	ST	IV	D1M1C11-L5B1-ST-IV
7	D1	M1	C13	L5	B1	SB	OH	D1M1C13-L5B1-SB-OH
8	D1	M1	C15	L5	B1	SB	IH	D1M1C15-L5B1-SB-IH
9	D1	M1	C17	L5	B1	SB	OV	D1M1C17-L5B1-SB-OV
10	D1	M1	C19	L5	B1	SB	IV	D1M1C19-L5B1-SB-IV
11	D1	M1	C21	L5	G2	GR	N1	D1M1C21-L5G2-GR-N1
12	D1	M1	C23	L5	G2	GR	S1	D1M1C23-L5G2-GR-S1
13	D1	M1	C25	L5	G3	GR	N1	D1M1C25-L5G3-GR-N1
14	D1	M1	C27	L5	G3	GR	S1	D1M1C27-L5G3-GR-S1
15	D1	M1	C29	L5	G3	GR	N2	D1M1C29-L5G3-GR-N2
16	D1	M1	C31	L5	G3	GR	S2	D1M1C31-L5G3-GR-S2
1	D1	M2	C01	L5	B2	ST	OH	D1M2C01-L5B2-ST-OH
2	D1	M2	C03	L5	B2	ST	IH	D1M2C03-L5B2-ST-IH
3	D1	M2	C05	L5	B2	ST	OV	D1M2C05-L5B2-ST-OV
4	D1	M2	C07	L5	B2	ST	IV	D1M2C07-L5B2-ST-IV
5	D1	M2	C09	L5	B2	SB	OH	D1M2C09-L5B2-SB-OH
6	D1	M2	C11	L5	B2	SB	IH	D1M2C11-L5B2-SB-IH
7	D1	M2	C13	L5	B2	SB	OV	D1M2C13-L5B2-SB-OV
8	D1	M2	C15	L5	B2	SB	IV	D1M2C15-L5B2-SB-IV
9	D1	M2	C17	L5	B2	XT	OH	D1M2C17-L5B2-XT-OH
10	D1	M2	C19	L5	B2	XT	IH	D1M2C19-L5B2-XT-IH
11	D1	M2	C21	L5	B2	XT	OV	D1M2C21-L5B2-XT-OV
12	D1	M2	C23	L5	B2	XT	IV	D1M2C23-L5B2-XT-IV
13	D1	M2	C25	L5	B2	XB	OH	D1M2C25-L5B2-XB-OH
14	D1	M2	C27	L5	B2	XB	IH	D1M2C27-L5B2-XB-IH
15	D1	M2	C29	L5	B2	XB	OV	D1M2C29-L5B2-XB-OV

16	D1	M2	C31	L5	B2	XB	IV	D1M2C31-L5B2-XB-IV
1	D1	M3	C01	L5	B3	ST	OH	D2M3C01-L5B3-ST-OH
2	D1	M3	C03	L5	B3	ST	IH	D2M3C03-L5B3-ST-IH
3	D1	M3	C05	L5	B3	ST	OV	D2M3C05-L5B3-ST-OV
4	D1	M3	C07	L5	B3	ST	IV	D2M3C07-L5B3-ST-IV
5	D1	M3	C09	L5	B3	SB	OH	D2M3C09-L5B3-SB-OH
6	D1	M3	C11	L5	B3	SB	IH	D2M3C11-L5B3-SB-IH
7	D1	M3	C13	L5	B3	SB	OV	D2M3C13-L5B3-SB-OV
8	D1	M3	C15	L5	B3	SB	IV	D2M3C15-L5B3-SB-IV
9	D1	M3	C17	L5	B3	XT	OH	D2M3C17-L5B3-XT-OH
10	D1	M3	C19	L5	B3	XT	IH	D2M3C19-L5B3-XT-IH
11	D1	M3	C21	L5	B3	XT	OV	D2M3C21-L5B3-XT-OV
12	D1	M3	C23	L5	B3	XT	IV	D2M3C23-L5B3-XT-IV
13	D1	M3	C25	L5	B3	XB	OH	D2M3C25-L5B3-XB-OH
14	D1	M3	C27	L5	B3	XB	IH	D2M3C27-L5B3-XB-IH
15	D1	M3	C29	L5	B3	XB	OV	D2M3C29-L5B3-XB-OV
16	D1	M3	C31	L5	B3	XB	IV	D2M3C31-L5B3-XB-IV
1	D1	M4	C01	L5	G4	GR	N1	D2M4C01-L5G4-GR-N1
2	D1	M4	C03	L5	G4	GR	S1	D2M4C03-L5G4-GR-S1
3	D1	M4	C05	L5	B4	ST	OH	D2M4C05-L5B4-ST-OH
4	D1	M4	C07	L5	B4	ST	IH	D2M4C07-L5B4-ST-IH
5	D1	M4	C09	L5	B4	ST	OV	D2M4C09-L5B4-ST-OV
6	D1	M4	C11	L5	B4	ST	IV	D2M4C11-L5B4-ST-IV
7	D1	M4	C13	L5	B4	SB	OH	D2M4C13-L5B4-SB-OH
8	D1	M4	C15	L5	B4	SB	IH	D2M4C15-L5B4-SB-IH
9	D1	M4	C17	L5	B4	SB	OV	D2M4C17-L5B4-SB-OV
10	D1	M4	C19	L5	B4	SB	IV	D2M4C19-L5B4-SB-IV
11	D1	M4	C21	L5	G5	GR	N1	D2M4C21-L5G5-GR-N1
12	D1	M4	C23	L5	G5	GR	S1	D2M4C23-L5G5-GR-S1
1	D2	M5	C01	L3	B1	ST	OH	D3M5C01-L3B1-ST-OH
2	D2	M5	C03	L3	B1	ST	IH	D3M5C03-L3B1-ST-IH
3	D2	M5	C05	L3	B1	ST	OV	D3M5C05-L3B1-ST-OV
4	D2	M5	C07	L3	B1	ST	IV	D3M5C07-L3B1-ST-IV
5	D2	M5	C09	L3	B1	SB	OH	D3M5C09-L3B1-SB-OH
6	D2	M5	C11	L3	B1	SB	IH	D3M5C11-L3B1-SB-IH
7	D2	M5	C13	L3	B1	SB	OV	D3M5C13-L3B1-SB-OV
8	D2	M5	C15	L3	B1	SB	IV	D3M5C15-L3B1-SB-IV
9	D2	M5	C17	L3	B1	XT	OH	D3M5C17-L3B1-XT-OH
10	D2	M5	C19	L3	B1	XT	IH	D3M5C19-L3B1-XT-IH
11	D2	M5	C21	L3	B1	XT	OV	D3M5C21-L3B1-XT-OV
12	D2	M5	C23	L3	B1	XT	IV	D3M5C23-L3B1-XT-IV
13	D2	M5	C25	L3	B1	XB	OH	D3M5C25-L3B1-XB-OH
14	D2	M5	C27	L3	B1	XB	IH	D3M5C27-L3B1-XB-IH

15	D2	M5	C29	L3	B1	XB	OV	D3M5C29-L3B1-XB-OV
16	D2	M5	C31	L3	B1	XB	IV	D3M5C31-L3B1-XB-IV
1	D2	M6	C01	L3	B2	ST	OH	D3M6C01-L3B2-ST-OH
2	D2	M6	C03	L3	B2	ST	IH	D3M6C03-L3B2-ST-IH
3	D2	M6	C05	L3	B2	ST	OV	D3M6C05-L3B2-ST-OV
4	D2	M6	C07	L3	B2	ST	IV	D3M6C07-L3B2-ST-IV
5	D2	M6	C09	L3	B2	SB	OH	D3M6C09-L3B2-SB-OH
6	D2	M6	C11	L3	B2	SB	IH	D3M6C11-L3B2-SB-IH
7	D2	M6	C13	L3	B2	SB	OV	D3M6C13-L3B2-SB-OV
8	D2	M6	C15	L3	B2	SB	IV	D3M6C15-L3B2-SB-IV
9	D2	M6	C17	L3	B2	XT	OH	D3M6C17-L3B2-XT-OH
10	D2	M6	C19	L3	B2	XT	IH	D3M6C19-L3B2-XT-IH
11	D2	M6	C21	L3	B2	XT	OV	D3M6C21-L3B2-XT-OV
12	D2	M6	C23	L3	B2	XT	IV	D3M6C23-L3B2-XT-IV
13	D2	M6	C25	L3	B2	XB	OH	D3M6C25-L3B2-XB-OH
14	D2	M6	C27	L3	B2	XB	IH	D3M6C27-L3B2-XB-IH
15	D2	M6	C29	L3	B2	XB	OV	D3M6C29-L3B2-XB-OV
16	D2	M6	C31	L3	B2	XB	IV	D3M6C31-L3B2-XB-IV
1	D2	M7	C01	L3	B3	ST	OH	D4M7C01-L3B3-ST-OH
2	D2	M7	C03	L3	B3	ST	IH	D4M7C03-L3B3-ST-IH
3	D2	M7	C05	L3	B3	ST	OV	D4M7C05-L3B3-ST-OV
4	D2	M7	C07	L3	B3	ST	IV	D4M7C07-L3B3-ST-IV
5	D2	M7	C09	L3	B3	SB	OH	D4M7C09-L3B3-SB-OH
6	D2	M7	C11	L3	B3	SB	IH	D4M7C11-L3B3-SB-IH
7	D2	M7	C13	L3	B3	SB	OV	D4M7C13-L3B3-SB-OV
8	D2	M7	C15	L3	B3	SB	IV	D4M7C15-L3B3-SB-IV
9	D2	M7	C17	L3	B4	ST	OH	D4M7C17-L3B4-ST-OH
10	D2	M7	C19	L3	B4	ST	IH	D4M7C19-L3B4-ST-IH
11	D2	M7	C21	L3	B4	ST	OV	D4M7C21-L3B4-ST-OV
12	D2	M7	C23	L3	B4	ST	IV	D4M7C23-L3B4-ST-IV
13	D2	M7	C25	L3	B4	SB	OH	D4M7C25-L3B4-SB-OH
14	D2	M7	C27	L3	B4	SB	IH	D4M7C27-L3B4-SB-IH
15	D2	M7	C29	L3	B4	SB	OV	D4M7C29-L3B4-SB-OV
16	D2	M7	C31	L3	B4	SB	IV	D4M7C31-L3B4-SB-IV

## Appendix D. SH 105 Bridge Live Load Testing Layout

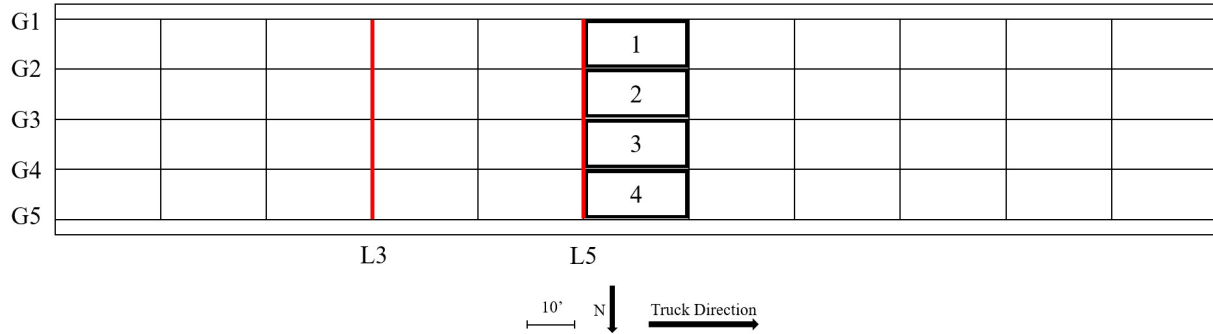


Figure D-1. SH 105 Bridge Load Case 1

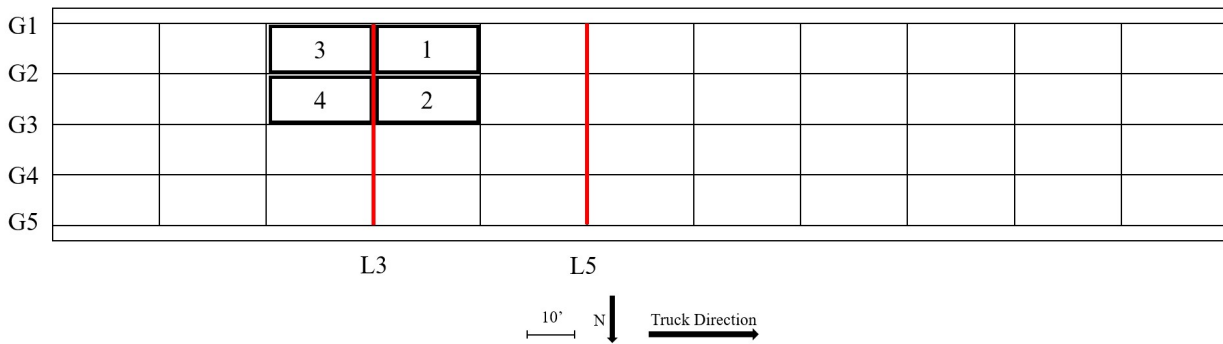


Figure D-2. SH 105 Bridge Load Case 2

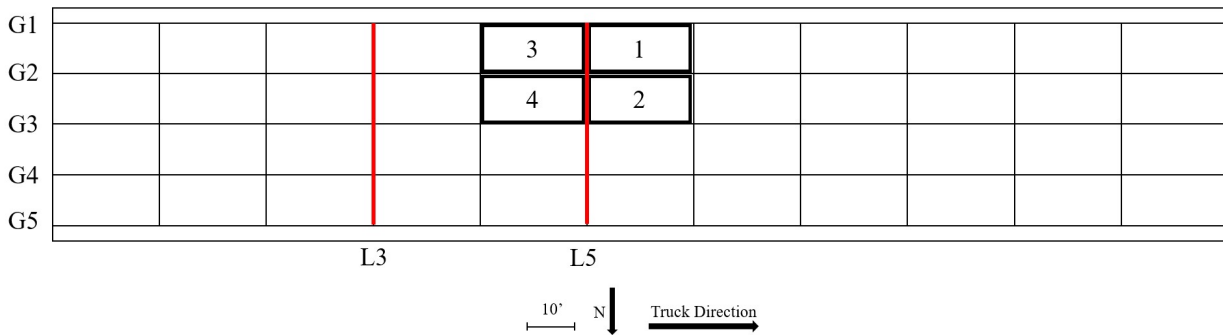


Figure D-3. SH 105 Bridge Load Case 3

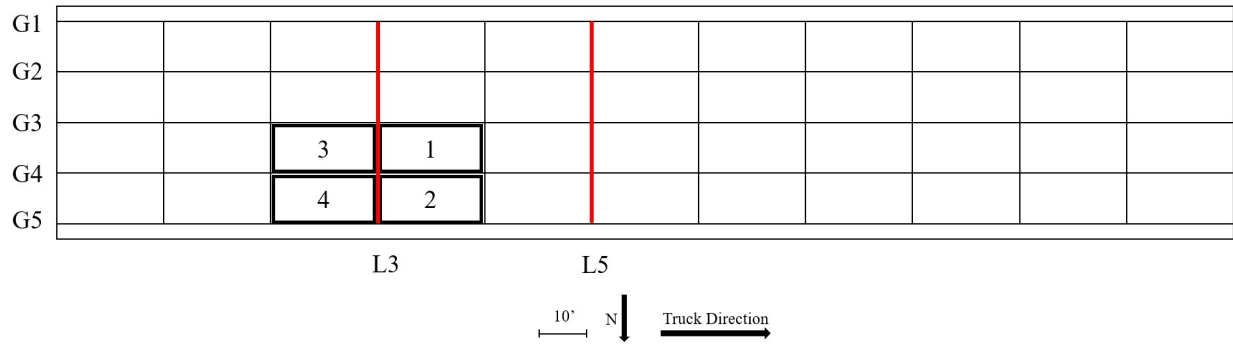


Figure D-4. SH 105 Bridge Load Case 4

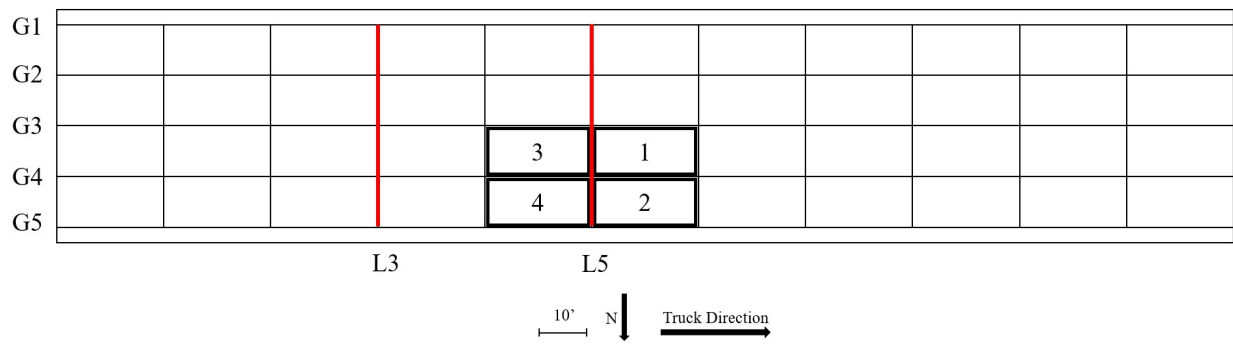


Figure D-5. SH 105 Bridge Load Case 5

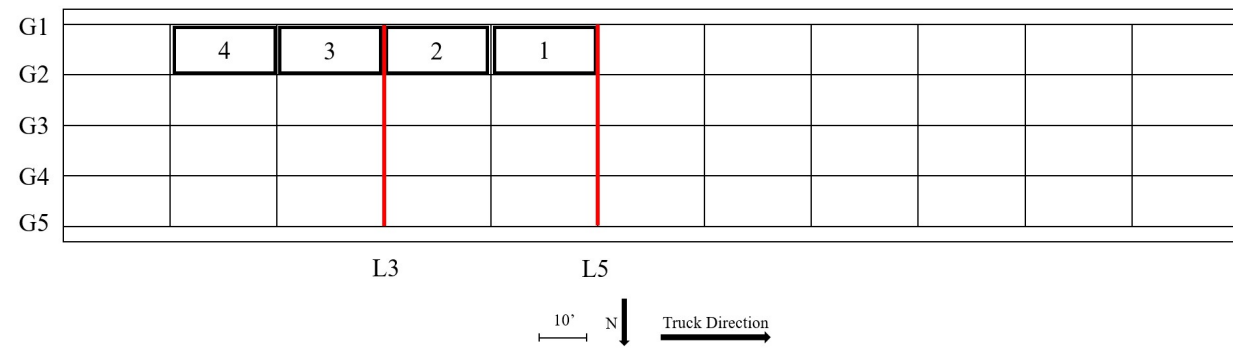


Figure D-6. SH 105 Bridge Load Case 6

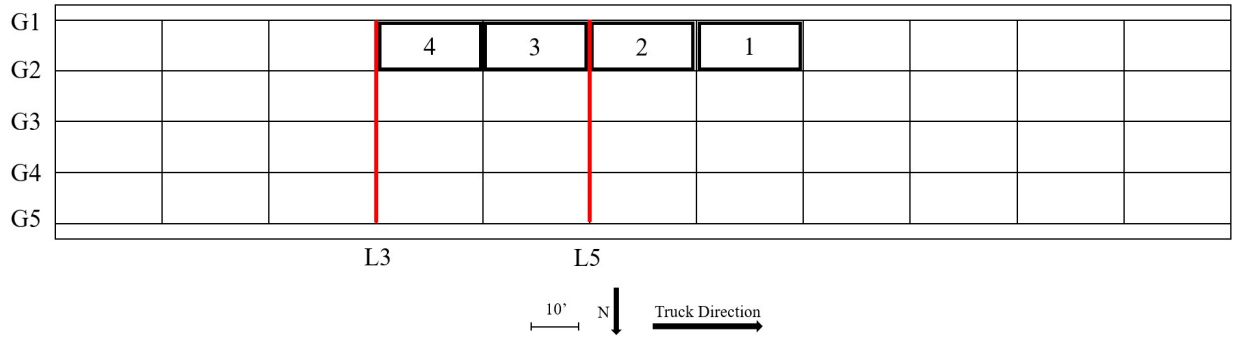


Figure D-7. SH 105 Bridge Load Case 7

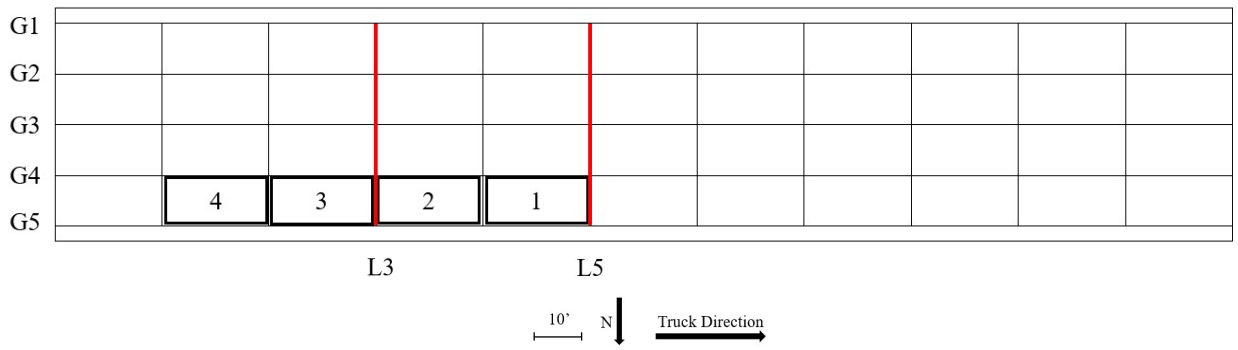


Figure D-8. SH 105 Bridge Load Case 8

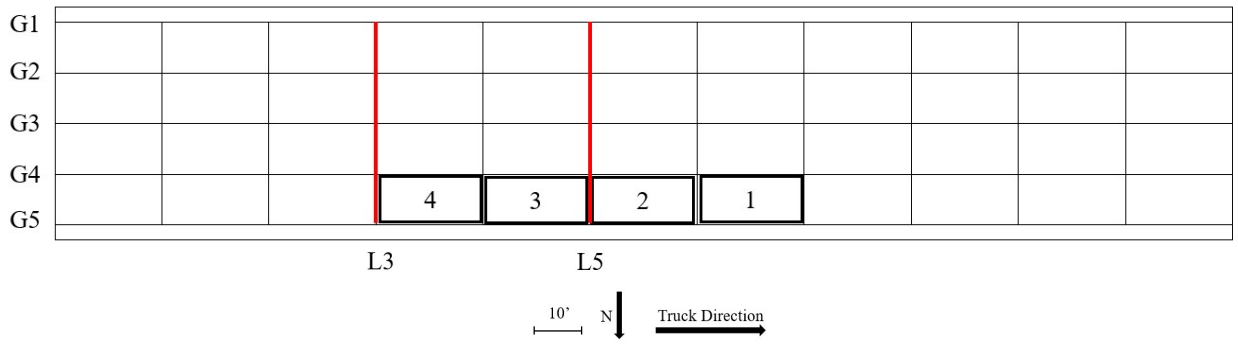


Figure D-9. SH 105 Bridge Load Case 9

## Appendix E. Chisholm Trail Bridge Sensor List Conventions

Table E-1. Chisholm Trail Bridge Sensor List Conventions

<b>Sensor List Conventions</b>		
Bay/ Girder #	G#	girder #
	B#	bay #
Member Type	GR	girder
	ST	strut top
	SB	strut bottom
	SBE	strut bottom east
	SBW	strut bottom west
	KE	k-frame east
	KW	k-frame west
Location on Member: Girders	N1	north bottom
	S1	south bottom
	N2	north middle
	S2	south middle
Location on Member: Single Angle	OH	outer horizontal
	IH	inner horizontal
	OV	outer vertical
	IV	inner vertical
Location on Member: Double Angle	OHN/S	outer horizontal north/south
	IHN/S	inner horizontal north/south
	IVN/S	inner vertical north/south



## Appendix F. Chisholm Trail Bridge Sensor List

Table F-1. Chisholm Trail Bridge Sensor List

Strain Gauge Count	Multiplexer	Channel	Cross-frame Line	Bay/Girder Number	Member Type	Location on Member	Label
1	M1	C01	L8	B1	ST	OH	M1C01-L8B1-ST-OH
2	M1	C02	L8	B1	ST	IH	M1C02-L8B1-ST-IH
3	M1	C03	L8	B1	ST	OV	M1C03-L8B1-ST-OV
4	M1	C04	L8	B1	ST	IV	M1C04-L8B1-ST-IV
5	M1	C05	L8	B1	SB	OH	M1C05-L8B1-SB-OH
6	M1	C06	L8	B1	SB	IH	M1C06-L8B1-SB-IH
7	M1	C07	L8	B1	SB	OV	M1C07-L8B1-SB-OV
8	M1	C08	L8	B1	SB	IV	M1C08-L8B1-SB-IV
9	M1	C09	L8	B2	ST	OH	M1C09-L8B2-ST-OH
10	M1	C10	L8	B2	ST	IH	M1C10-L8B2-ST-IH
11	M1	C11	L8	B2	ST	OV	M1C11-L8B2-ST-OV
12	M1	C12	L8	B2	ST	IV	M1C12-L8B2-ST-IV
13	M1	C13	L8	B2	SB	OH	M1C13-L8B2-SB-OH
14	M1	C14	L8	B2	SB	IH	M1C14-L8B2-SB-IH
15	M1	C15	L8	B2	SB	OV	M1C15-L8B2-SB-OV
16	M1	C16	L8	B2	SB	IV	M1C16-L8B2-SB-IV
1	M2	C01	L8	G3	GR	N1	M2C01-L8G3-GR-N1
2	M2	C02	L8	G3	GR	S1	M2C02-L8G3-GR-S1
3	M2	C03	L8	G3	GR	N2	M2C03-L8G3-GR-N2
4	M2	C04	L8	G3	GR	S2	M2C04-L8G3-GR-S2
5	M2	C05	L8	B3	ST	OH	M2C05-L8B3-ST-OH
6	M2	C06	L8	B3	ST	IH	M2C06-L8B3-ST-IH
7	M2	C07	L8	B3	ST	OV	M2C07-L8B3-ST-OV
8	M2	C08	L8	B3	ST	IV	M2C08-L8B3-ST-IV
9	M2	C09	L8	B3	SBE	OH	M2C09-L8B3-SBE-OH
10	M2	C10	L8	B3	SBE	IH	M2C10-L8B3-SBE-IH
11	M2	C11	L8	B3	SBE	OV	M2C11-L8B3-SBE-OV
12	M2	C12	L8	B3	SBE	IV	M2C12-L8B3-SBE-IV
13	M2	C13	L8	B3	SBW	OH	M2C13-L8B3-SBW-OH
14	M2	C14	L8	B3	SBW	IH	M2C14-L8B3-SBW-IH

15	M2	C15	L8	B3	SBW	OV	M2C15-L8B3-SBW-OV
16	M2	C16	L8	B3	SBW	IV	M2C16-L8B3-SBW-IV
1	M3	C01	L8	G4	GR	N1	M3C01-L8G4-GR-N1
2	M3	C02	L8	G4	GR	S1	M3C02-L8G4-GR-S1
3	M3	C03	L8	G4	GR	N2	M3C03-L8G4-GR-N2
4	M3	C04	L8	G4	GR	S2	M3C04-L8G4-GR-S2
5	M3	C05	L8	B3	KE	OH	M3C05-L8B3-KE-OH
6	M3	C06	L8	B3	KE	IH	M3C06-L8B3-KE-IH
7	M3	C07	L8	B3	KE	OV	M3C07-L8B3-KE-OV
8	M3	C08	L8	B3	KE	IV	M3C08-L8B3-KE-IV
9	M3	C09	L8	B3	KW	OH	M3C09-L8B3-KW-OH
10	M3	C10	L8	B3	KW	IH	M3C10-L8B3-KW-IH
11	M3	C11	L8	B3	KW	OV	M3C11-L8B3-KW-OV
12	M3	C12	L8	B3	KW	IV	M3C12-L8B3-KW-IV
13	M3	C13	L8	B4	ST	OH	M3C13-L8B4-ST-OH
14	M3	C14	L8	B4	ST	IH	M3C14-L8B4-ST-IH
15	M3	C15	L8	B4	ST	OV	M3C15-L8B4-ST-OV
16	M3	C16	L8	B4	ST	IV	M3C16-L8B4-ST-IV
1	M4	C01	L8	B4	SB	OH	M4C01-L8B4-SB-OH
2	M4	C02	L8	B4	SB	IH	M4C02-L8B4-SB-IH
3	M4	C03	L8	B4	SB	OV	M4C03-L8B4-SB-OV
4	M4	C04	L8	B4	SB	IV	M4C04-L8B4-SB-IV
5	M4	C05	L8	G5	GR	N1	M4C05-L8G5-GR-N1
6	M4	C06	L8	G5	GR	S1	M4C06-L8G5-GR-S1
7	M4	C07	L8	B5	ST	OH	M4C07-L8B5-ST-OH
8	M4	C08	L8	B5	ST	IH	M4C08-L8B5-ST-IH
9	M4	C09	L8	B5	ST	OV	M4C09-L8B5-ST-OV
10	M4	C10	L8	B5	ST	IV	M4C10-L8B5-ST-IV
11	M4	C11	L8	B5	SB	OH	M4C11-L8B5-SB-OH
12	M4	C12	L8	B5	SB	IH	M4C12-L8B5-SB-IH
13	M4	C13	L8	B5	SB	OV	M4C13-L8B5-SB-OV
14	M4	C14	L8	B5	SB	IV	M4C14-L8B5-SB-IV
15	M4	C15	L8	G6	GR	N1	M4C15-L8G6-GR-N1
16	M4	C16	L8	G6	GR	S1	M4C16-L8G6-GR-S1
1	M5	C01	L8	G1	GR	N1	M5C01-L8G1-GR-N1
2	M5	C02	L8	G1	GR	S1	M5C02-L8G1-GR-S1
3	M5	C03	L8	G2	GR	N1	M5C03-L8G2-GR-N1
4	M5	C04	L8	G2	GR	S1	M5C04-L8G2-GR-S1
5	M5	C05	L13	B1	ST	OH	M5C05-L13B1-ST-OH
6	M5	C06	L13	B1	ST	IH	M5C06-L13B1-ST-IH
7	M5	C07	L13	B1	ST	OV	M5C07-L13B1-ST-OV
8	M5	C08	L13	B1	ST	IV	M5C08-L13B1-ST-IV
9	M5	C09	L15	B1	SBE	OH	M5C09-L15B1-SBE-OH

10	M5	C10	L15	B1	SBE	IH	M5C10-L15B1-SBE-IH
11	M5	C11	L15	B1	SBE	OV	M5C11-L15B1-SBE-OV
12	M5	C12	L15	B1	SBE	IV	M5C12-L15B1-SBE-IV
13	M5	C13	L15	B1	SBW	OH	M5C13-L15B1-SBW-OH
14	M5	C14	L15	B1	SBW	IH	M5C14-L15B1-SBW-IH
15	M5	C15	L15	B1	SBW	OV	M5C15-L15B1-SBW-OV
16	M5	C16	L15	B1	SBW	IV	M5C16-L15B1-SBW-IV
1	M6	C01	L13	B1	SBE	OH	M6C01-L13B1-SBE-OH
2	M6	C02	L13	B1	SBE	IH	M6C02-L13B1-SBE-IH
3	M6	C03	L13	B1	SBE	OV	M6C03-L13B1-SBE-OV
4	M6	C04	L13	B1	SBE	IV	M6C04-L13B1-SBE-IV
5	M6	C05	L13	B1	SBW	OH	M6C05-L13B1-SBW-OH
6	M6	C06	L13	B1	SBW	IH	M6C06-L13B1-SBW-IH
7	M6	C07	L13	B1	SBW	OV	M6C07-L13B1-SBW-OV
8	M6	C08	L13	B1	SBW	IV	M6C08-L13B1-SBW-IV
9	M6	C09	L13	B1	KE	OH	M6C09-L13B1-KE-OH
10	M6	C10	L13	B1	KE	IH	M6C10-L13B1-KE-IH
11	M6	C11	L13	B1	KE	OV	M6C11-L13B1-KE-OV
12	M6	C12	L13	B1	KE	IV	M6C12-L13B1-KE-IV
13	M6	C13	L13	B1	KW	OH	M6C13-L13B1-KW-OH
14	M6	C14	L13	B1	KW	IH	M6C14-L13B1-KW-IH
15	M6	C15	L13	B1	KW	OV	M6C15-L13B1-KW-OV
16	M6	C16	L13	B1	KW	IV	M6C16-L13B1-KW-IV
1	M7	C01	L13	B2	ST	IHE	M7C01-L13B2-ST-IHE
2	M7	C02	L13	B2	ST	IVE	M7C02-L13B2-ST-IVE
3	M7	C03	L13	B2	ST	IHW	M7C03-L13B2-ST-IHW
4	M7	C04	L13	B2	ST	IVW	M7C04-L13B2-ST-IVW
5	M7	C05	L13	B2	SB	IHE	M7C05-L13B2-SB-IHE
6	M7	C06	L13	B2	SB	IVE	M7C06-L13B2-SB-IVE
7	M7	C07	L13	B2	SB	IHW	M7C07-L13B2-SB-IHW
8	M7	C08	L13	B2	SB	IVW	M7C08-L13B2-SB-IVW
9	M7	C09	L13	B3	ST	IHN	M7C09-L13B3-ST-IHN
10	M7	C10	L13	B3	ST	IVN	M7C10-L13B3-ST-IVN
11	M7	C11	L13	B3	ST	HIS	M7C11-L13B3-ST-HIS
12	M7	C12	L13	B3	ST	IVS	M7C12-L13B3-ST-IVS
13	M7	C13	L13	B3	SB	OHN	M7C13-L13B3-SB-OHN
14	M7	C14	L13	B3	SB	IVN	M7C14-L13B3-SB-IVN
15	M7	C15	L13	B3	SB	OHS	M7C15-L13B3-SB-OHS
16	M7	C16	L13	B3	SB	IVS	M7C16-L13B3-SB-IVS
1	M8	C01	L15	B1	KE	OH	M8C01-L15B1-KE-OH
2	M8	C02	L15	B1	KE	IH	M8C02-L15B1-KE-IH
3	M8	C03	L15	B1	KE	OV	M8C03-L15B1-KE-OV
4	M8	C04	L15	B1	KE	IV	M8C04-L15B1-KE-IV

5	M8	C05	L15	B1	KW	OH	M8C05-L15B1-KW-OH
6	M8	C06	L15	B1	KW	IH	M8C06-L15B1-KW-IH
7	M8	C07	L15	B1	KW	OV	M8C07-L15B1-KW-OV
8	M8	C08	L15	B1	KW	IV	M8C08-L15B1-KW-IV
9	M8	C09	L15	B2	ST	IHE	M8C09-L15B2-ST-IHE
10	M8	C10	L15	B2	ST	IVE	M8C10-L15B2-ST-IVE
11	M8	C11	L15	B2	ST	IHW	M8C11-L15B2-ST-IHW
12	M8	C12	L15	B2	ST	IVW	M8C12-L15B2-ST-IVW
13	M8	C13	L15	B2	SB	OHN	M8C13-L15B2-SB-OHN
14	M8	C14	L15	B2	SB	IVN	M8C14-L15B2-SB-IVN
15	M8	C15	L15	B2	SB	OHS	M8C15-L15B2-SB-OHS
16	M8	C16	L15	B2	SB	IVS	M8C16-L15B2-SB-IVS

# Appendix G. Chisholm Trail Bridge Live Load Testing Layouts

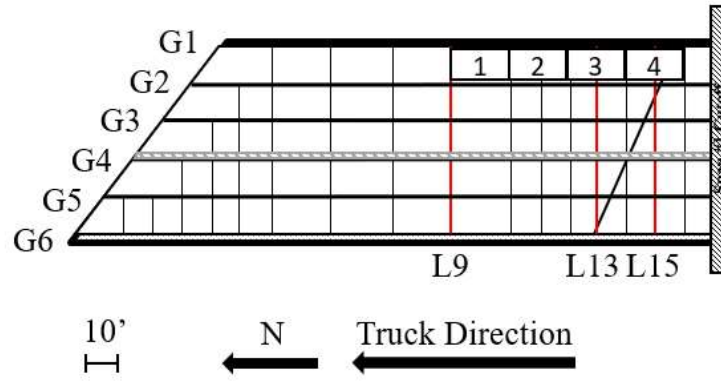


Figure G-1. Chisholm Trail Bridge Load Case 1

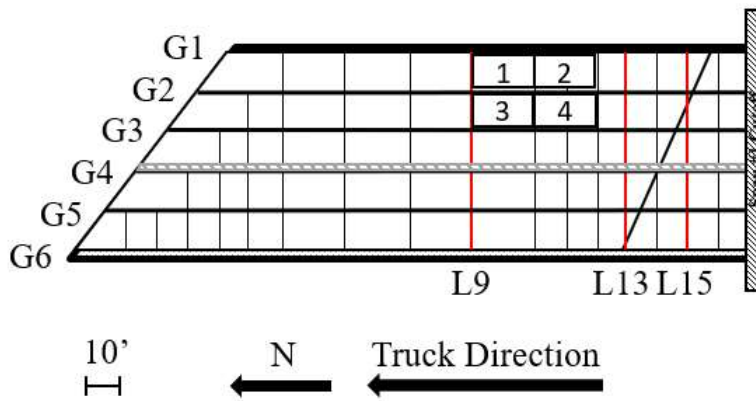


Figure G-2. Chisholm Trail Bridge Load Case 2

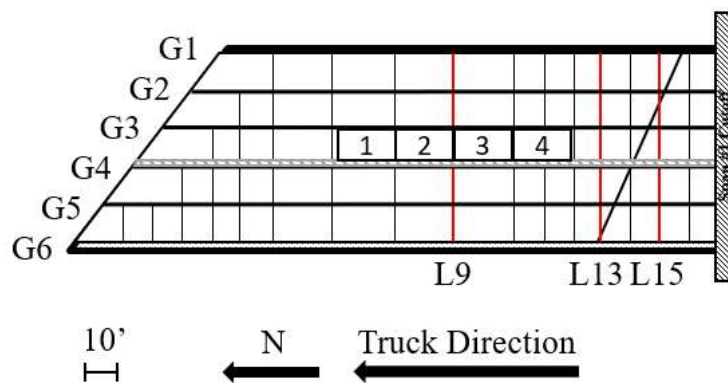


Figure G-3. Chisholm Trail Bridge Load Case 3

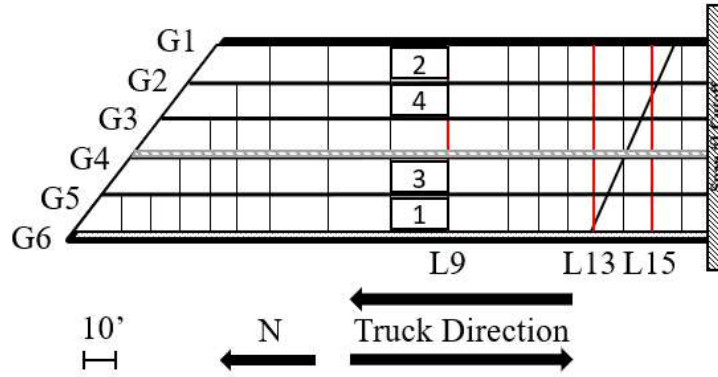


Figure G-4. Chisholm Trail Bridge Load Case 4

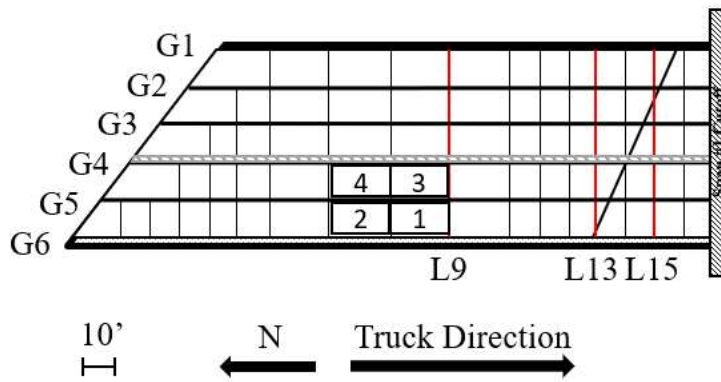


Figure G-5. Chisholm Trail Bridge Load Case 5

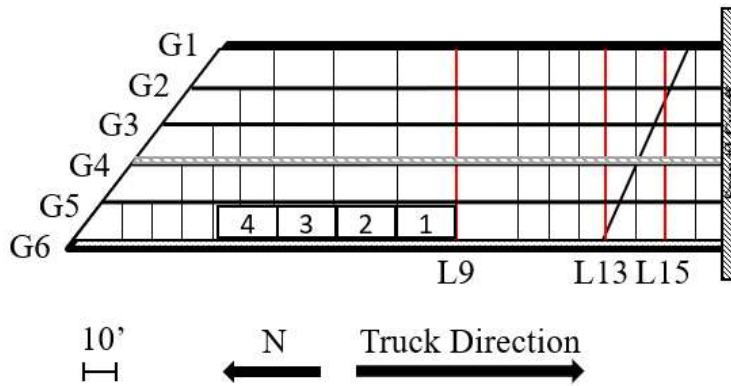


Figure G-6. Chisholm Trail Bridge Load Case 6

## Appendix H. Axial Force Sample Calculations

<b>Sample Problem - 20 kip Pure Axial Load</b>				
<b>Measured Strains and Locations</b>				
Area of member	$A := 6.45 \text{ in}^2$			
centroid i.e. origin of member:	$x0 := 0$	in	$y0 := 0$	in
strain 1 - OH	$\epsilon 1 := 107$	microstrain	$x1 := 3.3$	in
strain 2 - IH	$\epsilon 2 := 107$	microstrain	$x2 := 3.3$	in
strain 3 - OV	$\epsilon 3 := 107$	microstrain	$x3 := -1.7$	in
strain 4 - IV	$\epsilon 4 := 107$	microstrain	$x4 := -1.14$	in
<b>Calculations</b>				
$\epsilon b := \frac{\epsilon 1 + \epsilon 2 + \epsilon 3 + \epsilon 4}{4} = 107$				
$x b := \frac{x1 + x2 + x3 + x4}{4} = 0.94 \text{ in} \quad [\epsilon\_bar, x\_bar, y\_bar]$				
$y b := \frac{y1 + y2 + y3 + y4}{4} = -0.94 \text{ in}$				
$I_{11} := (x1 - x b)^2 + (x2 - x b)^2 + (x3 - x b)^2 + (x4 - x b)^2 = 22.435 \text{ in}^2$				
$I_{22} := (y1 - y b)^2 + (y2 - y b)^2 + (y3 - y b)^2 + (y4 - y b)^2 = 22.435 \text{ in}^2$				
$I_{12} := (x1 - x b)(y1 - y b) + (x2 - x b)(y2 - y b) + (x3 - x b)(y3 - y b) + (x4 - x b)(y4 - y b)$				
$I_{21} := I_{12} = 22.278 \text{ in}^2$				
$I_{10} := (x1 - x b)(\epsilon 1 - \epsilon b) + (x2 - x b)(\epsilon 2 - \epsilon b) + (x3 - x b)(\epsilon 3 - \epsilon b) + (x4 - x b)(\epsilon 4 - \epsilon b)$				
$I_{10} = 0 \text{ in}$				
$I_{20} := (y1 - y b)(\epsilon 1 - \epsilon b) + (y2 - y b)(\epsilon 2 - \epsilon b) + (y3 - y b)(\epsilon 3 - \epsilon b) + (y4 - y b)(\epsilon 4 - \epsilon b)$				
$I_{20} = 0 \text{ in}$				

Solve for b and c using  $I_{11} \cdot b + I_{12} \cdot c = I_{10}$  and  $I_{21} \cdot b + I_{22} \cdot c = I_{20}$

$$I_{11} \cdot b + I_{12} \cdot c = I_{10}$$

$$I_{21} \cdot b + I_{22} \cdot c = I_{20}$$

$$M := \begin{bmatrix} I_{11} & I_{12} \\ I_{21} & I_{22} \end{bmatrix}$$

$$v := \begin{bmatrix} I_{10} \\ I_{20} \end{bmatrix}$$

$$\begin{bmatrix} b \\ c \end{bmatrix} := M^{-1} \cdot v = \begin{bmatrix} 0 \\ 0 \end{bmatrix} \frac{1}{m}$$

$$a := \varepsilon b - b \cdot x b - c \cdot y b = 107 \quad \text{microstrain}$$

### Axial Stress

#### Axial Stress

$$E := 29000 \text{ ksi}$$

$$\sigma := E \cdot \frac{a}{10^6} = 3.103 \text{ ksi} \quad 10^6 \text{ for microstrain}$$

#### Axial Force

$$F := A \cdot \sigma = 20 \text{ kip}$$



## Sample Problem - 20 kip Axial and 0.01 k/ft Transverse Loading

\*\*\*orientation change for Strand7 validation

### Measured Strains and Locations

Area of member	$A := 6.45 \text{ in}^2$			
centroid i.e. origin of member:	$x0 := 0$	in	$y0 := 0$	in
strain 1 - OH	$\epsilon1 := 155$	microstrain	$x1 := 3.3$	$y1 := -1.7$ in
strain 2 - IH	$\epsilon2 := 131$	microstrain	$x2 := 3.3$	$y2 := -1.14$ in
strain 3 - OV	$\epsilon3 := -8.6$	microstrain	$x3 := -1.7$	$y3 := 3.3$ in
strain 4 - IV	$\epsilon4 := -14.5$	microstrain	$x4 := -1.14$	$y4 := 3.3$ in

### Calculations

$$\epsilon_b := \frac{\epsilon1 + \epsilon2 + \epsilon3 + \epsilon4}{4} = 65.725$$

$$x_b := \frac{x1 + x2 + x3 + x4}{4} = 0.94 \text{ in} \quad [\epsilon\_bar, x\_bar, y\_bar]$$

$$y_b := \frac{y1 + y2 + y3 + y4}{4} = 0.94 \text{ in}$$

$$I_{11} := (x1 - x_b)^2 + (x2 - x_b)^2 + (x3 - x_b)^2 + (x4 - x_b)^2 = 22.435 \text{ in}^2$$

$$I_{22} := (y1 - y_b)^2 + (y2 - y_b)^2 + (y3 - y_b)^2 + (y4 - y_b)^2 = 22.435 \text{ in}^2$$

$$I_{12} := (x1 - x_b)(y1 - y_b) + (x2 - x_b)(y2 - y_b) + (x3 - x_b)(y3 - y_b) + (x4 - x_b)(y4 - y_b)$$

$$I_{21} := I_{12} = -22.278 \text{ in}^2$$

$$I_{10} := (x1 - x_b)(\epsilon1 - \epsilon_b) + (x2 - x_b)(\epsilon2 - \epsilon_b) + (x3 - x_b)(\epsilon3 - \epsilon_b) + (x4 - x_b)(\epsilon4 - \epsilon_b)$$

$$I_{10} = 727.824 \text{ in}$$

$$I_{20} := (y1 - y_b)(\epsilon1 - \epsilon_b) + (y2 - y_b)(\epsilon2 - \epsilon_b) + (y3 - y_b)(\epsilon3 - \epsilon_b) + (y4 - y_b)(\epsilon4 - \epsilon_b)$$

$$I_{20} = -736.196 \text{ in}$$

Solve for b and c using  $I_{11} \cdot b + I_{12} \cdot c = I_{10}$  and  $I_{21} \cdot b + I_{22} \cdot c = I_{20}$

$$I_{11} \cdot b + I_{12} \cdot c = I_{10}$$

$$I_{21} \cdot b + I_{22} \cdot c = I_{20}$$

$$M := \begin{bmatrix} I_{11} & I_{12} \\ I_{21} & I_{22} \end{bmatrix}$$

$$v := \begin{bmatrix} I_{10} \\ I_{20} \end{bmatrix}$$

$$\begin{bmatrix} b \\ c \end{bmatrix} := M^{-1} \cdot v = \begin{bmatrix} -406.5097 \\ -1.6956 \cdot 10^3 \end{bmatrix} \frac{1}{m}$$

$$a := \varepsilon b - b \cdot x b - c \cdot y b = 115.914 \quad \text{microstrain}$$

### Axial Stress

#### Axial Stress

$$E := 29000 \text{ ksi}$$

$$\sigma := E \cdot \frac{a}{10^6} = 3.362 \text{ ksi} \quad 10^6 \text{ for microstrain}$$

#### Axial Force

$$F := A \cdot \sigma = 22 \text{ kip}$$

## Appendix I. Lubbock Bridge Axial Forces

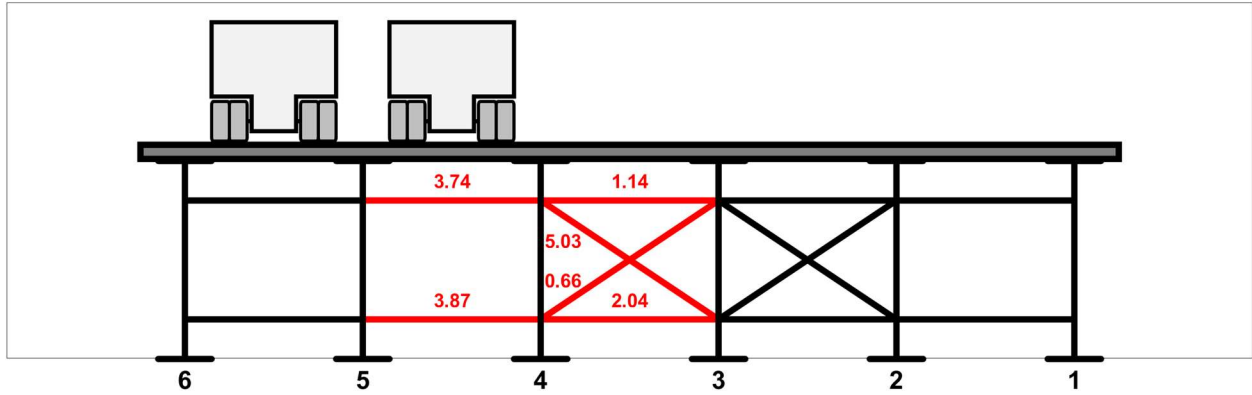


Figure I-1. Lubbock Bridge Load Case 1 CFL 7 Axial Force [kip]

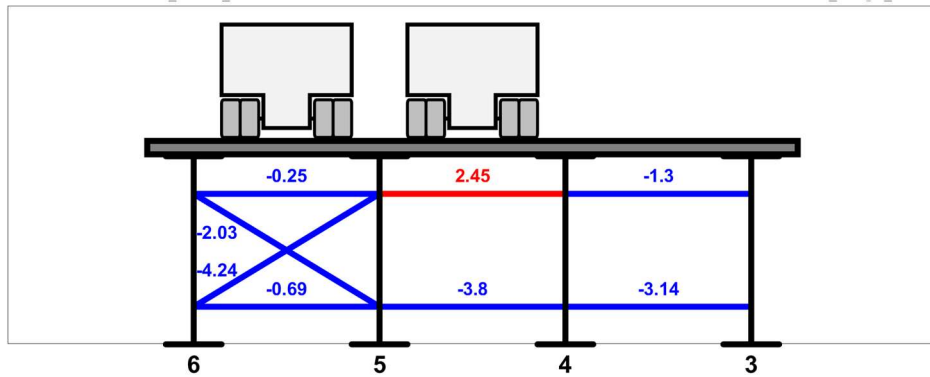


Figure I-2. Lubbock Bridge Load Case 1 CFL 3 Axial Force [kip]

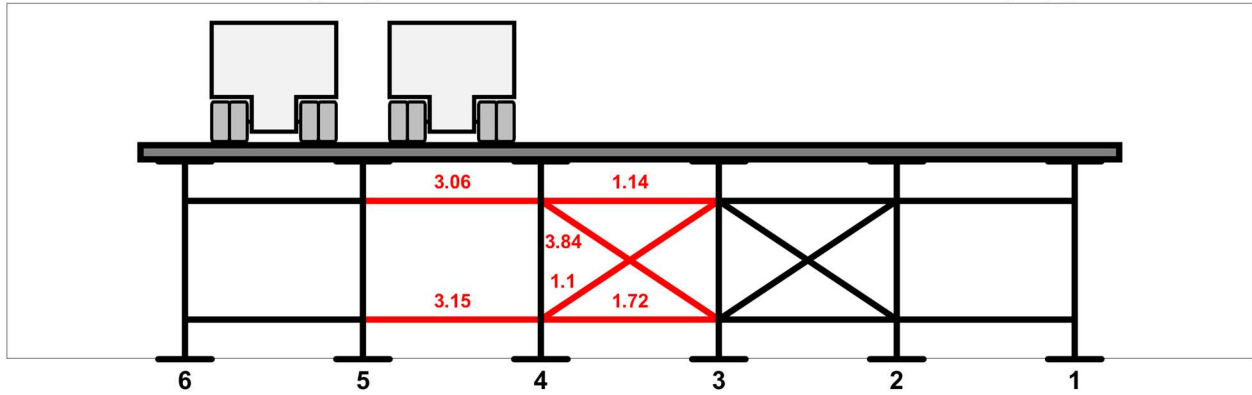


Figure I-3. Lubbock Bridge Load Case 2 CFL 7 Axial Force [kip]

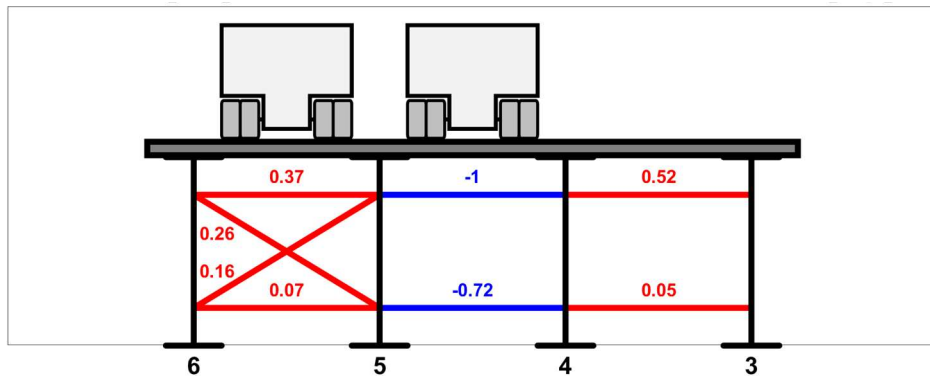


Figure I-4. Lubbock Bridge Load Case 2 CFL 3 Axial Force [kip]

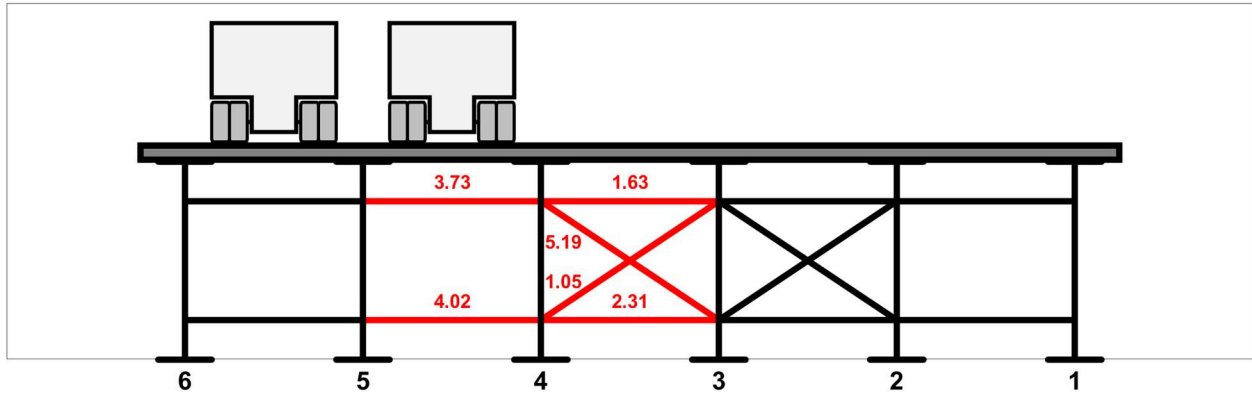


Figure I-5. Lubbock Bridge Load Case 3 CFL 7 Axial Force [kip]

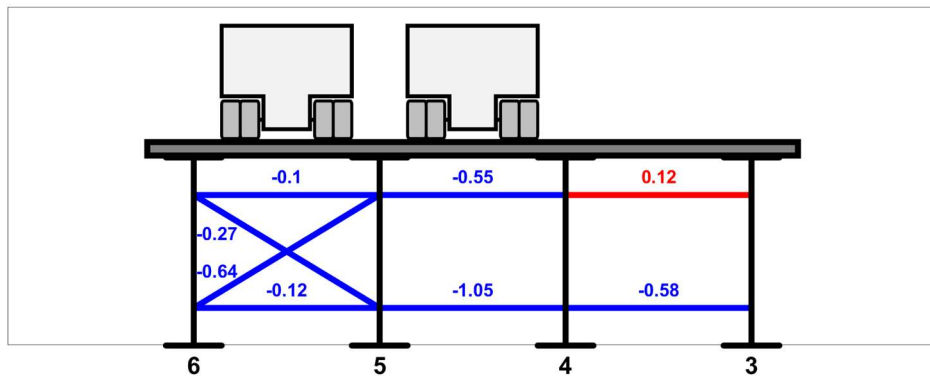


Figure I-6. Lubbock Bridge Load Case 3 CFL 3 Axial Force [kip]

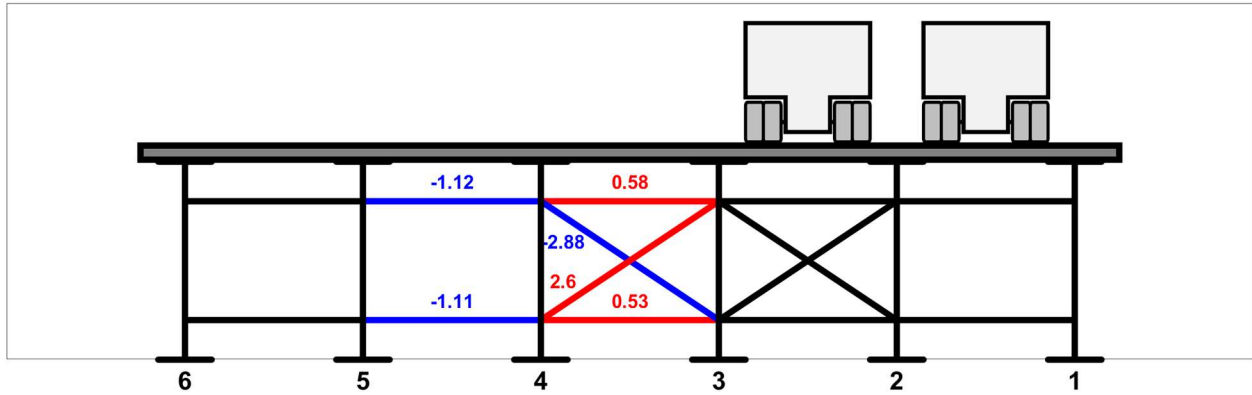


Figure I-7. Lubbock Bridge Load Case 4 CFL 7 Axial Force [kip]

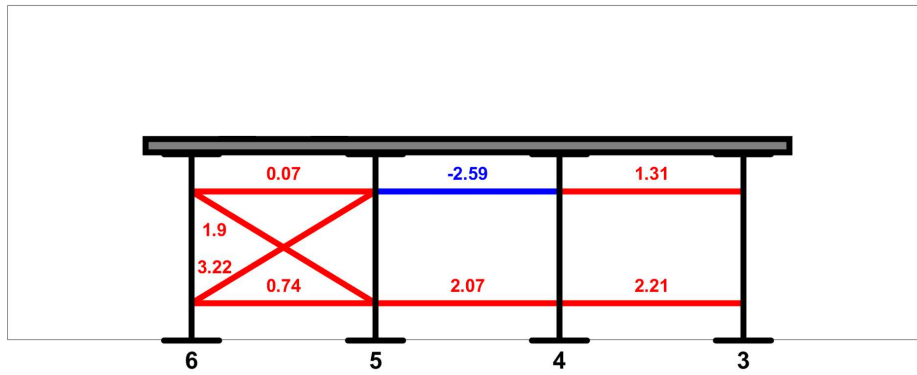


Figure I-8. Lubbock Bridge Load Case 4 CFL 3 Axial Force [kip]

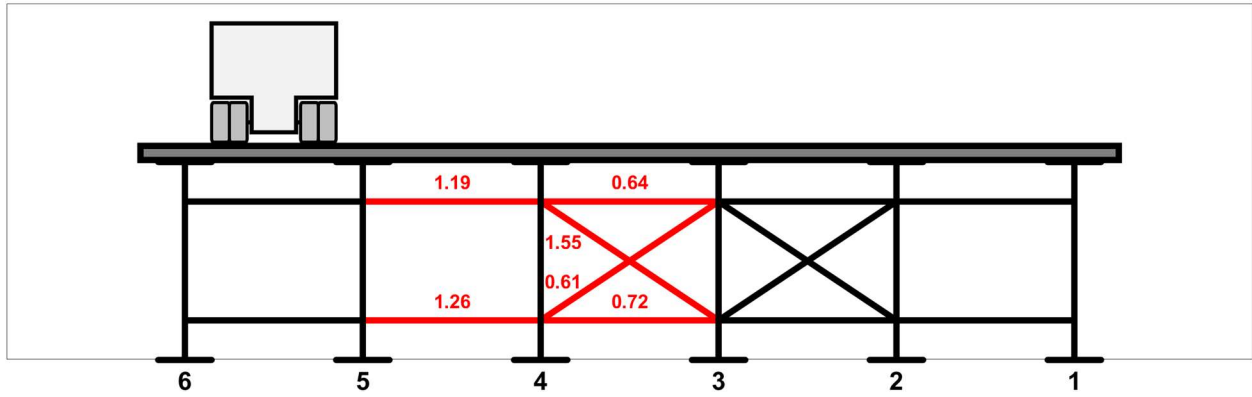


Figure I-9. Lubbock Bridge Load Case 5 CFL 7 Axial Force [kip]

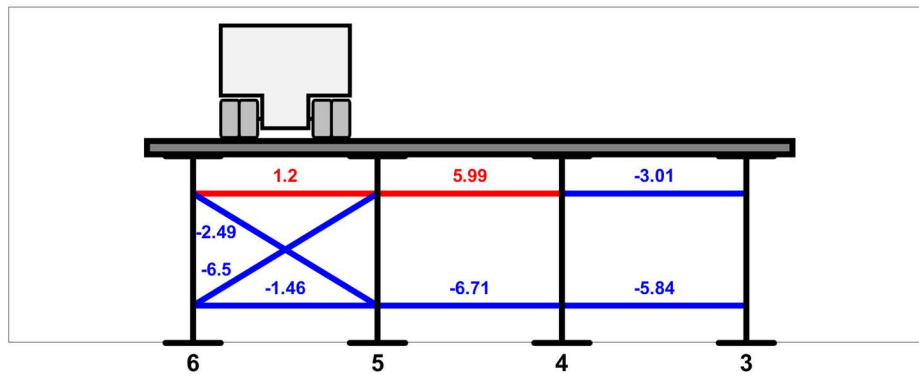


Figure I-10. Lubbock Bridge Load Case 5 CFL 3 Axial Force [kip]

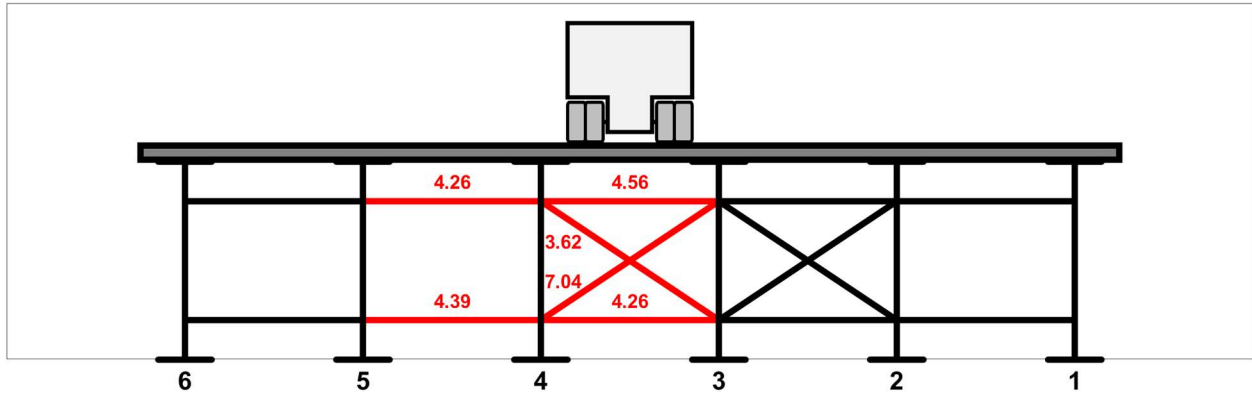


Figure I-11. Lubbock Bridge Load Case 6 CFL 7 Axial Force [kip]

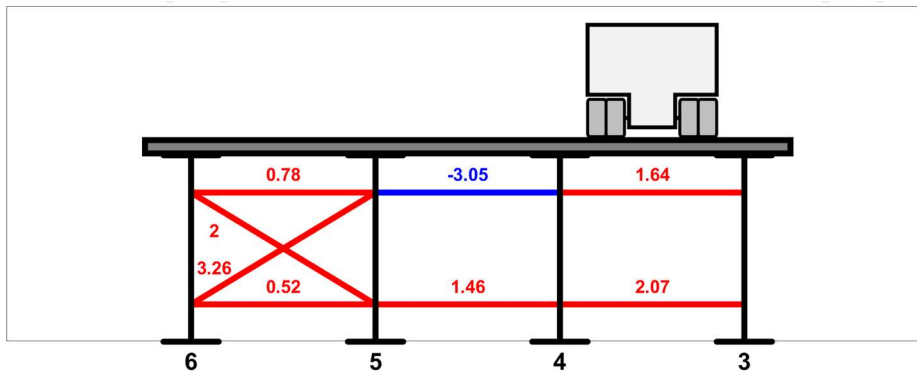


Figure I-12. Lubbock Bridge Load Case 6 CFL 3 Axial Force [kip]



## Appendix J. SH 105 Bridge Axial Forces and Deflections

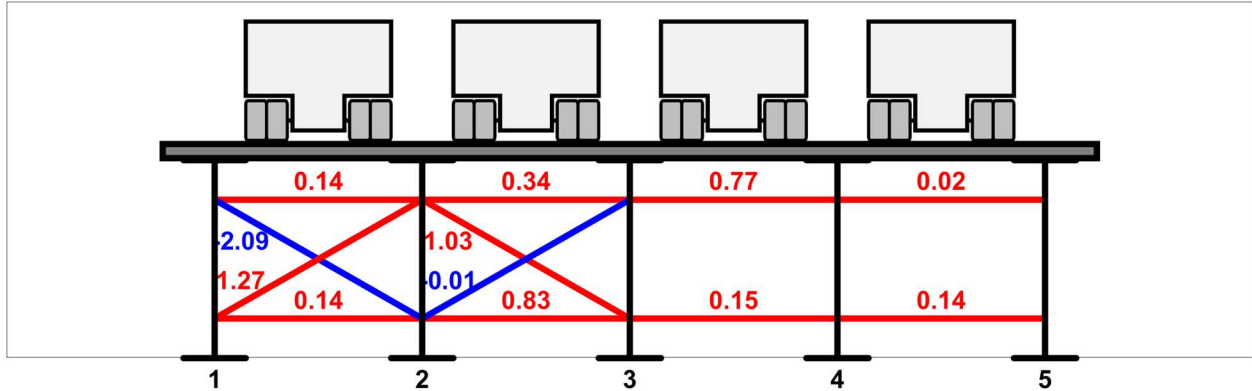


Figure J-1. SH 105 Bridge Load Case 1 CFL 3 Axial Force [kip]

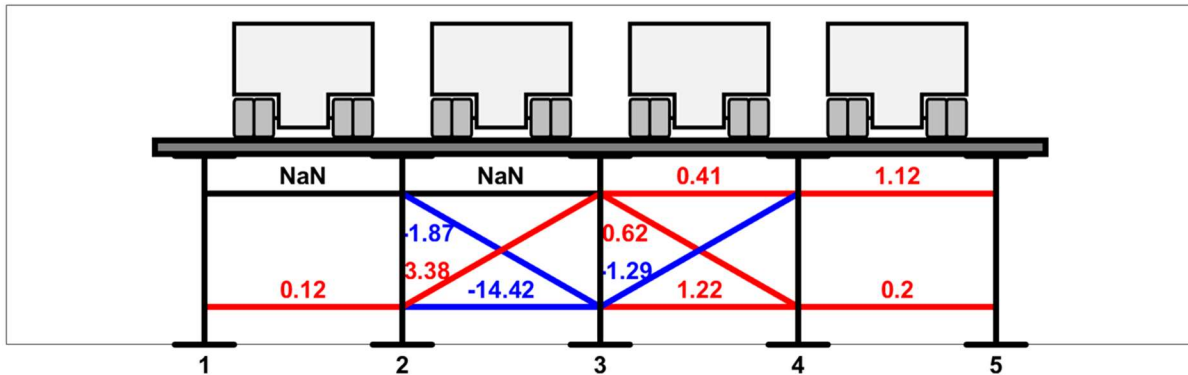


Figure J-2. SH 105 Bridge Load Case 1 CFL 5 Axial Force [kip]

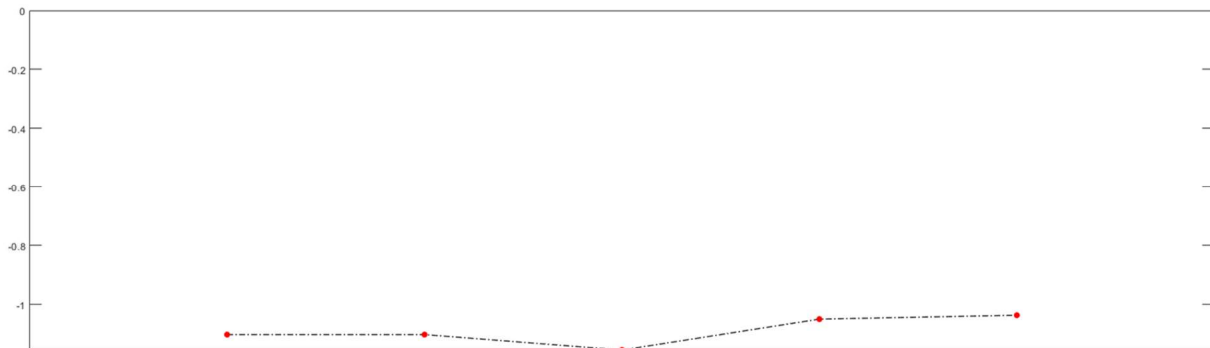


Figure J-3. SH 105 Bridge Load Case 1 CFL 5 Deflections [in]

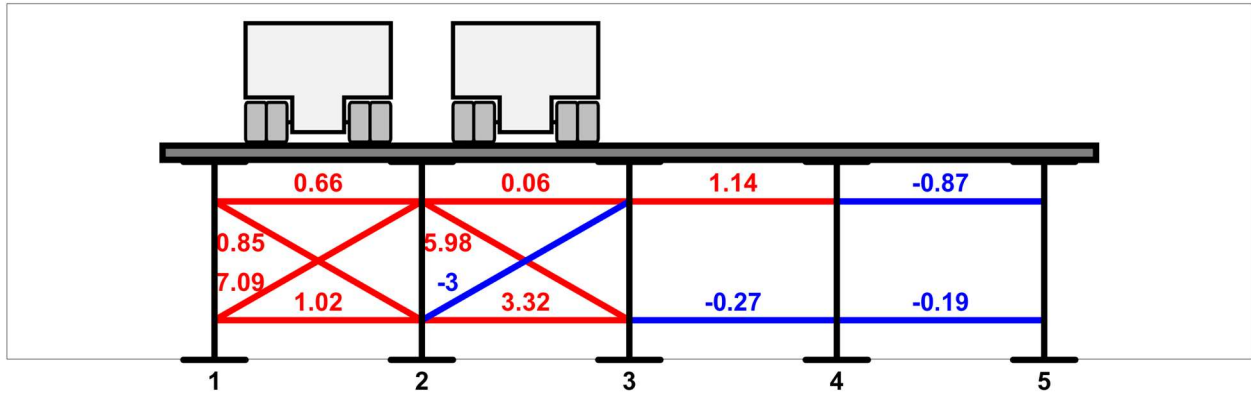


Figure J-4. SH 105 Bridge Load Case 2 CFL 3 Axial Force [kip]

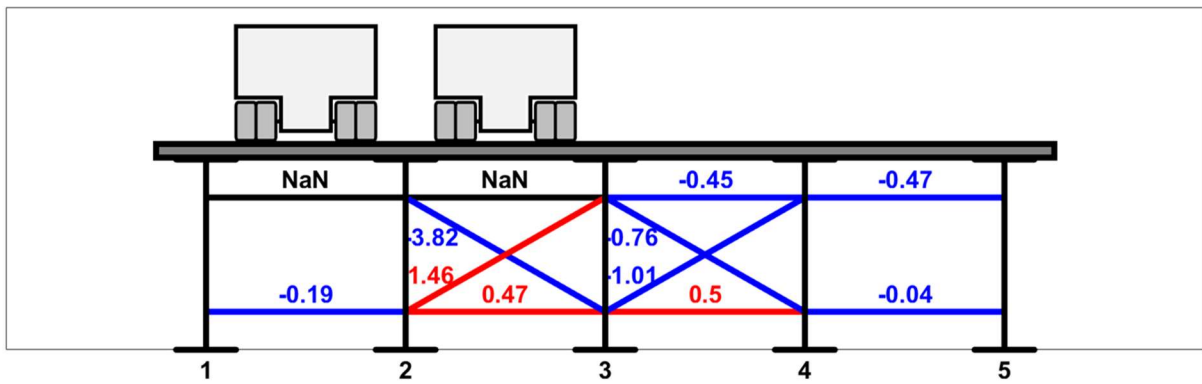


Figure J-5. SH 105 Bridge Load Case 2 CFL 5 Axial Force [kip]

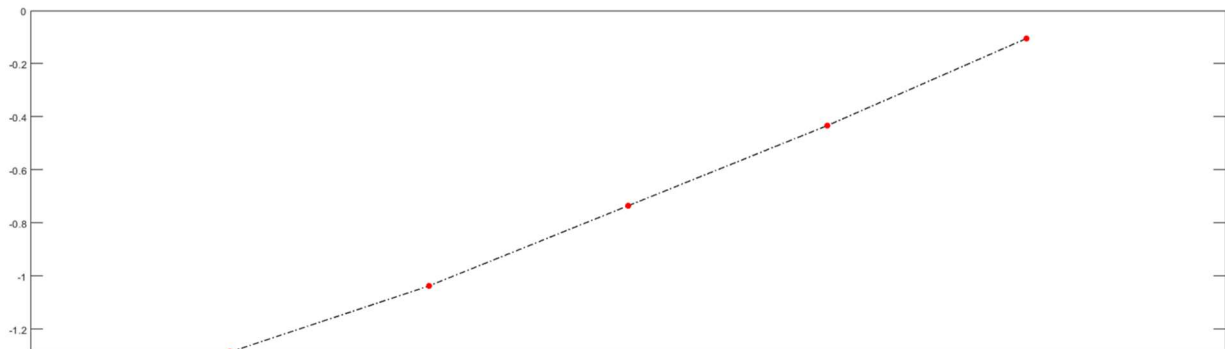


Figure J-6. SH 105 Bridge Load Case 2 CFL 5 Deflections [in]

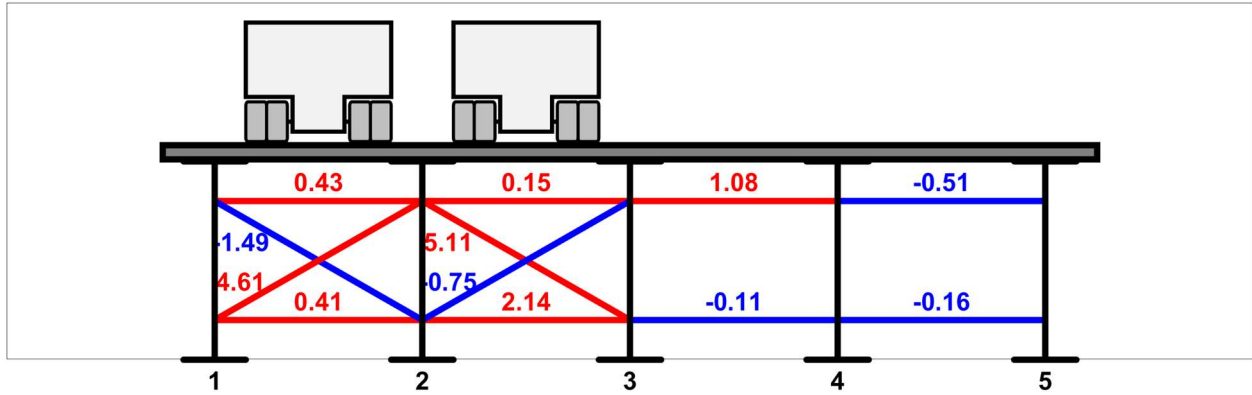


Figure J-7. SH 105 Bridge Load Case 3 CFL 3 Axial Force [kip]

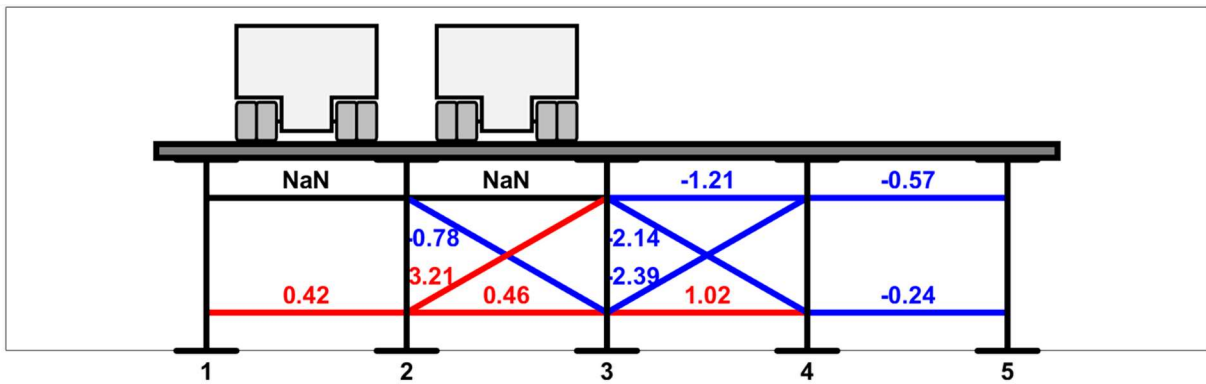


Figure J-8. SH 105 Bridge Load Case 3 CFL 5 Axial Force [kip]

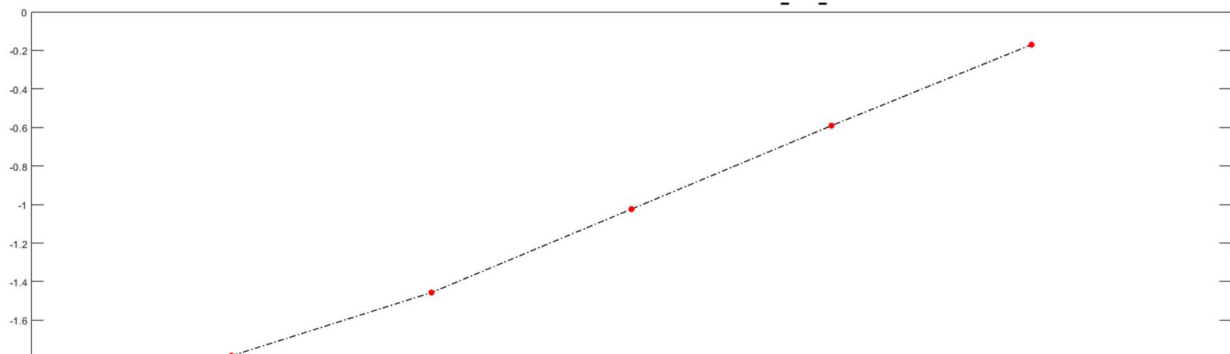


Figure J-9. SH 105 Bridge Load Case 3 CFL 5 Deflections [in]

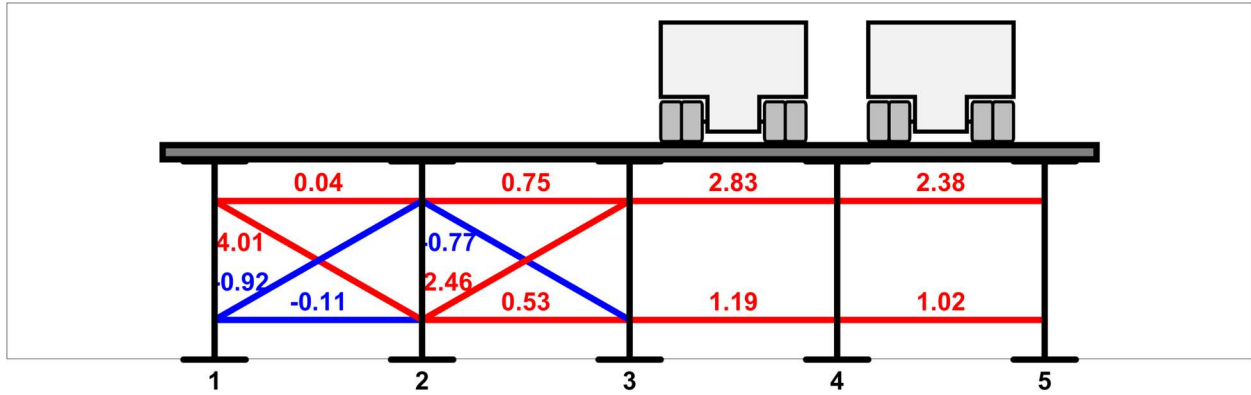


Figure J-10. SH 105 Bridge Load Case 4 CFL 3 Axial Force [kip]

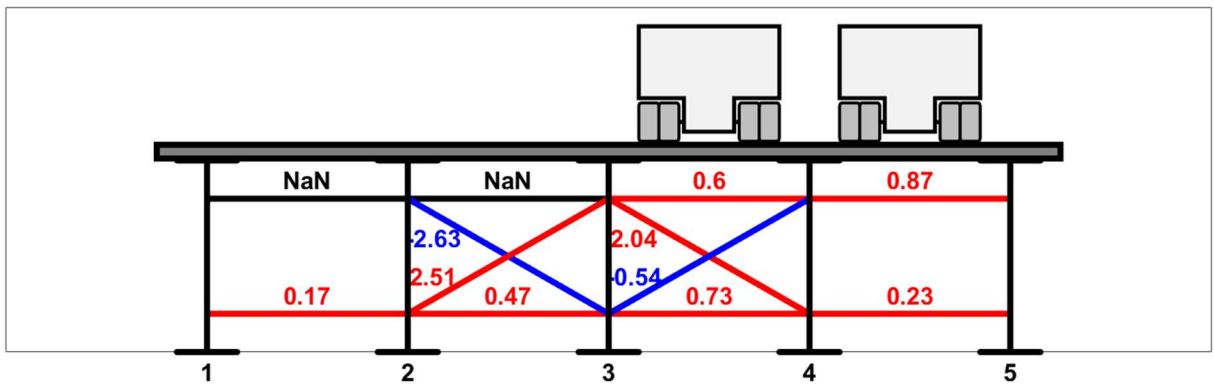


Figure J-11. SH 105 Bridge Load Case 4 CFL 5 Axial Force [kip]

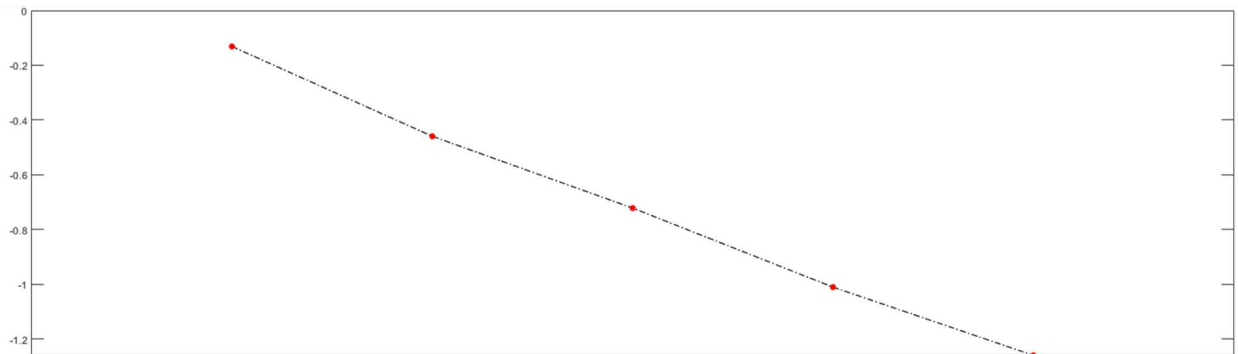


Figure J-12. SH 105 Bridge Load Case 4 CFL 5 Deflections [in]

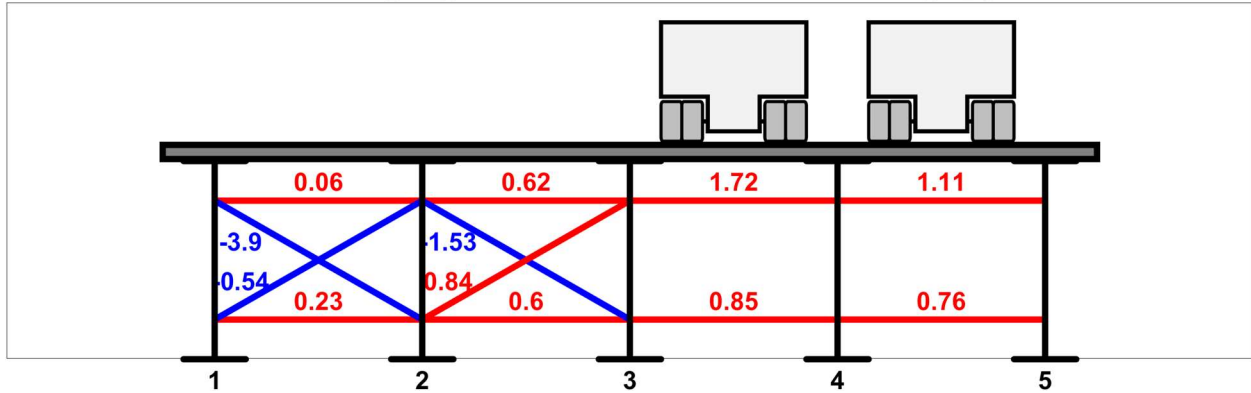


Figure J-13. SH 105 Bridge Load Case 5 CFL 3 Axial Force [kip]

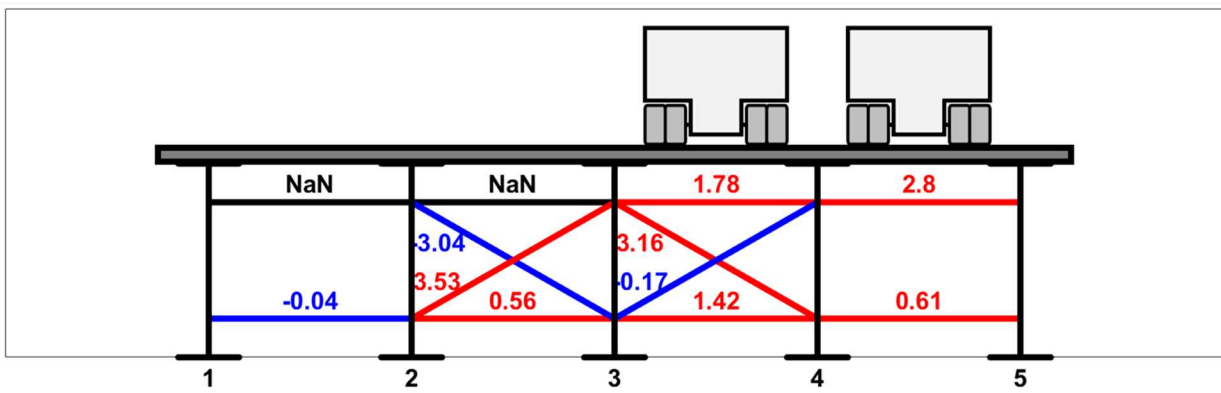


Figure J-14. SH 105 Bridge Load Case 5 CFL 5 Axial Force [kip]

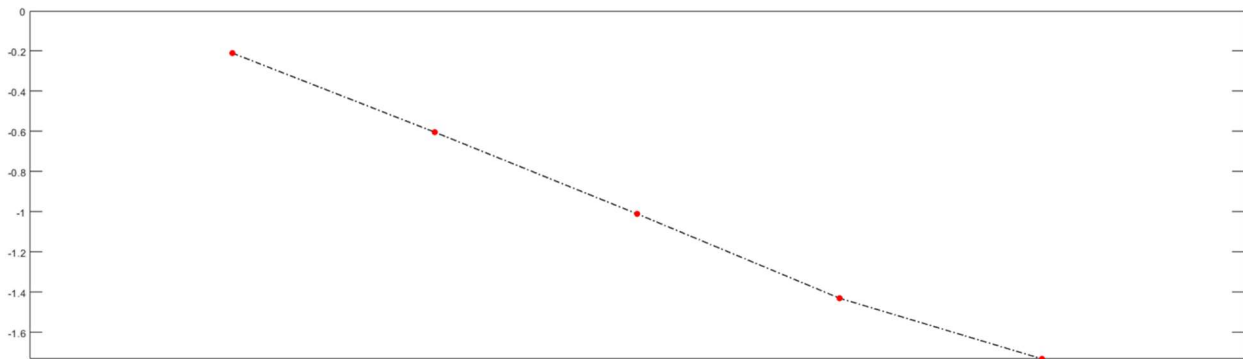


Figure J-15. SH 105 Bridge Load Case 5 CFL 5 Deflections [in]

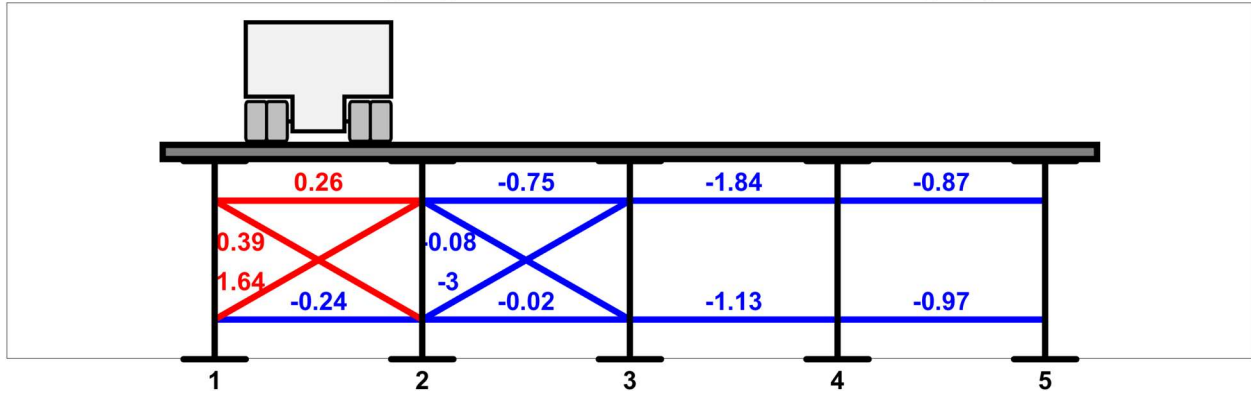


Figure J-16. SH 105 Bridge Load Case 6 CFL 3 Axial Force [kip]

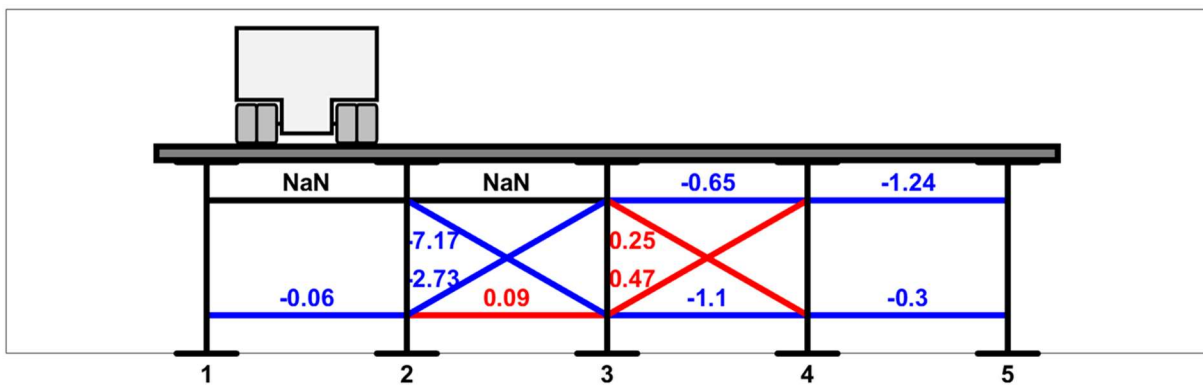


Figure J-17. SH 105 Bridge Load Case 6 CFL 5 Axial Force [kip]

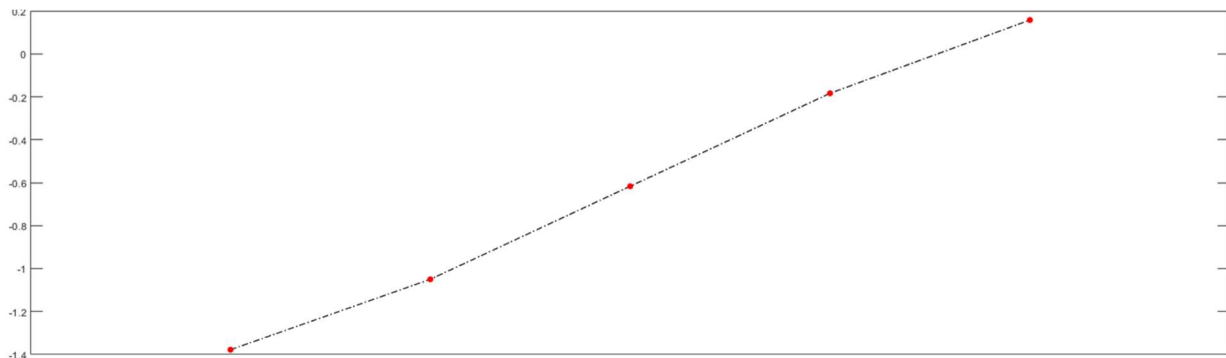


Figure J-18. SH 105 Bridge Load Case 6 CFL 5 Deflections [in]

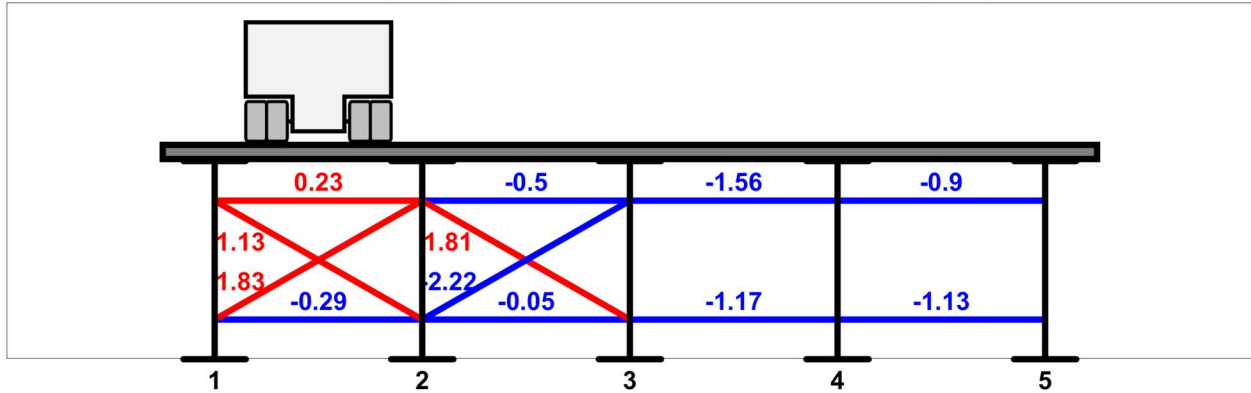


Figure J-19. SH 105 Bridge Load Case 7 CFL 3 Axial Force [kip]

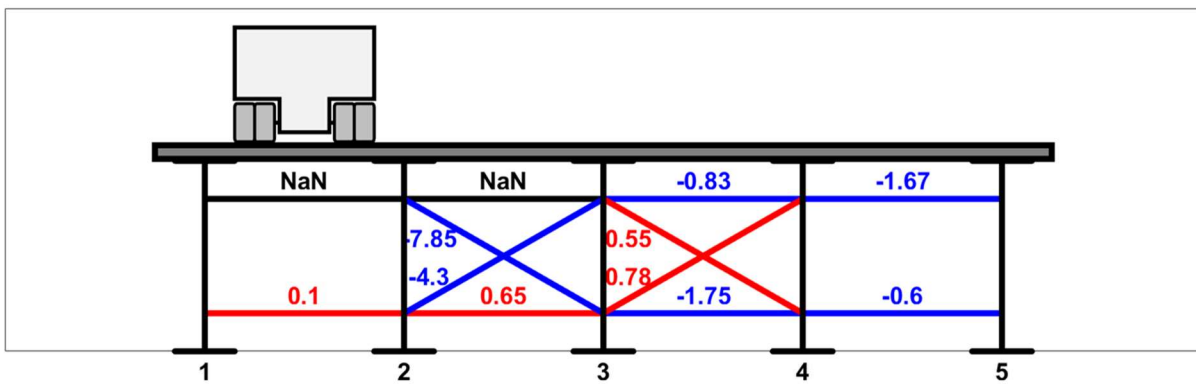


Figure J-20. SH 105 Bridge Load Case 7 CFL 5 Axial Force [kip]

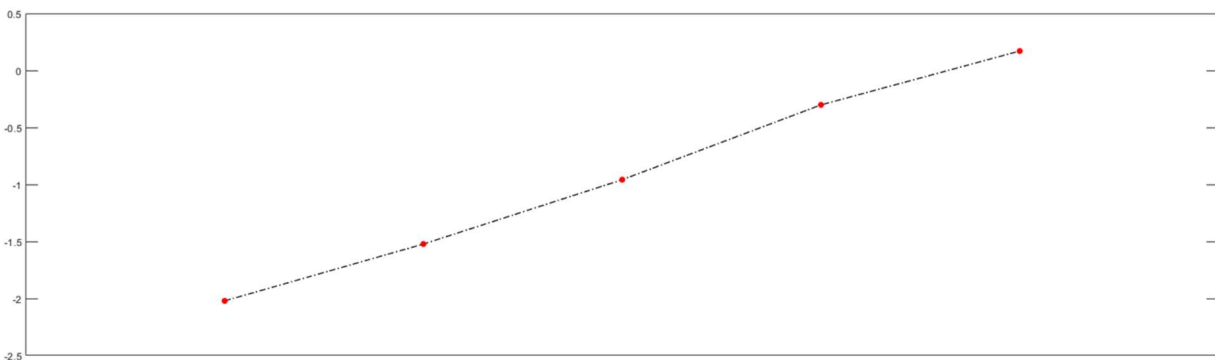


Figure J-21. SH 105 Bridge Load Case 7 CFL 5 Deflections [in]

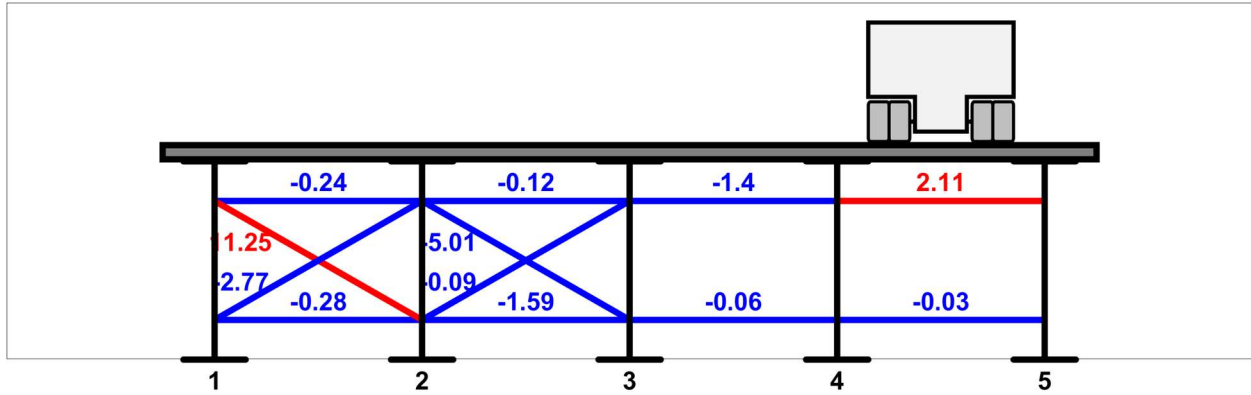


Figure J-22. SH 105 Bridge Load Case 8 CFL 3 Axial Force [kip]

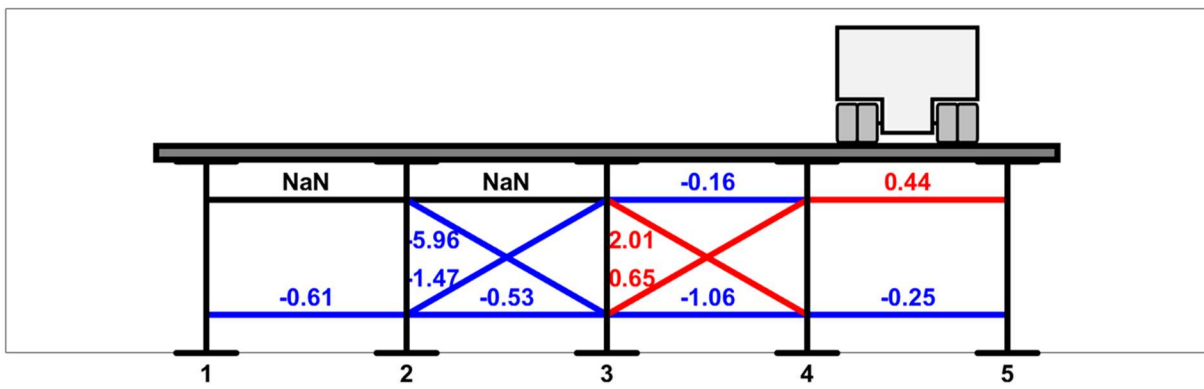


Figure J-23. SH 105 Bridge Load Case 8 CFL 5 Axial Force [kip]

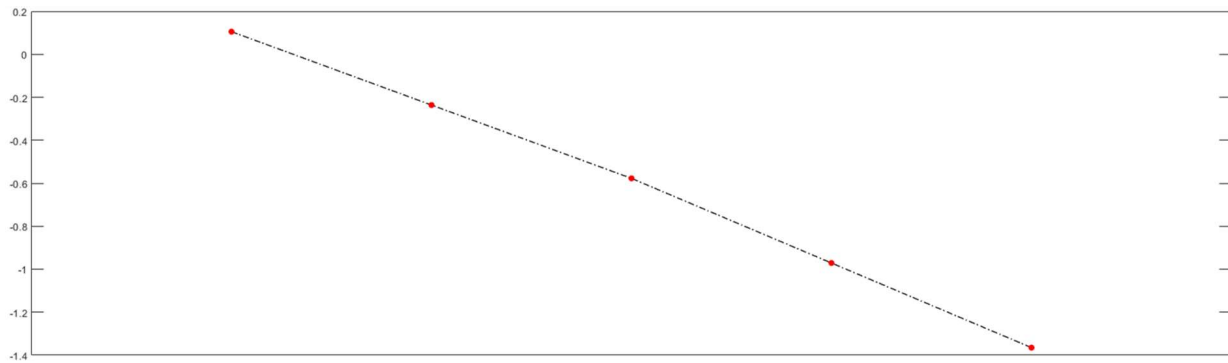


Figure J-24. SH 105 Bridge Load Case 8 CFL 5 Deflections [in]



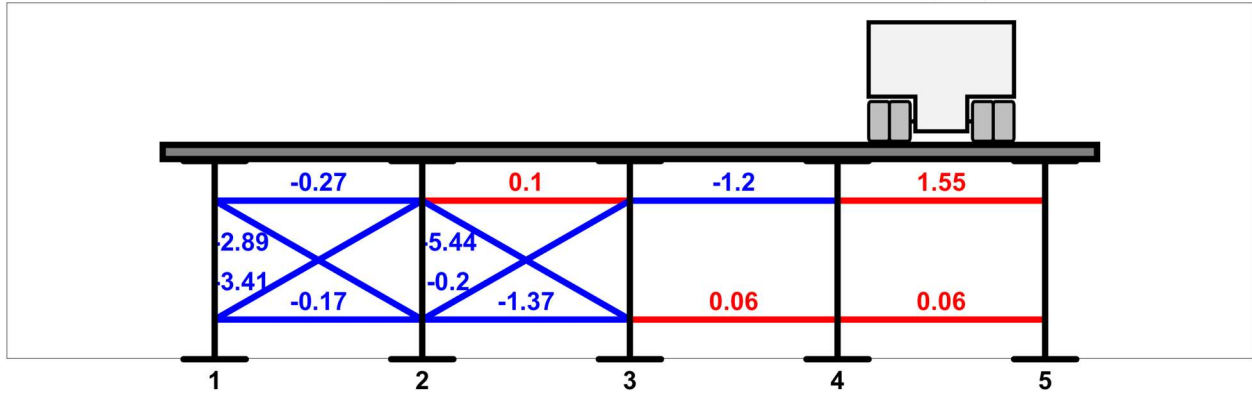


Figure J-25. SH 105 Bridge Load Case 9 CFL 3 Axial Force [kip]

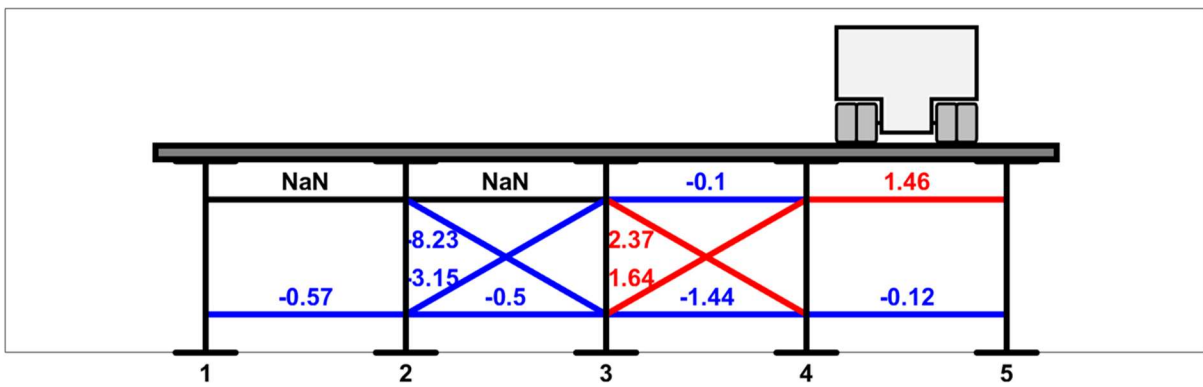


Figure J-26. SH 105 Bridge Load Case 9 CFL 5 Axial Force [kip]

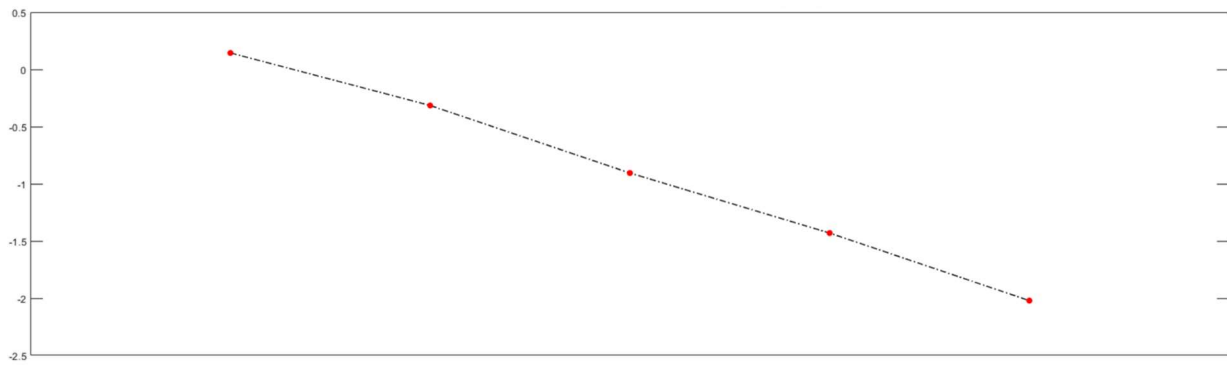


Figure J-27. SH 105 Bridge Load Case 9 CFL 5 Deflections [in]

## Appendix K. Chisholm Trail Bridge Axial Forces and Deflections

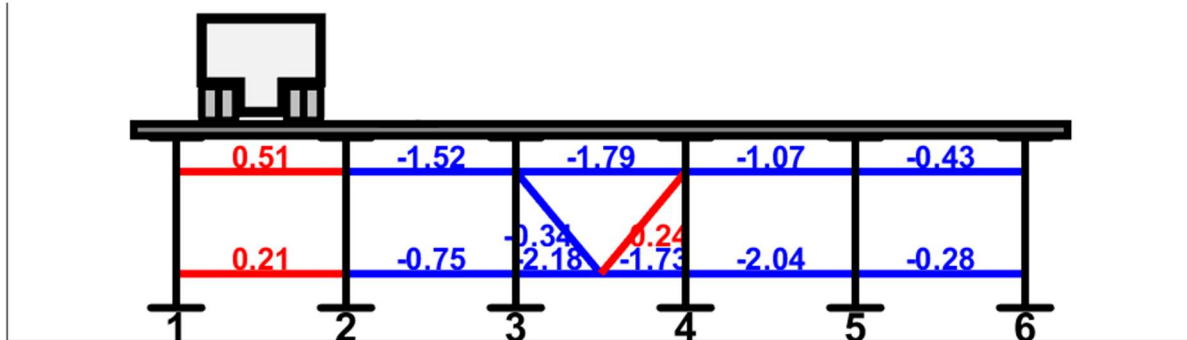


Figure K-1. Chisholm Trail Bridge Load Case 1 CFL 9 Axial Forces [kip]

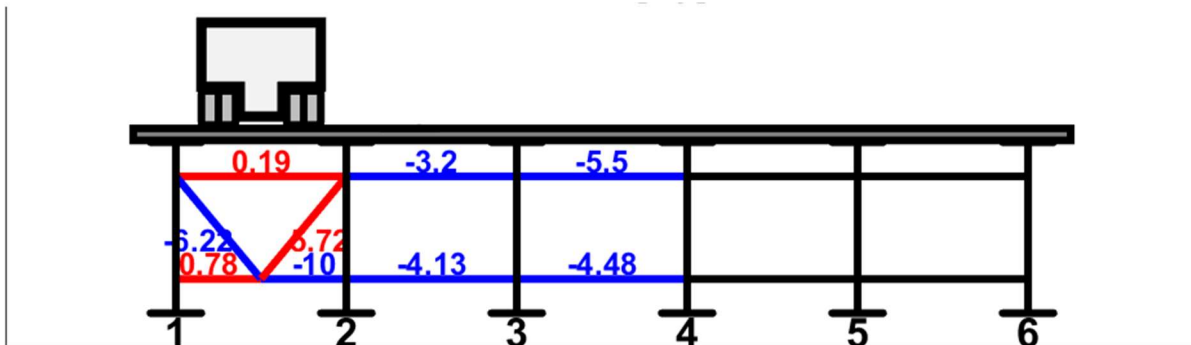


Figure K-2. Chisholm Trail Bridge Load Case 1 CFL 13 Axial Forces [kip]

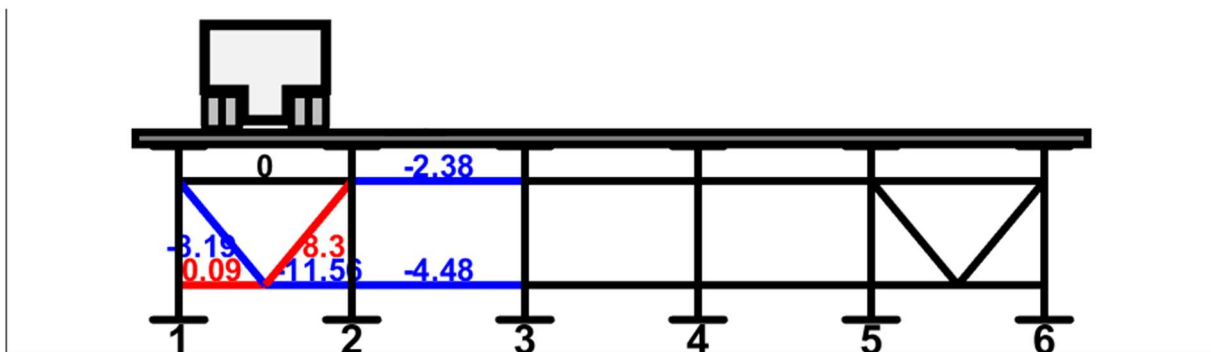


Figure K-3. Chisholm Trail Bridge Load Case 1 CFL 15 Axial Forces [kip]

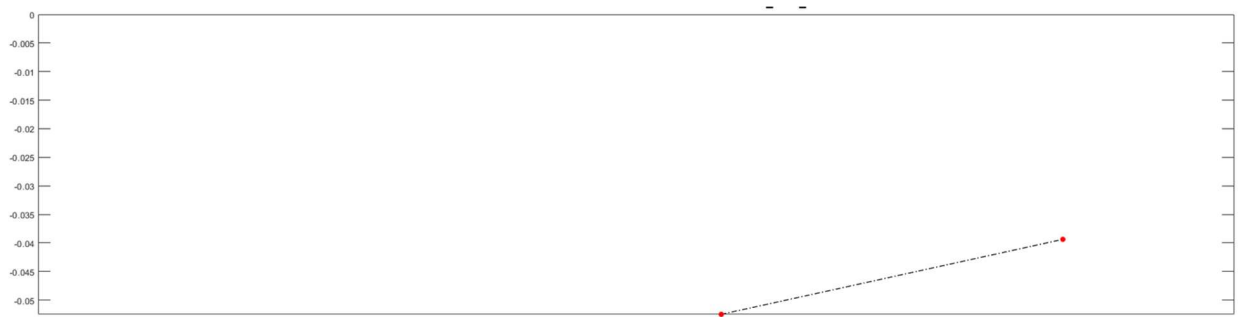


Figure K-4. Chisholm Trail Bridge Load Case 1 CFL 8 Deflections [in]

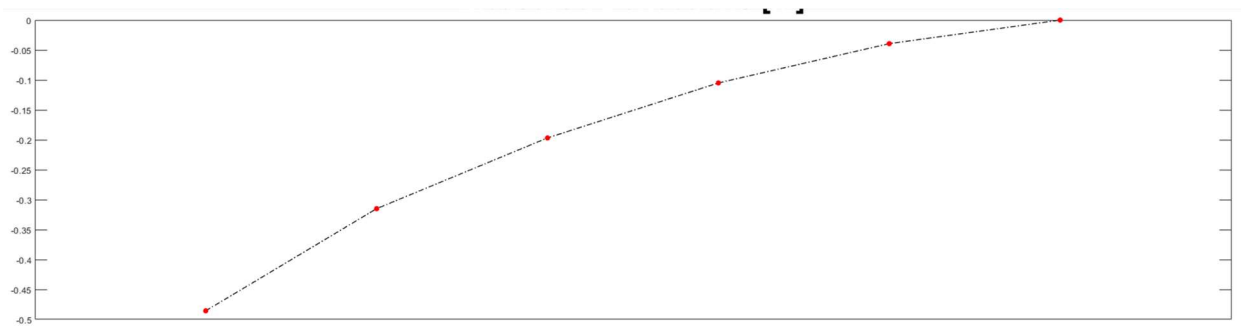


Figure K-5. Chisholm Trail Bridge Load Case 1 CFL 10 Deflections [in]

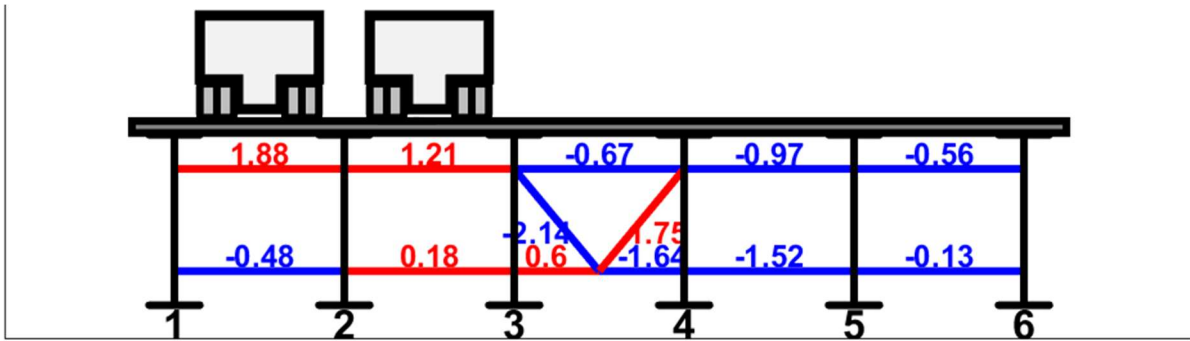


Figure K-6. Chisholm Trail Bridge Load Case 2 CFL 9 Axial Forces [kip]

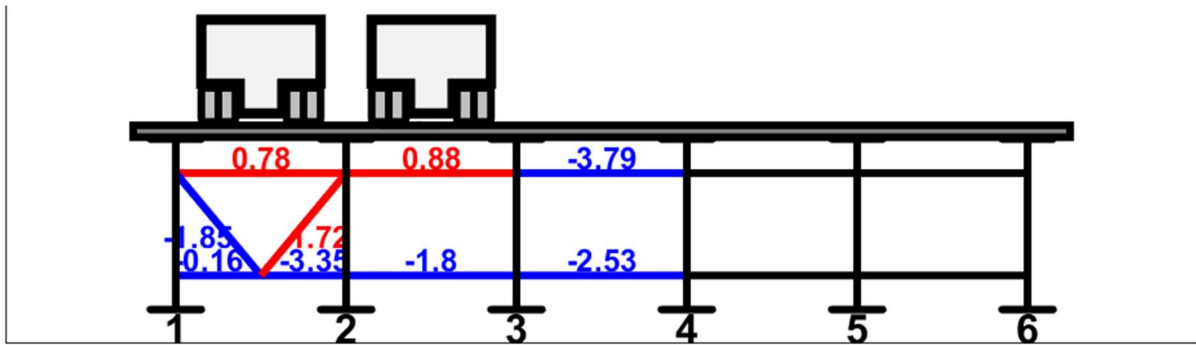


Figure K-7. Chisholm Trail Bridge Load Case 2 CFL 13 Axial Forces [kip]

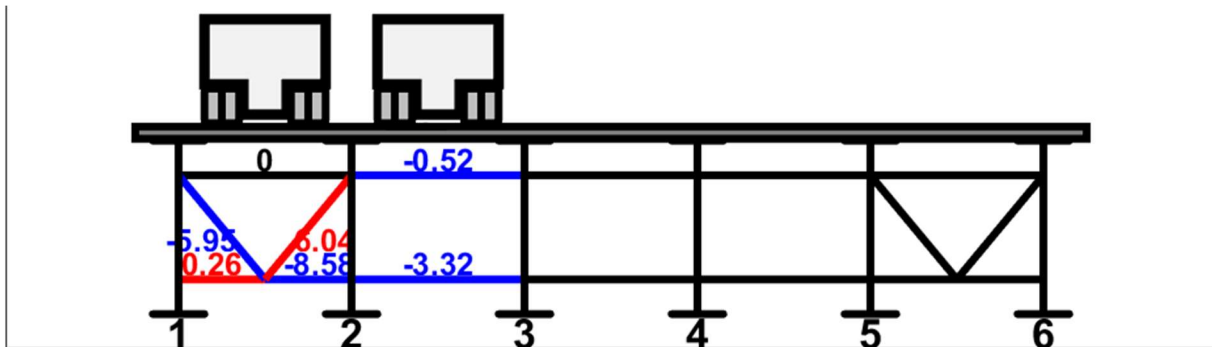


Figure K-8. Chisholm Trail Bridge Load Case 2 CFL 15 Axial Forces [kip]

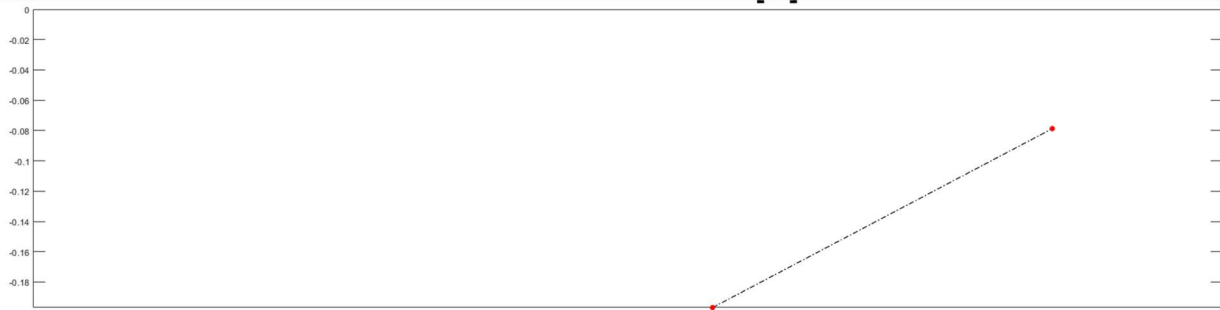


Figure K-9. Chisholm Trail Bridge Load Case 2 CFL 8 Deflections [in]

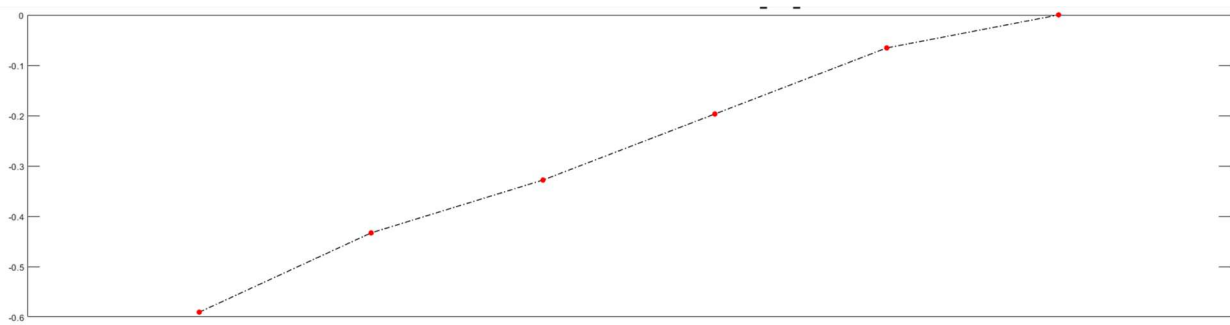


Figure K-10. Chisholm Trail Bridge Load Case 2 CFL 10 Deflections [in]

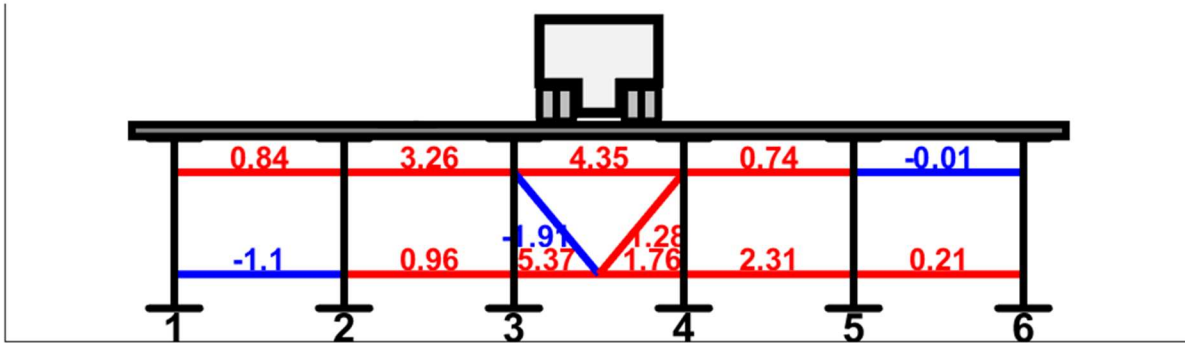


Figure K-11. Chisholm Trail Bridge Load Case 3 CFL 9 Axial Forces [kip]

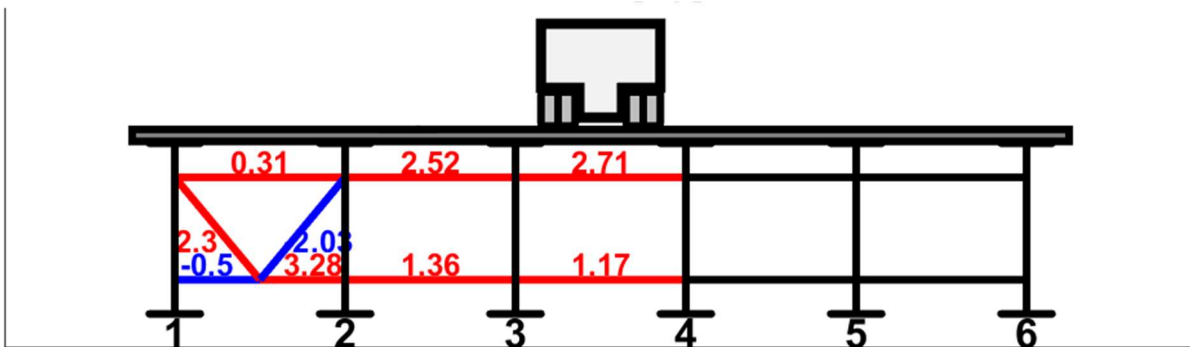


Figure K-12. Chisholm Trail Bridge Load Case 3 CFL 13 Axial Forces [kip]

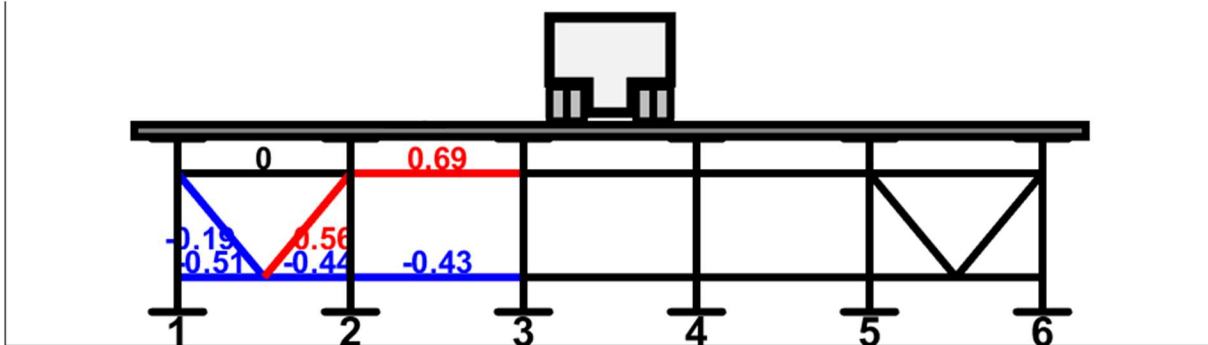


Figure K-13. Chisholm Trail Bridge Load Case 3 CFL 15 Axial Forces [kip]

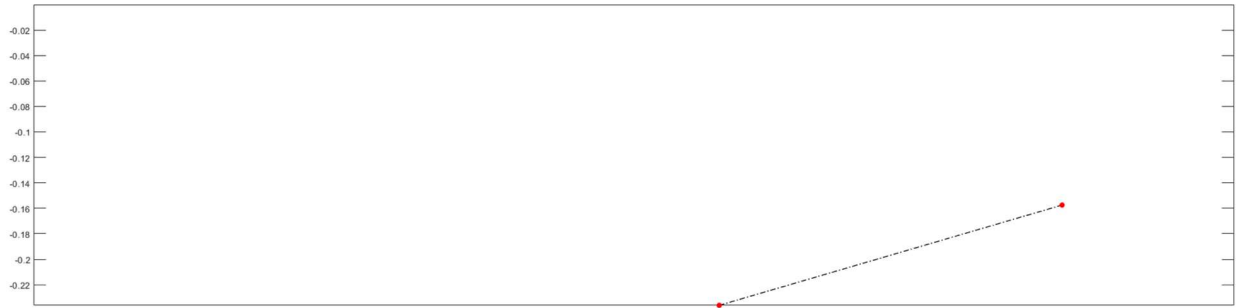


Figure K-14. Chisholm Trail Bridge Load Case 3 CFL 8 Deflections [in]

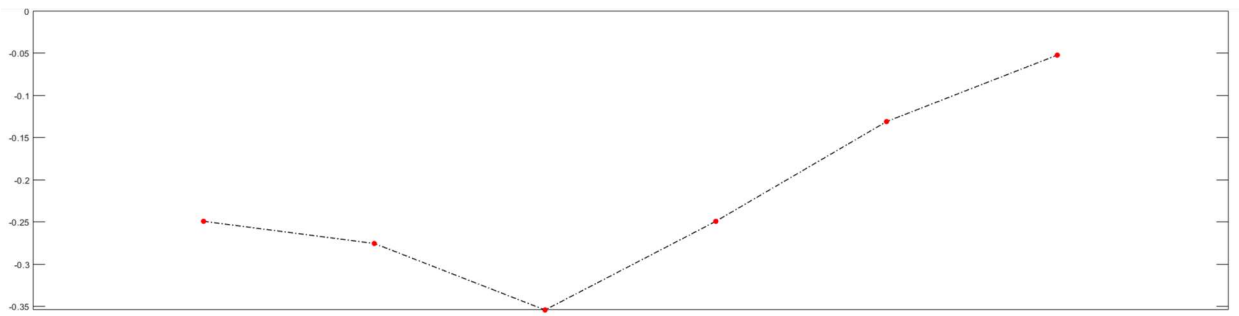


Figure K-15. Chisholm Trail Bridge Load Case 3 CFL 10 Deflections [in]

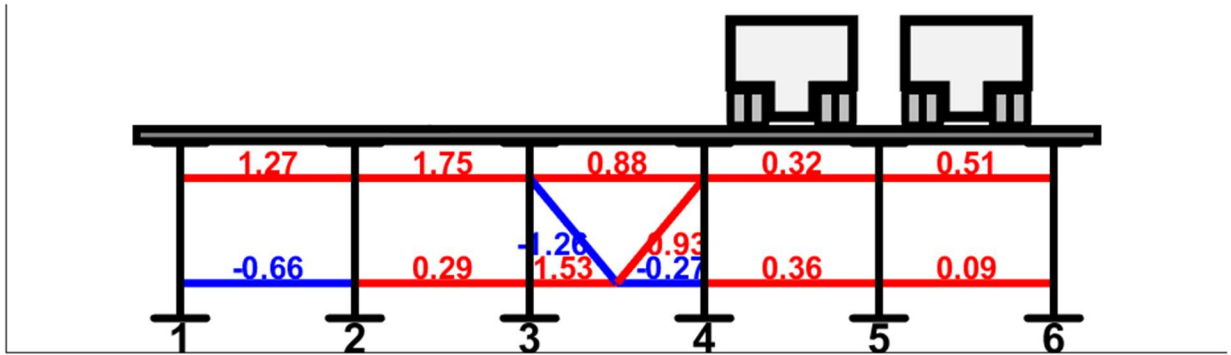


Figure K-16. Chisholm Trail Bridge Load Case 5 CFL 9 Axial Forces [kip]

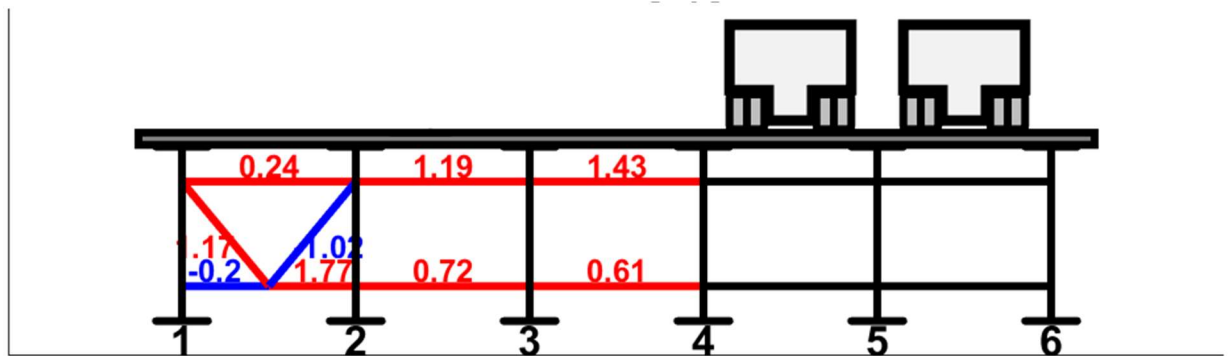


Figure K-17. Chisholm Trail Bridge Load Case 5 CFL 13 Axial Forces [kip]

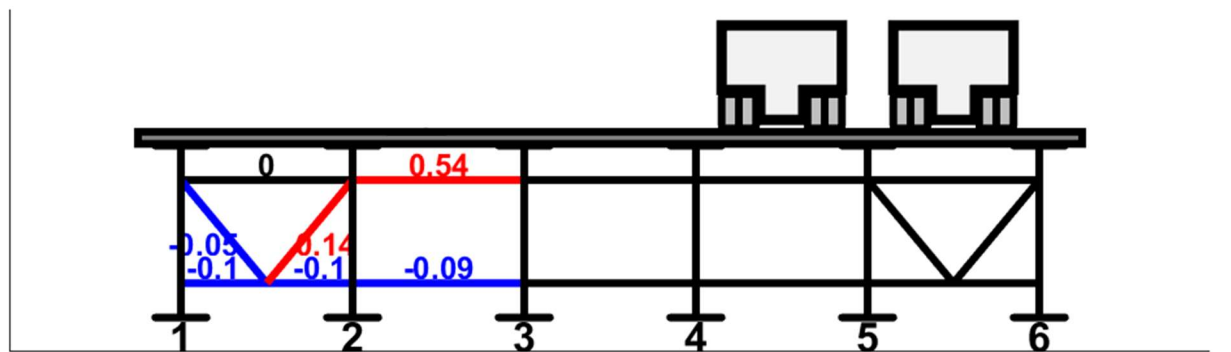


Figure K-18. Chisholm Trail Bridge Load Case 5 CFL 15 Axial Forces [kip]



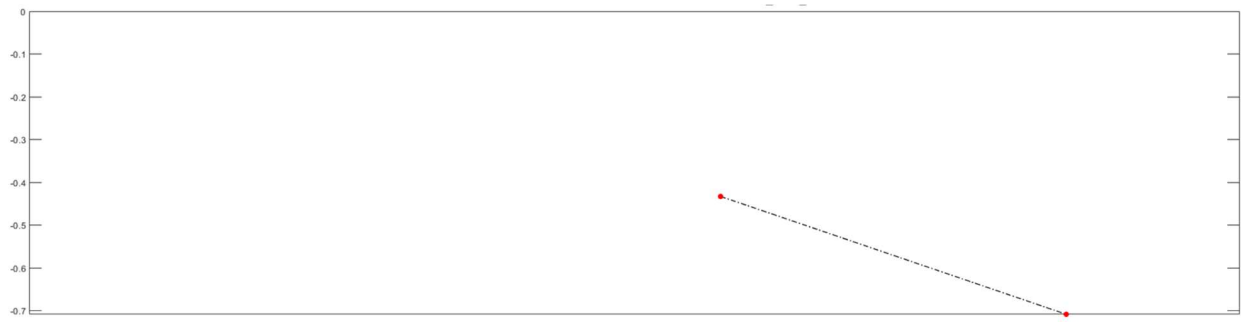


Figure K-19. Chisholm Trail Bridge Load Case 5 CFL 8 Deflections [in]

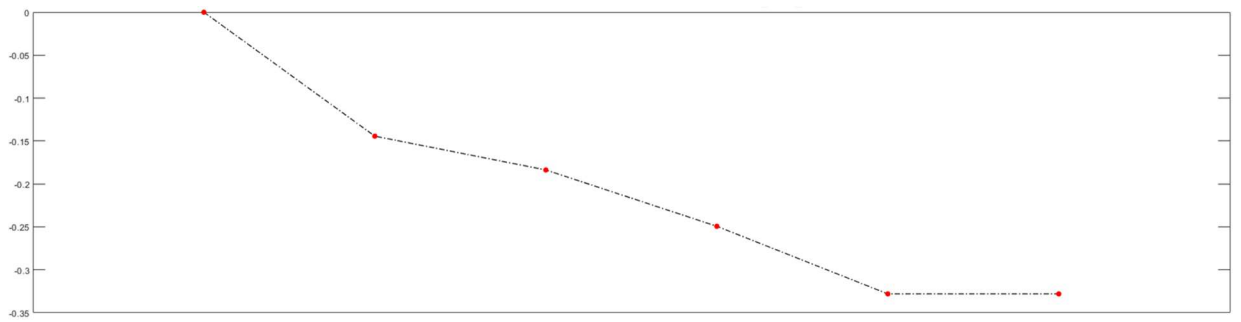


Figure K-20. Chisholm Trail Bridge Load Case 5 CFL 10 Deflections [in]

## **Vita**

Claire Elizabeth Gasser was born in Fairfax, Virginia. She graduated from the University of Notre Dame in 2020 with a Bachelor of Science in Civil Engineering. She immediately began graduate studies at Texas A&M University and earned her Master of Science in Civil Engineering in 2022. She moved to Auburn University in January 2023 to complete her doctoral program.